Fabrication and Characterization of Aluminum Composites by Squeeze Infiltration and Compocasting Techniques

Thesis Submitted to AcSIR for the Award of the Degree of

DOCTOR OF PHILOSOPHY

in Engineering Sciences

By

Sree Manu K.M.

Registration No: 20EE12A39018

Under the guidance of

Dr. T.P.D. Rajan

Materials Science and Technology Division

CSIR - National Institute for Interdisciplinary Science and Technology

(CSIR-NIIST)

THIRUVANANTHAPURAM-695 019, KERALA, INDIA

November 2016

Dedicated to…

Mr. S.M. Nair, Mrs. V.A. Kumari, Mrs. Aswathy.S.Nair,

Mr. S.A. Anurudh & Dr. T.P.D. Rajan

DECLARATION

I hereby declare that the matter embodied in the thesis entitled: "**Fabrication and Characterization of Aluminum Composites by Squeeze Infiltration and Compocasting Techniques**" is the result of the investigations carried out by me at the Materials Science and Technology Division, CSIR-National Institute for Interdisciplinary Science and Technology (CSIR-NIIST), Trivandrum, under the supervision of Dr. T.P.D. Rajan and the same has not been submitted elsewhere for any other degree.

In keeping with the general practice of reporting scientific observations, due acknowledgement has been made wherever the work described is based on the findings of other investigators.

Thiruvananthapuram
November 23, 2016

Sree Manu K.M.

COUNCIL OF SCIENTIFIC & INDUSTRIAL RESEARCH
CSIR - NATIONAL INSTITUTE FOR INTERDISCIPLINARY SCIENCE AND TECHNOLOGY (CSIR-NIIST)
Industrial Estate P.O., Trivandrum - 695 019, India

Dr. T.P.D. Rajan
Senior Scientist
Materials Science and Technology Division

Tel: 91-471-2515327
Fax: +91-471-2491712
E-mail: tpdrajan@niist.res.in

November 23, 2016

CERTIFICATE

This is to certify that the work incorporated in this Ph.D. thesis entitled "**Fabrication and Characterization of Aluminum Composites by Squeeze Infiltration and Compocasting Techniques**" submitted by **Mr. K. M. Sree Manu** to Academy of Scientific and Innovative Research (AcSIR), in partial fulfilment of the requirements for the award of the **Degree of Doctor of Philosophy in Engineering Sciences**, embodies original research work under my supervision and guidance at the Materials Science and Technology Division of the CSIR-National Institute for Interdisciplinary Science and Technology (CSIR-NIIST), Trivandrum. I further certify that this work has not been submitted to any other University or Institution in part or full for the award of any degree or diploma. Research material obtained from other sources has been duly acknowledged in the thesis. Any text, illustration, table etc., used in the thesis from other sources, have been duly cited and acknowledged.

Sree Manu K.M.
(Student)

Dr. T.P.D. Rajan
(Thesis Supervisor)

ACKNOWLEDGEMENTS

I would like to express my deep sense of gratitude to my supervising guide, **Dr. T.P.D. Rajan**, Senior Scientist, MMS/MSTD, for his timely suggestions, consistent support, advice, enthusiastic and excellent guidance throughout my Ph.D. career. I could benefit a lot from his excellent ideas and invaluable academic experience, which would certainly help me in future. He gave full freedom to develop my individuality and self-sufficiency to carry out the work independently. Under his supervision, I have grown up to be a more mature and more qualified researcher.

My sincere gratitude's to Dr. A. Ajayaghosh, Director, CSIR-NIIST and Dr. Suresh Das former Director, CSIR-NIIST, Thiruvananthapuram, for providing all the necessary facilities to carry out my research.

My deepest gratitude's to Dr. U.T.S. Pillai, Dr. S. Savithri and Dr. U.S. Hareesh (my Doctoral Advisory Committee members) for their valuable suggestions and assistances at different instances.

I would like to thank Dr. R. Luxmi Varma and Dr. Mangalam S. Nair, present and former AcSIR co-ordinators.

I wish to express my sincere thanks to present and former Head of MMS/MSTD, all scientists and staffs of Materials Science and Technology Division and CSIR-NIIST for their help and support.

I am extremely grateful to Dr. B. C. Pai, CSIR-NIIST and Dr. Manoj Gupta, NUS, Singapore, for their valuable discussions and encouragement.

I convey my sincere thanks to Mr. M. Brahmakumar, Mr. V. Antony and Mr. A. Peer Mohamed, CSIR-NIIST, for the help received during castings, optical micrographs, and TGA/DTA.

I wish to thank Dr. K. Udaya Bhat and Mr. Prashant, NITK, Surathkal for their help in TEM analysis.

I would like to thank Dr. K. Manisekar, Professor and Head, Department of Centre for Manufacturing Science, National Engineering College, Kovilpatti.

I am grateful to thank Mr. P. Narayanasamy, Mr. P.S. Rahul, Mr. K. Sreeraj, Mr. L. Ajay Raag, Mr. Riyas Mohammed, Mr. S. Arun Kumar, Mr. M.G. Akhil, Mr. Abhilash Viswanath, Mr. K.R. Athul, Mr. Hari Sanil, Mr. E. Jayakumar, Mr. Jithu Jayaraj, Mr. N. Anand, Mr. Prince Joseph, Mr. Nikhil Koshy, Ms. K. Jerin Pancrecious, Ms. R. Remya, Mrs. R. Aiswarya, and all other friends at CSIR-NIIST for their help, care, and support which made my research and life in NIIST memorable.

Heartfelt thanks to my parents (S.M. Nair and V. Anandha Kumari Amma) for providing me a good education, endless love, encouragement and untiring support. Special thanks to my wife (Aswathy. S. Nair) and son (S.A. Anurudh).

The financial assistance from Council of Scientific and Industrial Research (CSIR), New Delhi is gratefully acknowledged.

Above all, I thank Almighty for giving me all these people to help and encourage me, and for the skills and opportunity for the successful completion of this thesis.

Sree Manu K.M.

Contents

List of Tables

List of Figures

Preface

Metallic composites are one of the advanced materials widely used for aerospace, automotive, defense, and general engineering applications. They can be tailored to have superior properties such as enhanced high-temperature performance, high specific strength and stiffness, increased wear resistance, better thermal and mechanical fatigue, and creep resistance than those of unreinforced alloys. In the present scenario of materials world, evolution of aluminum matrix composites (AMCs) from science and intellectual interest to an industrial technology is due to their unique combination of engineering properties. To fabricate such composites with ideal properties, the processing technique has to ensure high volume fraction of reinforcement incorporation, uniform distribution of the reinforcement and acceptable adhesion between the matrix and the reinforcing phase without unwanted interfacial reactions which degrades the mechanical properties. Liquid metal infiltration into porous ceramic preforms, compocasting and squeeze casting techniques stands out to be the economic and distinct methods for fabricating AMC with aforesaid properties compared to other conventional processes.

Squeeze infiltration is a liquid state fabrication method, in which the reinforcing phases are constructed into a high dimensional interconnected porous body called preform followed by liquid metal infiltration through the preform under pressure. The wetting between the matrix and the reinforcement can be overcome by external pressure; also it can yield ancillary assistance like eradication of shrinkage and porosities, refined microstructure since solidification under pressure, and reduced chemical reactions due to enhanced processing speed last for few seconds. Use of high volume fraction of reinforcement, uniform microstructure due to the use of a highly ordered inceptive preform, and development of near net shape and selectively reinforced components are an added advantage of squeeze infiltration. Compocasting is a solid-liquid state method in which a vortex is created in the semisolid molten metal (between the solidus and liquidus temperature of the matrix alloy) using an impeller driven by an electric motor, and the reinforcements are added into the vortex under stirring. Distinct advantages are low casting temperature, uniform distribution of

reinforcement without agglomeration, good wettability and better matrix-reinforcement bonding. During compocasting process, the higher viscosity of semisolid molten metal slurry transmits shear force over the agglomerated reinforcements which lead to better dispersion and distribution of reinforcement in the matrix. The compocast melt are further solidified using squeeze casting technique. The objective of the current research work is to fabricate AMC employing a variety of micron and nano size reinforcement's combinations like Al-carbon fiber, Al-aluminosilicate fiber, Al-micorsilica and Al-nano Al_2O_3 by squeeze infiltration and compocasting techniques to obtain superior properties for strategic and societal applications.

The thesis comprises of six chapters. The first chapter gives a brief introduction to metallic composites, preform materials, infiltration and compocasting processes. Further, an extensive and exclusive literature review on the development of MMC (Metal matix composites) by various infiltration and compocasting techniques, their process parameters, characteristics, and applications carried out worldwide also incorporated towards the end of this chapter.

The second chapter deals with the development of bidirectional carbon fiber fabric reinforced 6061 aluminum composites by squeeze infiltration technique. Bidirectional (BD) satin weave polyacrylonitrile (PAN) based carbon fiber (C_f) fabric preform was successfully infiltrated with Al6061 alloy by direct squeeze infiltration process and their properties were evaluated. The infiltrated composite shows uniform distribution of carbon fibers in the matrix with the elimination of porosities, fiber damage and close control in deleterious aluminum carbide (Al_4C_3) phase formation, by using optimized process parameters. C_f/Al6061 composite exhibits superior wear resistance compared to unreinforced alloy due to the formation of self-lubricant tribo-film on the pin surface, which intercepts the matrix metal to counter surface contact. The introduction of BD carbon fiber in the matrix enhanced the hardness and compressive strength of the composite remarkably by restraining the matrix plastic flow behavior. The tensile strength of composite decreased due to interfacial delamination of transverse oriented fibres at lower load. HRTEM observation shows the presence of Al_2O_3 and $MgAl_2O_4$ spinel, confirmed by EDS and SAD pattern, at the interface and controls

the growth of Al_4C_3 crystals. The C_f/Al6061 shows lower density of 2.16 g/cm^3 which is a major advantage for weight reduction compared to the monolithic alloy (2.7 g/cm^3). Electrochemical and Immersion test of composite shows no significance reduction in corrosion characteristics.

The third chapter deals with the structure and properties of squeeze infiltrated zirconia grade-aluminosilicate short fiber reinforced aluminum composites. Squeeze infiltration process is successfully adopted to develop Al6061 metal matrix composite reinforced with zirconia grade aluminosilicate fiber using 15 and 20 vol% preforms. Composites microstructure depicts uniform distribution of fiber throughout the matrix with the elimination of preform breakage, porosities, and shrinkage. TEM observation shows the formation of Al_2O_3 at the interface, which controls the chemical interaction between the matrix and the fiber. Infiltrated composite shows enhanced wear resistance behavior compared to that of base alloy, and it improves with the increase in volume fraction of the reinforcement. However, sliding speed overcomes the volume fraction concept in improving the wear resistance of the composite by the quick formation of mechanically mixed layer (MML) at increased sliding speed. The tensile and impact strength of the base alloy is slightly higher than that of the composite due to its ductile nature. Incorporation of fiber in the matrix improves the CTE, hardness, compression and corrosion properties of the composite.

The fourth chapter deals with the structure and properties of modified compocast microsilica reinforced aluminum matrix composite. A356 aluminium alloy reinforced with 7 wt. % microsilica composites were produced by the three different processing routes viz. liquid metal stir casting followed by gravity casting, compocasting followed by squeeze casting and modified compocasting route and their properties were examined. Microstructure of liquid metal stir cast Al MMC shows agglomeration of particles leading to high porosity level in the developed material. Adopting new route of compocasting followed by squeeze casting process prevent the agglomeration sites with uniform distribution and dispersion of the dispersoids in the matrix metal. Modified compocasting process reduces the segregation of particles in the final composites thus enhancing the mechanical, tribological and corrosion properties of the composites. Superior wear-resistance properties were exhibited by the modified compocast composite

compared to the unreinforced squeeze cast alloy and abrasive type wear mechanism was observed in the case of composite. Increasing the sliding speed resulted in the quick evolution of tribolayer and the wear rate of composite gets reduced. Presence of phases like $MgAl_2O_4$ spinel, $NaAlSi_3O_8$ and $KAlSi_3O_8$ has a favorable effect on increased corrosion resistance of the composite. Microsilica particles significantly enhanced the compressive strength of modified compocast composites compared to the unreinforced squeeze cast Al alloy.

The fifth chapter deals with the strengthening of cast aluminum alloy by alumina nanoparticles through interpenetrating interfacial adhesion with the matrix. Incorporation of nanodispersoids tends to strengthen the aluminum alloys along with the fine precipitates and the enhancement in properties depends on effective dispersion, distribution and bonding of nanoparticles in the alloy. The study evaluates the effect of varying weight percentage of alumina nanoparticles in strengthening of cast A356 aluminum alloy by modified compocasting followed by solidification using squeeze casting. Addition of 0.5 wt% Al_2O_3 nanoparticles to cast alloy shows remarkable enhancement in the yield strength from 204 to 323 MPa. They also exhibit higher hardness, UTS, compressive strength, thermal and tribological properties. HRTEM image showed the effective role of interfaces on formation of strong adhesion between the matrix and nanoparticle, where the insertion of Al lattice into the Al_2O_3 crystalline lattice are observed contributing to strengthening of the alloy. The Al_2O_3 nanoparticles and the β'' are involved in the Orowan strengthening of Al nanocomposite. The presence of hard Al_2O_3 nanoparticles and the stronger bonding between particle and alloy constrain the dislocation motion leading to dislocation bowing. The theoretical estimation of Al - 0.5 wt% Al_2O_3 nanocomposite yield strength shows that the contribution of Hall-Petch is predominant followed by Orowan and solid solution strengthening. The major results of the work carried out are summarized in chapter six and the scope for future work is also described.

Chapter 1

Introduction

1.1. Metallic Composites

The inclusion of high strength and modulus ceramic reinforcements to a ductile metal matrix forms the metallic composites having unique combination of properties offering high resilience, high temperature applications compared to polymer and ceramic matrix composites. From tribological perspective, the addition of hard ceramic reinforcements increases the wear resistance of the metallic matrix. Ultimate combination of properties of MMCs depends on a number of factors related to matrix, reinforcement, processing and heat treatment. Samer et al. recommended that the young's modulus, UTS and maximum elongation of the composite depend on the particle size of the reinforcements and obtained superior properties in composites containing nanoparticles (~70nm) when compared to composites containing micrometer range particles in Al/TiC system.[1] Formation of ductile intermetallic phases during solidification and potential of the material to be strengthened by precipitation are considered as distinct advantages in metallic composites, which empower the mechanical properties of the composite.

The properties of the MMCs are also determined by the type and morphology of reinforcement incorporated in the molten metal matrix like particulates, whiskers, continuous fiber, discontinuous fiber, etc. Aluminum, magnesium and titanium alloys are the most commonly used matrix materials for MMC processing due to their low specific gravity and those find wide range of applications in automotive and aerospace sectors. In metallic composites the thermal stress caused due to thermal mismatch between matrix and reinforcement can be reduced from the matrix plastic deformation phenomena.[2] Nowadays, fabrication of MMC focuses on nanocomposites where the matrix alloys are coupled with nanoparticle reinforcements like carbon nanotubes, SiO_2, Y_2O_3, SiC, Al_2O_3, graphene, etc.[3,4]

1.2. Infiltration Process

Liquid metal infiltration of ceramic preform is apparently the best suited fabrication method to produce metal matrix composite components with variety of complex shapes having high volume fraction of reinforcement. Infiltration is a liquid state fabrication method, in which a porous preform (reinforcement) such as ceramic particles, fibers, woven etc are impregnated in a molten matrix metal, which fills the pores between the dispersed phase inclusions. Synthesis of porous ceramic preform with sufficient mechanical strength, uniform pore distribution, pore size and porosity level is one of the crucial steps involved in infiltration processing of composites.[5,6] The captivating properties of these ceramic foams such as thermal resistance, low density, controlled permeability, low thermal conductivity, high surface area and high structural uniformity make them potential candidates for multiple engineering applications.[7,8] Some of the important fabrication methods for porous ceramic foams are polymer replica techniques, gel casting, direct foaming of suspensions and using pore forming agents (PFA).[9-15] Al, Mg and Cu based alloys have been successfully used as matrices to contrive MMCs through liquid infiltration, as they can be easily melted and handled in the liquid state. Difference from one infiltration method to another is based on the technique that is used to drive the molten metal to enter the preform. The literature review below gives the state-of-art knowledge on the various infiltration processing and compocasting methods of MMCs and their characteristics.

1.3. Preform Materials

The porous ceramic preforms contemplate as scaffolding, are considered to be the base of the composite materials processed by infiltration technique. The properties of the composite depend upon the strength, distribution, type and structure of the interconnected pores in the porous body to facilitate the liquid metal infiltration. Thus, the process parameters have to be optimized for synthesizing quality composites. Assorted type of fundamental works by varying the processing, pore former (NaCl, PEG, carbon fiber, tylose), reinforcement (Al_2O_3, SiC, Si_3N_4) and binding agent (aluminum, poly vinyl alcohol) have been carried out by several investigators. However, the depth and speed of the

infiltration is influenced by the coefficient of permeability in the preform, which alters with the volume fraction of reinforcement. Yamanaka et al.[16] concluded that the temperature, wettability and the volume fraction of reinforcement in the preform regulate the coefficient of permeability in the system. An increase in the volume fraction of reinforcement reduces the gaps and open porosity in the porous preform, which reduces the ability of the liquid molten metal to get penetrated. Based on the experimental studies it is found that the permeability k of a porous preform is directly proportional to the square of the mean diameter of the reinforcement.[17]

$$k = aD^2 \qquad (1)$$

where a is the constant which depends on the reinforcement morphology. Dobrzanski et al.[18] fabricated Al_2O_3 based preforms using carbon fiber as the pore forming agent and observed the increase of permeability with an increase in pore former content.

The strength of the porous preform is negatively affected by increasing the pore former content because it increases the porosity level and by randomness in distribution of pores. In accordance with the above factor, non uniform distribution of pores in the preform will create difference in the collateral wall thickness and cause inability to withstand localized stress concentration resulting in deformation.[19] The grain size of the particles has great impact on the porosity hike and strength of the preform. Increase in the grain size is inversely proportional to the mechanical strength of the preform owing to low diffusion on grain boundaries.[20] The morphology of the pores in the preform depends on the kind and type of pore former used in the system. Raddatz et al.[21] created hollow channels in the ceramic preform by integrating cylindrical shaped polymer fibers as pore forming agent. The binding agent in the preform plays a dual role, which imparts strength to the green body as well as the sintered porous structure by bridging between the particles. Moreover, the selected binder should not pave way for the interfacial reactions with the reinforcement and molten metallic matrix during infiltration. Mechanical strength of the porous preform basically depends on the kind and the type of binding agent used for fabrication; metallic binders can be used for partial coating on reinforcements to improve wettability.

1.4. Processing Techniques

The liquid infiltration processes can be broadly classified into two categories: a) spontaneous infiltration and b) forced infiltration (Figure 1.1). When capillary action of the reinforcement phase acts as a driving force for infiltration, the category of processes is termed as spontaneous infiltration. In forced infiltration an external pressure such as gaseous, mechanical, squeeze, electromagnetic etc. are applied to the liquid matrix phase which accelerates the infiltration of molten metal through the preforms. The processing details are briefly discussed here.

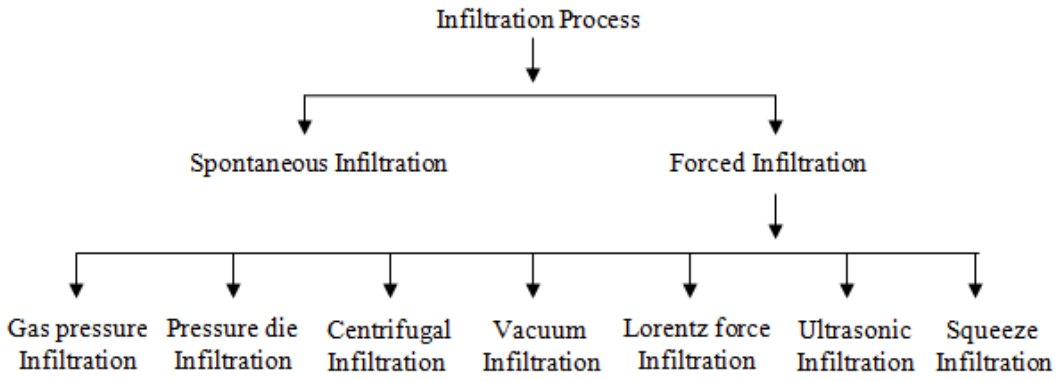

Figure 1.1. Classification of infiltration process for the fabrication of metal matrix composites.

1.4.1. Spontaneous / Pressure-less Infiltration

In spontaneous infiltration, the molten liquid metal invades into the voids of the porous body without the application of any external forces (Figure 1.2).[22-27] This can be accomplished with the help of controlled temperature and gas atmosphere ensuring good wetting conditions are maintained for self-permeation.[28] Numerous studies in pressure-less infiltration have been carried out using Al–Si, Al–Zn, Al–Mg alloys into porous SiC preform and however, there are some challenges that should be tackled to develop spontaneous infiltration a very promising and industrially adaptable method. Conventional drawback of the infiltration synthesis method is the poor wettability between the matrix and the reinforcement resulting from the formation of oxide layer on the melt surface.[29] Poor wettability negatively influences the infiltration process by slowing down the infiltration process leading to undesirable reactions at the interface resulting in

the formation of intermetallics such as Al_4C_3 and Al_3SiC_4 in aluminum -SiC based systems.[30] Many researchers had investigated the effect of activator content in pressure-less infiltration of metal matrix composites.[31] Dwell time and activator primarily controls the rate of infiltration. More the activation more will be the infiltration depth. The amount of porous areas and residual porosity also govern the infiltration quality but this can be reduced by increasing the activator content.[32] The wettability of preform by liquid molten metal is an essential parameter for processing composites by pressure-less infiltration technique. Wittig et al. suggest that the addition of titanium in the steel matrix composites reinforced with ZrO_2 particles helps in improving the wetting behavior of liquid metal to ceramic preforms.[33] Contreras et al. successfully infiltrated liquid magnesium into TiC preforms by pressure-less technique.[34] Previous studies suggest that the wettability can be improved by adding 3 - 4.7 mass percent of magnesium to the melt and also by using 100% nitrogen atmosphere in the furnace.

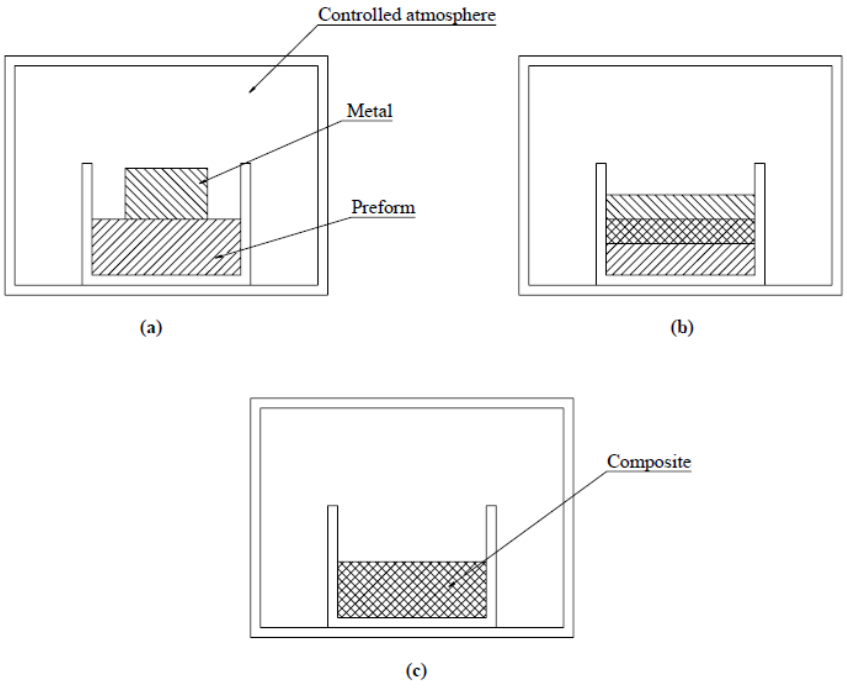

Figure 1.2. Schematic diagrams showing the working principle of spontaneous infiltration process: (a) infiltration takes place at controlled atmosphere, (b) progressiveness of infiltration, and (c) final composite.

Magnesium is known to be a powerful surfactant that accumulates oxygen from the surface of the melt and forms $MgAl_2O_4$ spinel at the interface. The

reaction results in attenuating the oxide layer and act as driving force to promote wetting.[35] Schiroky et al. reported the PRIMEX™ pressure-less infiltration process of SiC and alumina infiltration by Al-Mg alloy. During the pressure-less infiltration process, the Mg in the Al-Mg alloy at 800^{o}C vaporizes and reacts with the nitrogen gas used as atmosphere for the process to form Mg_3N_2 and deposits on the reinforcement surface. During aluminum alloy infiltration, Al reacts with Mg_3N_2 to form AlN and Mg which promotes better wetting with the reinforcement.[36] Even though, the primary motive for the use of nitrogen during infiltration is the prevention of Al alloy oxidation it aids in reinforcement wetting also. The effective chemical reaction between the constituents in the molten metal and trapped gases in the porous preform causes pressure drop in the preform and thereby improves the ease of molten metal penetration. Nake et al. study the spontaneous infiltration mechanism of Al-Si-Mg alloy on SiC preform with the addition of Fe_2O_3 in the preform as additives to improve wettability. The pressure reduction in the preform improves the suction of the molten metal which helps to break the oxide film present at the interface between the metal and the preform (Figure 1.3) formed due to the reaction between the molten metal and the adsorbed moisture at the infiltration front.[37]

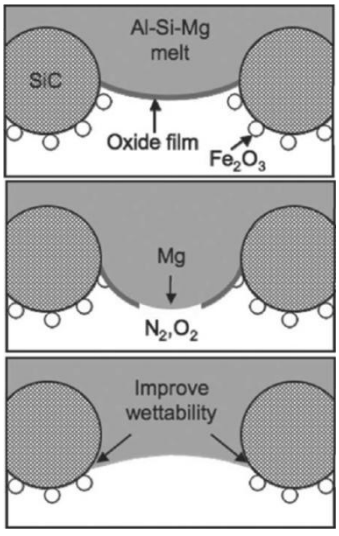

Figure 1.3. Schematic diagram showing the penetration of molten metal into the SiC preform by breaking the oxide film at the interface during spontaneous infiltration. [37]

Generally, the wetting system of solid by a liquid is stipulated by contact angle (Figure 1.4) and the contact angle, θ, at the solid, liquid and gas/vapour is related by the Young-Dupre's equation.[38]

$$\gamma_{lv}\cos\theta = \gamma_{sv} - \gamma_{sl}\,, \qquad (2)$$

where γ_{lv}, γ_{sv} and γ_{sl} are the liquid metal surface tension, surface energies of solid/vapour and solid/liquid respectively. The molten metal will wet the solid preform, if $\gamma_{sv} > \gamma_{sl}$, that is, when $\theta < 90^{o}$. Similarly, if the above process is reverse in the case of nonwetting system a minimum pressure (threshold pressure) is to be exerted for infiltration.

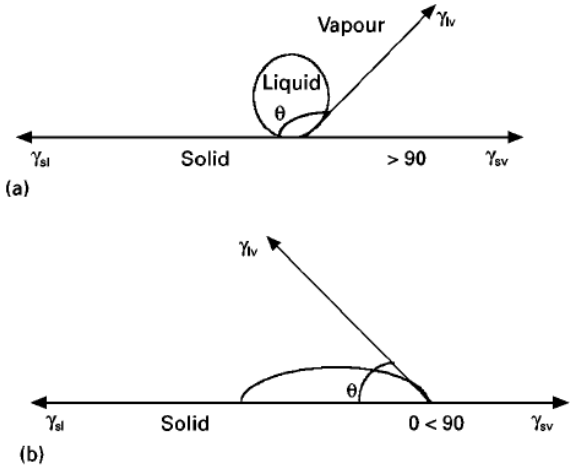

Figure 1.4. Schematic illustrations showing the contact angle in a (a) nonwetting system and (b) wetting system. [38]

As stated by Darcy's law, the infiltration rate of molten metal into porous preform is[39]

$$\nu = \frac{k}{\mu}\frac{dp}{dx}, \qquad (3)$$

where ν is the flow rate, k is the permeability which depends on the shape and sizes of the interconnected channels through which the molten metal flows, μ is the viscosity of the molten metal, p is the pressure (capillary pressure for spontaneous) correlated with the size and shape of the pores that are in contact with the molten metal, and x is the infiltration distance. Surface modification of reinforcements is also an effective method to circumvent interfacial reactions and enhance wetting. Treatments include metallic coatings like Cu, Ni, Zn, Ag, Si etc

and high-temperature treatment, for example, of SiC leads to the formation of very stable surface layer of amorphous silica.[40, 41] It has also been reported that the coating of K_2ZrF_6, ZrO_2, and Na_2O in the fillers helps pressure-less infiltration.[42-44] Continual investment and further process optimization can ensure spontaneous infiltration techniques to remain an attractive technique to synthesize composites in the time to come.

1.4.2. Forced Infiltration

The infiltration process in which the aid of an external pressure or mechanical force governs the infiltration of liquid metal into the porous reinforcement is called forced infiltration. Poor wetting between the molten metal and porous structure can be overcome by endowing mechanical energy to force the metal into the porous preform. There are various types of forced infiltration methods and these are described below.

1.4.2.1. Gas Pressure Infiltration

An infiltration process in which pressurized gas (Figure 1.5) is used as driving force for the penetration of molten metal into the porous body. Gas infiltration process is normally carried out in combination with vacuum at the other end of the preform to get rid of entrapped air to facilitate easy penetration at lower gas pressures.[45] Qi et al. suggest that the anti-pressure of gas in the porous preform significantly slows down the rate of infiltration, which increases with increase in infiltration depth and the temperature. As a result high pressure is needed for complete infiltration of molten metal, hence, anti-pressure of gases is to be considered during the analysis of threshold pressure. With the ideal gas equation PV = nRT, the anti pressure of gas can be expressed as[46]

$$p_g(z) = \frac{p_0 T_z L}{T_0\,[L-z]}, \qquad (4)$$

where p_0 is the pressure of gas at initial time, T_0 is the initial time temperature, L is the preform total length, and T_z is the temperature of the gas when the infiltration attains a height z. Enhance in the infiltration temperature and pressure during gas pressure infiltration process improves the relative density of the component, which shows an effect on the mechanical properties of the final composite.[47] Joseph Blucher concluded that the fabrication of MMC by hydrostatic gas pressure infiltration holds certain advantages like low acquisition cost, high operational

flexibility for research purposes etc.[48] Al alloys reinforced with Ni and Cu coated chopped, unidirectional carbon fibers and porous graphite preforms were successfully fabricated using gas pressure infiltration technique.[49-51] Non coated fibers can also be used in gas pressure infiltration technique due to the short contact time of the matrix with the reinforcement. Drawback of the gas infiltration technique is the added cost of pressurized gas which usually is an inert gas.

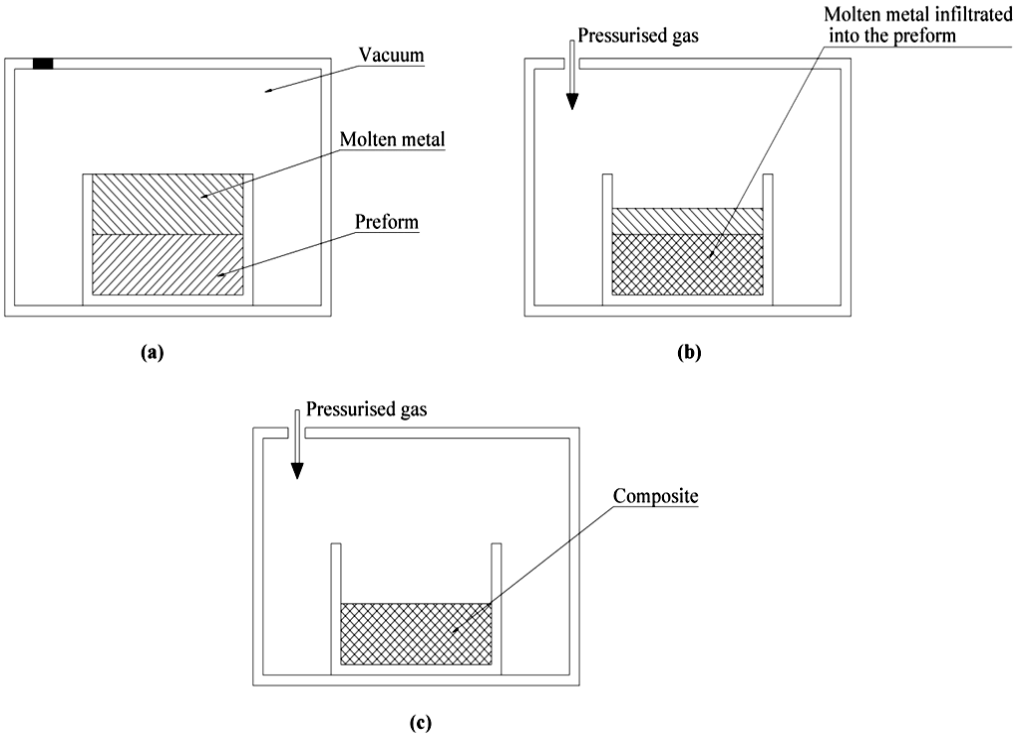

Figure 1.5. Schematic illustrations of gas pressure infiltration process for the fabrication of MMCs: (a) infiltration process carried out with vacuum to remove the entrapped air in the preform to facilitate easy molten metal penetration, (b) applying pressurized gas as a driving force for metal infiltration, and (c) final composite.

1.4.2.2. Pressure Die Infiltration

Pressure die infiltration process involves placing a porous preform inside a solid die and applying pressure with the help of a movable piston to allow penetration of liquid metal in the porous preform (Figure 1.6 (a and b)). Process parameters that are optimized include speed, die temperature, and pressure of the piston. Main advantages of this process are low cost and ability to fabricate components of high complexity and precision. The deformation of preform due to

the pressure of the molten metal before and during infiltration will be high for pressure die casting compared to squeeze casting owing to high compression rate of preform during infiltration. Rasmussen et al. suggest that by increasing the volume fraction of the reinforcement leads to stronger preform which can prevent preform deformation, but at the same time it will prohibit the ease of infiltration.[52]

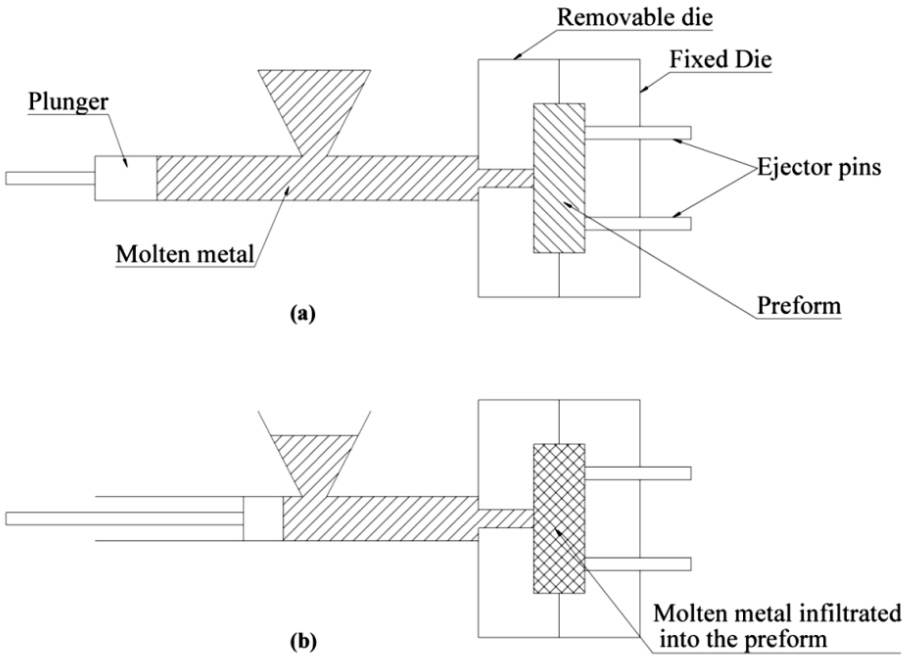

Figure 1.6. Schematic diagrams of pressure die infiltration process for the fabrication of MMCs: (a) before applying pressure to molten metal using plunger and (b) after applying pressure to molten metal using plunger to form the composite.

1.4.2.3. Centrifugal Infiltration

In centrifugal infiltration process, rotational / centrifugal force is used to infiltrate porous preform with liquid molten metal. During the fabrication of composites porous reinforcement material is positioned inside a mold (at the end) having an elongated runner, which was filled with molten metal. Large rotational velocities of the runner initiate centrifugal force with required drive for infiltration to overcome the threshold pressure for melt penetration and viscous forces of the molten metal to flow in the preform. The molten metal pressure exerted on the porous preform during centrifugal force is given by[53]

$$p_c = \frac{1}{2}\rho\omega^2(L_2^2 - L_1^2), \qquad (5)$$

Where ρ is the density of molten metal, $= \frac{2\pi\Omega}{60}$, Ω is the rotational speed in rpm, and L_2 and L_1 are the outer and the inner molten metal's level from the rotation axis. To develop the near net shape components and to avoid the material wastage typical centrifugal infiltration technique is adopted (Figure 1.7a).

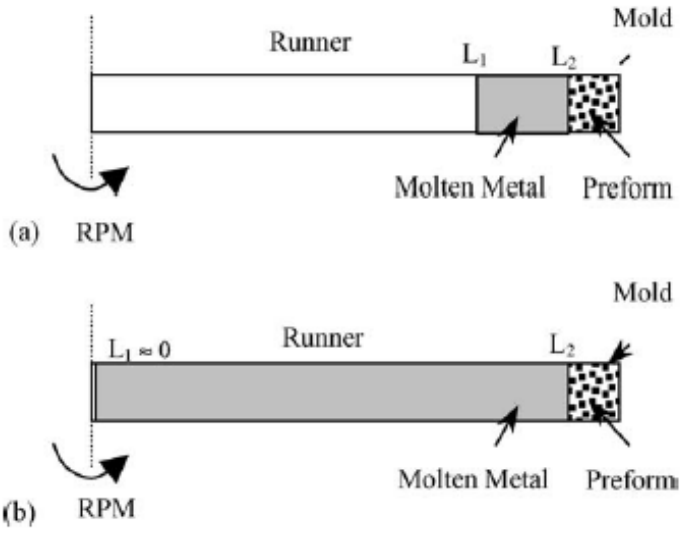

Figure 1.7. Schematic diagrams of (a) a traditional centrifugal infiltration process and (b) a high pressure centrifugal infiltration process. [53]

In order to achieve high pressure centrifugal infiltration, a slight modification within the same centrifugal system used for conventional process is made by extending the inner molten metal level *L_1* from the rotational axis (Figure 1.7b). In such cases liquid metal pressure acting on the preform will be given by

$$p_c = \frac{1}{2}\rho\omega^2 L_2^2 \qquad (6)$$

Surface-coated and noncoated carbon short fiber preforms were successfully infiltrated by centrifugal process and the optimum preform preheating temperature for non coated fiber for the smooth penetration of molten metal is above 873 K (600 ^oC), whereas for nickel-coated carbon fiber preform is 673 K (400 ^oC).[54] In addition, surface pressure of the porous preform is reduced perceptibly as the molten metal starts to infiltrate and once when the metal gets penetrated into the preform the pressure of the infiltrated region falls under the threshold pressure. The adhesion between the molten metal and the

reinforcement will not get separated due to the fall of pressure in the infiltrated zone below the threshold pressure. However, to achieve a complete infiltration of molten metal throughout the porous preform, the pressure on the infiltration front should exceed the threshold pressure.[55]

1.4.2.4. Lorentz Force Infiltration

Lorentz force infiltration process is a novel infiltration process in which electromagnetic force is used to propel the molten metal into the ceramic preforms. During the process, the preform gets immersed in a liquid molten metal which is subjected to a high-frequency magnetic pulse. Simultaneously, eddy current persuaded in the liquid metal gets to interact with the magnetic pulse and develop a Lorentz body force in the liquid molten metal causing the liquid metal to enter into the ceramic preform at a high speed. Richard M. Andrews and Andreas Mortensen had successfully fabricated void-free aluminum/Al_2O_3 fiber composite by Lorentz force infiltration technique. They suggested that the infiltration depth depends on the nature and number of discharges.[56]

1.4.2.5. Ultrasonic Infiltration

In ultrasonic infiltration process, pressure waves generated by the ultrasonic vibration assists in the penetration of the molten matrix material in the ceramic preform. When ultrasonic vibration is actuated through a horn in the liquid molten metal, acoustic cavitations (bubbles) are originated. The air entrapped in the porous preform and the dissolved gas in the molten metal can become the cavitations nuclei. When a bubble collapses shock wave originates close to the molten metal resulting in infiltration process (Figure 1.8).[57, 58]

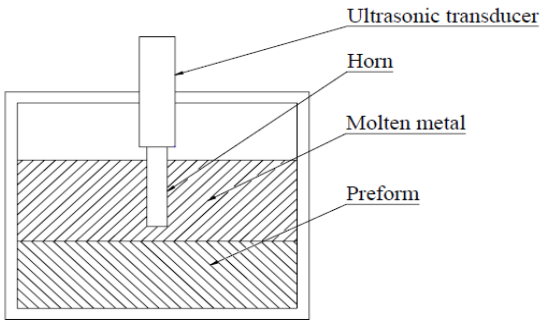

(a)

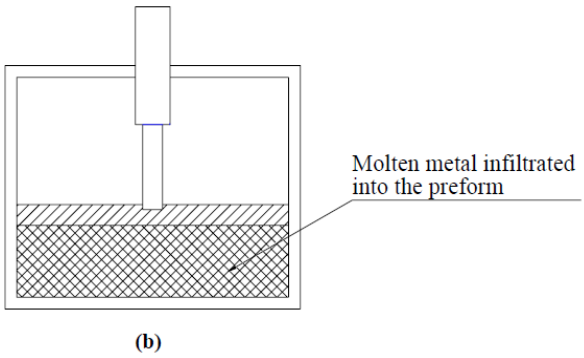

Figure 1.8. Schematic diagrams of ultrasonic infiltration process for the fabrication of MMCs: (a) before ultrasonic vibration and (b) after ultrasonic vibration using transducer as a driving force to penetrate molten metal into the ceramic preform.

The important process parameters considered for the ultrasonic infiltration is ultrasonic power, hole in the horn, and fabrication speed. Increase in the diameter of the hole in the horn decreases the infiltration ratio due to the depletion in the formation of acoustic cavitations and studies show that optimum diameter of the hole is 5 mm. Studies have shown that the infiltration can be made more effective by the addition of 2.4 mass % magnesium to liquid Al metal coupled with an ultrasonic power of 200 W. Similarly, infiltration ratio decreases with increase in the fabrication speed, but at the same time addition of magnesium in the molten metal for wettability helps to increase the fabrication speed with better infiltration ratio.[59,60] Gen sasaki et al. studied the effect of ultrasonic vibration on the wettability during infiltration using contact angle technique of polyester resin on glass substrate with and without ultrasonic vibration (Figure 1.9). The system which undergoes ultrasonic vibration shows reduction in contact angle due to heavy vibration acceleration and thereby improving wettability.[61]

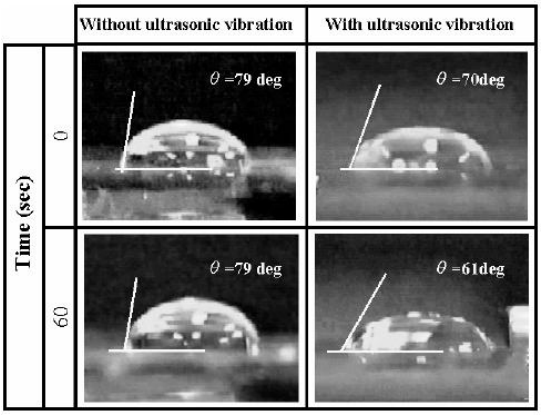

Figure 1.9. Effect of ultrasonic vibration on contact angle. [61]

1.4.2.6. Vacuum Infiltration

Vacuum infiltration involves a negative pressure infiltration in which matrix metal gets penetrated into the evacuated preform due to the application of suction pressure (Figure 1.10). Process parameters like infiltration temperature, infiltration time and applied vacuum (~300-500 mmHg) plays a crucial role in this process.[62] Infiltration rate gets increased with increasing the molten metal temperature and by applying coating on the reinforcement, thereby reducing the infiltration incubation period to avoid brittle interfacial reactions.[63] Low solidification rate of the final component during processing can be stepped up as one of the disadvantage of vacuum infiltration which enhances the grain growth of the matrix metal and interfacial reaction between matrix and the reinforcement.[64] To avoid the liquid molten metal getting into the vacuum pump by chance during infiltration process one portion of the connection pipe is filled with metal chips, so that the molten metal entering into the pipe gets solidified in that particular area without damaging the vacuum pump. Studies have shown that Al and Mg based composite materials with more than 50 vol. % reinforcement can be successfully fabricated using vacuum infiltration technique.[65]

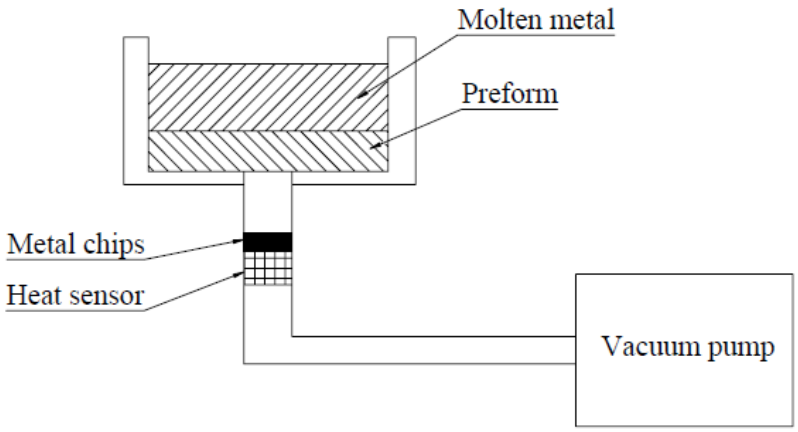

Figure 1.10. Schematic diagram showing the working principle of vacuum infiltration process for the fabrication of MMCs.

1.4.2.7. Squeeze Infiltration

Squeeze infiltration is one of the widely used methods for the production of near net shape metal matrix composites with close control over shape, volume fraction, chemistry and distribution of reinforcement.[66-72] This process offers

advantages over other conventional methods for fabricating composite components which are difficult to be machined. The process involves the formation of porous preform as the reinforcement and its infiltration with the molten matrix material under pressure (Figure 1.11) typically in the range of 50-100 MPa.[22]

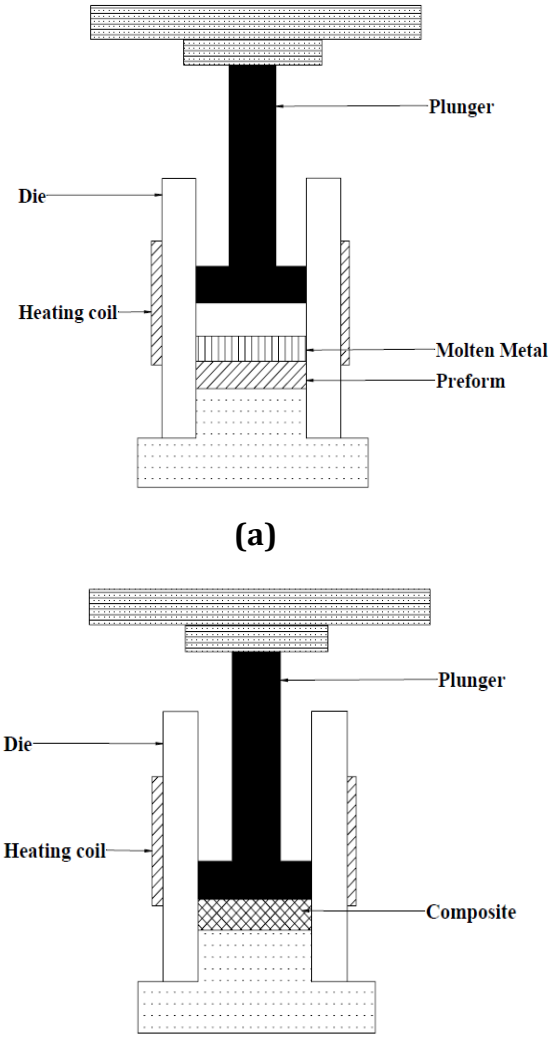

Figure 1.11. Schematic diagrams of squeeze infiltration process for the fabrication of MMCs: (a) before the application of squeeze pressure and (b) after the application of squeeze pressure as a driving force to infiltrate molten metal into the preform.

The appropriate magnitude of applied pressure ensures eradication of porosities, refined microstructure, enhanced processing speed, and termination of chemical reactions. For the development of quality composites processing parameters of

squeeze infiltration have to be optimized. In light of the above, the application of higher squeeze pressure accelerates the infiltration process but leads to crumpling or cracking of the porous preform.

Numerous studies regarding infiltration pressure have been done by many researchers. Guan et al.[73] investigated the threshold pressure and infiltration behavior of liquid metal into the porous preform. The infiltration rate can be improved effectively by raising infiltration pressure, but the effect will gradually diminish with the advancement in time. Increase in infiltration pressure minimizes porosity, reduces the heat loss and hinders the solidification of liquid metal front effectively. According to Darcy's law, the expression for the square of infiltration height as a function of infiltration time and difference in infiltration pressure of the liquid metal is[74]

$$h^2 = \frac{2kt}{\mu(1-V_s)}(p - p_0), \qquad (7)$$

where p is the applied pressure, p_0 is the threshold pressure for the initiation of infiltration, infiltration time t, μ is the viscosity of molten metal, v_s is the volume fraction of solid, and k is the permeability of the porous solid. The threshold pressure p_0 for infiltration can be obtained as[75]

$$p_0 = 6\lambda\gamma_{lv}\cos\theta\,\frac{V_s}{(1-V_s)D}, \qquad (8)$$

Where λ is a geometrical factor that represents the deviations from particle/fiber shape, surface roughness, and actual particle/fiber size distribution. The basic governing phenomenon for the infiltration of metals, ceramics, and polymers into the porous preforms are fluid flow, capillarity, and the behaviour of preform deformation, which in turn are decided by preform permeability, volume fraction of reinforcement, preform stress-strain behaviour, pressure-dependant saturation of melt in the porous preform, and the melt viscosity.

The strength and stability of preform during infiltration depends on the mode of fabrication of preform, type of binder and the reinforcement used. Reinforcements having lubrication nature enhance the tendency of sliding over one another thereby increasing the chance for deformation of the preform. Similarly during the fabrication of layered preform, equality in the stacked layers reduces the preform compliance.[76] A new technique for the direct measurement

of capillary force is by drainage curve method through which the corresponding volume fraction of the molten metal in the porous preform as a function of applied pressure is plotted and the method adopted is also suitable for measuring contact angle and infiltration kinetics.[77] Higher temperatures of liquid metal, preform, and die initiate unwanted chemical reactions at liquid metal/fiber interface and prolong the solidification time.[78] Delaying the application of pressure after pouring the molten metal above preform in the mold causes the formation of oxide layer around the preform, which decelerates the infiltration process.[79] Oxide inclusions, porosity and voids, blistering, cold laps and cold shuts, and sticking of casting with the die surface are the major casting defects that occur in the squeeze cast process.[80] Alhashmy et al. processed carbon fiber reinforced aluminum matrix composite by squeeze infiltration technique.[81] They suggested that the inclusions can be avoided using filters and turbulence must also be completely avoided while pouring. Porosity can be avoided by increasing the squeeze pressure. The main cause for blistering is the entrapment of gas from the melt and can be avoided by reducing the pouring temperature and degassing the melt. Die temperature and metal pouring temperature can be increased to avoid cold laps and better lubrication or die coating to avoid sticking of casting with the die surface.

1.5. Squeeze Infiltration of Aluminum MMC and FGM

Squeeze infiltration processing setup for Al MMC has been designed and developed at CSIR-NIIST. During squeeze infiltration parameters like the design of die, the preform preheating temperature, mold and molten metal temperature, and squeeze pressure plays a vital role for the depth of penetration of liquid metal throughout the porous preform. Some of the highlights of the work carried out by the authors are presented here. Silicon carbide porous preform was made by salt leach out technique and aluminum powder as the binder. Porous preform was placed in a die and infiltrated with liquid 6061 alloy. Macrograph of the infiltrated specimen (Al 6061-50vol% SiC~42 μm) and porous preform used for infiltration process are shown in Figure 1.12 (a). It can be rendered from the representation that the components fabricated can also act as a selectively reinforced composite with the eradication of cold shuts, blistering and other casting defects.

Microstructure in Figure 1.12 (b) shows the uniform distribution of SiC particles in the matrix resulted due to the good quality of preform used and the effective penetration of the liquid metal even in minute voids in the preform.[82] These infiltrated composites find potential application for electronic packaging systems and armor materials.

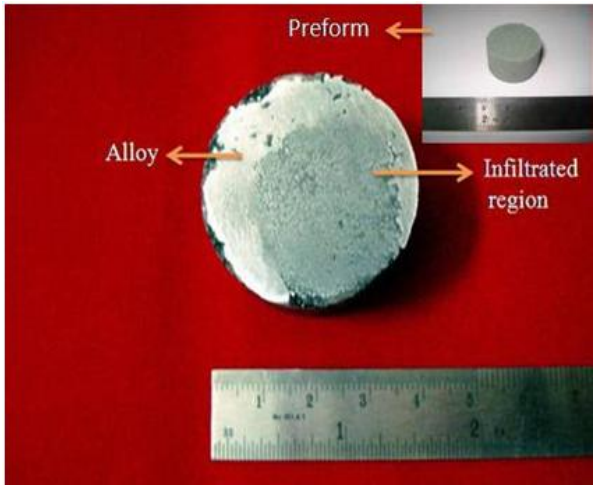

(a)

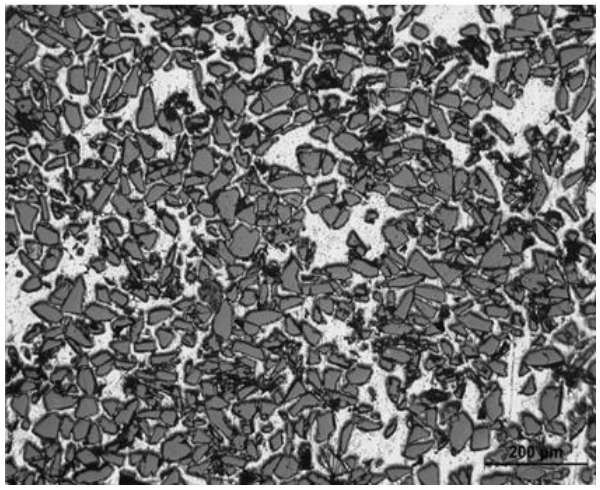

(b)

Figure 1.12. Images of (a) macrograph of infiltrated specimen and porous preform and (b) microstructure of aluminum 6061–50vol% SiC infiltrated composite. [82]

The emerging new generation advanced composites are the functionally graded materials in which properties vary along a specified direction to provide functional performance for the components. The variation in properties is effected through the change in microstructure and/or composition in the required direction. The ability of these tailored materials to replace sharp interfaces

manifests in composite materials by gradient interfaces thereby providing smooth transition from ductile matrix metal to hard ceramic phase is an added advantage.[83] The Squeeze infiltration is one of the effective fabrication methods for synthesizing functionally graded materials. Process involves the framing of graded porous ceramic preform with adequate interconnecting porosity and its infiltration with the molten metal under pressure. The gradation in preforms can be obtained by various techniques like the usage of graded particle sizes for green body compaction which leads to the formation of porosity gradient during sintering and also by the use of graded pore forming agents and their volume fractions which create porosity gradient during the burn out of fugitive pore former while sintering.[84] Figure 1.13 shows the macrograph and microstructure of functionally graded Al-SiC composite developed by squeeze infiltration method in CSIR-NIIST, India.

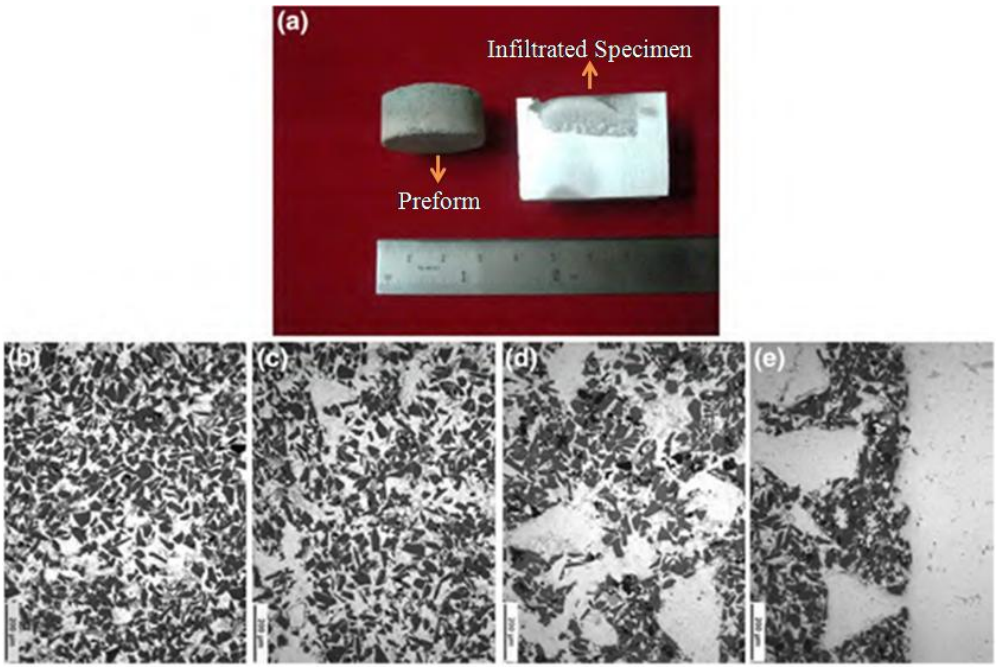

Figure 1.13. Images of (a) macrograph of graded preform and aluminum–SiC infiltrated composite specimen. Microstructures of functionally graded Al (6061)–SiCp composite produced by squeeze infiltration: (b) starting from outer layer, (c) middle layer, (d) inner layer in 12mm thick casting, and (e) interface region. [85]

Macrograph depicts (Figure 1.13a) the graded sintered porous preform (three layers) and its infiltration with Al 6061 molten metal. Microstructure description

stipulates the graded distribution of SiC Particles in Al 6061 matrix, starting from outer layer (Figure 1.13b) having high volume fraction of reinforcement (low porosity) to middle layer (Figure 1.13c) having medium volume fraction of reinforcement (medium porosity) and ends in inner layer (Figure 1.13d) having low volume fraction of reinforcement (high porosity) in 12mm thick casting. Figure 1.13e shows the interface region between the aluminum 6061 molten metal and the first layer of the preform (from inner side).[85]

1.6. Characteristics of Infiltrated Composites

1.6.1. Structural Characteristics

Infiltration processed composites have more isotropic microstructure compared to other conventional methods due to the use of judiciously designed porous preform as reinforcement. In preform, particles/fibers are tightly packed with binders ensuring regular uniform distribution of pores (pores are artificially created). The aptness to develop complex shaped components with high volume fraction of reinforcement is an added advantage to the infiltration process compared to other systems. Wetting must be ensured to procure good adhesion between the molten matrix material and ceramic reinforcement especially for spontaneous infiltration processes. Interfacial reactions between the metal matrix and the ceramic reinforcement highly depend on the processing methodology. Preform and die preheat temperature, infiltration pressure, melt pouring temperature, and infiltration time are the major process parameters that govern the infiltration quality. Preform and die preheat temperatures circumvent the sudden solidification of the melt due to lower temperature gradient. More the infiltration time and melt temperature more will be the formation of brittle and undesirable phases like Al_4C_3 (Figure 1.14).

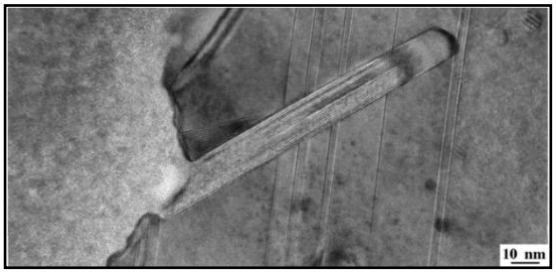

Figure 1.14. HRTEM images of Al_4C_3 grains as lath type morphology. [99]

Studies have established that when these kinds of components are used in service, carbide phases present in it have the tendency to react with atmospheric moisture to form CH_4 (flammable gas) resulting in porosity and failure of the composite.[86] It may be noted that limited interfacial reactions are desirable and improve the wettability between the matrix and reinforcement thereby enhancing the mechanical properties of the composite.[87–89] During heterogeneous bonding, process temperature and holding time have an impact on the microstructure of the composites prepared by pressure-less infiltration technique. The thickness of the interfacial reaction layer is dominated by the infiltration bonding temperature than the holding time (Figure 1.15). However, decrease in the holding time cause pores at the interface and this pores can be limited by increasing the holding time.[90]

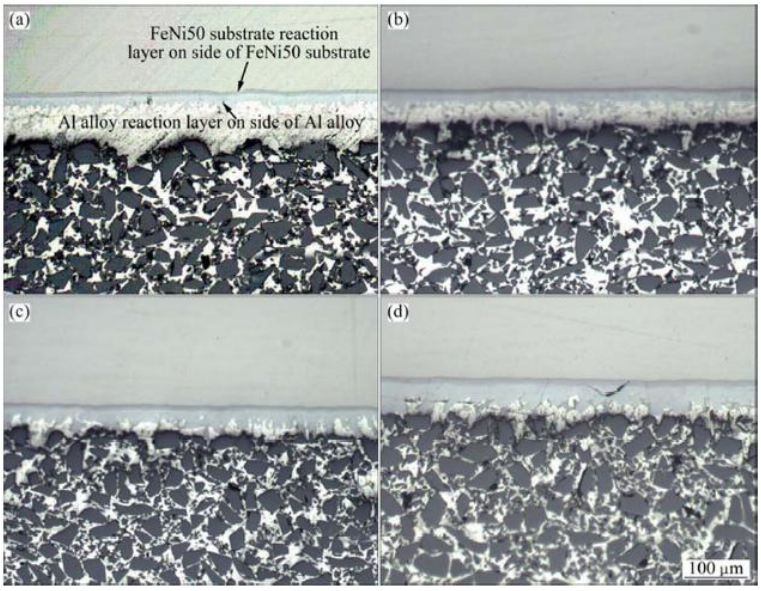

Figure 1.15. Effect of infiltration temperature on the thickness of the interfacial reaction layer: (a) 943 K (670 °C), (b) 963 K (690 °C), (c) 983 K (710 °C) and (d) 1003 K (730 °C). [90]

Matrix alloying is the most appropriate method to enhance the interface bonding strength for continuous carbon fiber reinforced magnesium matrix composites.[91] The alloying elements are prone to segregation at the interface during the solidification of composites in the form of nanoscale compounds by reacting with matrix or reinforcement. But high quantity of alloying elements may slow down the infiltration rate by reducing the viscosity of the liquid molten

metal.[92] Nagendra et al. investigated the microstructures and properties of Al_2O_3/Al–AlN composites by pressure-less infiltration of Al alloys.[93] Al_2O_3 was chosen as the preform and liquid aluminum in which AlN is precipitated by nitridation process was selected as the matrix material. They concluded that the processing temperature has a great impact on microstructures. At higher temperature above 1273 K (1000 ^oC) porosity was observed in the matrix. The presence of AlN at the interface significantly improves the hardness and elastic moduli of the composite. In the study done by Zhang et al. it was reported that in Cu/SiC composite, the increased infiltration temperature (1698 K (1425 °C)) resulted in the melting of sharp edges of SiC particles (Figure 1.16) in the preform. The degradation of SiC leads to the releasing of Si and C (black layer around the particle) into the matrix metal.[94]

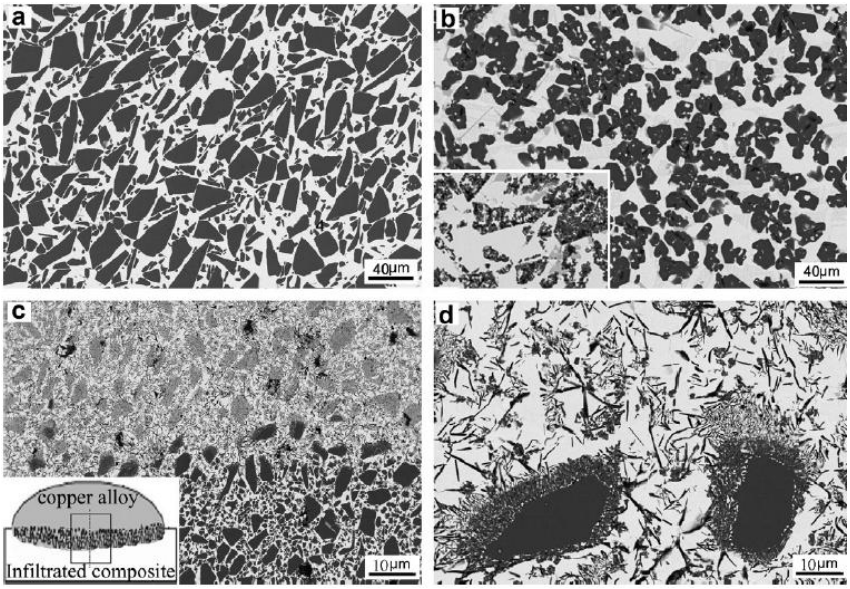

Figure 1.16. Microstructure of SiCp/Cu composite: (a) infiltrated at 1698 K (1425 ^oC) for 1 h, (b) infiltrated at 1723 K (1450 ^oC) for 2 h, (c) cross section of the interface region, and (d) higher magnification of the region (c) in which SiC particles gets melted at an infiltration temperature of 1723 K (1450 ^oC). [94]

Warrier et al. prepared Ti MMC by rapid infiltration process where the continuous graphite fibers are kept inside a graphite crucible and a calculated quantity of the matrix was placed on top of the fibers. Pressure-less infiltration was carried out at temperatures about 50 °C above the liquidus of the matrix in about 1-2 min. Five different alloys ranging from 40 to 85 wt % Ti showed that the thickness of

reaction zone at the matrix/reinforcement interface was found to be increased with increase in the titanium content in the matrix alloy.[95] Matrix-preform interfacial reactions can also be suppressed by nickel coating, SiC coating, copper coating, pyro carbon coating etc on the preform material especially in the case of carbon fiber preform.[96-101] Dobrzanski et al. concluded that the particle reinforced composite materials synthesized by infiltration process exhibit higher crack resistance along grain boundaries than fiber. The above phenomenon was attributed to the certainty with which each and every particle will act as an obstacle to crack growth. While considering fiber reinforced composites, propagation of crack will occur over the long distance due to the length of the fiber without any resistance.[102]

1.6.2. Physical Properties

By decreasing the reinforcement particle size and increasing the volume fraction, low coefficient of thermal expansion composite can be fabricated especially for electronic packaging and structural applications. Etter et al. synthesized graphite preform based composites with pure aluminum and AlSi7Mg alloy as matrix by pressure infiltration technique and the composites were thermally cycled between 333 K (60 ^{o}C) and 573 K (300 ^{o}C) up to 1020 cycles to investigate their response to thermal damage. The electrical conductivity of the composites was not affected by thermal cycling, however, it reduced the CTE of the composites because of stress relaxation processes. Before thermal cycling, composite with AlSi7Mg alloy as matrix shows higher CTE than the one having pure aluminum as matrix due to the precipitation reaction of Mg_2Si phase at 473 K (200 ^{o}C). During thermal cycling Mg_2Si particles were precipitated inside the metal phase of the AlSi7Mg based composites and thereby show similar CTE values to that of pure aluminum based composites during the CTE measurement after thermal cycling.[103] Ren et al.[104] investigated the effect of adding Mg and Si to aluminum matrix on the physical properties of the SiCp/Al composites processed by pressure-less infiltration. Si content above 12 wt% retards the interfacial reactions between alloy and SiC by precipitating at the interface (Figure 1.17). Formation of reaction product Al_4C_3 needles at the interface between the Al-SiC is observed in Figure 1.17a without the addition of Si. Increase in the silicon content eliminates the interfacial reaction products thereby providing a smooth interface

between the Al-SiC composites (Figure 1.17b-d). Also the addition of Si improves the thermal conductivity and reduces the CTE of the composites. The thermal and mechanical properties of the composites are affected by porosities, where poor wettability between the matrix and reinforcement can be one of the reasons behind it.[105] The addition of Si in the liquid metal helps in reducing the viscosity of the melt thereby improves the wettability between the matrix and the reinforcement, results in smooth penetration during infiltration.[106] Si content less than 6 wt% and Mg content less than 4 wt% results in poor thermo mechanical properties due to poor wettability between matrix and reinforcement. Formation of brittle intermetallic compound such as Al_3Mg_2 is reported by the addition of magnesium more than 4.7 by mass percent, which wanes the properties of the final composites.[59]

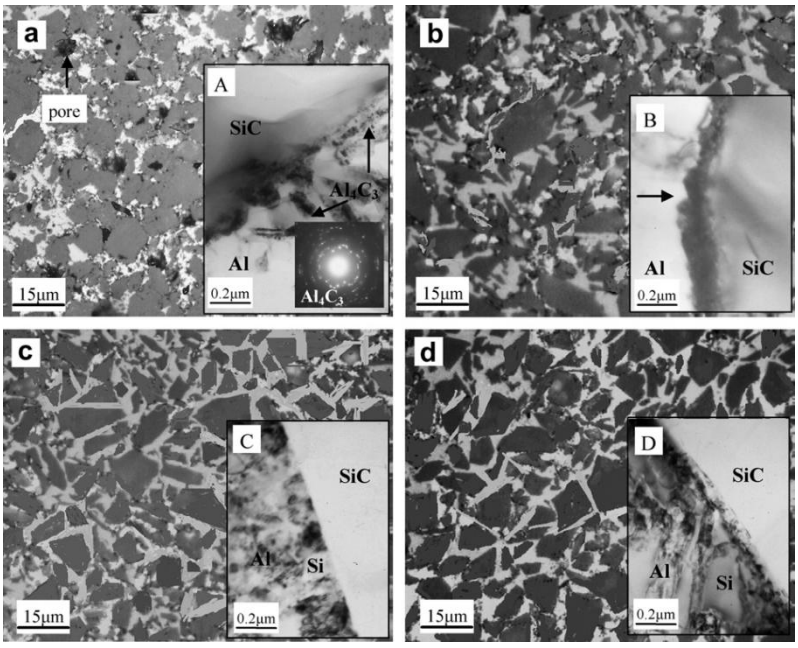

Figure 1.17. Optical and TEM images of the interface between Al-SiC composite with the addition of Si: (a and A) 0 wt%, (b and B) 6 wt%, (c and C) 12 wt% and (d and D) 18 wt% to reduce the interfacial reactions. [104]

The thermal conductivity was more influenced by the interfacial reactions between matrix and reinforcement. Lee et al. investigated the effect of Al_4C_3 formation on thermal conductivity (TC) of carbon fiber reinforced aluminum matrix composites and found that there is considerable decrease in thermal conductivity with increase in Al_4C_3 formation. The main reason for decrease in TC

was the surface damages to the carbon fibers (Figure 1.18) due to the growth of Al_4C_3.[107]

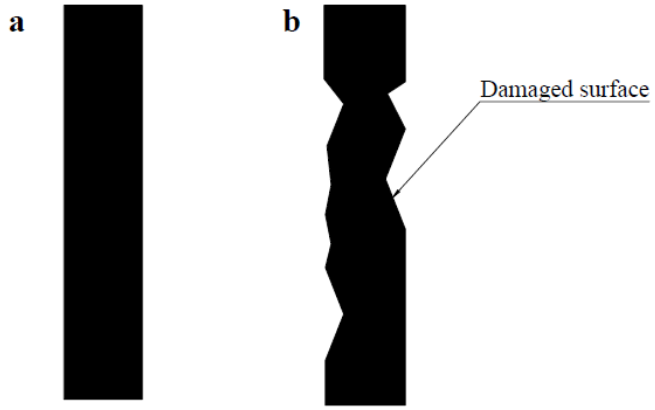

Figure 1.18. Change in the diameter of carbon fiber due to the formation of aluminum carbide: (a) before aluminum carbide formation and (b) after aluminum carbide formation.

The formation of AlN phase from the reactive infiltration of Al/Al alloys into porous α-Si_3N_4 preforms shows great impact on the thermal conductivity (TC) and CTE of the composites. Kalemtas et al. suggests that the connectivity of reactive phases (AlN), porosity in the composite, particle size of ceramic phase, and intrinsic properties of the ceramic phase are some of the factors markedly affects the TC and CTE of the composite. Non uniform distribution of the major phases like AlN, Si and Al reduces the connectivity of phases which reduces the thermal conductivity of the material.[108] Similarly decrease in the particle size of the ceramic phase increases the grain boundary volume which increases the scattering of conductive electrons leading to low thermal conductivity of the material.[109] The CTE value for AlN is very low and its uniform distribution in the material reduces the usage of Al phase during the process of thermal expansion.

1.6.3. Mechanical Properties

The mechanical properties of the composite are determined to study the effects of the type of reinforcement used, chemical composition of matrix alloy, infiltration processing temperature and the interfacial reactions. The reinforcement with finer particle size imparts additional interface area assisting the nucleation sites for the grain formation during infiltration process. Obviously developed composite dispense restrictions to the following factors like plastic flow

during deformation, grain growth during heat treatment and dislocation, resulting in higher mechanical strength.[110] Mechanical properties of the composite processed by infiltration technique also depend on the technique adopted for infiltrating molten metal into the preform. Mechanical properties will be less for pressure-less and low pressure infiltration techniques when compared to squeeze infiltration technique, since it offers lower infiltration time which circumvent the growth of interfacial reaction products. Due to the properties like ultra-high temperature ablation, strength retention at elevated temperatures, excellent thermal stability and moderate thermal expansion, ZrC particle reinforced tungsten composites (ZrC\W) had gained much attention in the aerospace applications.[111] Dense ZrC\W matrix composite fabricated by Zhao et al. under reactive infiltration of melted Zr_2Cu alloy into a porous WC preform provides mechanical properties, which are similar to the properties of ZrC\W composites prepared by other processing technique like hot-pressing and reactive sintering. $Zr_xCu_yC_z$ nanoparticles formed at the grains of ZrC due to the dissolution Cu in the ZrC matrix act as a pinning point for dislocations (Figure 1.19) and cracks thereby changing the direction of crack propagation, resulting in high fracture toughness and fracture strength.[112]

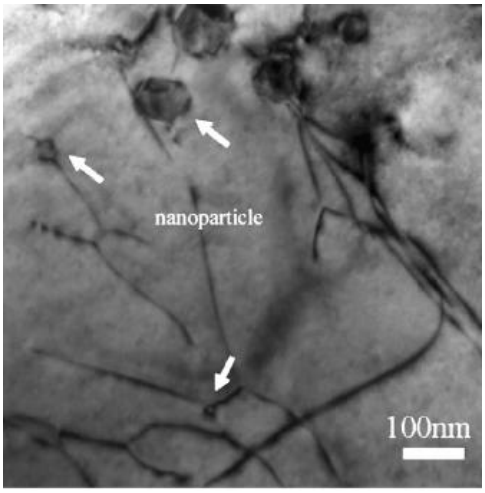

Figure 1.19. Dislocation pinning by the intragranular nanoparticles in the ZrC matrix.[112]

The infiltration time also plays a major role on mechanical properties of metal matrix composites. Tong et al. investigated the effect of infiltration time on mechanical properties of the C/C-SiC composite and found that the reaction

between the infiltrated molten metal and carbon preform is time dependent and the preform with higher porosity shows inferior mechanical properties (Figure 1.20). More the preform porosity more will be the melt and fiber contacts and thus more will be the interfacial reactions with an increase in infiltration time, which will negatively affect the mechanical strength of the composite.[113]

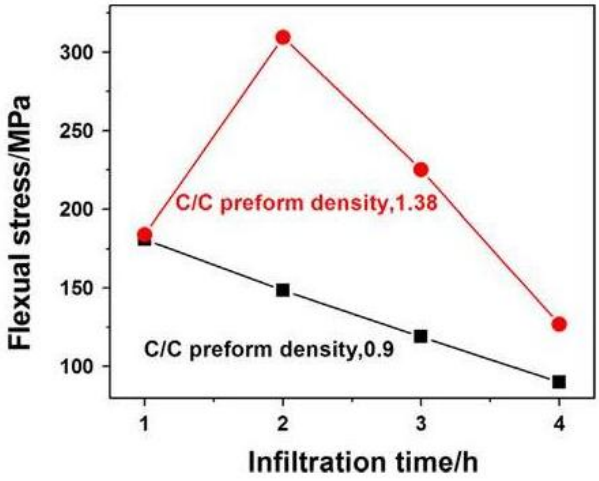

Figure 1.20. Flexural strength of C/C-SiC composites prepared in different infiltration time.[113]

An increased mechanical strength can be achieved by reducing the infiltration time thereby avoiding the formation of interfacial phases. The flexural strength of an infiltrated composite depends more on their fiber matrix interface and porosity. Heat treatment temperatures also have a great influence on the flexural strength of the composites. Higher heat treatment temperature will lead to decrease in flexural strength and elastic modulus due to the volatilization of residual metal.[114] Elastic modulus can also be enhanced by increasing the Si content in the matrix (Al) but heat treatment can provide appreciable improvement in hardness.[115,116] The composite having matrix material with high Cu content can provide better elastic properties and bending strength.[117] Another factor that adversely affects the mechanical strength is the preform materials contact with each other especially carbon fiber–carbon fiber contact in the case of carbon fiber reinforced composites. Increase in fiber volume fraction will lead to more and more direct fiber contacts and thus less tensile strength.[118] In a study done by Schlenther et al.[119], it was reported that the impact toughness of MMCs depends on the reinforcement particle size. Finer the particle size lower

will be the impact toughness due to lower inter-particle distance. Use of coarse reinforcements will provide more inter-particle distance leading to large interface area for good bonding between the matrix and reinforcement, so that crack propagation will be over the matrix material which provides energy in the form of plastic deformation before fracture, as a result crack branching occurs (Figure 1.21). However, increase in the particle diameter leads to increasing the possibility of particle cracking.[120] Additionally, several investigations suggested that some of the intermetallic phases flourished at the interface during infiltration process had the ability to enhance the hardness of the composite. Sanchez et al. inferred from their studies that during centrifugal infiltration process, nickel coated on the carbon fiber gets dissolved in the matrix to form Al_3Ni hard intermetallic compounds, which increase the hardness of the system. They also concluded that the hardness of the composite, in addition, depends on the volume fraction of the reinforcement.[54]

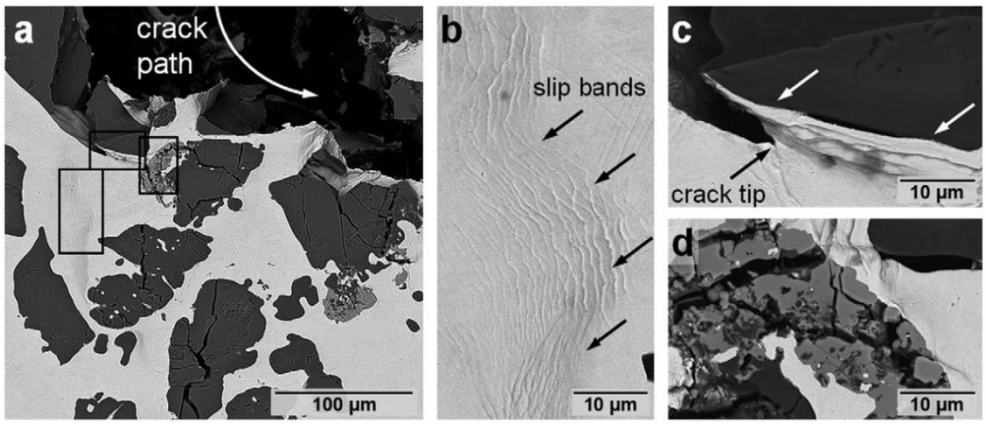

Figure 1.21. SEM images of the composite showing: (a) crack propagate through particle, (b) plastic deformation in the matrix zone, (c) good interfacial bonding between the particle and the matrix due to inter-particle distance, and (d) Severe crack propagation without any plastic deformation in fine particles or agglomerated zone due to lower inter-particle distance.[119]

1.6.4. Tribology and Corrosion Behaviour

The tribological property of the composites developed using the infiltration process is directly proportional to the size of the particle and the volume fraction of the reinforcement used. While considering an example, larger ceramic particles will exhibit superior wear resistance but inferior mechanical properties to those

containing smaller particles.[121] Zhang et al. also studied the effect of porosity in composites prepared by pressure-less infiltration of liquid copper into SiC preform and found that porosity has a significant influence on wear resistance. More the amount of porosity less will be the wear resistance and composite with low porosity shows remarkable wear resistance when compared to those with higher porosity.[122] Many investigations are already done on tribological behavior of carbon fiber reinforced metal matrix composites processed by infiltration technique. The carbon fibers are milled into very fine particles and get squeezed in between the sliding surfaces to form a tribo-layer or a solid lubricant layer.[123] Metal matrix composites containing carbon nanotubes also exhibit better wear resistance properties and the composite shows decreasing effect of wear rate with increase in CNT volume fraction.[124] Chang et al.[125] studied the wear behavior of composites processed by infiltrating Al-8%Mg into Al_2O_3 preform and found that the wear behavior is governed by foam density and cell size of the preform (Figure 1.22).

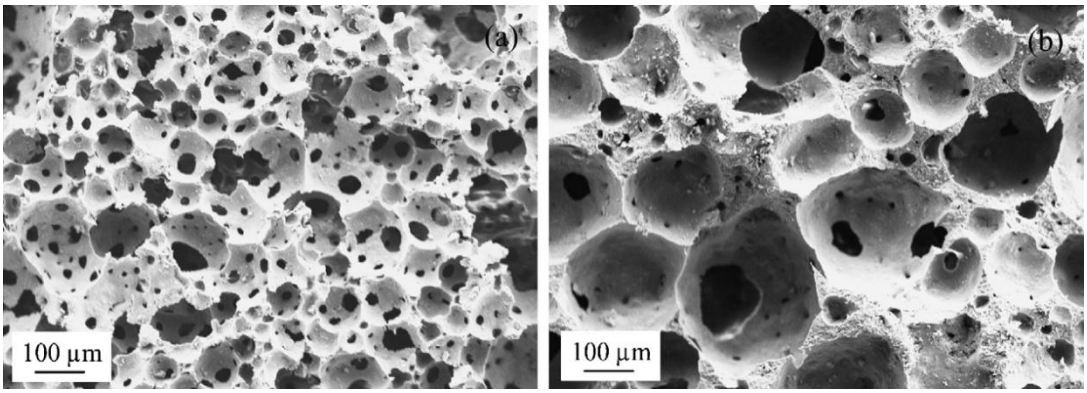

Figure 1.22. SEM images of (a) Al_2O_3 prefrom having 15% density with ~50-100 μm cell size and (b) Al_2O_3 prefrom having 27 % density with ~150-200 μm cell size.[125]

Composite with lower foam density shows more wear rate when compared to that with higher foam density due to the increase in the contact area of the infiltrated matrix with the counter disc during sliding (Figure 1.23a). Increasing the cell size of the preform forms large ridges of Al_2O_3 (Figure 1.23b and c) throughout the composite, which prevents the direct wearing of matrix alloy by counter surface.

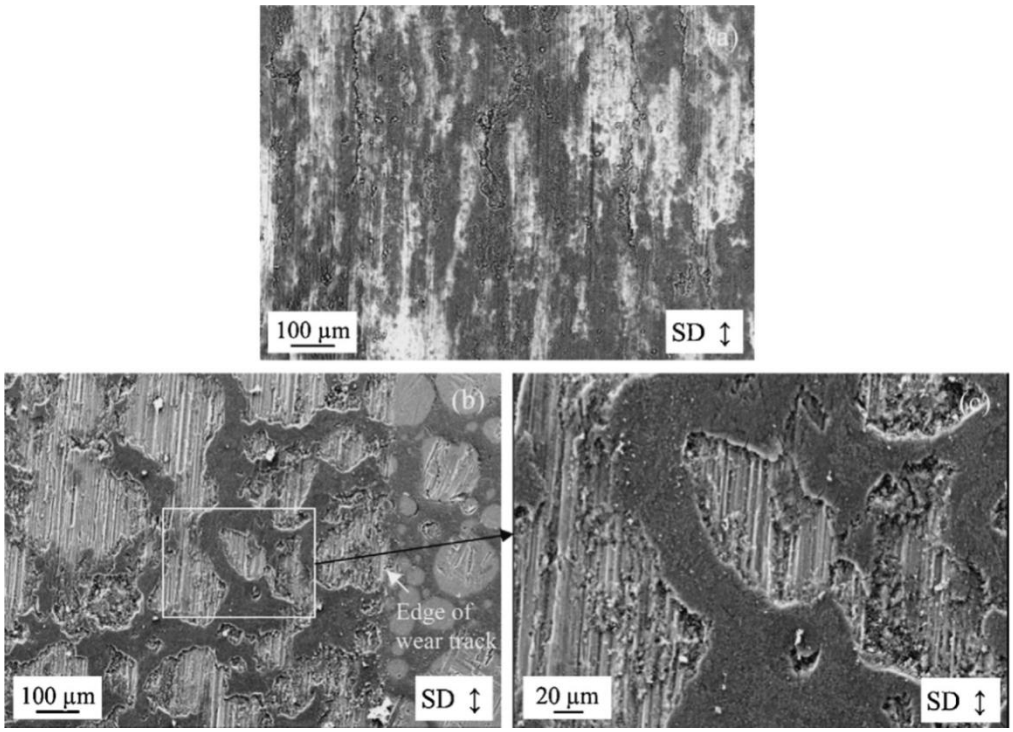

Figure 1.23. SEM images of worn out surface of infiltrated composite developed from (a) Al_2O_3 prefrom having 15% density with ~50-100 μm cell size and (b and c) Al_2O_3 prefrom having 27 % density with ~150-200 μm cell size.[125]

Dobrzanski et al.[126] stated that increase in volume fraction of the reinforcement in composite materials improves the general and pitting corrosion resistance. The higher volume content of the reinforcement phase (surface of the part undergoing testing) does not allow the current to conduct thus retarding electrochemical corrosion. The formation of intermetallic phases during processing, alloying element in the matrix, volume fraction, and the type of reinforcements are the pivotal features affecting the corrosion properties of the composite. The brittle intermetallic phases like Mg_2Si can have the tendency to act as anodic region to the matrix leading to the catastrophic localized corrosion. Escalera et al. studied the corrosion behavior of hybrid SiC/fly ash composites infiltrated with Al-8Si-15Mg and Al-3Si-15Mg (wt.%) as matrix alloys. The composite infiltrated with Al-8Si-15Mg results in the formation of Mg_2Si precipitation, which leads to the degradation of materials (Figure 1.24) due to the aggressive localized corrosion when exposed to ambient atmosphere for certain period.

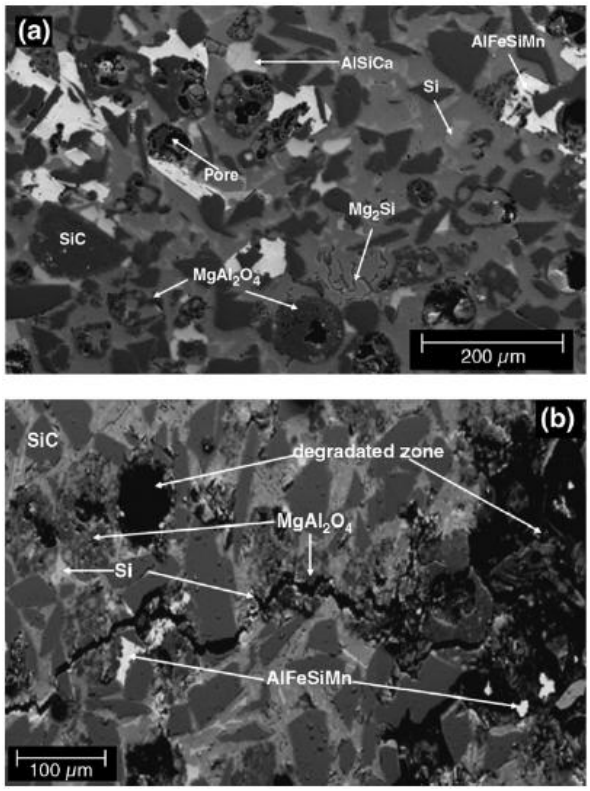

Figure 1.24. SEM micrographs of composite infiltrated with Al-8Si-15 Mg as alloy: (a) after processing and (b) after exposure to ambient atmosphere for 1 month.[127]

The composite infiltrated with Al-3Si-15Mg reveals no physical degradation even when exposed to humid environment for long duration (Figure 1.25) due to the termination of Mg_2Si phase, as the silicon content was low enough for the precipitation.[127] At the same time, some studies show that the reinforcement with small mean diameter and addition of Mg in matrix metal during pressure infiltrated composite enhances the corrosion resistance of the material when exposed to longer duration in NaCl. The formation of reaction products like Mg_2Si at the intersection of the reinforcements blocks the continuity of the metal matrix in the inner side of the developed composite through which the pitting during corrosion propagates and the concentration of interfacial reaction products in smaller reinforcements will be high due to their increased surface area contact with the melt.[128-130] The studies on corrosion behavior of infiltrated composites have shown varying nature of corrosion resistance by different investigators. Hence a detailed investigation is further necessary to generalize the corrosion nature.

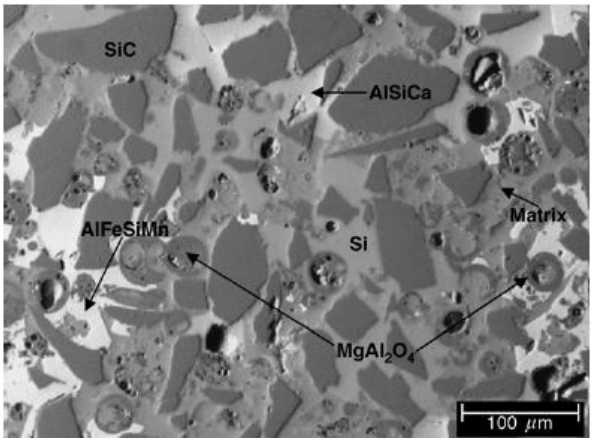

Figure 1.25. SEM micrograph of composite infiltrated with Al-3Si-15Mg as alloy after exposure for 11 months in humid environment.[127]

1.7. Applications

Recognizing the ability of liquid metal infiltration processes to assist in the further development of MMC components for aerospace, automotive, defense, electronics packaging, and in general engineering sectors, significant extent of research work is being carried out worldwide. Aluminum matrix composites with high volume fraction ceramic particles synthesized by infiltration process find potential application as integrated heat sinks and microprocessor lids in electronic packaging.[131] Properties like high thermal conductivity and low thermal expansion coefficient make aluminum nitride (AlN) reinforced aluminum matrix composites suitable for substrate and packaging applications in microelectronic sector. Low coefficient of thermal expansion makes the composite suitable for lightweight structural parts and heat sink applications.[132] Electronic packaging components with high volume fraction of reinforcement used in thermal management applications minimize the thermal stresses generated by the thermal expansion mismatch between them by dispelling the heat induced from the semiconductor.[133] The automotive industry has successfully implemented liquid metal infiltration technique to develop components like pistons,[134] clutch disk,[135] engine blocks with integral MMC piston liners,[136] etc by Al/SiC and Al/Al_2O_3 composites (Figure 1.26 a, b and c).

(a) **(b)**

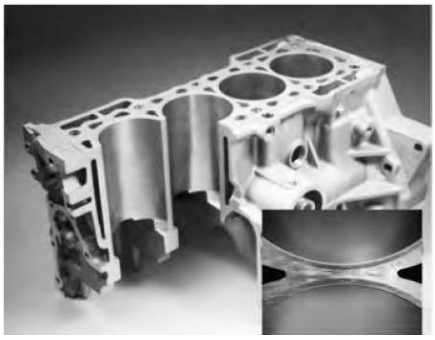

(c)

Figure 1.26. (a) Diesel engine piston selectively reinforced at the top ring groove area by infiltration process, [134] (b) automotive clutch disc manufactured by preform infiltration of aluminum using High Pressure Die Casting (HPDC), [135] and (c) cross section of Honda engine block with integral MMC piston liners fabricated by infiltration process.[136]

Honda manufactures have developed aluminum engine block using cylindrical hybrid preform of short alumina and carbon fibers by squeeze infiltration process there by replacing the commercial cast iron engine blocks thus providing weight reduction and higher performance.[137] Coal/lignite fly ash reinforced aluminum matrix composite made by pressure infiltration technique is a prime material for wear applications.[138] AlSi7Mg with 20 volume percentage SiC particles, liquid AlSi9Mg alloy infiltrated in Al_2O_3 preform by squeeze infiltration are quite worthy for brake discs and piston head of internal combustion engine, respectively.[139] Short alumina fiber reinforced aluminum matrix composites processed by squeeze infiltration technique is widely used in pistons.[131] The potential automotive components fabricated using infiltration processes are given in Table 1.1.

Table 1.1: Aluminum Infiltrated Components developed and used in automobiles.

Composite System	Automotive Component	Manufacturer
Al-Alumina$_{(f)}$	Diesel Engine Piston	Toyota
Al-$Al_2O_{3(sf)}$ -$C_{(sf)}$	Engine	Honda
Al -$FP_{(CF)}$	Connecting Rod	Du-pont
Al-$SUS_{(CF)}$	Connecting Rod for Petrol Engine	Honda
Al-$SiC_{(W)}$	Diesel Engine Piston	Niigata
Al-$SiC_{(w)}$	Connecting Rod	Nissan
Al-Alumina$_{(f)}$	Piston Ring Grove	Toyota

Molten metal infiltration of particle reinforced aluminum matrix composites such as B_4C, SiC, TiC, TiB_2, Al_2O_3 etc are successfully used as components in opto-mechanical assemblies and aerospace applications. Boron carbide, because of its high hardness and other magnificent mechanical properties like low density, high impact and wear resistance, excellent resistance to chemical agents, high melting point, and high capability for neutron absorption, finds application in structural neutron absorber, substrate material for computer hard disc, and as armor plate materials. It is tough to fabricate dense B_4C materials for industrial applications because of its high sensitivity to brittle fracture. This problem can be overcome by the fabrication of B_4C reinforced aluminum matrix composites by infiltration process. For example in the case of neutron shielding applications aluminum matrix provides fracture toughness and strength to the composites while boron carbide absorbs neutron.[140] AMC with 40 vol% SiC particles is used as flight control hydraulic manifolds and the aerospace application further extends to fuel access cover door, ventral fins, fan exit guide vane in the gas turbine engine, rotating blade sleeves in helicopters etc. Particle reinforced aluminum matrix composites also shows their ingenuity in developing braking system of trains and cars and it also finds extensive automotive applications such as gear parts, valves, crankshafts, and suspension arms.[131] Table 1.2 summarises the major industries producing components by infiltration process.[141]

Table 1.2: The major companies producing components by infiltration process.[141]

Sl. No.	Industries manufacturing MMC by infiltration
1.	3M Company, Specialty Fibers and Composites, USA (www.3M.com/mmc)
2.	CPS Technologies (http://www.alsic.com/)
3.	Ford Motor Company, USA (www.ford.com)
4.	General Motors, USA (www.gm.com)
5.	Honda Motor Company, Ltd, Japan (www.honda.com)
6.	M-Cubed Technologies, Inc, USA (www.mmmt.com)
7.	Mazda Motor Corporation, Japan
8.	Metal Matrix Cast Composites (MMCC), USA (www.mmccinc.com)
9.	Motorola, Inc, USA (www.motorola.com)
10.	Porsche, Germany (www.porsche.com)
11.	Toyota Motor Corporation, Japan (http://www.toyota.com/)
12.	Triton Systems Inc, USA (www.tritonsys.com)
13.	Thermal Transfer Composites, LLC (http://www.thermaltc.com/)

1.8. Compocasting Process

In recent years, researchers have identified compocasting as one of the economic and efficient methods for fabricating aluminum matrix composites (AMC) over other conventional methods due to its advantages like low casting temperature, uniform distribution of reinforcement without agglomeration, good wettability and better matrix-reinforcement bonding.[142] Compocasting is a solid-liquid state method in which a vortex is created in the semisolid molten metal (between the solidus and liquidus temperature of the matrix alloy) using an impeller driven by an electric motor, and the reinforcements are added into the vortex under stirring (Figure 1.27). During compocasting process, the higher viscosity of semisolid molten metal slurry transmits shear force over the agglomerated reinforcements which lead to better dispersion and distribution of reinforcement in the matrix. Both the micron and nano size reinforcements are successfully incorporated into the matrix by compocasting process.

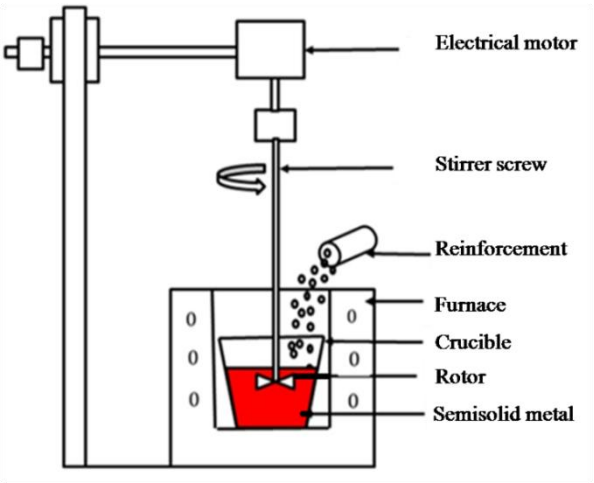

Figure 1.27. Schematic diagram of compocasting process.[143]

The major process parameters considered during compocasting process are (i) crucible size (ii) size and shape of the stirrer (iii) semisolid metal temperature (iv) stirring time (v) stirring speed (vi) mold temperature and (vii) reinforcement feeding rate. The properties of the final composite depend on the aforesaid process parameters.[144] Mortensen et al.[145] concluded that in composite the wetting behavior and the reinforcement uniform distribution depends on the rheology of composite and nucleation of the matrix. Mazahery et al.[146] reported that the vigorous agitation during compocasting process cause the dendrites to break and leads to refined microstructure without using grain refiner. The studies show that the tribological and the mechanical characteristics of the composite depends on the matrix microstructure, reinforcement distribution and the porosity content, which can be satisfied by the semi-solid stir casting process. Even for the higher volume fraction of reinforcement homogenous distribution of reinforcement in the matrix is obtained by compocasting process.[147] Khosravi et al.[148] fabricated A356-SiCp composites by compocasting process and observed that by increasing the stirring speed, time and temperature the porosity level in final composite increases. However, uniform particle distribution and enhanced tensile strength were obtained for the composite processed at the parameters of 400 rpm (stirring speed), 590 °C (stirring temperature) and 30 min (stirring time).

The compocasting process has two variations namely semisolid–semisolid (SS) and semisolid–liquid (SL) routes, in which the matrix alloy during casting step is either in partially liquid or in fully liquid state respectively. However, during

compocasting process the matrix will be in the semi-solid state for both the variations and the reinforcements are added into it. Both the variations have its advantages and disadvantages, some of the benefits of SS route are (a) low processing temperature (b) lower interfacial reaction (c) low solidification shrinkage, etc. While considering the benefits of SL route they are (a) ease of casting (b) less porosity etc.[149] Rajan et al.[150] fabricated A356/fly ash composites by three processing routes namely stir casting process, compocasting process and modified compocasting followed by squeeze casting process. In stir casting process, the addition of fly ash particles into the molten metal and the pouring of composite slurry into the mold were carried out above the liquidus temperature of the matrix aluminum. In compocasting process, both the addition of fly ash particles and the pouring of composite slurry into the mold were carried out at semi-solid state. While in the case of modified compocasting process, the addition of fly ash particles was carried out at matrix semisolid state and pouring of the composite slurry was done above the matrix material liquidus temperature, followed by solidification under squeeze pressure. They found that the modified compocasting cum squeeze casting process results in the better distribution of reinforcements in the matrix followed by compocasting and squeeze casting processes. The processing method also plays a critical role in determining the mechanical properties of the composite. The previous study showed that the porosity content and grain size of the composite fabricated by compocasting process was lower than composite processed by stir casting process due to low wettability in stir casting process.[151] To improve the wettability between the reinforcement and matrix during stir casting process, several techniques were suggested like adding wettability agent and fluxes, preheating the reinforcements, coating of reinforcements, etc but it will increase the overall fabrication cost.[152,153,154] Allwyn et al. reported the studies on AA6061/ rice husk ash (RHA) particulate reinforced composite fabricated by compocasting process and concluded that the uniform distribution of RHA in the matrix was observed, which refines the grain size. Also, the interface between the matrix and reinforcement was smooth without any interfacial reactions with better bonding, which leads to enhanced mechanical properties.[155]

1.9. Aluminum Nanocomposites

Aluminum matrix composites containing the second phase as nanoscale reinforcements (<100 nm) or the grain size of matrix below 100 nm are termed as aluminum matrix nanocomposites (AMNCs). AMNC has emerged as a new class of lightweight materials exhibiting excellent characteristics like good specific stiffness, improved ultimate tensile strength (UTS) and yield strength (YS), better thermal stability and creep resistance etc than those of unreinforced Al alloys and aluminum micron size reinforcement added composites. The special strengthening factors enhancing the characteristics of AMNCs over Al micron size reinforcement added composites are orowan mechanism, grain refinement, enhanced dislocation density, intimate adhesion between the matrix and reinforcement, and effective load bearing capacity.[156] It is reported that the microparticles are usually located at the boundaries of the eutectic grains, which leads to lower fracture toughness and high-temperature properties of the composite. At the same time, nanoparticles get distributed on the dendrites of the primary solid solution which in turn helps in improving the aforesaid properties of the composite.[157] AMNCs provide better performance in structural, thermal, high precision and tribological applications. Al reinforced with nano SiC offers excellent dimensional stability and can be used for thermal applications. Nano reinforcements like Al_2O_3, SiO_2 and TiO_2 coupled with Al matrix find wide applications for components and car body materials in automotive industry.[158]

Sajjadi et al. studied the effect of micro (20-30 μm) and nano (50 nm) Al_2O_3 reinforcement on the properties of Al A356 composites and reported that the Al-Al_2O_3 nanocomposite exhibits higher hardness value over micron size particle added composites due to the influence of nanoparticles on the orowan mechanism.[159] Mazahery et al. reported that the enhancement in the mechanical properties of the Al-Al_2O_3 nanocomposite is due to the resistance to dislocation motion offered by the nonshearable nanoparticles and it increases with increase in the particle volume fraction. They also concluded that the increase in UTS and YS of the Al nanocomposite is due to the use of small particle size and its uniform distribution in the matrix which helps in effective transfer of applied tensile load from the matrix to the reinforcement Al_2O_3.[160-161] Ede et al. reported that the addition of SiC nanoparticles into the aluminum alloy increase the mechanical

properties of the composite, however, increase in the addition of nano SiC above the critical value lowers the mechanical properties due to the SiC clusters.[162] Mahallawi et al. compared the effect of incorporating three different types of reinforcements like Al_2O_3, TiO_2 and ZrO_2 in Al A356 alloy and found that the composite reinforced with Al_2O_3 obtains the highest strength properties compared to other reinforcement added composites.[163]

1.10. Scope of the Investigation

The literature review carried out on aluminum composite processed by liquid metal infiltration and compocasting techniques have shown the potential for fabricating composites with enhanced mechanical and tribological properties for various engineering applications. Liquid metal squeeze infiltration is one of the important and suitable method for making composites with large volume fraction and continuous fiber systems. However the compocasting finds potential applications in making composites with ultrafine, nano and assorted particle size reinforcements with uniform distribution. There is a large scope for exploring new metallic composite systems for industrial application.

In the present study, Al metallic composites are aimed for fabrication using squeeze infiltration and compocasting techniques. Bidirectional (BD) satin weave polyacrylonitrile (PAN) based carbon fiber (C_f) fabric preform and discontinuous zirconia grade aluminosilicate fiber preform is used for infiltration process. Direct squeeze infiltration technique is adopted for developing fiber composites due to its distinct advantages like the ability to form selectively reinforced composite, refined microstructures due to high solidification rate, eradication of shrinkage and porosities since solidification under squeeze pressure and uniform microstructure due to the use of a highly ordered inceptive preform. These types of composites developed by infiltration process find wide applications for engineering components in aerospace, automotive, defense, electronics and general engineering sectors. The controlled process parameters of molten metal temperature, preform and die preheating temperature, dwell time, and applied squeeze pressure were used for the infiltration of liquid aluminum into the preform. The wide scopes of the work carried out by infiltration process are

- Aluminum matrix composites with high volume fraction of reinforcement.
- Complete Infiltration of aluminum metal throughout the tiny interspaces of the preform without the solidification in the infiltration front is challenging.
- Conventional infiltration process is carried out in vacuum / inert gas atmosphere to control the fiber degradation and interfacial reactions leading to higher processing cost. Scope for developing a new process with low temperature preform preheating and liquid metal infiltration in ambient temperature and atmosphere.

Compocasting stands out to be one of the economic and effective methods to produce Al matrix composites (AMCs) by reducing the casting temperature and adding ceramic particles into the semi-solid state aluminum, which enhances wettability and better distribution of reinforcement particles in the matrix. Fine size microsilica and nano Al_2O_3 particles are used as reinforcements for compocasting process. Solidification of composites is carried out under squeeze pressure to refine the grain size and to reduce the porosity in the final composites. Aluminum alloys with nanodispersions are gaining considerable attention as lightweight metallic materials in high-performance application areas of aerospace, defense and recreation sectors. There is a wide scope for preparing micro and nano-composites by compocasting process due to

- Capability for uniform distribution of fine and nano size reinforcement in the aluminum matrix which is really challenging by other methods.
- Tailoring the processing parameters to obtain high strength aluminum matrix composites through nanodispersoids and maintaining the semisolid temperature during dispersion.

1.11. Objectives of the Investigation

The present investigation aims at processing of aluminum based metallic composites by two potential and industrially applicable processes of squeeze infiltration and compocasting techniques. Squeeze infiltration is adopted for high volume fraction fibre reinforcement containing composite system and Compocasting is applied for fine and nanosize particle dispersed metallic composites. The fabricated composites are to be evaluated for their structural, physical, mechanical, tribological, interfacial and corrosion characteristics. The important mechanism dealing with various property improvements are discussed.

Squeeze infiltration technique is applied for fabricating and evaluating

- Bidirectional carbon fiber reinforced Al 6061 composite (Cf AMC) and study the effect of carbon fiber on the properties of composites.
- Al6061 matrix composite reinforced with low-cost zirconia grade aluminosilicate short fiber using 15 and 20 vol% preforms and study the structure and properties of the composite.

Compocasting technique is modified and applied for

- Microsilica reinforced A356 aluminum composite and evaluating their properties.
- Nano alumina reinforced A356 Al nanocomposites solidified under squeeze casting process. Studies are to be carried out on the interfacial characteristics between the nanoparticles and matrix on strengthening of cast aluminum alloys.

Chapter 2

Development of Bidirectional Carbon Fiber Fabric Reinforced 6061 Aluminum Composites by Squeeze Infiltration Technique

Abstract

Bidirectional (BD) satin weave polyacrylonitrile (PAN) based carbon fiber (C_f) fabric preform was successfully infiltrated with Al6061 alloy by squeeze infiltration process and their properties were evaluated. The infiltrated composite shows uniform distribution of carbon fibers in the matrix with the elimination of porosities, fiber damage and close control in deleterious aluminum carbide (Al_4C_3) phase formation, by using optimized process parameters. C_f/Al6061 composite exhibits superior wear resistance compared to unreinforced alloy due to the formation of self-lubricant tribo-film on the pin surface, which intercepts the matrix metal to counter surface contact. The introduction of BD carbon fiber in the matrix enhanced the hardness and compressive strength of the composite remarkably by restraining the matrix plastic flow behavior. The tensile strength of composite decreased due to interfacial delamination of transverse oriented fibers at lower load. HRTEM observation shows the presence of Al_2O_3 and $MgAl_2O_4$ spinel, confirmed by EDS and SAD pattern, at the interface and controls the growth of Al_4C_3 crystals. The C_f/Al6061 shows lower density of 2.16 g/cm^3 which is a major advantage for weight reduction compared to the monolithic alloy (2.7 g/cm^3). Electrochemical and Immersion test of composite shows no significance reduction in corrosion characteristics.

2.1. Introduction

The potential application and increased usage of carbon fiber globally in aerospace, automotive, and defense sectors is due to its high specific strength and stiffness, good flexibility and low density.[164] The demand of carbon fiber in transport sector is to focus on developing vehicles with light weight construction, greater fuel efficiency and higher payload capacity. Modern innovation in this

sector is the launch of the BMW i3 electric vehicle with its carbon fiber composite passenger compartment.[165] Aluminum alloys are considered as the prime matrix material for composites due to its ductility, low density and high specific strength. Carbon fiber reinforced aluminum matrix composites (C_fAMC) shows unique combination of properties than those of the monolithic materials. Formation of brittle interfacial reaction product Al_4C_3 between carbon fiber and the aluminum is one of the common problem encountered in C_fAMC, which affects the final properties of the composite.[107,99,166,167] Several studies have been conducted by many researchers on coating of carbon fibers using Cu, Ni, Al_2O_3, SiC etc to avoid the detrimental reaction with the molten matrix metal during composite preparation.[98,96,168,169,67] However, some of the factors like change in density of the reinforcement, dissolution of coatings into the matrix material forming brittle reaction products, increasing thickness of coating leads to brittleness and reduce the ductility of the composites set limitations to the coating process.[170] Also, based on the fabrication methods of composite better bonding between the matrix and reinforcement and smooth interface without any unwanted reaction products can be obtained.

Different fabrication techniques have been implemented to develop fiber reinforced metal matrix composites like stir casting, infiltration, powder metallurgy, diffusing bonding etc.[72,171,172] Among these squeeze infiltration of liquid metal into porous preform technique stands out one of the economic and distinct method compared to other conventional methods. The wetting between the matrix and the reinforcement can be overcome by external pressure; also it can yield ancillary assistance like eradication of shrinkage and porosities, refined microstructure since solidification under pressure, and reduced chemical reactions due to enhanced processing speed last for few seconds. Use of high volume fraction of reinforcement and development of near net shape and selectively reinforced components are an added advantage of squeeze infiltration. Squeeze infiltration is a liquid state fabrication method, which begins with the formation of mechanically stable porous preform and its infiltration with the liquid metal under pressure.[85,173,75] Most of the research has been carried out on using carbon short fibers, unidirectional fibers and carbon nanotube reinforced composite.[174-178] Carbon in the form of graphite,[179] graphene[180-181] and

diamonds[182] of particles size in the range of micro and nano were also used for the preparation of aluminum composites. In contrast, the studies on the development of bidirectional satin weave PAN based carbon fiber fabric reinforced aluminum matrix composites are limited. The present investigation attempts to fabricate bidirectional carbon fiber reinforced Al6061 composite (C_fAMC) by direct squeeze infiltration process and study the effect of carbon fiber on the properties of composites. The design of the die and optimized process parameters like preform and die preheating temperature, liquid metal temperature and squeeze pressure plays a major role in the complete infiltration of molten aluminum into the carbon fiber preform. The composites will be characterized with respect to structural, interfacial, physical, mechanical, tribological and corrosion characteristics.

2.2. Experimental Methods

2.2.1. Processing of BD C_f/Al6061Infiltrated Composite

Al6061 is chosen as the matrix alloy since it is one of the most widely used wrought alloy for the structural application in aerospace, automotive, naval and defence sectors. Al6061 alloy of composition Al-1.2 Mg-0.8 Si (in wt. %) supplied by Sargam Metals, India was employed. Satin weave PAN based 3K bidirectional carbon fiber fabric was used as the reinforcement having 3000 carbon fibers in each tow. The average diameters of the fibers were 7 μm with a density of 1.8 g/cm^3.The carbon fiber mat was cut into pieces and stacked together to fabricate the preform for molten metal infiltration of dimension 8cm length and 1cm width. The layers of the carbon fiber mat in the preform were stitched together with the help of carbon fiber strands and then the preform was preheated to 350 °C for 1 hour. Direct squeeze infiltration technique was adopted for fabricating bidirectional C_f/Al6061 composite. The die of 120×50×60 mm cavity was designed and fabricated using tool steel. The following processing parameters were optimized and used for squeeze infiltration. The die and punch was fixed in a 25T hydraulic press and preheated to a temperature of 220 °C for one hour. Simultaneously 6061 alloy was melted in a resistance heating furnace to a temperature of 750 °C and magnesium (1 wt. %) in pure form was added into the molten metal to improve the wettability during infiltration. When the aluminum

melt temperature becomes 780 °C the preheated carbon fiber preform was put into the preheated die, liquid metal was poured over it and subsequently high pressure of 40 MPa was applied on the molten metal to get infiltrated into the preform. The squeeze pressure was maintained for about 2-3 minutes until the solidification was complete. The unreinforced Al6061 alloy was subjected to squeeze casting process for comparison of characteristics with respect to the composite.

2.2.2. Characterization

As cast samples of unreinforced squeeze cast alloy and infiltrated composite were used for characterization in the present study. Microstructural characteristics of alloy and composite were characterized using JEOL SEM with Oxford EDAX and Leica DMRX Optical Microscope. Initial polishing using 100, 220, 400, 600 and 1000 grit size emery papers were adopted for preparing metallographic samples followed by final selvyt cloth polishing using diamond paste of particle size 6, 3 and 0.25 μm. Philips X-ray Diffraction (XRD) was used to characterize the extracted fibers from infiltrated composite using Cu K_α radiation (wavelength λ =0.154 Å) to identify the phases. The hardness tests were carried out using Zwick Brinell hardness testing machine with a 2.5 mm ball indenter and 62.5 kg load. The dry wear tests were conducted using DUCOM (TR20LE) pin-on-disk tribometer at two conditions; constant velocity of 2 and 4 m/s with varying loads of 20, 30, 40 and 50 N and at constant load of 30 and 50 N with varying velocities of 1, 2, 3 and 4 m/s at a constant sliding distance of 1500 m. EN31 high carbon alloy steel with chemical composition, Fe-1 C-0.5 Mn-1.4 Cr-0.25 Si (in wt. %), hardness of 63HRC and surface roughness (R_a) of 0.4μm measured using Bruker profilometer was used as the counter disk for pin-on-disk wear testing. Cylindrical specimens having dimension of 6 mm diameter and 30 mm length with the surface roughness of the wear surface as 0.5μm were used as the wear testing pin. The differential thermal analysis (DTA) and thermo gravimetric analysis (TGA) were performed using a Hitachi STA7300 (TG-DTA) instrument at a heating rate of 10 ^oC/min. The density and compression tests were evaluated using Archimedes principle and Instron machine respectively. The tensile tests of alloy and composite were done using FIE make universal testing machine (UNITEK-94100). Interface characterization of C_f/Al6061composite were examined in JEOL-

JEM-2100 transmission electron microscope operated at 200 kV with Oxford EDS. Electrochemical analysis and Immersion test were carried out to evaluate the corrosion behavior of alloy and composite. In electrochemical analysis the corrosion behavior of the alloy and composite were examined by an electrochemical workstation (CH Instruments, Model CHI680) using a three-electrode cell, with Al6061 unreinforced squeeze cast alloy and Al6061-C_f infiltrated composite as working electrode, platinum as auxiliary electrode and calomel as reference electrode using a potentiodynamic system. The working electrode, in each case the material under study, was subjected to 3.5 wt. % NaCl solution and the scan rate was 0.2 mV/sec. In immersion test method, the material under study (alloy and composite) having dimension of 0.6×0.5 cm (cuboidal) was immersed in 3.5 wt. % NaCl for 7, 14 and 21 days and measure the weight loss of the material after the exposure to NaCl. Nitric acid was used to remove the corrosion products from the corroded samples.

2.3. Result and Discussion

2.3.1. Structural Characteristics

The SEM photomicrographs of as received and surface treated carbon fibers are shown in Figure 2.1. As received carbon fiber shows a glossy surface finish (Figure 2.1a) originates from the polymer coatings. For the smooth weaving of carbon fiber mat and to evade the formation of static charges due to friction between carbon fibers, normally polymer coating is applied on the surface of carbon fibers. This coating may inhibit wettability between the matrix and reinforcement and adversely affect the molten metal infiltration into the fiber mat preform. Obviously, the carbon fiber undergoes surface treatment in acetone and distilled water to remove coating and dried in an oven. The treated carbon fibers reveals an uneven surface finish due to the peel up of coatings (Figure 2.1b) and some of them which gets sticked on the surface of the fiber (Figure 2.1c). The macrograph of the infiltrated Al 6061-BD carbon fiber composite and the preform made of satin woven 3K carbon fiber mat are shown in Figure 2.2. It can be rendered from the macrograph that the developed composite is free from porosities caused by gas inclusions and provoking the concept of selectively reinforced composites (SRC). The application of selective infiltration can lead to

advanced functionally graded composite materials through which location specific properties can be achieved.

Optical microstructure of the polished surface of BD C_f/Al 6061 composite by squeeze infiltration process is portrayed in Figure 2.3. The tiny interspaces between the carbon fiber fabrics gets completely infiltrated by liquid aluminum, stipulating the effect of squeeze pressure exceeding the wettability between matrix and the reinforcement. Uniform distribution of fiber mat is perceived in the matrix aluminum due to the use of an inceptive preform having isotropic arrangements of two dimensional woven fibers for infiltration. However there is no sign of fiber agglomeration, fiber damage and drift in the preform due to high pressure melt penetration, since the plane of BD arrangement is disturbed no more. Perfect adhesion between the carbon fiber and liquid aluminum is observed in the microstructure with the elimination of porosities and cracks, which can be accredited to the solidification process that takes place under pressure (Figure 2.3a). The cross section of C_f/Al 6061 composite in Figure 2.3b depicts the depth of penetration by liquid molten metal into the multiple stacks of fiber mat preform and the infiltration was observed even through single fiber. Moreover, a single layer of fiber mat in the preform contains combination of fiber arranged in the transverse and longitudinal direction. Totally around 20 layers of such carbon fiber mat preform is successfully infiltrated. Figure 2.3c shows the final layer of the mat preform in the composite in which the cross section of carbon fiber strands used for stitching the preform mat layers together can be identified, which gets invaded into the longitudinal fiber arrangement. The junction between the transverse and longitudinal alignment of woven carbon fiber fabrics are clearly seen in the microstructure (Figure 2.3a). While polishing the longitudinal laid fibers on oblique plane are cut along as cross section and thus seen as elliptical shape (Figure 2.4).

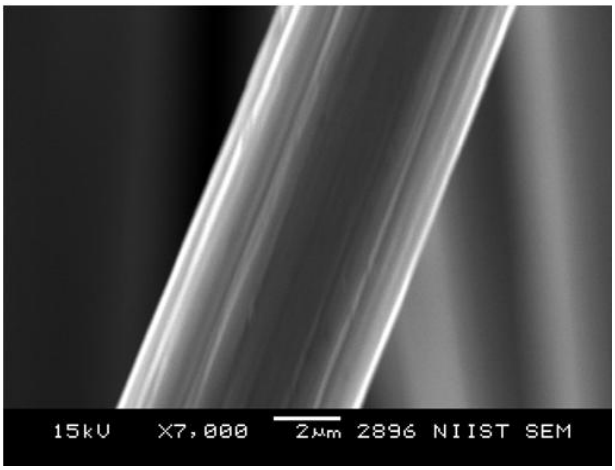

(a)

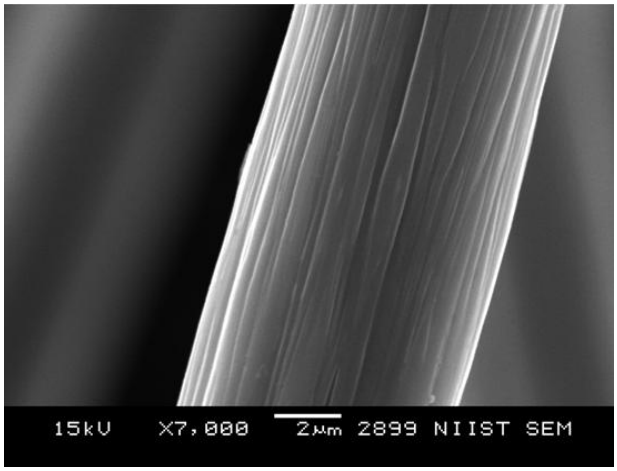

(b)

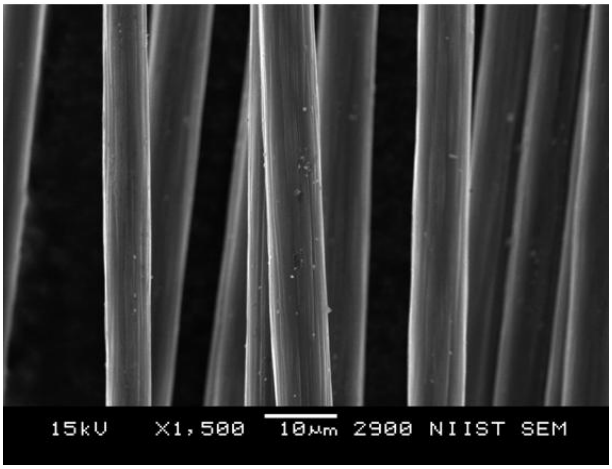

(c)

Figure 2.1. SEM photomicrographs of (a) untreated carbon fiber (b) surface treated carbon fiber (c) surface treated carbon fiber in which some amount of polymer coatings get sticked on it.

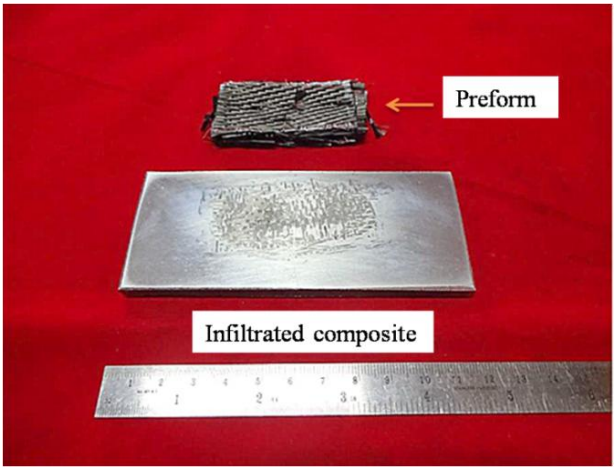

Figure 2.2. Macrographs of the carbon fiber mat preform and the BD C_f/ Al 6061 Infiltrated composite.

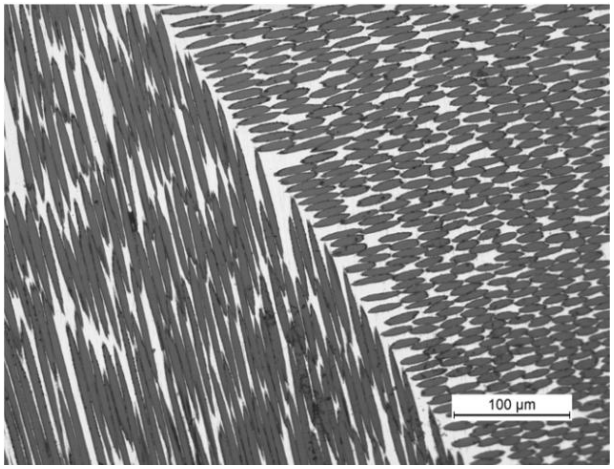

(a)

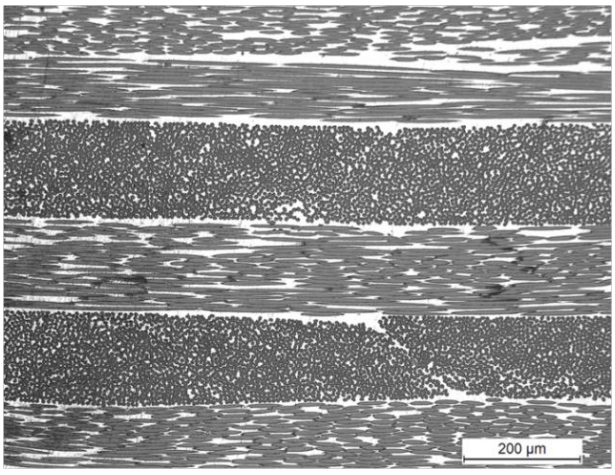

(b)

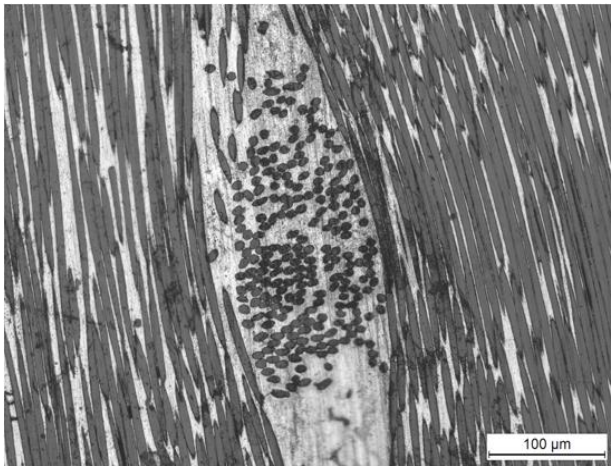

(c)

Figure 2.3. Optical micrographs of (a) BD C_f fabric/Al6061 infiltrated composite (b) cross section of the infiltrated composite (c) cross section of fiber strand used for stitching the preform in infiltrated composite.

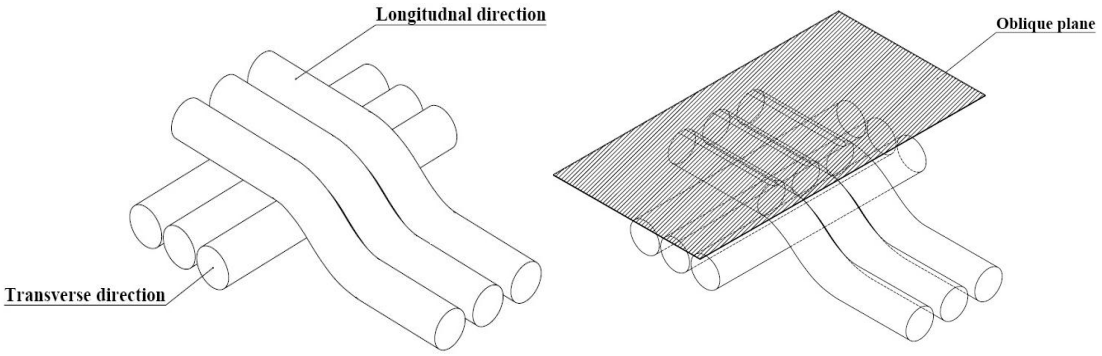

(a) **(b)**

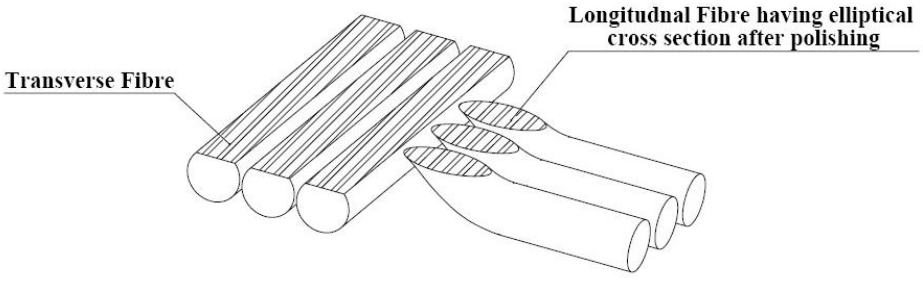

(c)

Figure 2.4. Schematic representation denoting the orientation of carbon fiber in the infiltrated composite while polishing for metallographic preparations.

The SEM image (Figure 2.5a and b) of the squeeze infiltrated composite reveals the intimate interfacial bonding between the aluminum and carbon fiber. The interface between the matrix and reinforcement seems to be lustrous and free from defects with adequate wetting behavior. Figure 2.6a shows the SEM images of the extracted carbon fiber from the composite. The surface of the fiber seems to be smooth without any remarkable interfacial reactions, which stipulate the perception of squeeze infiltration process parameters. The excess development of familiar brittle reaction phase like Al_4C_3 in Al-carbon composite cause notch shape damages on the surface of the fiber[183] resulting in degradation of properties, which is very limited in this system. EDAX on the surface of the extracted fiber (Figure 2.6b) shows the presence of carbon, oxygen, aluminum and magnesium. However, the nature of compound present on the surface can be determined by XRD analysis.

Figure 2.7a shows the TEM image of interface region between BD C_f/Al6061 composite developed by squeeze infiltration process. The presence of oxide layers like Al_2O_3 and $MgAl_2O_4$ spinel can be observed on the interface between the matrix and carbon fiber, which are confirmed by the elemental analysis by EDS (Al_2O_3 atomic%: Al-42.57, O-57.43; $MgAl_2O_4$ atomic%: Al-35.56, O-56.95, Mg-7.48). During squeeze infiltration process, oxygen presents in the atmosphere and in the pores of the preform reacts with molten aluminum and its alloying elements to form oxide layer on the infiltration front. Major portion of the oxide layers formed at the interface are found to be Al_2O_3 and the Figure 2.7b shows the HRTEM image of crystalline lattice planes and the d_{012} interplanar distance of 0.34 nm correlated to the Al_2O_3 structure. The perfect arrangement of atoms in Al_2O_3 lattice can be depicted from the deconstructed TEM image using FFT (Fast Fourier Transform) in Gatan Microscopy suite software. The oxide layer formed at the interface improves the bonding strength between matrix/reinforcement and also obstructs the diffusion of matrix aluminum into the carbon fiber, thereby reducing the formation of interfacial reaction product, Al_4C_3.

Very limited formation of Al_4C_3 crystals as lath like shape is observed (Figure 2.8a) in the oxide-matrix interface region, which is confirmed by TEM-EDS (Al_4C_3 atomic%: Al-81.59, C-18.41) and selected area diffraction analysis (SAD)

with an interplanar distance d_{107} of 0.23 nm. Studies shows that the main reason behind the Al_4C_3 formation in Al/Carbon fiber composite is the dissolution of carbon fiber in the liquid aluminum followed by solidification process.[184] In higher magnification single twinned regions are identified in Al_4C_3 crystals (Figure 2.8b) with a cross section of about 7 nm and it can be visible from the auxiliary electron diffraction reflexes in SAD. The formation of additional spots due to twinning effect is demonstrated by SAD pattern interpretation in Figure 2.8c. Similar morphology of Al_4C_3 was reported by Steffens et.al in their studies.[185] The difference in thermal expansion coefficient between Al_4C_3 and matrix aluminum cause compressive strain in the carbide crystals during solidification, which can cause surface twinning in Al_4C_3. Very few precipitates of intermetallic phase Mg_2Si is observed on the composite interface region, which results from the reaction of Mg and Si present in the Al 6061 matrix alloy (Mg_2Si atomic%: Mg-67.74, Si-32.26) (Figure 2.9).

2.3.2. XRD Analysis

The XRD diffractogram of extracted fibers from the infiltrated composite using NaOH solution is shown in Figure 2.10. The major diffraction peaks observed in the extracted composite particles belongs to C and precipitated phases like $Al_{12}Mg_{17}$, $MgAl_2O_4$, Al_2O_3 and Al_4C_3 which manifest more crystalline nature respectively. Chemical interaction between the magnesium and the matrix material leads to the formation of intermetallic phase $Al_{12}Mg_{17}$, which helps is enhancing the mechanical properties of the material. Simultaneously, magnesium reduces the surface tension of the molten aluminum during infiltration by accumulating oxygen from the melt surface and forms $MgAl_2O_4$ spinel. The reaction results in attenuating the oxide layer and act as driving force to promote wetting. Due to the poor solubility of carbon in aluminum the formation of brittle interfacial reaction like Al_4C_3 is recurrent in the aluminum carbon composites. The detrimental reaction product Al_4C_3 reduces the properties of the final composite by catastrophic crack propagation owing to its fragile nature. Studies shows that, when these kind of components are used in service, carbide phases present in it have the tendency to react with atmospheric moisture to form CH_4 resulting in porosity and cause failure to the composite.[186]

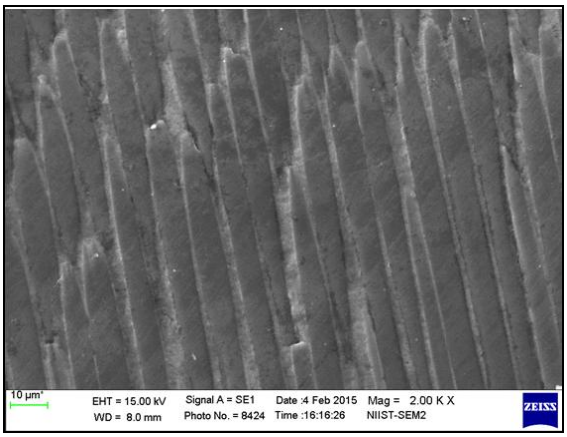

(a)

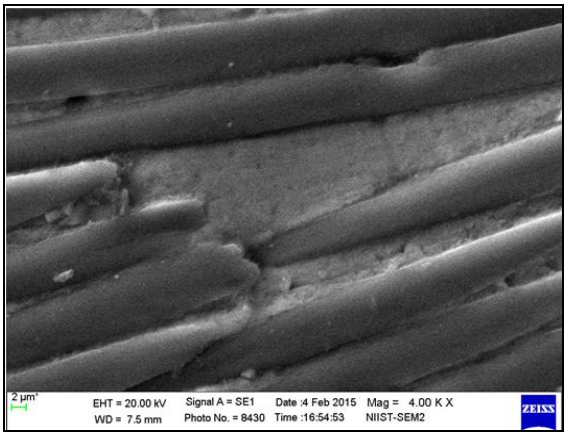

(b)

Figure 2.5. (a and b) SEM photo micrographs of carbon fiber mat reinforced aluminum matrix composite.

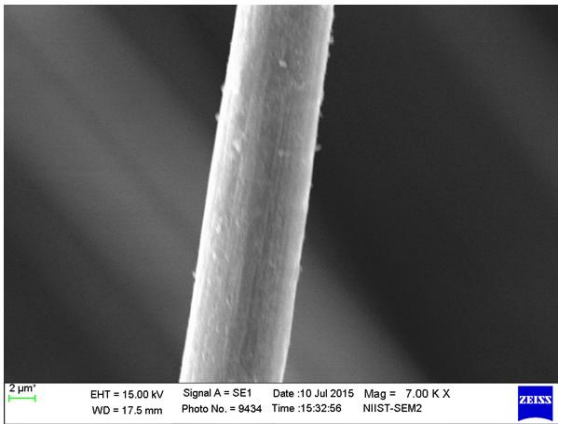

(a) **(b)**

Figure 2.6. (a) SEM photo micrographs and (b) EDX spectrum of extracted carbon fiber from the infiltrated composite.

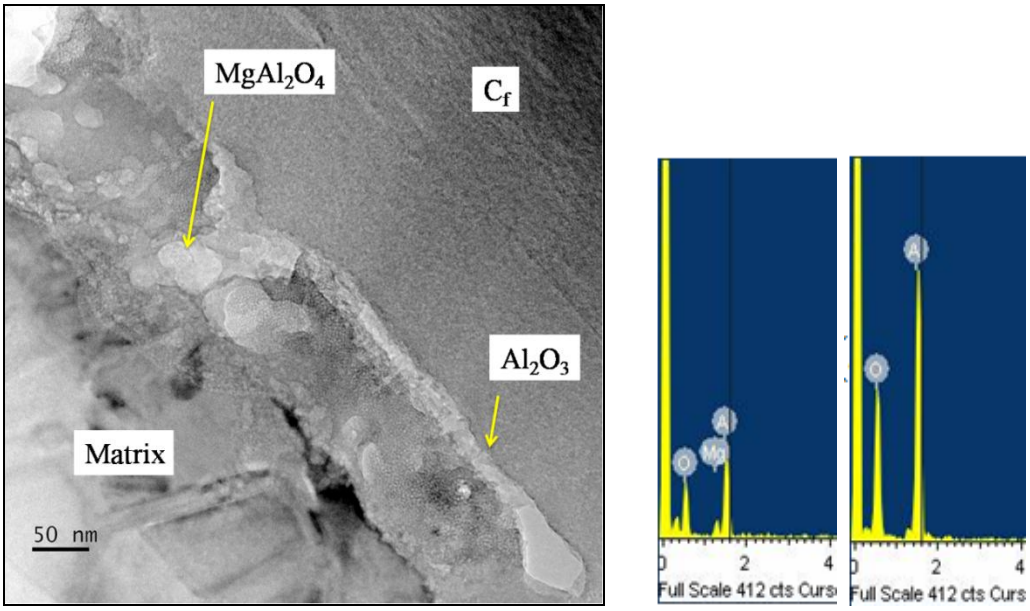

(a)

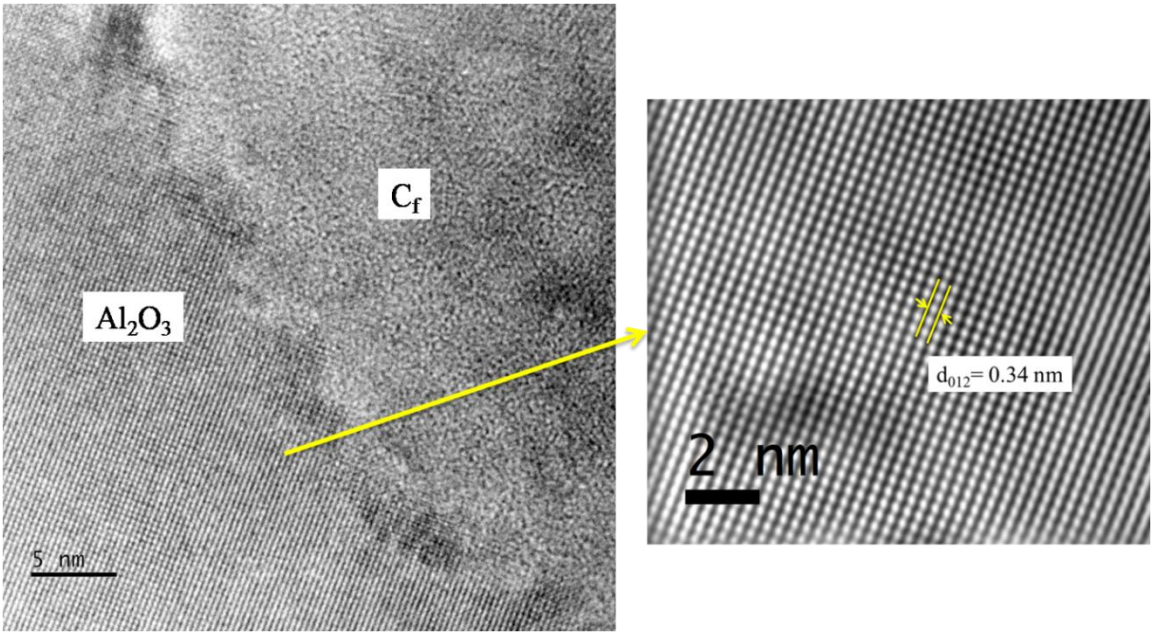

(b)

Figure 2.7. TEM observation of the interface region between C_f/Al6061 infiltrated composite. (a) Composite interface shows the presence of oxide layers like Al_2O_3, $MgAl_2O_4$ spinel and its corresponding TEM-EDS. (b) A high-resolution TEM image shows the crystalline lattice planes in Al_2O_3 formed at the C_f/Al6061 interface.

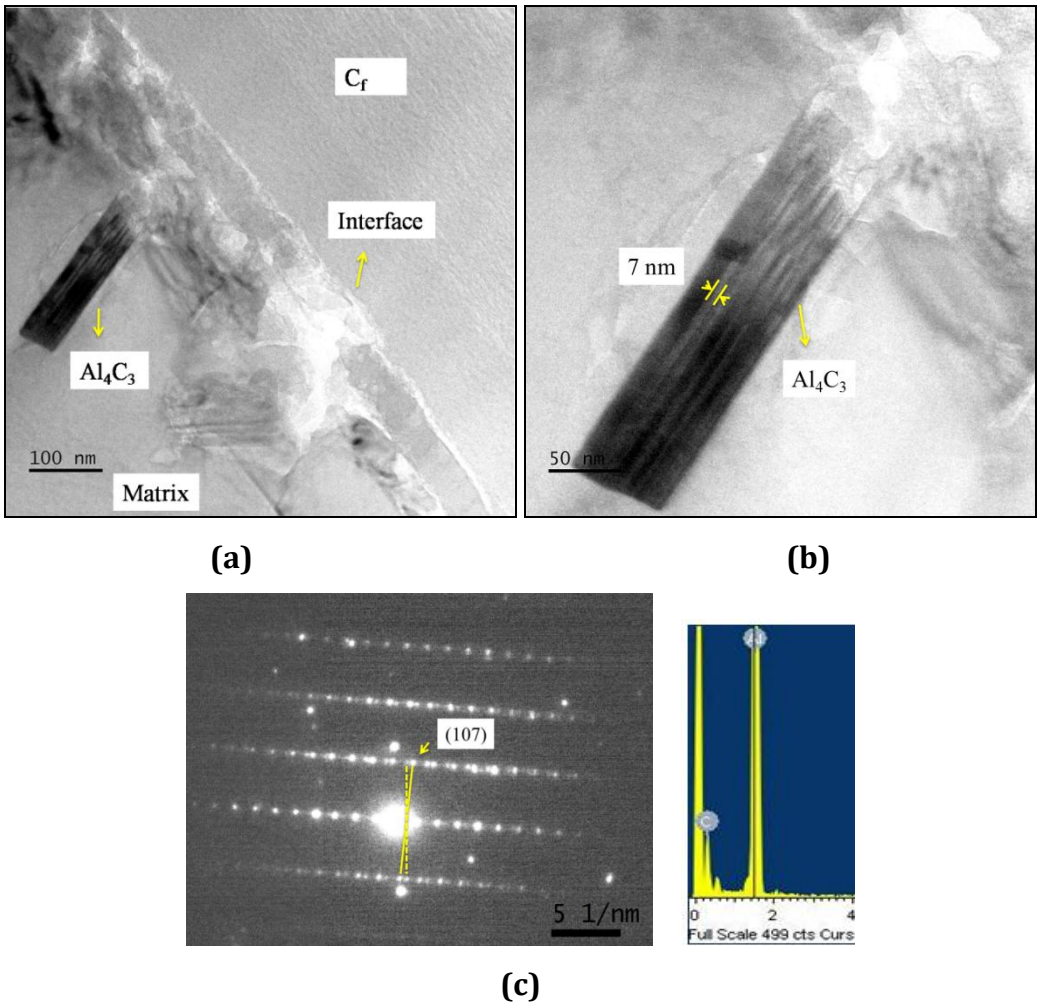

Figure 2.8. Recognition of Al_4C_3 crystals. (a) TEM image of the reaction product Al_4C_3 at the Al/fiber interface. (b) A high magnification image shows the twinned carbide crystal texture, (c) SAD pattern of Al_4C_3 phase and its EDS.

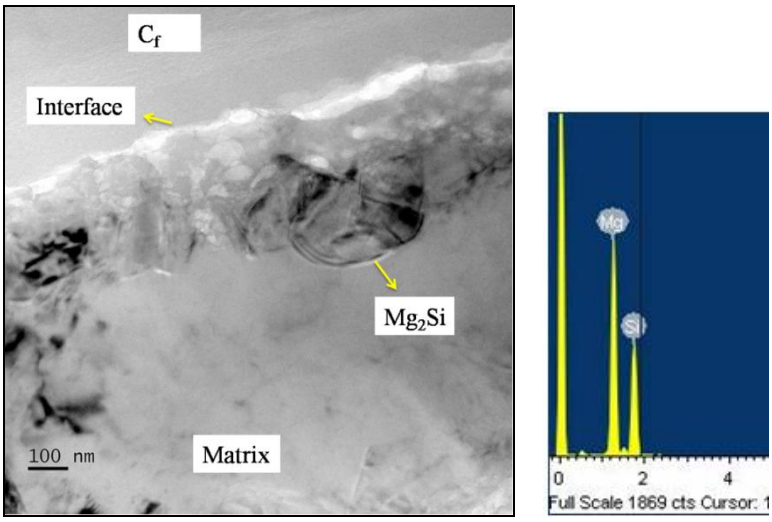

Figure 2.9. TEM image shows the precipitation of Mg_2Si at the composite interface and its corresponding TEM-EDS.

Hence, the growth of Al_4C_3 in this study is controlled by the optimized infiltration process parameters like temperature, pressure and dwell time and also the presence of $MgAl_2O_4$ spinel, Al_2O_3 and $Al_{12}Mg_{17}$ intermetallic, which protects the carbon fiber from the formation of deleterious interfacial reaction product, Al_4C_3. Also the prospect of Al_4C_3 needle formation escalates if the melt temperature is high and cooling rate is slow. The high heat transfer coefficient of squeeze infiltration technique increase the cooling rate and the possibility of Al_4C_3 evolution is less.

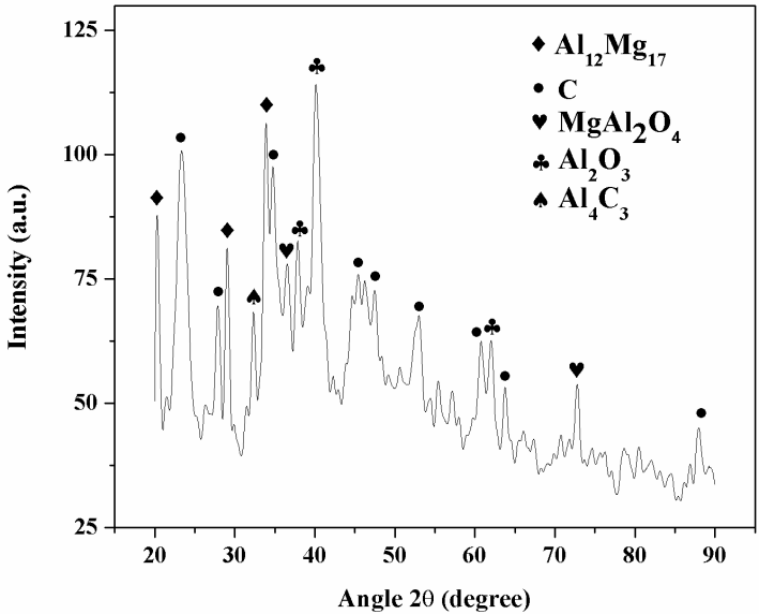

Figure 2.10. XRD pattern of extracted fibers from the infiltrated composite using NaOH solution showing interfacial reaction products.

2.3.3. Thermal and Physical Characteristics

Figure 2.11 showed the TGA curve of surface treated carbon fiber to evaluate the thermal stability of the material. The carbon fiber is stable during heating in air atmosphere till 600 °C and the rapid decomposition occurs after that. Instability of carbon fiber above 600 °C is due to the oxidation of carbon, as the temperature increases the rate of fiber oxidation also increases simultaneously. Hence the preform preheating and metal infiltration can be carried out below the decomposition temperature in air atmosphere. Higher temperature can be used only if it is carried out in inert or vacuum atmosphere.

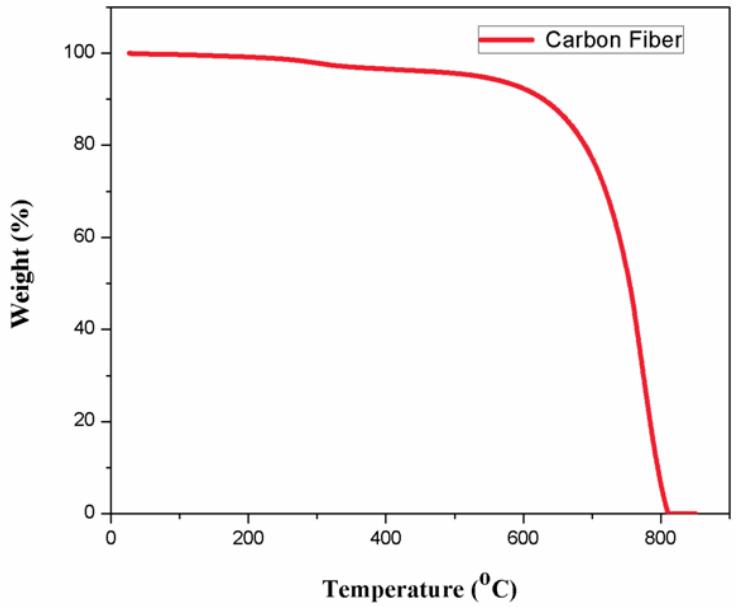

Figure 2.11.TGA curve of carbon fiber.

Differential thermal analysis (DTA) of the alloy and composites (Figure 2.12) are done to transpire the phase transformation and the onset temperature at which it eventuate, area under the peak is the change in enthalpy. The major endothermic peak at 660 ˚C corresponds to L → α-Al dendrites due to the melting of aluminum matrix.

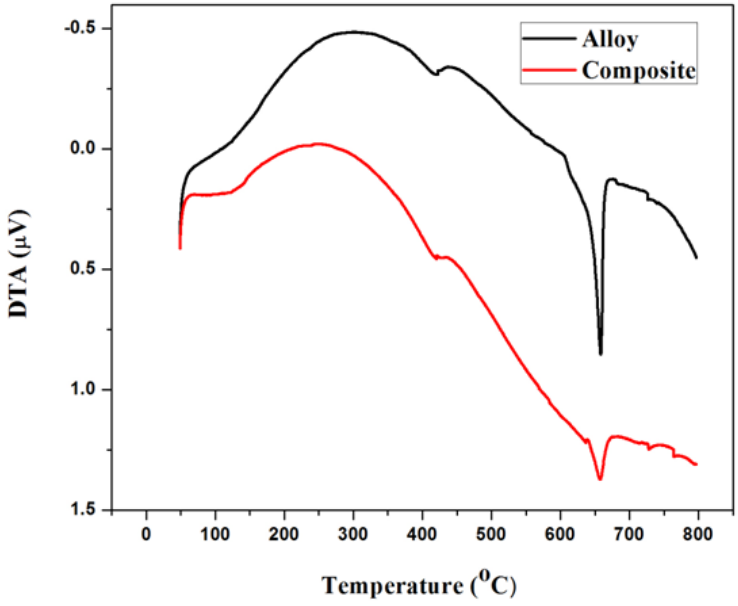

Figure 2.12.DTA of unreinforced squeeze cast Al6061 alloy and infiltrated composite.

The density of the woven carbon fiber fabric reinforced aluminum matrix composite sample is 2.16 g/cm^3 which is lower than those of the monolithic alloy (2.7 g/cm^3). The reduction in density is due to synergisitc effect of lower density of carbon fiber (1.8 g/cm^3) with matrix alloy in the composite. The volume percentage of carbon fiber determined by extraction method shows 63% of fiber in the infiltrated composite. The electrical resistivity measured by four probe method of base 6061 alloy is 3.1 x 10^{-8} Ωm and for the carbon fiber infiltrated 6061 aluminum composite is 18.8 x 10^{-8} Ωm.

2.3.4. Mechanical Characteristics

The hardness value of unreinforced squeeze cast alloy and composite tested by Brinell hardness tester is shown in histogram (Figure 2.13). Carbon fiber reinforced composite manifest superior hardness properties in both top surface and cross section when compared to base alloy. The existence of hard and stiff carbon fiber in the matrix shares the load generated from the indenter and being a continuous fiber it act as a fence to matrix dislocation. The base alloy without reinforcement is relatively softer compared to the reinforced composite and it undergoes plastic deformation easily. Further it is observed that the top surface of the composite give higher hardness value compared to cross section in the composite. This may be due to higher resistance offered by both longitudinal and transverse oriented fibre at the top surface and in the later case only longitudinal orientation of fibre will give resistance for the indenter

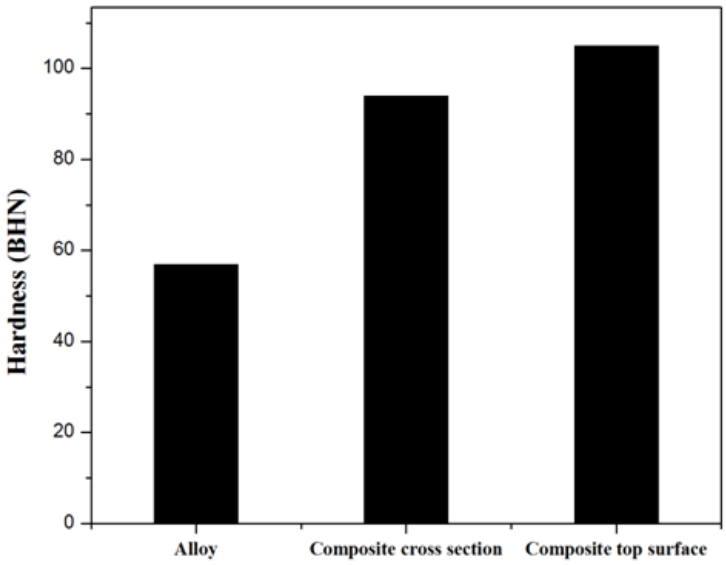

Figure 2.13. Hardness properties of unreinforced squeeze cast Al6061alloy and squeeze infiltrated composite.

The average compressive strength in cast condition obtained for BD C_f/Al 6061 composite is 290 MPa, which is considerably higher than that of the unreinforced alloy (223 MPa). The supplement of bidirectional woven carbon fiber in the matrix enhance the compressive strength of the composite by holding the load in both the directions due to the nature of fiber orientation there by restrain the matrix plastic flow behavior. Figure 2.14a and b shows the compressive stress-strain curve and fractograph of compression test sample of squeeze infiltrated C_f/Al 6061 composite. The compression test curve showed a rise in stress during the fracture after barreling due to the resistance to deformation offered by the longitudinal fibers. The SEM image showed one of the longitudinal layer gets compressed when load is applied and gets fractured after withstanding the compression load, the next transverse layer slides off after delamination of the fiber from the matrix during compressive loading.

The ultimate tensile strength of as cast infiltrated composite is 101 MPa. Whereas the squeeze cast alloy under similar condition give a UTS of 189MPa. In composite, during tensile loading the reinforced fiber aligned towards the tensile axis bears the load and the fiber oriented in the transverse direction bears very minimum load. The fracture surface (Figure 2.15a and b) of the composite tensile specimen exhibits two modes of fracture viz., the ductile fracture by matrix and brittle fracture by the reinforcement. Figure 2.15a showed the fractograph of bidirectional fiber region of both interfacial delamination of transverse oriented fibers and breakage of longitudinal oriented fibers with respect to tensile loading direction. The interfacial delamination of transverse oriented fibers contributes to lowered tensile values in BD C_f/Al 6061 composites. The fractograph of longitudinally oriented fibers in the composite is shown in Figure 2.15b, where the well infiltrated matrix alloy region looks ductile and surface appears smooth and silky due to plastic nature of the material, while brittle fracture is observed in reinforced fiber surface. Crack initiation and crack propagation is observed around the carbon fiber leading to the interfacial debonding of carbon fiber from the matrix material, which in turn acts as one of the fracture initiation point during tensile loading in these composite. The necking of ductile infiltrated metal matrix region around the carbon fiber leads to the

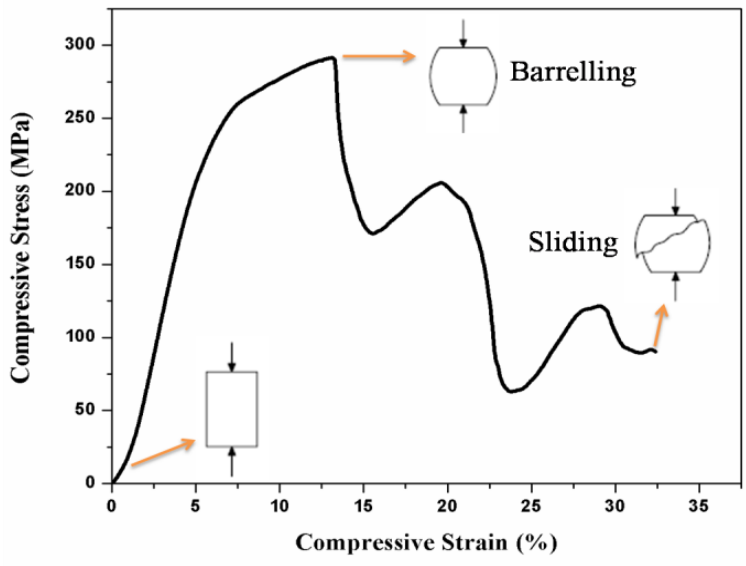

(a)

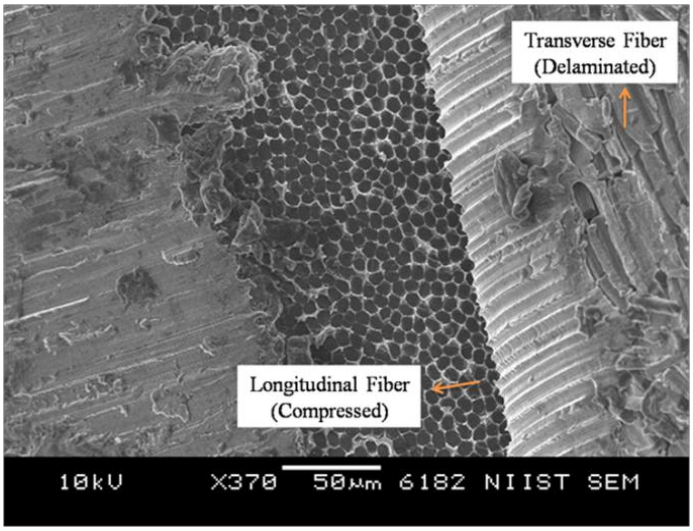

(b)

Figure 2.14. (a) Compressive stress-strain curve (b) SEM photomicrograph of compression test specimen fracture surface of squeeze infiltrated C_f/Al 6061 composite.

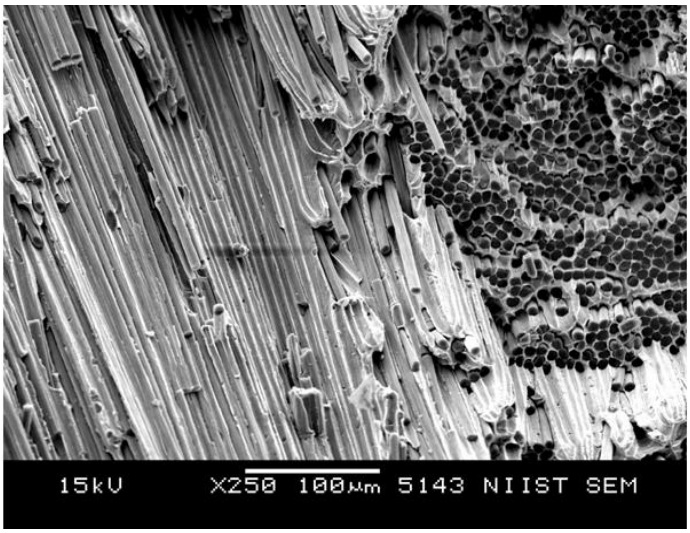

(a)

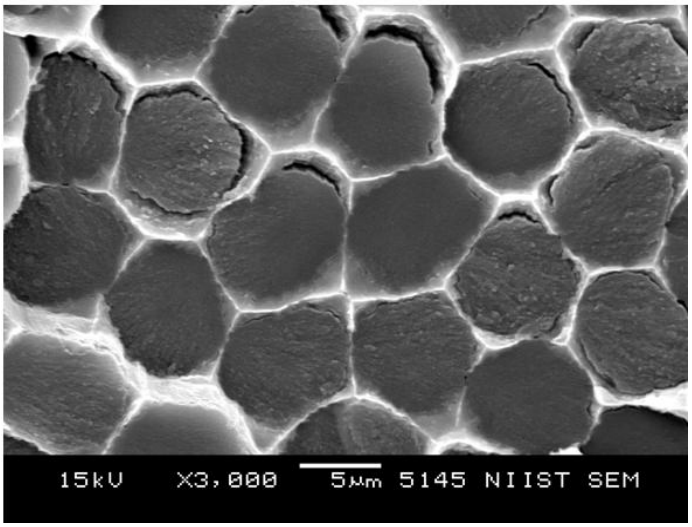

(b)

Figure 2.15. SEM photomicrograph of tensile fracture of squeeze infiltrated C_f/Al 6061 composite (a) Fracture surface showing bidirectional fiber region of both interfacial delamination of transverse oriented fibers and breakage of longitudinal oriented fibers with respect to tensile loading direction (b) Fractograph showing fracture surface of infiltrated composite with longitudinally oriented carbon fiber.

narrow cell wall type morphology resembling the honeycomb structure. The carbon fiber shows a brittle failure once the tensile load reaches the maximum.

2.3.5. Tribological Characteristics

The pin on disk wear behavior of unreinforced Al 6061 squeeze cast alloy and BD C_f/Al 6061 composite with respective to constant velocity and variation in load is shown in Figure 2.16a. The wear rate of unreinforced squeeze cast alloy at 2m/s increases enormously with increase in load owing to the generation of higher temperature, which leads to thermal softening and plastic deformation of the material caused by shear stress at higher load. The unreinforced alloy experiences a galling seizure above the load of 40 N followed by heavy noise, vibration and transfer of the pin material to the counter surface, consequently the tests were stopped. The mild wear to sever wear transition occurs at 30 - 40 N load in the case of unreinforced alloy whereas the composite shows the mild wear regime even up to 50N. The wear rate of CF fabric/Al composite is phenomenally lower than the base alloy due to the incorporation of carbon fiber there by suppressing the transition to a severe wear rate. The curves of composite for 2 m/s and 4 m/s overlap each other due to the spacing of ordinate scale while considering the weight loss of alloy, which was much higher when compared to that of composite. Figure 2.16b shows the extensive graph of the composite for 2 m/s and 4 m/s and it can be attributed from the curve that increasing the load in 2 m/s and 4 m/s velocities results in increased but negligible weight loss due to the intensity of heat generated.

Figure 2.16c presents the effect of variation in velocity at constant loads on the wear of C_f/Al 6061 composite. In this case also the composite shows extreme wear resistance at increase in velocity with constant loads of 30 N and 50 N, however imperceptible amount of wear loss is observed in the composite by increasing the sliding velocity in both the conditions. The incorporation of carbon fiber in the matrix alloy yields a self-lubrication phenomenon on the friction surface, by the formation of a lubricating tribolayer intercepting the matrix metal to counter surface contact. Additionally, the major portion of the stress concentration during friction is conveyed by the carbon fiber in the composite there by reducing the severe plastic deformation of the soft matrix alloy.

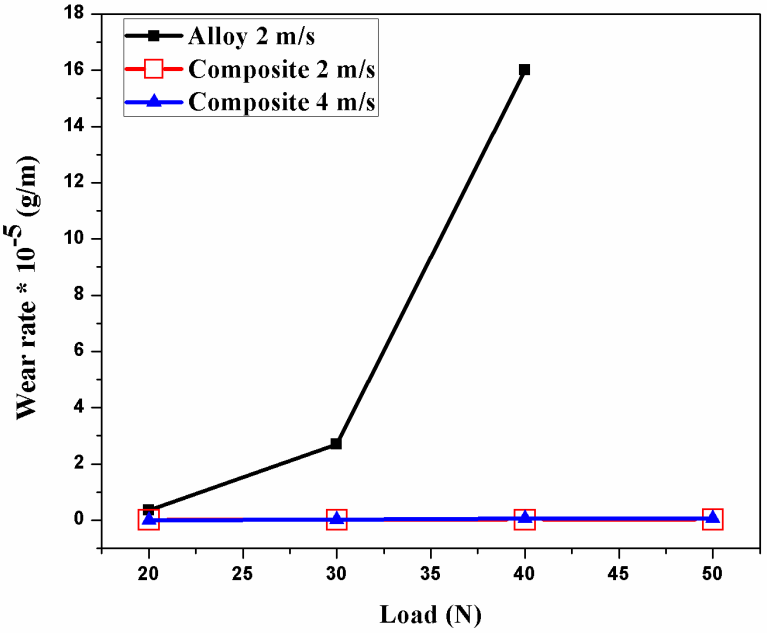
Alloy 2 m/s
Composite 2 m/s
Composite 4 m/s
Wear rate * 10-5 (g/m)
Load (N)
0
2
4
6
8
10
12
14
16
18
20
25
30
35
40
45
50

(a)

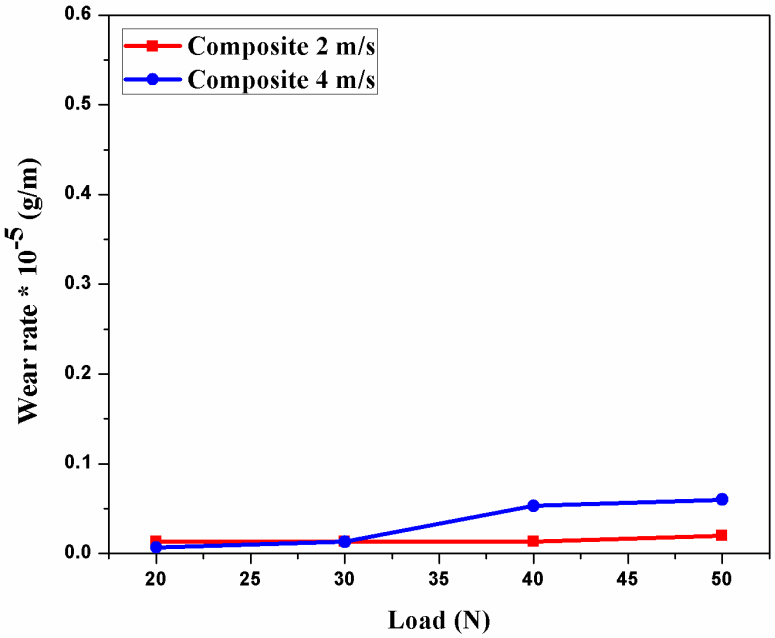
Composite 2 m/s
Composite 4 m/s
Wear rate * 10-5 (g/m)
Load (N)
0.0
0.1
0.2
0.3
0.4
0.5
0.6
20
25
30
35
40
45
50

(b)

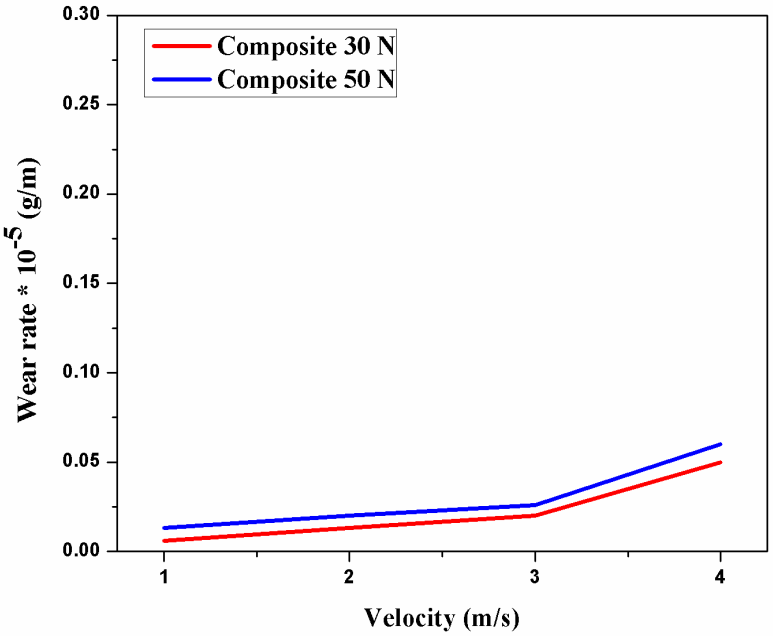

(c)

Figure 2.16. Wear rate of (a) unreinforced squeeze cast alloy and C_f/Al 6061 infiltrated composite with respective to constant velocity and variation in load (b) extensive graph of the composite at constant velocity and variation in load (c) effect of variation in velocity at constant load on the wear of composite.

The SEM characterization of the worn surfaces of the unreinforced squeeze cast alloy sliding at constant velocity in varying load in room temperature is shown in Figure 2.17. From the micrograph it can be revealed that squeeze cast alloy undergoes shallow and wider grooves (marked as G) with material flow (MF) at a speed of 2 m/s at 20 N load (Figure 2.17a). A severe shearing is observed in alloy by increasing the load of 30 N (Figure 2.17b) with deeper grooves (marked as DG), surface deformation and the wedges of damaged material regions (marked as W) along the sliding directions. The degree of surface delamination of materials as wedges extents due to the propagation of the surface cracking (arrow marked). During the wear mechanism, the cyclic stresses induced due to frictional force under varying load conditions leads to rise in the degree of heat expelled between the surfaces. Obviously the alloy loses its toughness and yield strength due to repeated thermal stress and undergoes heavy plastic flow of the material.

Figure 2.18 shows the worn surface of the C_f/Al composite at constant velocity in varying load, which seems to be relatively smoother compared to alloy

with the formation of tribolayer or mechanically mixed layer (MML) on the sliding surface. The remarkable termination of cracking and delamination phenomenon is observed on the worn surface of the composite. It can be depicted from the micrograph that there is no debonding of carbon fiber from the matrix during friction that insight the strength of the interfacial bonding. Even at higher load the composite manifest good wear resistance and also all the wear tracks are almost same irrespective of load conditions. A trivial amount of matrix and fiber loss is observed in composite at increase in load for 2 m/s and 4 m/s velocities may be attributed to the nature of plastic flow at higher load. The orientation of carbon fiber with respect to sliding direction plays an important role in the wear resistance of the composite. Similar observation has been depicted in the investigation on Al_2O_{3f}/SiCp/Al hybrid composites.[187]

The worn surface of the composite at constant loads with varying sliding velocity in Figure 2.19 also delineate the formation of lubrication film with relatively flat surface compared to alloy. It can be observed that small kind of granules are formed between and above the fibers, which can be ascribed to the plastic deformation of the metal that covers the carbon fiber when it comes in contact with the rotating counter disc. The degree of metal granules increases with increase in velocity in both the load conditions is due to the frequent contact surface of the composite pin on the counter disc causing rise in localized surface temperature. The large platelets of the lubrication film (MML) gets broken, separated and equally distributed (Figure 2.19b) on the friction surface of the composite as a wear resistance tribolayer.

The evolution of tribolayer or MML at the interface of the two frictional materials makes the C_f/Al 6061 composite superior wear resistance compared to unreinforced alloy. Figure 2.20a portrayed the distinct formation of lubricating tribolayer spreads over the sliding surface of the composite. The PAN based carbon fiber has the enhanced susceptibility to perform the self-lubricating phenomenon due to its turbostratic structure in which the aromatic sheets of planes (similar to graphite) are randomly oriented. In hexagonal graphite structure the aromatic sheets containing carbon atom sits on the centre of the hexagon of the adjacent plane and the orientation is uniform. The carbon atoms connected in each planes are strong covalent bond, however due to the longer

interspacing between the adjacent planes the bonding between them is weak van der waals bonding. Carbon elevates its self-lubricating advantage by van der waals debonding, so that easy slip and transfer of one plane over another happens.[188] The adsorption of water vapor on the carbon surface increases the lubrication process by weakening the interspace bonding energy between the planes.[189] Owing to the random orientation in turbostratic structure, the interspacing between the planes of aromatic sheets in PAN based carbon fiber becomes further longer compared to hexagonal graphite structure. The increase in interspacing of planes weakens the bonding between adjacent planes on a great extent thereby improving the gliding of planes one over the other, promoting and enhancing the self-lubrication feature. During wear, the carbon fiber interacts with moisture from the atmosphere causing the interspacing bonding between the carbon atom planes fragile. As a result surface plane of the carbon fiber starts shearing and gliding and these joined to form a solid lubricant film (tribolayer).The developed tribolayer is directly proportional to the volume fraction of the carbon fiber. The lubricant gets spread on the sliding surface of the composite there by improving the wear resistance, as a result of hindering the metal to metal contact on the friction surface. EDS analysis on the layer above the surface of the Carbon fiber/Al composite (Figure 2.20b) imparts the presence of carbon, aluminum, chromium, iron and oxygen. The emergence of lubricating layer (MML) is confirmed by the presence of oxidation reaction and other elements present in the layer on the sliding surface of the composite.

2.3.6. Corrosion Analysis

2.3.6.1. Electrochemical Method

Electrochemical workstation was used for the measurement of corrosion potential and corrosion current of unreinforced squeeze cast alloy and the infiltrated composites through the extrapolation of anodic and cathodic Tafel lines. The potentiodynamic polarization curves (Figure 2.21) shows that the alloy has a corrosion potential (E_{corr}) value of (-0.87 V) to that of composite (-0.83V). From the polarization measurements the corrosion current density (i_{corr}) value of the composite (15 μA/cm^2) seems to be slightly higher when compared to the (i_{corr}) value of the unreinforced alloy (7μA/cm^2), indicating a comparable corrosion

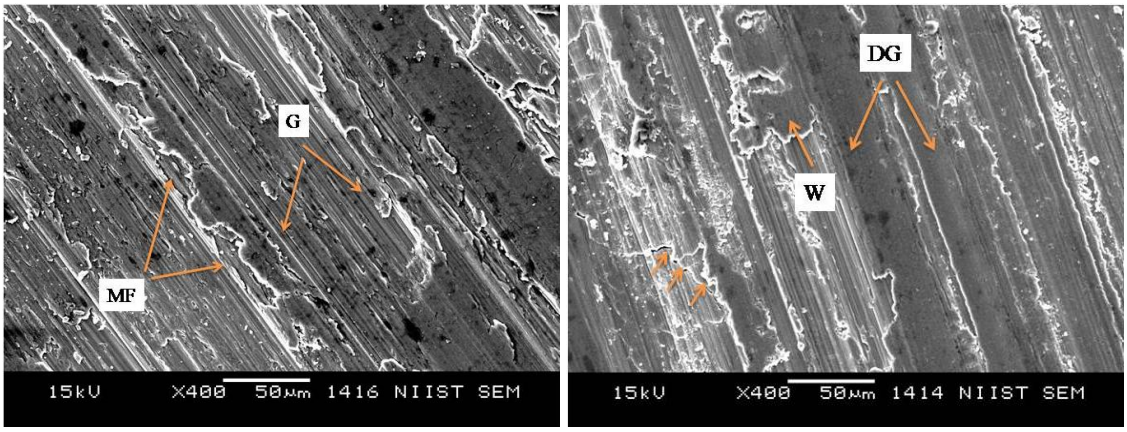

(a) **(b)**

Figure 2.17. SEM micrographs of worn out surface of squeeze cast Al6061 unreinforced alloy with respective to variation in load at constant velocity (a) applied velocity of 2 m/s in 20 N load and (b) 2 m/s in 30 N load.

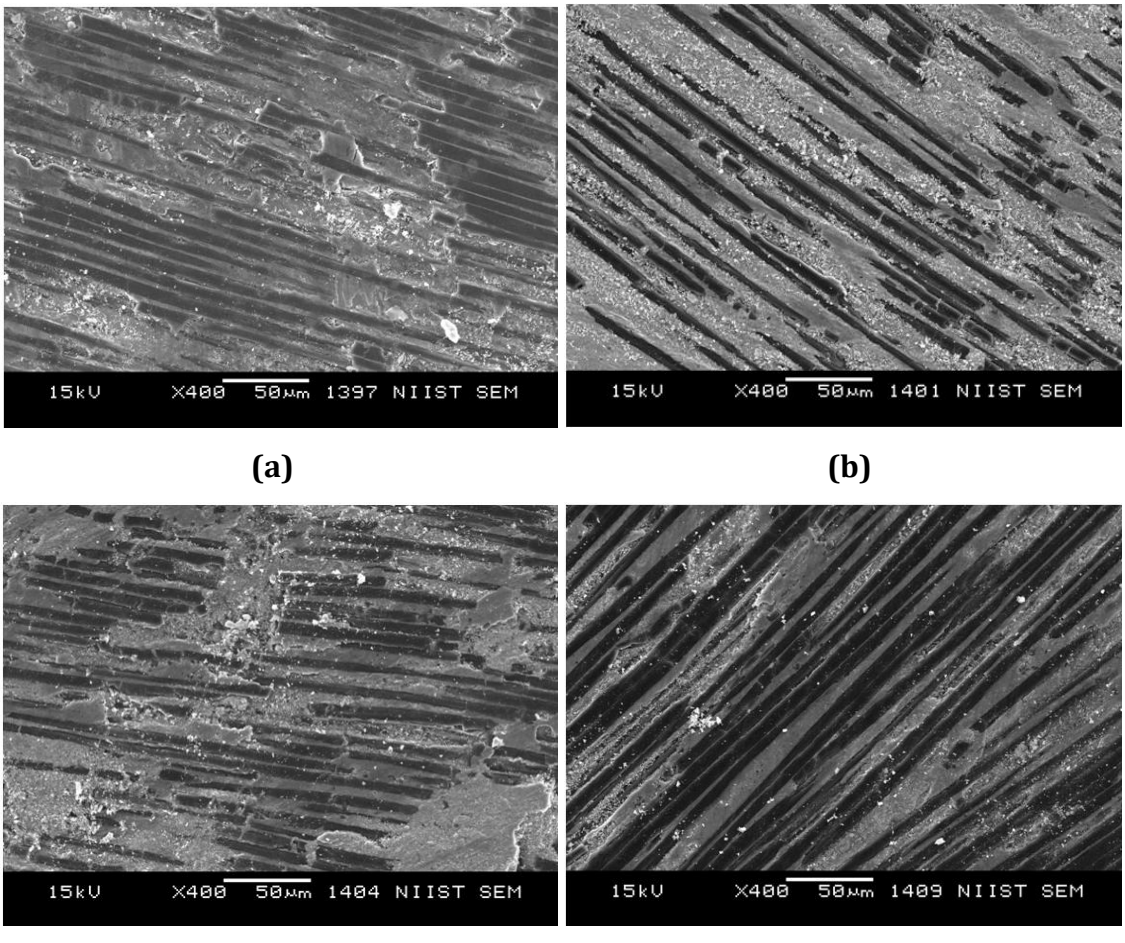

(a) **(b)**

(c) **(d)**

Figure 2.18. SEM micrographs of worn out surface of infiltrated composite with respective to variation in load at constant velocity (a) applied velocity of 2 m/s in 20 N load (b) 2 m/s in 50 N load (c) 4 m/s in 20 N load (d) 4 m/s in 50 N load.

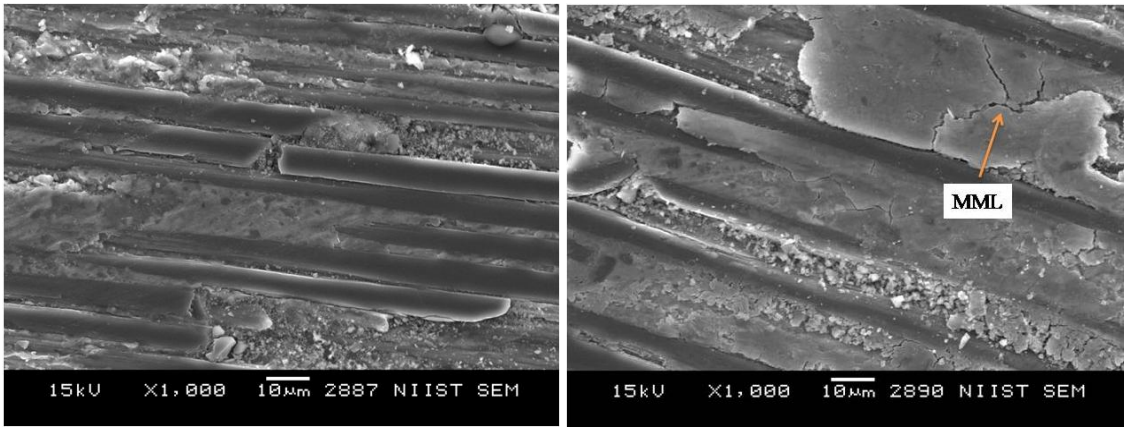

(a) **(b)**

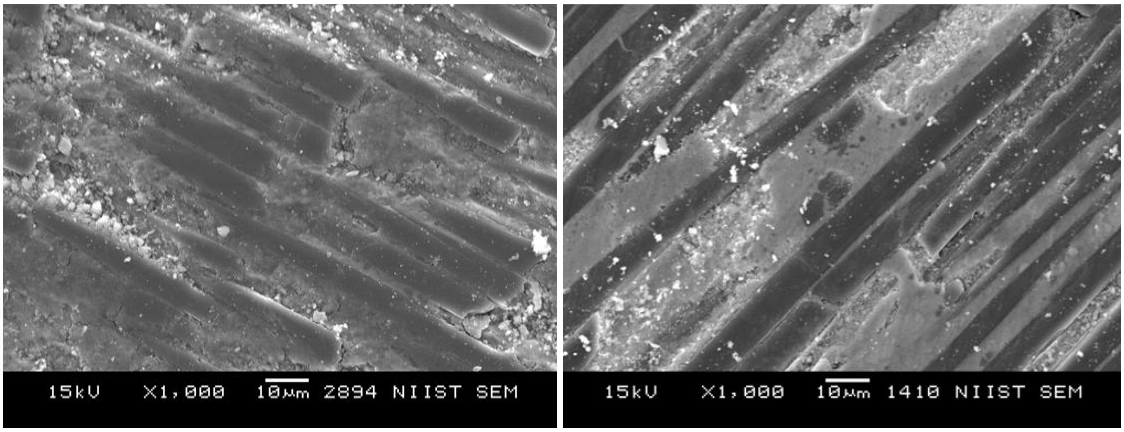

(c) **(d)**

Figure 2.19. SEM micrographs of worn out surface of composite with respective to variation in velocity and constant load (a) applied load of 30 N in 1 m/s velocity (b) 30 N in 4 m/s velocity (c) 50 N in 1 m/s velocity (d) 50 N in 4 m/s velocity.

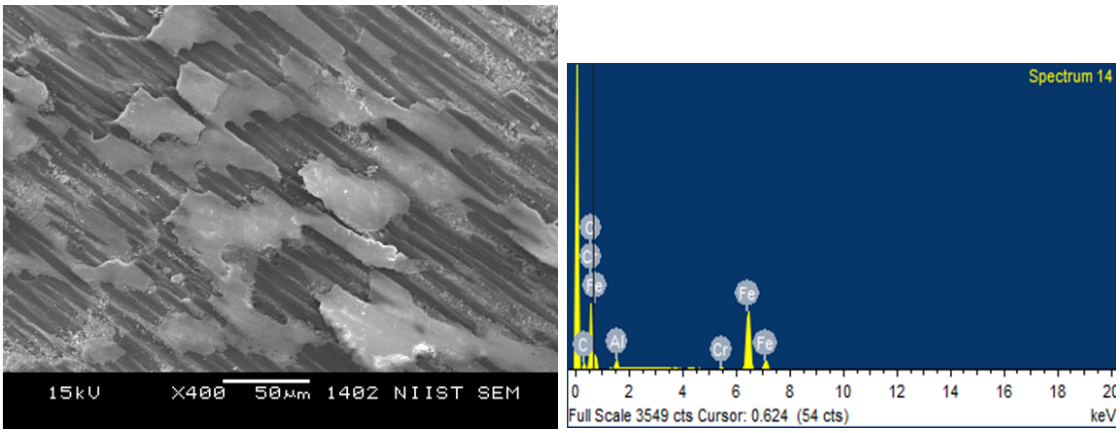

(a) **(b)**

Figure 2.20. (a) SEM photomicrographs and (b) EDX spectrum of self-lubricating tribolayer (MML) spreads over the sliding surface of the composite.

characteristics of composite with the alloy. The anodic polarization curve of the unreinforced alloy exhibits a small slope, may be due to the formation of strong passive oxide layer Al_2O_3. The variation in the corrosion behavior of composite is due to the potential difference at the matrix reinforcement interface.

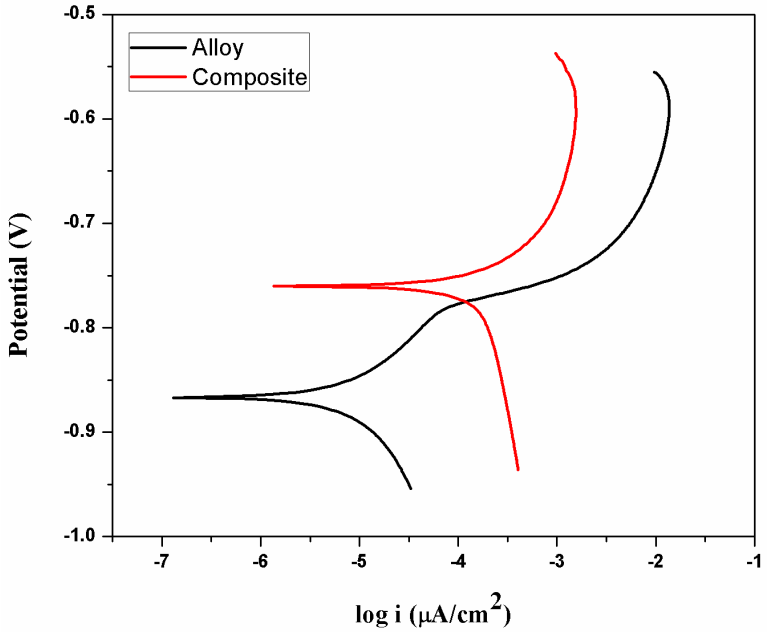

Figure 2.21. Potentiodynamic polarizations curves of Al6061 squeeze cast alloy and squeeze infiltrated C_f/Al 6061 composite exposed to 3.5 wt.% NaCl aerate solution with calomel as reference electrode.

2.3.6.2. Immersion Test

Table 2.1 shows the corrosion rate of unreinforced squeeze cast alloy and the BD C_f/Al 6061 composite during immersion test.

Table 2.1: Corrosion rate of 6061 alloy and BD C_f infiltrated composite.

Sample	Exposure period (Days)	Weight Loss (g)	Corrosion rate (mm/year)
Alloy	7	0.0006	0.06
Alloy	14	0.0010	0.05
Alloy	21	0.0025	0.08
Composite	7	0.0100	1.3
Composite	14	0.0251	1.6
Composite	21	0.0507	2.2

It is observed that the corrosion rate of alloy is negligible and the trend is reduced with increasing the exposure time due to the formation of strong passive oxide layer. With increase in time to 21 days, the corrosion layer breaks and the corrosion tends to increase. The corrosion rate of carbon fiber reinforced aluminum composite seems to be higher compared to the unreinforced alloy due to galvanic corrosion and the trend is increased with increasing the exposure time. Figure 2.22 shows the SEM images of the surface topography of the corroded samples of alloy immersed for 7, 14 and 21 days. The formation of strong passive oxide layer (Al_2O_3) on the surface of the unreinforced alloy increases with increase in the exposure time.

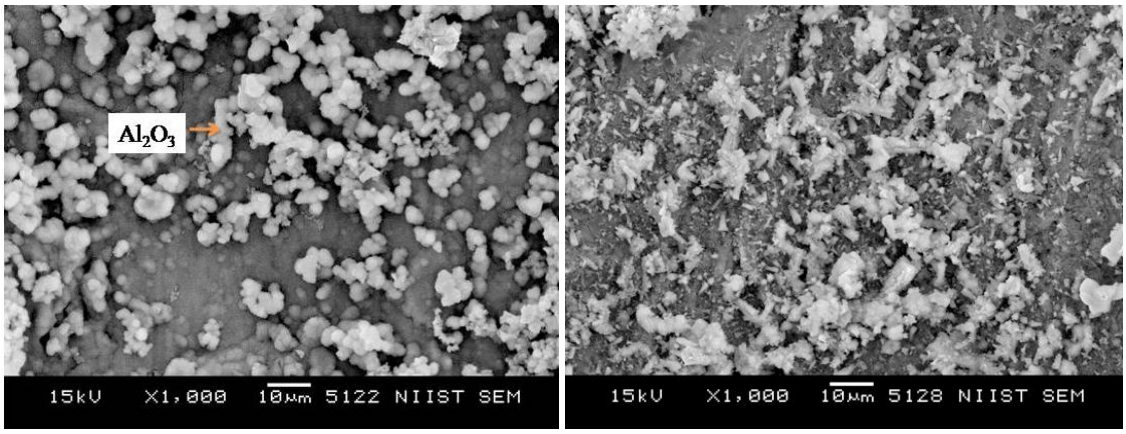

(a) **(b)**

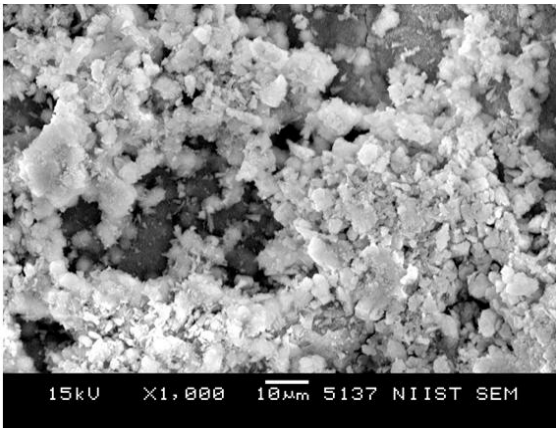

(c)

Figure 2.22. SEM photomicrographs of the surface topography of the corroded samples of Al6061 alloy immersed for (a) 7 days (b) 14 days (c) 21 days.

The carbon fiber reinforced aluminum matrix composite is more susceptible to galvanic corrosion due to the noble potential of carbon fiber, which act as a passive region. Aluminum alloy 6061 act as active region from which the flow of electrons and material loss takes place. From the Figure 2.23 it can be observed that the formation of oxide layer Al_2O_3 is less in composite compared to alloy due to the cathode (carbon fiber) to anode (alloy) volume ratio. Formation of crack and pitting is observed in the case of composite, ascribed to the removal of active 6061 aluminum alloy causing the carbon fiber to project outside. EDS spectrum on the top surface of the corrosion sample having the same morphology in alloy and composite confirms the presence of oxide layer Al_2O_3 (Figure 2.23d).

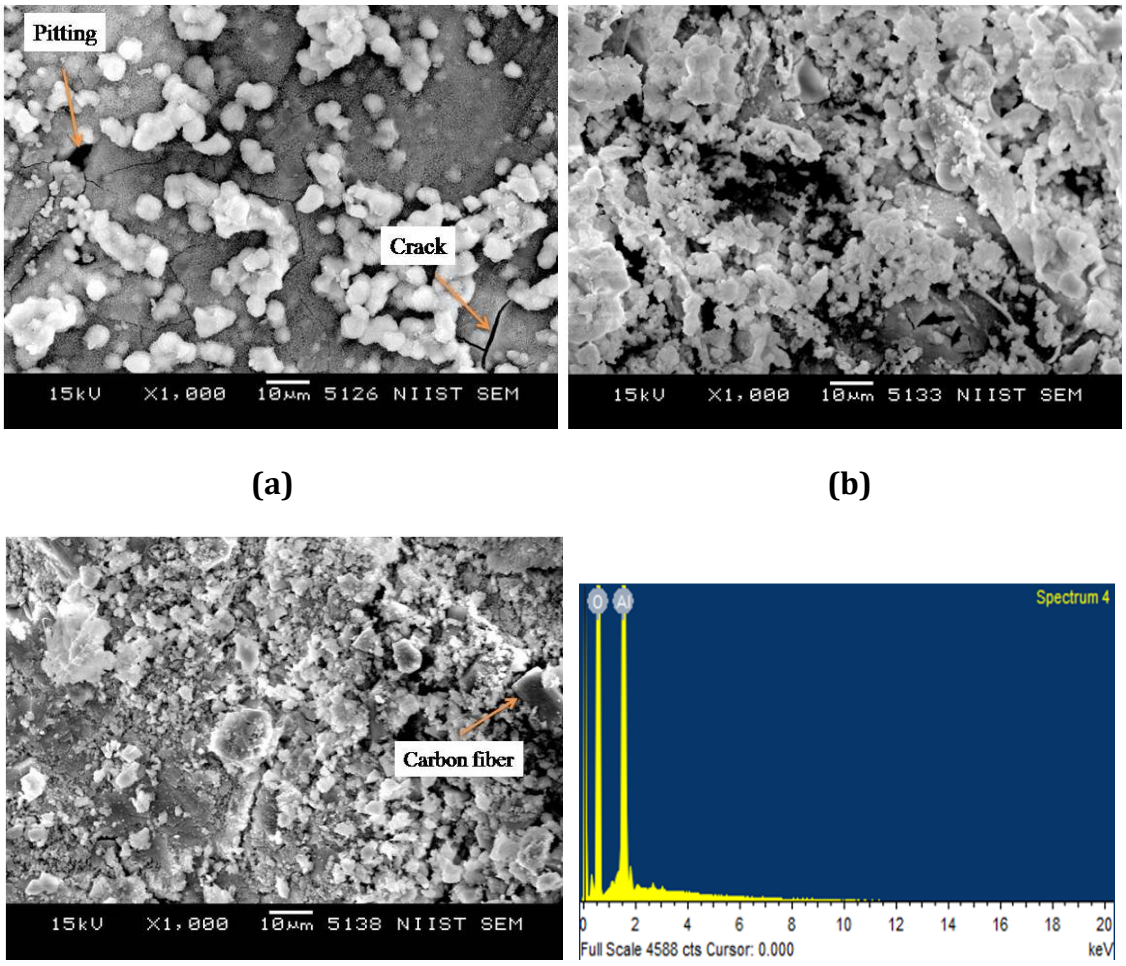

Figure 2.23. SEM photomicrographs of the surface topography of the corroded samples of C_f/Al6061 infiltrated composite immersed for (a) 7 days (b) 14 days (c) 21 days (d) EDAX spectrum of the oxide layer.

2.4. Conclusion

The carbon fiber woven fabric reinforced 6061 aluminum composite was successfully fabricated by direct squeeze infiltration process with high volume fraction and uniform distribution of carbon fiber in the matrix material. The major conclusions of the present investigation are:

- The composites have shown complete penetration of molten aluminum metal between each and every carbon fiber in the preform with perfect adhesion between the carbon fiber and aluminum. The elimination of porosities without fiber damage and free from agglomeration is maintained in the composite by the use of optimized process parameters during squeeze infiltration.
- The surface of the extracted carbon fiber from the infiltrated composite are found to be relatively smooth without any damage showing no remarkable interfacial reaction product of Al_4C_3. The major diffraction peaks observed in the XRD analysis were C, $MgAl_2O_4$ spinel, Al_2O_3 and $Mg_{17}Al_{12}$.
- HRTEM studies have shown the presence of Al_2O_3 and $MgAl_2O_4$ spinel at the interface between carbon fiber and the matrix thereby protecting the fiber from deleterious interfacial reaction of Al_4C_3. However, very few traces of Al_4C_3 crystals are observed at the interface.
- The lower density of 2.16 g/cm^3obtained for the woven carbon fiber fabric reinforced aluminum matrix composite is a major advantage for weight reduction compared to the monolithic alloy (2.7 g/cm^3).
- Electrical resistivity of carbon fabric reinforced composite increased significantly compare to the alloy.
- Al6061/C_f reinforced composite provide remarkable enhancement in hardness and compressive strength compared to unreinforced squeeze cast alloy. The tensile strength of the composite is reduced due to interfacial debonding of the transverse oriented fibers in the infiltrated composite.
- The tensile fractrograph of the composite shows multimode fracture of ductile matrix failure and brittle fiber breakage. Honey comb cell

morphology is observed around the longitudinal fiber due to the necking of ductile aluminum matrix.

- Carbon fiber mat reinforced aluminum composite exhibits remarkable wear resistance compared to unreinforced squeeze cast alloy due to self-lubricating phenomenon of carbon fiber thereby developing tribolayer (MML) on the friction surface.
- Electrochemical and Immersion corrosion studies reveal that the carbon fiber reinforced composite shows slight reduction in corrosion resistance compared to base squeeze cast alloy. The formation of strong passive oxide layers are observed in alloy. Galvanic corrosion is observed in the case of composite with the formation of crack.

Chapter 3

Structure and Properties of Squeeze Infiltrated Zirconia Grade Aluminosilicate Short Fiber Reinforced Aluminum Composites

Abstract

Squeeze infiltration process is successfully adopted to develop Al6061 metal matrix composite reinforced with zirconia grade aluminosilicate fiber using 15 and 20 vol% preforms. Composites microstructure depicts uniform distribution of fiber throughout the matrix with the elimination of preform breakage, porosities, and shrinkage. TEM observation shows the formation of Al_2O_3 at the interface, which controls the chemical interaction between the matrix and the fiber. Infiltrated composite shows enhanced wear resistance behavior compared to that of base alloy, and it improves with the increase in volume fraction of the reinforcement. However, sliding speed overcomes the volume fraction concept in improving the wear resistance of the composite by the quick formation of mechanically mixed layer (MML) at increased sliding speed. The tensile and impact strength of the base alloy is slightly higher than that of the composite due to its ductile nature. Incorporation of fiber in the matrix improves the CTE, hardness, compression and corrosion properties of the composite.

3.1. Introduction

Discontinuous aluminosilicate fiber reinforced Al MMC find wide applications for engineering components in aerospace, automotive, defense, electronics and general engineering sectors due to its high specific strength, wear resistance, low CTE and product cost.[190-191] The low cost of aluminosilicate fiber makes this material as a prime reinforcement for the fabrication of MMC with performance comparable to other short fibers like carbon, alumina and SiC.[192] Aluminum alloys are considered to be one of the finest matrix materials for MMC due to its ductility, low density, high specific strength and corrosion resistance characteristics. Various processing methods have been developed for the

fabrication of fiber reinforced metal matrix composites like infiltration, stir casting, electromagnetic casting, etc.[46,171,193,194] Due to a series of distinct advantages, squeeze infiltration method stands out to be an economic and efficient method for the fabrication of fiber reinforced composite. Squeeze Infiltration process comes under the classification of liquid state fabrication method in which the reinforcing phases are constructed into a high dimensional interconnected porous body called preform, followed by liquid metal infiltration through the preform under pressure.[85-195] The poor wettability and chemical reaction between the reinforcement fiber and the molten matrix metal can be avoided by supplying external pressure and with enhanced processing speed, which last for few seconds. The advantages of infiltration process are its ability to form selectively reinforced composite, refined microstructures due to high solidification rate, eradication of shrinkage and porosities since solidification under squeeze pressure and uniform microstructure due to the use of a highly ordered inceptive preform.[78-196] Aluminum and magnesium alloys have been successfully infiltrated into the coated and non- coated carbon fiber, alumina fiber, and saffil fiber preforms by pressure infiltration technique.[96,197,198] Clegg et al. reported that the Al-saffil fiber composite produced by squeeze infiltration process exhibits strong fiber/ matrix bond, which helps in improving the load transfer capability of the fiber from the matrix material during service conditions thereby improving the mechanical and tribological properties of the material.[199] Friend et al. identified that the incorporation of alumina short fibers into the aluminum alloy had a significant effect on altering the age hardening characteristics of the matrix.[200] Wu et al. reported that the incorporation of aluminosilicate fiber in the aluminum matrix by squeeze infiltration process reduces the formation of microcracks on the worn surface by preventing plastic deformation, thereby improving the wear resistance of the composite during high temperature wear tests.[201] However, studies on cost effective zirconia containing aluminosilicate fiber reinforced aluminum matrix composites by squeeze infiltration process are limited.

In the present study, attempts are made to fabricate Al6061/aluminosilicate composite by squeeze infiltration process using low-cost zirconia grade aluminosilicate fiber preform with 15 and 20 vol% and to evaluate the structure and properties of the composite. The controlled process parameters

of molten metal temperature, preform and die preheating temperature, dwell time and applied squeeze pressure are used for the infiltration of liquid aluminum into the aluminosilicate fiber preform. The samples are subjected to structural, physical, mechanical, tribological, interfacial and corrosion characteristics.

3.2. Experimental Procedure

3.2.1. Processing of Al6061/Aluminosilicate Fiber Infiltrated Composite

Al6061 alloy supplied by Sargam Metals, India was chosen as the matrix material and the chemical composition of the alloy is given in Table 3.1.

Table 3.1: Composition of 6061 alloy.

Component	Mg	Si	Cu	Zn	Ti	Cr	Fe	Mn	Al
Amount (wt%)	1.2	0.8	0.40	0.25	0.15	0.35	0.7	0.15	Rest

Discontinuous zirconia grade aluminosilicate fiber preforms with the volume percentage of 15 and 20% (M/s Murugappa Morgan Thermal Ceramics Ltd., Chennai, India) were chosen as the reinforcement with an average fiber diameter of 5 μm. The properties and chemical composition of reinforcement were given in Tables 3.2 and 3.3.[202]

Table 3.2: Properties of zirconia grade aluminosilicate fiber.

Properties	**Value**
Melting point, ^{o}C	1650
Density	2.6 g/cc
Fiber diameter, μm (arithmetic means)	5

Table 3.3: Composition of zirconia grade aluminosilicate fiber.

Constituents	**Percentage %**
Al_2O_3	32 to 36
SiO_2	44 to 48
ZrO_2	16.5 to 19.5
Others	traces

Direct squeeze infiltration technique was adopted for the development of Al6061/aluminosilicate fiber reinforced composite using a die of 120×50×60 mm cavity fabricated using tool steel (Figure 3.1). The present die is designed and fabricated with close clearance in order to aid complete infiltration of liquid metal without any splashing.

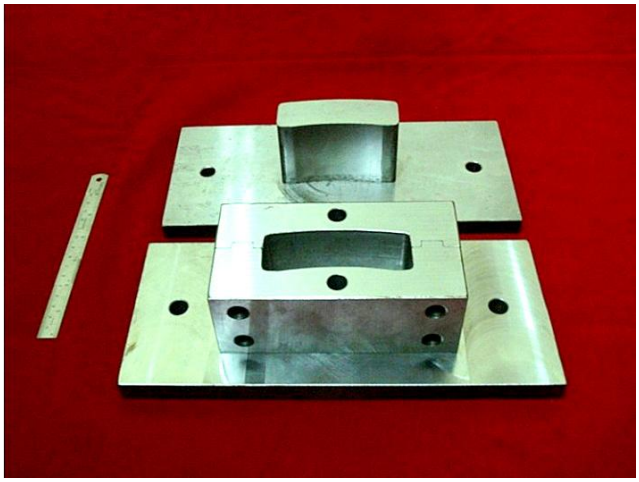

Figure 3.1. Die used for squeeze infiltration process.

The important process parameters followed for the infiltration process are given below. The preform was preheated to a temperature of 430 ^{o}C; meanwhile, Al6061 alloy with a melting point of 650 ^{o}C was melted in a resistance heating furnace to a temperature of 750 °C. Magnesium (1 wt%) in pure form was added into the molten metal to improve the wettability between the matrix and the reinforcement during the infiltration process. The die and punch were fixed in a 25T hydraulic press and preheated to a temperature of 220 °C for one hour. The liquid aluminum at 780 °C was poured into the preheated aluminosilicate fiber preform placed inside the preheated die, and subsequently, a high pressure of 40 MPa was applied on the molten aluminum metal to get penetrated into the preform. Squeeze pressure was maintained for about 3-4 minutes until the solidification was complete and for the comparison of characteristics with the squeeze infiltrated composite the base unreinforced Al6061 alloy was also subjected to squeeze casting process.

3.2.2. Characterization

Both the base unreinforced squeeze cast alloy, and the infiltrated composite was used for characterization in the present study. The T6 heat

treatment schedule was carried out for both Al6061 alloy and the infiltrated fiber composite, i.e., solution treatment (535 °C for 4 h) followed by quenching in warm water (80 °C) and then precipitation or age hardening at 175 °C for 8 h. For mechanical properties and tribological characterization, heat treated specimens are used. Alloy and composites were characterized using Leica DMRX Optical Microscope and JEOL SEM with Oxford EDS. Philips XRD was used to characterize the extracted fibers from the infiltrated composite using Cu K_α radiation (wavelength λ =0.154 Å) to identify the phases. The Hardness of alloy and composites were measured using Zwick Brinell hardness testing machine with a 2.5 mm ball indenter and 62.5 kg load. The test was conducted at room temperature, and the hardness measurements were taken at five different places on each sample to obtain an average value of hardness. The dry wear behavior of samples was investigated using DUCOM (TR20LE) pin-on-disk tribometer with various loads of 10, 20, 30 and 40 N at a sliding velocity of 2 m/s and 4 m/s for the constant sliding distance of 1500 m. The differential thermal analysis (DTA) of alloy and composites were conducted using Hitachi STA7300 (TG–DTA) instrument at a heating rate of 10 °C/min in the argon atmosphere. The compression and tensile tests were carried out using Instron and FIE make universal testing machine (UNITEK-94100) at a strain rate of 0.0005 s^{-1} and 0.0008 s^{-1} respectively. The Charpy V-notch impact test was adopted for alloy and composites. The geometry of tensile, impact and compression specimens of alloy and composites were shown in Figure 3.2 and the measurements were carried out using three samples in each condition to obtain an average value. The density measurements of alloy and composites were evaluated using Archimedes principle. Interface characterization of Al6061/aluminosilicate fiber reinforced infiltrated composite was examined in JEOL-JEM-2100 transmission electron microscope operated at 200 kV with Oxford EDS. The corrosion characteristics of alloy and composites were analysed by a potentiodynamic electrochemical workstation (CH Instruments) in 3.5 wt% NaCl solution at room temperature, and the scan rate was 0.2 mV/s. The instrument consists of three-electrode cell system: unreinforced Al6061 squeeze cast alloy and Al6061/aluminosilicate fiber reinforced composite as working electrode, platinum as auxiliary electrode and calomel as the reference electrode.

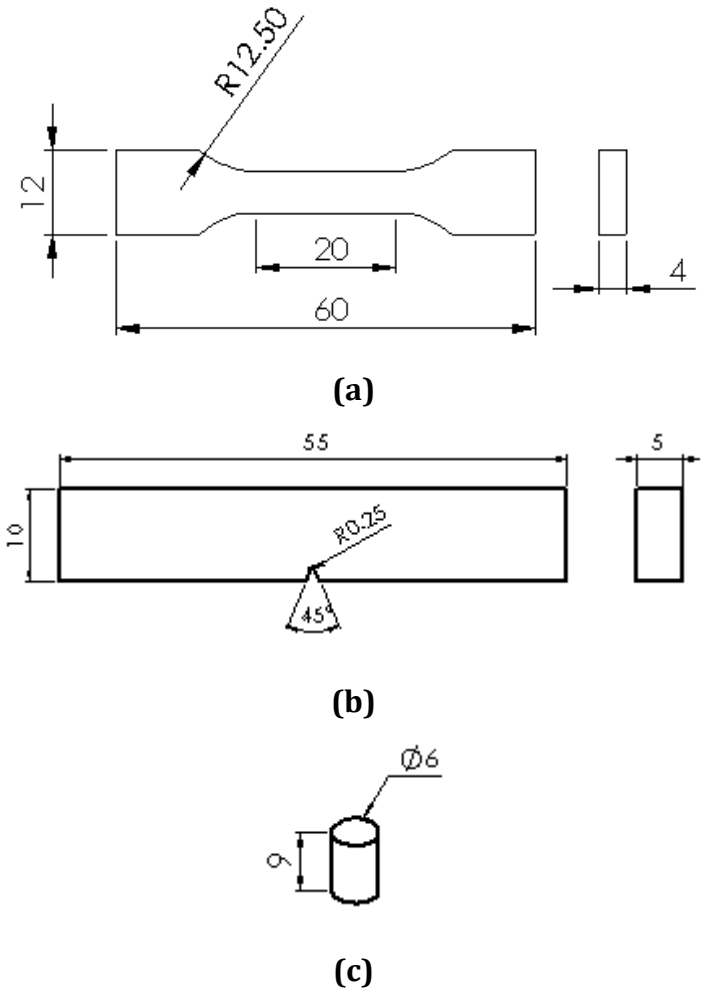

Figure 3.2. Geometry of (a) Tensile specimen (ASTM-E8) (b) Impact specimen (ASTM-E23) (c) Compression specimen (ASTM-E9).

3.3. Results and Discussion

3.3.1. Structural Characteristics

Figure 3.3a shows the macrograph of the zirconia grade aluminosilicate fiber preform used for the squeeze infiltration process of aluminum 6061 alloy. The SEM micrograph and the EDS spectra of the surface of aluminosilicate fiber used in the fabrication of preform are shown in Figure 3.3(b and c). EDS analysis confirms the chemical constituents of aluminosilicate fiber made of zirconia-grade. Figure 3.4(a and b) depicts the optical microstructure of Al6061 – aluminosilicate composite reinforced with a volume fraction of 15 and 20% fiber fabricated by squeeze infiltration process. Uniform dispersion of aluminosilicate fibers in the matrix is observed without the formation of porosities and cracks owing to the solidification of the composite, which takes place under pressure. No fiber

agglomeration is discerned in the microstructure, which percept the elimination of preform damage during high pressure melt infiltration. The aluminum melt gets thoroughly infiltrated into the lower and higher volume fraction of the randomly oriented fine fibrous network providing a smooth interface with better adhesion between the matrix and the reinforcement. While polishing some of the fibers oriented in the polishing direction are cut along as cross section and thus resembles elliptical shape like phenomenon in the microstructure.

Figure 3.5a shows the HRTEM image of the interface region between Al6061/aluminosilicate fiber reinforced composite developed by squeeze infiltration process. The presence of oxide layer Al_2O_3 can be observed in the interface region between the aluminum and aluminosilicate fiber, which is confirmed by the elemental analysis by EDS (Atomic%: Al-42.57, O-57.43) (Figure 3.5b). During squeeze infiltration process, oxygen present in the atmosphere and in the pores of the preform reacts with molten aluminum to form an oxide layer on the infiltration front. The oxide layer formed at the interface gets "Keyed-in" to the surface of the fiber as well as matrix aluminum thereby providing mechanical interlocking effect between the matrix/reinforcement, which in turn improves the interfacial bonding strength.[203] Simultaneously, it also obstructs the diffusion of matrix aluminum into the zirconia grade aluminosilicate fiber, thereby reducing the interfacial reactions. The low solubility of Si in aluminum (maximum solubility of Si in α-Al is 1.65 (wt%) at 577 ^{o}C [204]) results in the segregation of silicon on the composite interface region during the solidification of metal (Figure 3.6(a and b)) (Atomic%: Si-100).

(a)

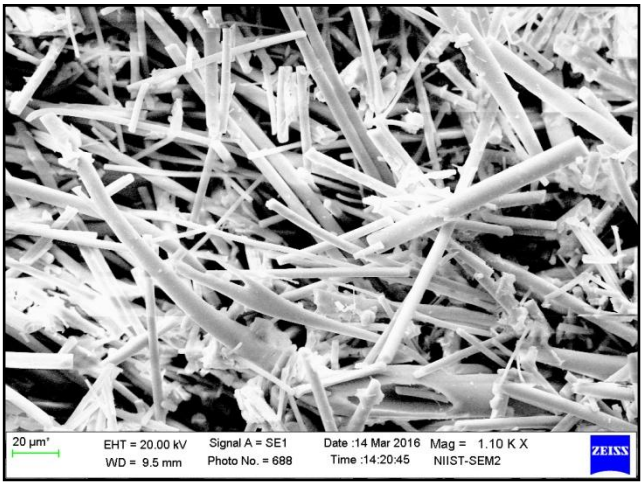

(b)

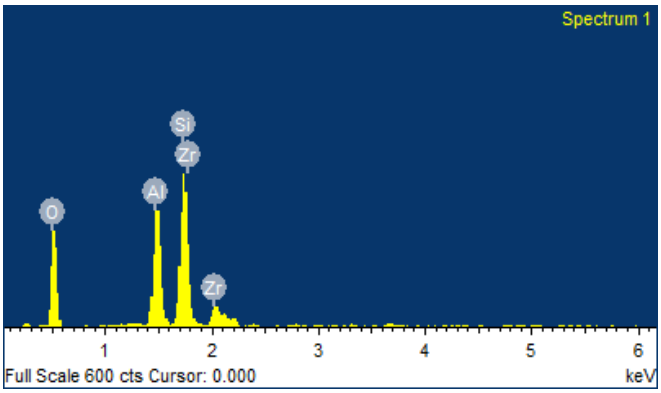

(c)

Figure 3.3. (a) Macrograph of the zirconia grade aluminosilicate fiber preform (b) SEM image and (c) EDX spectrum of zirconia grade aluminosilicate fiber used in the preform fabrication.

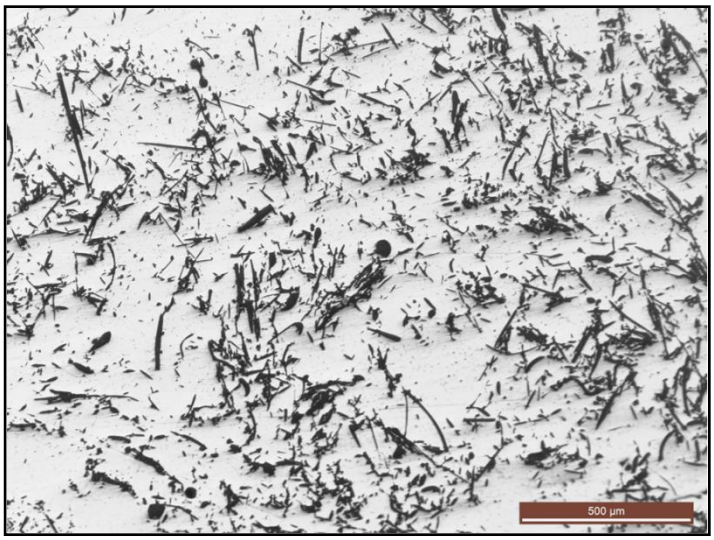

(a)

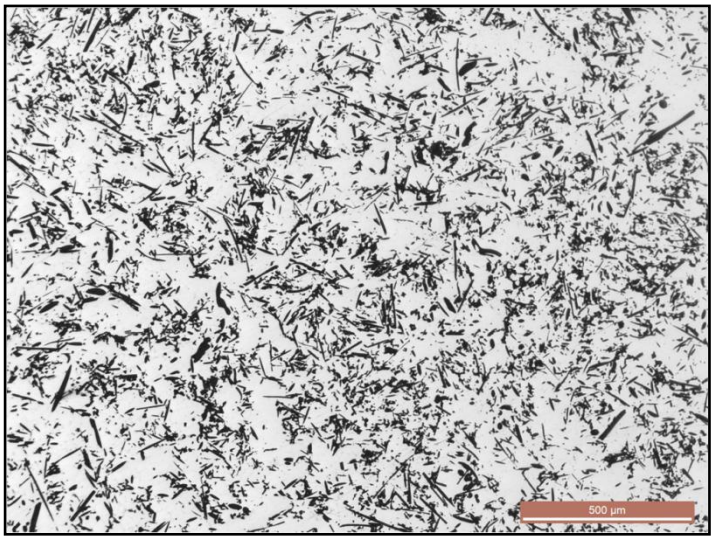

(b)

Figure 3.4. The optical microstructure of Al6061-aluminosilicate composite reinforced with (a) 15 vol% of fiber (b) 20 vol% of fiber by squeeze infiltration process.

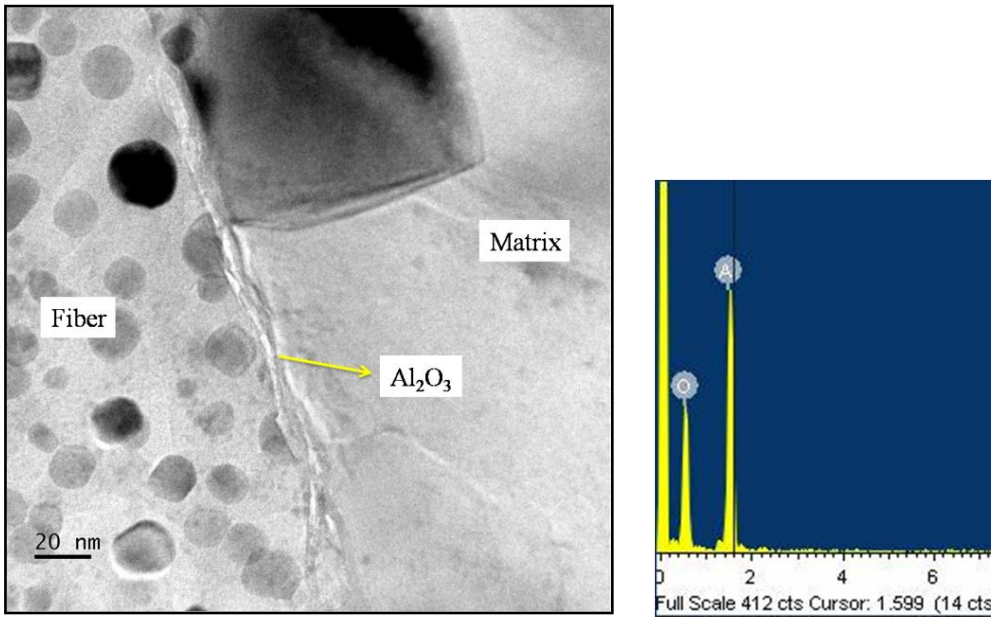

(a) **(b)**

Figure 3.5. (a) HRTEM observation of the interface region between Al6061-aluminosilicate fiber infiltrated composite showing the presence of oxide layer Al_2O_3 (b) Corresponding EDS.

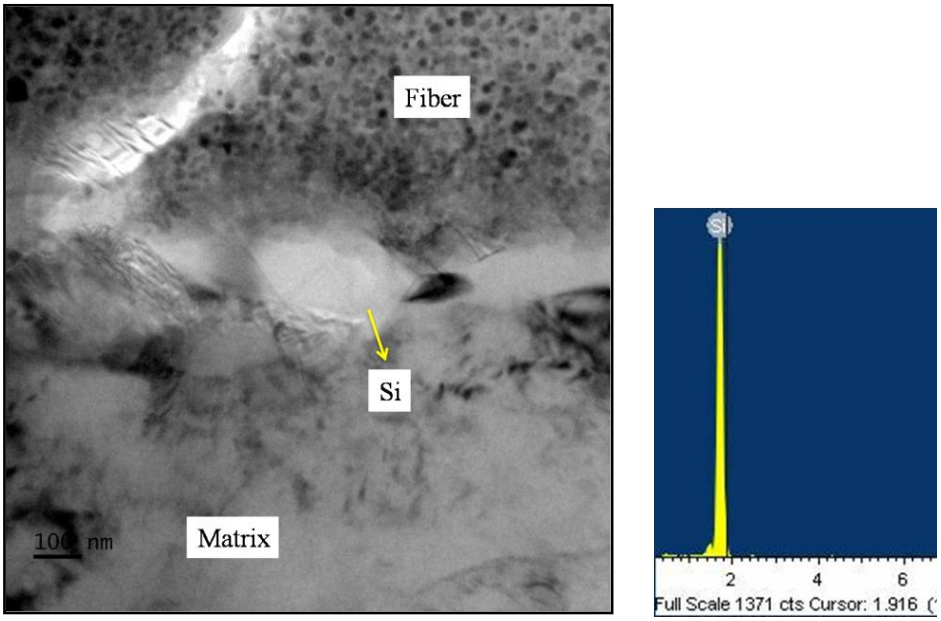

(a) **(b)**

Figure 3.6. (a) TEM image showing the presence of Si at the interface region in the infiltrated composite (b) Corresponding EDS.

3.3.2. XRD Analysis

Figure 3.7(a and b) shows the XRD pattern of as received and extracted fiber from the infiltrated composite using NaOH solution. Significant diffraction peaks discerned from the extracted sample belongs to $MgAl_2O_4$ spinel (JCPDS Card No: 01-077-0438), Al_2O_3 (JCPDS Card No: 00-047-1771), SiO_2 (JCPDS Card No: 01-080-0367), ZrO_2 (JCPDS Card No: 00-041-0017) and $ZrAl_3$ (ICDD Card No: 065-2750) phases. The possible chemical interaction of matrix Al and Mg with Al_2O_3 and SiO_2 present in the fiber results in the following interfacial reactions.[205]

$$3Mg_{(1)} + 4Al_2O_{3(s)} \rightarrow 3MgAl_2O_{4(s)} + 2Al_{(1)} \quad [1]$$

$$\Delta G_{1000K} = -258 \text{ kJ mol}^{-1}$$

$$4Al_{(1)} + 3SiO_{2(s)} \rightarrow 2Al_2O_{3(s)} + 3Si_{(s)} \quad [2]$$

$$\Delta G_{1000K} = -532 \text{ kJ mol}^{-1}$$

$$2Al_{(1)} + Mg_{(1)} + 2SiO_{2(s)} \rightarrow MgAl_2O_{4(s)} + 2Si_{(s)} \quad [3]$$

$$\Delta G_{1000K} = -441 \text{ kJ mol}^{-1}$$

The addition of Mg in the molten matrix helps in improving the wettability between the matrix and the reinforcement during infiltration by scavenging the oxygen from the melt surface and forms $MgAl_2O_4$ spinel.[206] Besides, matrix Al and Mg reacts with ZrO_2 (zirconia grade aluminosilicate fiber) to form the following reactions

$$13Al_{(1)} + 3ZrO_{2(s)} \rightarrow 2Al_2O_{3(s)} + 3ZrAl_{3(s)} \quad [4]$$

$$\Delta G_{1000K} = -448 \text{ kJ mol}^{-1}$$

$$2Mg_{(1)} + ZrO_{2(s)} \rightarrow 2MgO_{(s)} + Zr_{(s)} \quad [5]$$

$$\Delta G_{1000K} = -77 \text{ kJ mol}^{-1}$$

$$Mg_{(1)} + 8Al_{(1)} + 2ZrO_{2(s)} \rightarrow MgAl_2O_{4(s)} + 2ZrAl_{3(s)} \quad [6]$$

$$\Delta G_{1000K} = -344 \text{ kJ mol}^{-1}$$

Equation [4] is the most possible reaction due to high negative Gibbs free energy for the formation of stable $ZrAl_3$ intermetallic phase in these systems with aluminum.

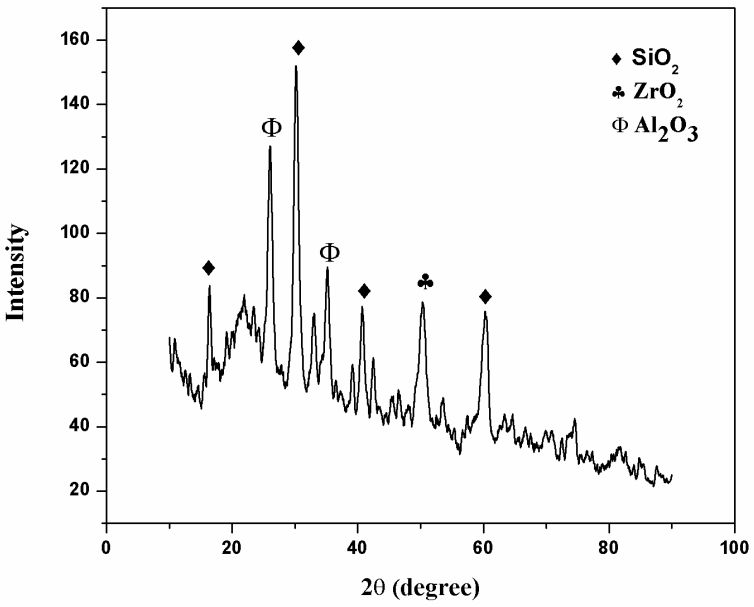

(a)

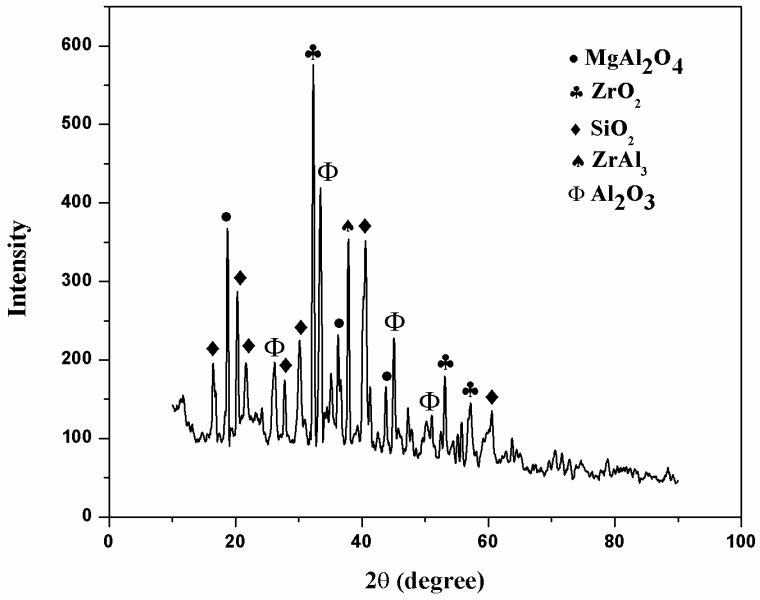

(b)

Figure 3.7. XRD pattern of (a) As received zirconia based aluminosilicate fiber (b) Extracted fiber from the infiltrated Al6061-aluminosilicate fiber reinforced composite using NaOH solution showing interfacial reaction products.

3.3.3. Thermal and Physical Characteristics

Differential thermal analysis curves of the squeeze cast alloy and the infiltrated composites in Figure 3.8 shows a major endothermic peak at 650 ˚C corresponds to α-Al → L dendrites due to the melting of the aluminum matrix. A

minor shift in the liquidus temperature of 15 and 20 vol% fiber reinforced composite towards the lower temperature is due to the colligative property of depression in freezing point by the addition of aluminosilicate fiber into the matrix aluminum.

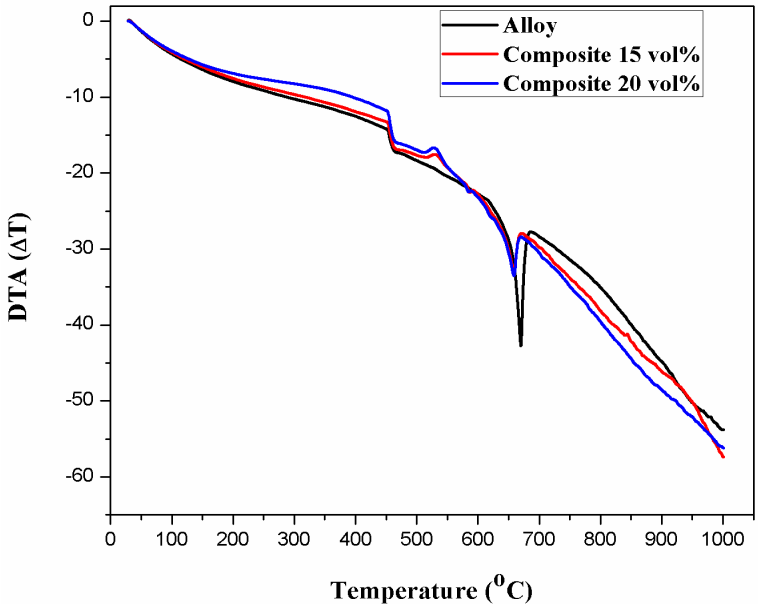

Figure 3.8. DTA analysis of unreinforced squeeze cast Al6061 alloy and the infiltrated composite reinforced with 15 and 20 vol% fiber.

As shown in Figure 3.9, the measured CTE value of Al6061-aluminosilicate fiber reinforced composite decreases with increase in the volume fraction of the fiber. Increasing the volume fraction of reinforcement fiber reduces the matrix content, at the same time, low CTE value of aluminosilicate fiber than that of aluminum helps in reducing the CTE of the composite material. The density of the squeeze infiltrated Al6061-aluminosilicate composite reinforced with 15 and 20 vol% fibers are 2.67 g/cc and 2.66 g/cc respectively, which is lower than the monolithic Al6061 alloy (2.7 g/cc). The electrical resistivity measured by four probe method for infiltrated Al6061-aluminosilicate composite reinforced with 15 and 20 vol% fibers are 4.76 × 10^{-2} Ωm and 5 × 10^{-2} Ωm which is higher compared to that of unreinforced squeeze cast Al6061 alloy (4.35× 10^{-2} Ωm). This is due to the resistivity offered by the aluminosilicate fiber and it improved with increase in the volume fraction.

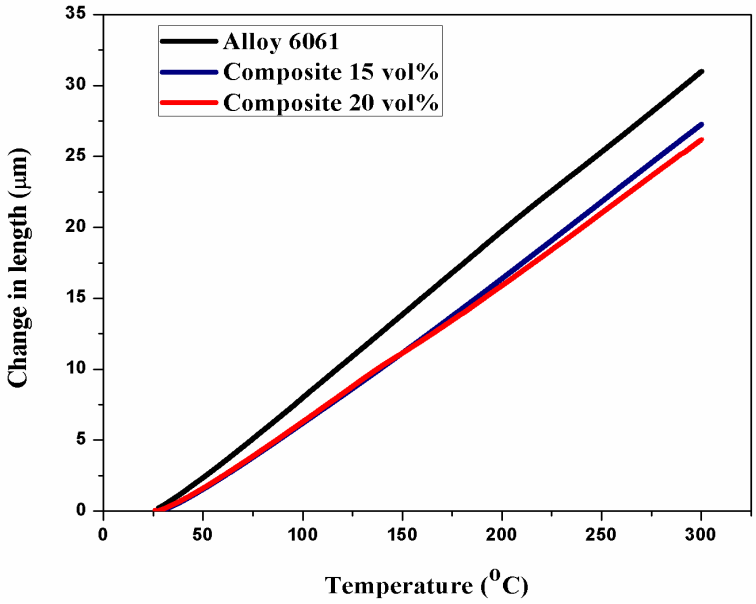

Figure 3.9. CTE analysis of unreinforced squeeze cast Al6061 alloy and the infiltrated composite reinforced with 15 and 20 vol% fiber.

3.3.4. Mechanical Characteristics

3.3.4.1. Hardness

The Brinell hardness values of unreinforced Al6061 squeeze cast alloy and the infiltrated composite in as-cast and heat treated conditions are shown in the histogram (Figure 3.10). The inclusion of aluminosilicate fiber in the aluminum matrix significantly enhances the hardness properties of the composite, and it increases with increase in the volume fraction of the reinforcement. Higher hardness in the composite is ascribed to the fact that the hard fiber shares the load developed by the indenter with the matrix and its tendency to develop heterogeneous nucleation sites for grain refinement, which act as a barrier for dislocation. The Heat-treated samples provided higher hardness compared to as cast samples due to the precipitation hardening effect. The unreinforced squeeze cast alloy undergoes plastic deformation under applied stress easily due to soft nature resulting in lower hardness value.

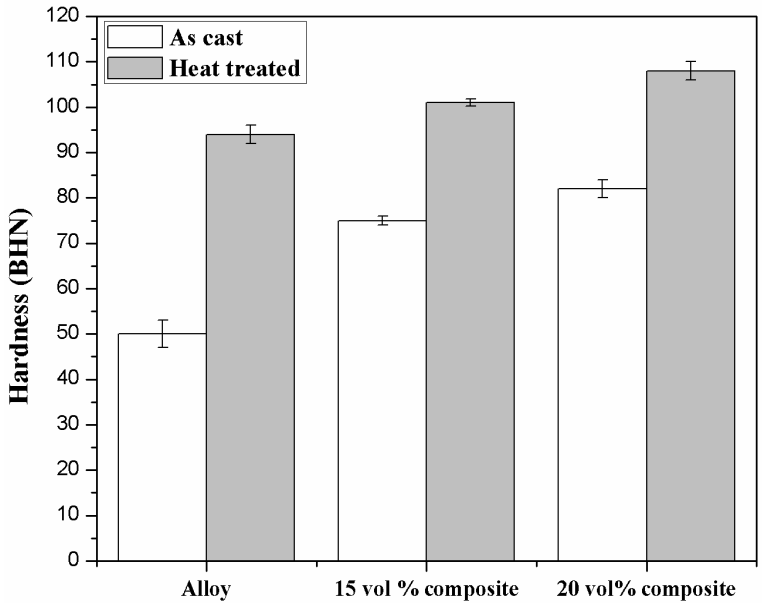

Figure 3.10. Hardness values of base unreinforced alloy and infiltrated composite reinforced with 15 and 20 vol% fiber in as-cast and heat treated conditions.

3.3.4.2. Compression

The average compressive strength obtained for the infiltrated composite reinforced with 15 and 20 vol% aluminosilicate fibers are 750 MPa (standard deviation-5MPa) and 770 MPa (standard deviation-7MPa) respectively, which are higher than that of the unreinforced squeeze cast alloy (725 MPa, standard deviation-5MPa). Meanwhile, the increase in fiber content shows a marginal change in the compression strength of the composite. The familiar isotropic behavior of randomly oriented aluminosilicate fiber in the infiltrated composite equally holds the load in all directions thereby restricting the soft matrix plastic flow behavior. Figure 3.11 shows the compressive stress-strain curve of the base alloy and the squeeze infiltrated Al6061/aluminosilicate fiber composite. Unreinforced squeeze cast alloy undergoes a failure which is entirely different from that of fiber reinforced infiltrated composite that fails in a progressive manner. The drop in compressive stress in the composite is due to the debonding at fiber-matrix interface during barreling and a rise in stress during the fracture after barreling is due to the resistance to deformation offered by the randomly oriented fibers.

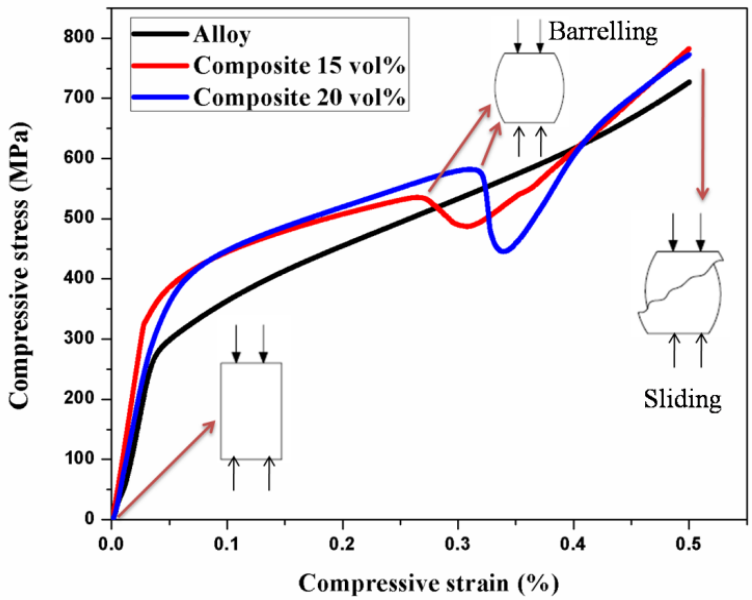

Figure 3.11. Compressive stress-strain curve of the typical base squeeze cast alloy, and the squeeze infiltrated composite reinforced with 15 and 20 vol% fiber.

3.3.4.3. Tensile Strength

The ultimate tensile strength of the infiltrated composite reinforced with 15 and 20 vol% fiber was 198 MPa (standard deviation-4MPa) and 220 MPa (standard deviation-6MPa), respectively. UTS appears to increase with the increase in fiber content, which is contributed to the high concentration of fibre and effective load transfer from the matrix to reinforced fiber during tensile loading. The UTS value of unreinforced squeeze cast alloy is 258 MPa (standard deviation-3MPa) which is slightly higher than that of infiltrated composite due to its tough and ductile nature.

Figure 3.12 shows the SEM images of the tensile fracture surface of alloy and infiltrated composite. Large numbers of dimples are observed on the fracture surface of the matrix alloy due to the progressiveness of plastic deformation during tensile fracture, and the surface appears smooth with the formation of necking during failure (Figure 3.12a). The composite exhibits a mixed mode of fracture caused by ductile matrix fracture and brittle reinforcement failure. The randomly oriented fibers in the preform break and cause the composite fracture. The necking of ductile infiltrated metal matrix region around the aluminosilicate fiber is observed in the composite. Both delamination and fracture of fibres are observed in the fractographs (Figure 3.12 b &c).

3.3.4.4. Impact Strength

The impact strengths of the infiltrated composite reinforced with 15 and 20 vol% fiber are 28 J (standard deviation-3 J) and 25 J (standard deviation-3 J) respectively. The energy absorbed by the composite during impact test shows that the increase in the fiber volume fraction decreases the impact strength. The low impact energy absorbed by the composite is due to the brittle nature of fiber which intercepts the dislocation movement thereby inhibiting plastic deformation before crack initiation. An increase in the fiber content in the matrix reduces the ductility of the material and cause various stress concentration areas, which acts as the favorable sites for crack initiation and propagation. Unreinforced squeeze cast alloy naturally being a ductile material absorbs high energy (38 J, standard deviation-5 J) during impact test than that of the composite.

The SEM images in Figure 3.13 shows the impact fracture surface of the unreinforced squeeze cast alloy and the infiltrated composites reinforced with 15 and 20 vol% fiber. The fracture surface of the alloy shows the homogeneous formation of deep and shallow dimples with shear deformation, which shows the response of matrix to ductility (Figure 3. 13a). It can be apparent from the fracture surface of the composite that the formations of stress concentration sites (marked as SC) are in the interface region causing matrix-fiber debonding (Figure 3.13b). Infiltrated composite depicts the evidence of matrix cracking coupled with reinforcement failure, which results in the brittle mode of fracture (Figure 3.13c). Composite reinforced with 20 vol% fiber shows more fiber breakage region due to the incorporation of higher reinforcement content.

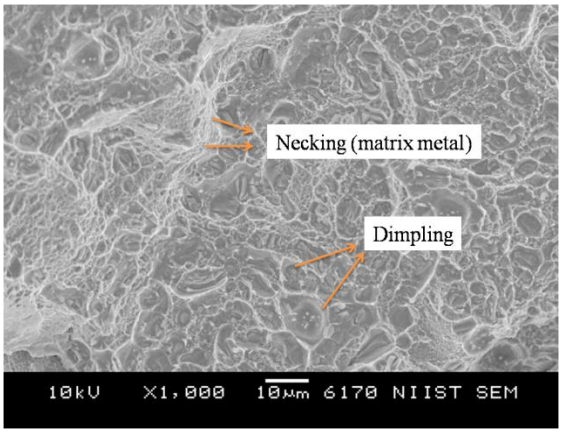

(a)

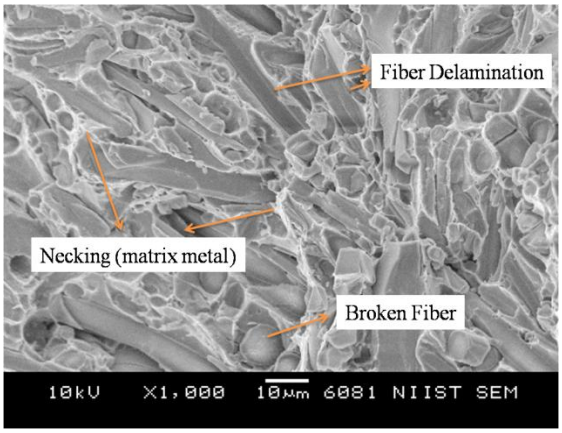

(b)

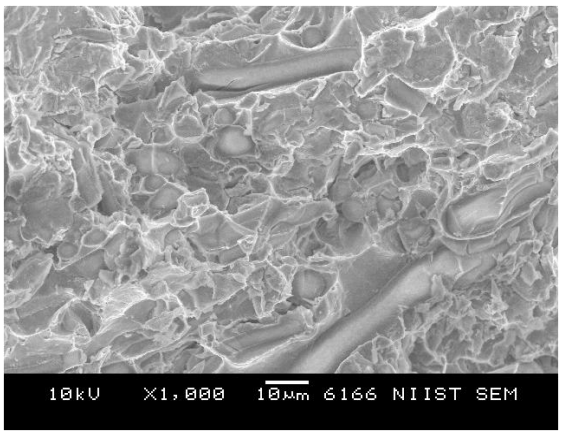

(c)

Figure 3.12. SEM photomicrograph of the tensile fracture surface of (a) Squeeze cast Al6061 alloy (b) Composite reinforced with 15 vol% fiber (c) Composite reinforced with 20 vol% fiber.

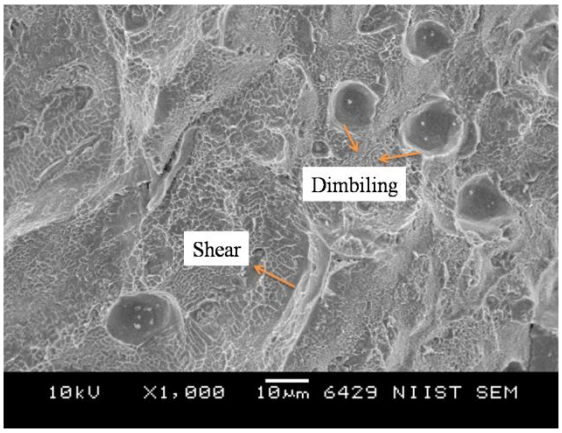

(a)

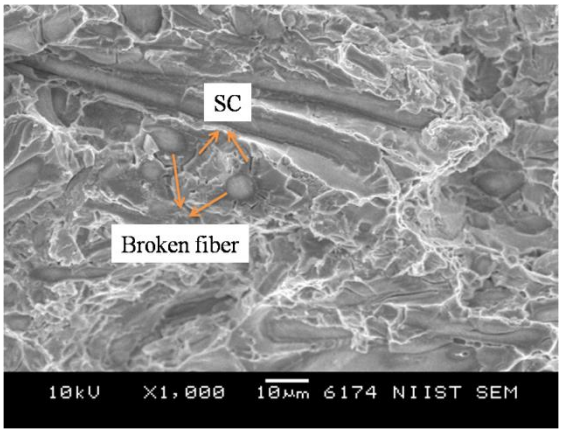

(b)

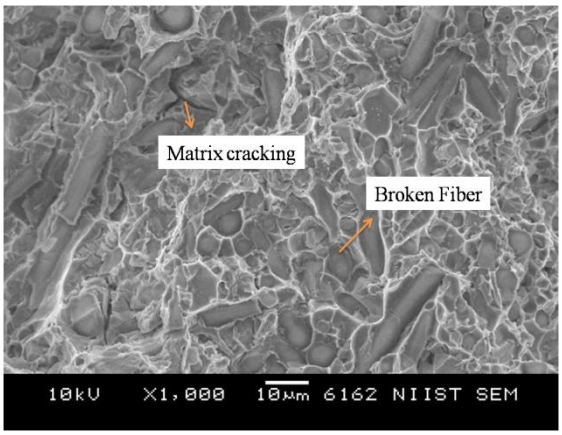

(c)

Figure 3.13. SEM images of the impact fracture surface of (a) Unreinforced squeeze cast Al6061 alloy (b) Infiltrated composite reinforced with 15 vol% fiber (c) Infiltrated composite reinforced with 20 vol% fiber.

3.3.5. Wear Behavior

The effect of variation in load and velocity on the wear behavior of unreinforced Al6061 squeeze cast alloy and the infiltrated composites reinforced with 15 and 20 vol% of aluminosilicate fiber are shown in Figure 3.14.

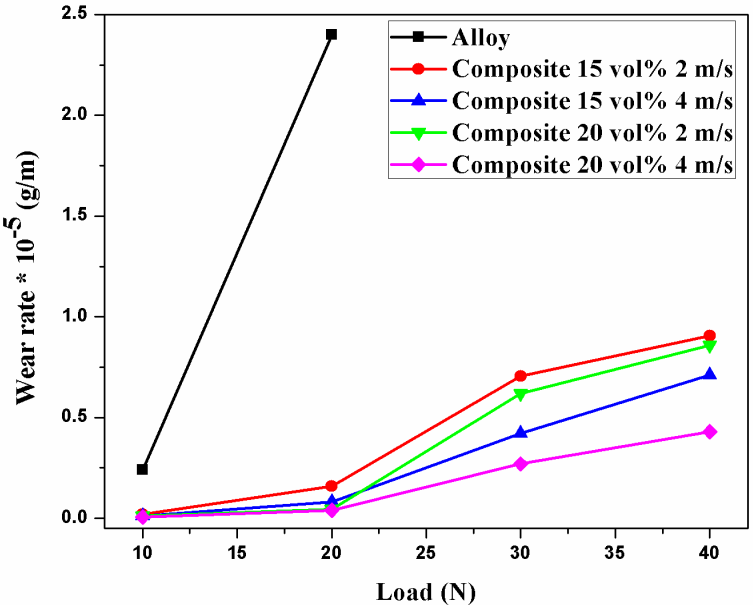

Figure 3.14. Wear rate of unreinforced squeeze cast Al6061 alloy, and the squeeze infiltrated Al6061-aluminosilicate composite reinforced with 15 and 20 vol% fiber.

It is apparent from the graph that the wear rate of both alloy and composite increases with increase in load due to the temperature generated by the shear stress while sliding at higher load. A severe wear transition region is observed in the case of the unreinforced alloy at a speed of 2 m/s in 20 N load, and a further increase in load causes heavy vibration and damage to the pin material; consequently, the test for unreinforced alloy was stopped. Unreinforced alloy being a soft material undergoes heavy plastic deformation due to thermal softening of the material under higher load as discussed above results in higher wear rate. The addition of randomly oriented aluminosilicate fiber in the matrix significantly reduces the wear rate of composite compared to that of base alloy. Hard reinforcement in the matrix prevents the direct wear of matrix alloy by counter surface and reduces the severe plastic deformation in it thereby reducing the intensity of heat generated during sliding at varying load. Also, it can be

depicted from the plot that increases in the volume fraction of reinforcement decrease the wear rate of composite and the present result confirms the previous statement. However, sliding speed dominates over the volume fraction of the reinforcement. An increase in the sliding speed at 4 m/s for composite reinforced with 15 vol% fiber shows decreased wear rate compared to that of composite reinforced with 20 vol % fiber sliding at 2 m/s. The decrease in wear rate while increasing the sliding speed is attributed to the quick evolution of tribolayer or MML (Mechanically Mixed Layer) on the pin surface formed by the mixing of plastically deformed wear debris and oxidized particles during sliding, which acts as a wear resistance coating.[207]

3.3.5.1. Worn Surface Analysis using SEM

The SEM images of the worn out surfaces of the unreinforced squeeze cast alloy and infiltrated composites reinforced with 15 and 20 vol% fiber are shown in Figure 3.15. Unreinforced alloy at a speed of 2 m/s in 20 N load undergoes heavy plastic deformation with patches and flow of material along the sliding direction. The higher degree of shear in the soft alloy during wear develops thermal stresses which induce surface cracking and results in the delamination of material (Figure 3.15a). Worn surface of the composite reinforced with 15 vol% fiber rotated at a speed of 2 m/s in 40 N load shows the formation of metal granules with a restriction in the material delamination and plastic deformation due to the incorporation of aluminosilicate fibers, thereby improving the hardness of the composite (Figure 3.15b). Composite reinforced with 15 vol% fiber rotated at a speed of 4 m/s in 40 N load (Figure 3.15c) shows smooth worn surface with the elimination of material fragments compared to that of composite reinforced with 20 vol% fiber rotated at a speed of 2m/s in 40 N load (Figure 3.15d) due to the formation of mechanically mixed layer (MML). The MML formed on the pin surface act as a tribofilm which intercepts the direct contact between the sliding pin and the counter disc, thereby preventing the plastic flow of the material. Composite reinforced with 20 vol % fiber rotated at a speed of 4 m/s in 40 N load (Figure 3.15e) shows remarkable smooth wear surface compared with other wear specimens of alloy and composite due to the coupled effect of higher fiber content in the matrix and the formation of tribofilm at increased sliding speed.

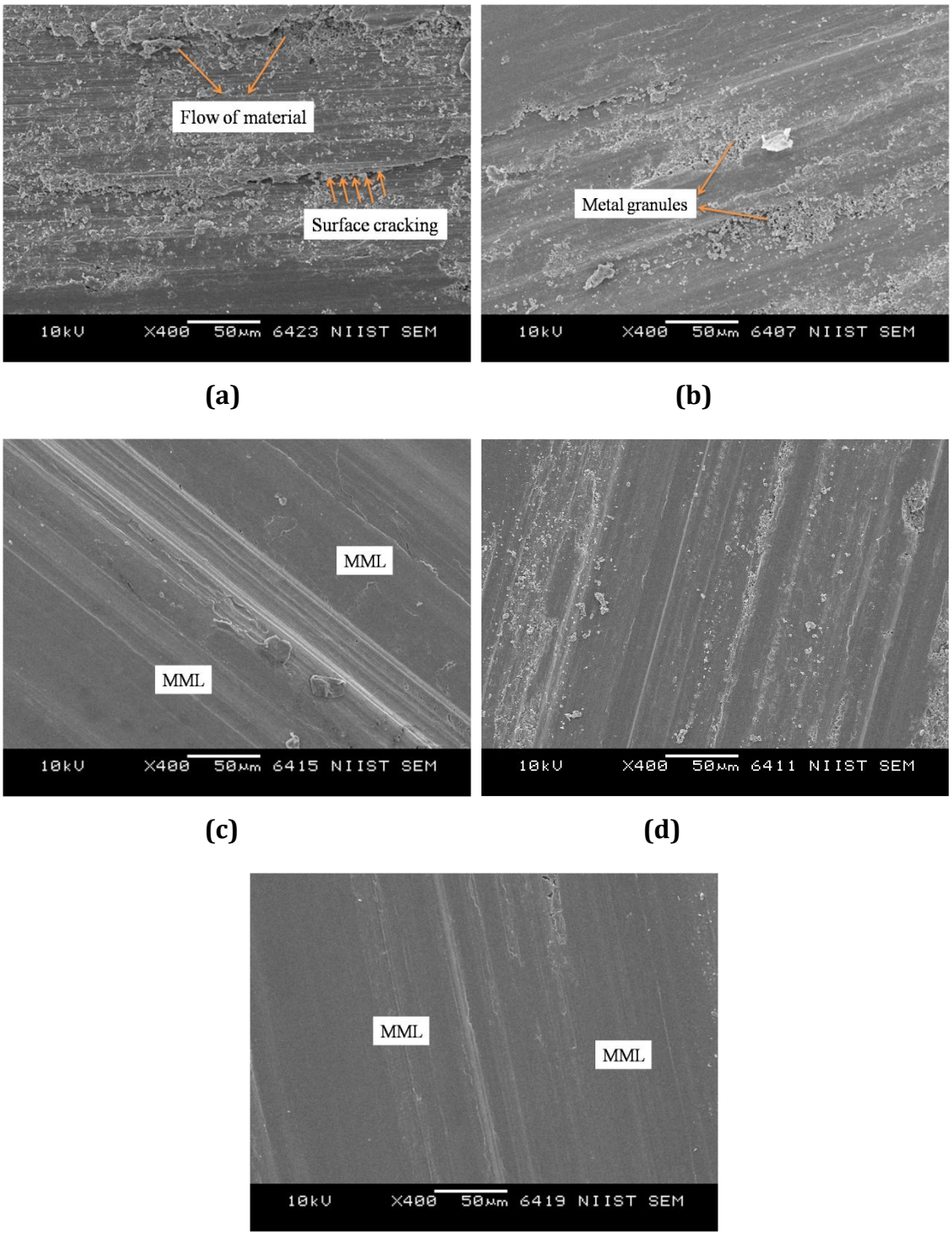

Figure 3.15. SEM photomicrographs of worn out surface of (a) Unreinforced squeeze cast Al6061 alloy at an applied velocity of 2 m/s in 20 N load (b) 15 vol% fiber reinforced composite 2 m/s in 40 N load (c) 15 vol% fiber reinforced composite 4 m/s in 40 N load (d) 20 vol% fiber reinforced composite 2 m/s in 40 N load (e) 20 vol% fiber reinforced composite 4 m/s in 40 N load.

EDS spectrum on the worn surface of the Al6061- 20 vol% aluminosilicate fiber reinforced composite sliding at a speed of 4 m/s in 40 N load (Figure 3.16) shows the presence of Fe, Si and the possible oxide layers like MgO, Al_2O_3 and $MgAl_2O_4$. MML or the wear resistant tribolayer formed on the pin and plate interface is composed of plastically deformed wear debris and oxidized particles during wear.

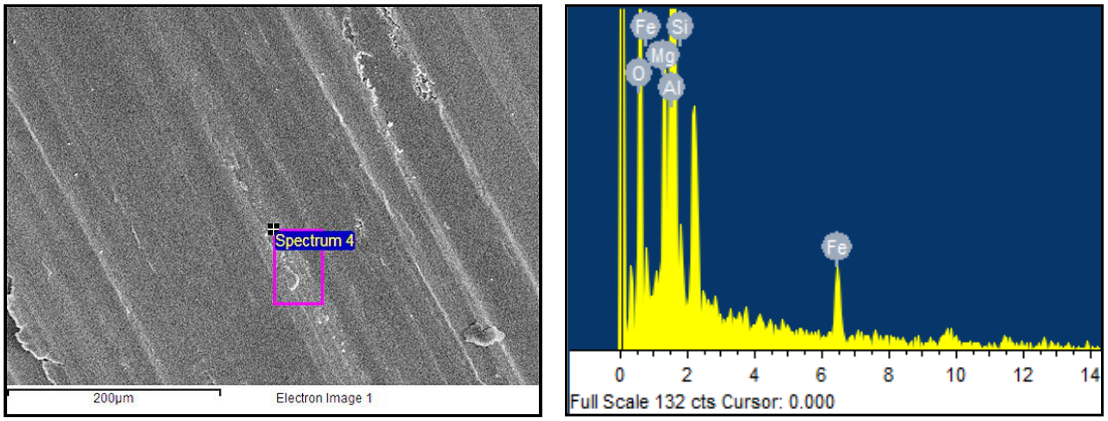

Figure 3.16. SEM and EDS spectrum on worn surface of Al6061- 20 vol% aluminosilicate fiber reinforced composite sliding at a speed of 4 m/s in 40 N load.

3.3.6. Corrosion Behavior

The Potentiodynamic scanning curves through the extrapolation of anodic and cathodic Tafel lines and the corrosion parameters of unreinforced squeeze cast alloy and the infiltrated composites are shown in Figure 3.17 and Table 3.4.

Table 3.4: Corrosion parameters of unreinforced squeeze cast Al6061 alloy and the infiltrated composite reinforced with 15 and 20 vol% aluminosilicate fiber.

Sample type	E_{corr} Corrosion potential (V)	i_{corr} Corrosion current ($\mu A/cm^2$)	Resistance (Ω)
Alloy	-0.81	10	2143
Composite 15 vol %	-0.87	2.8	8035
Composite 20 vol %	-0.96	2.7	13063

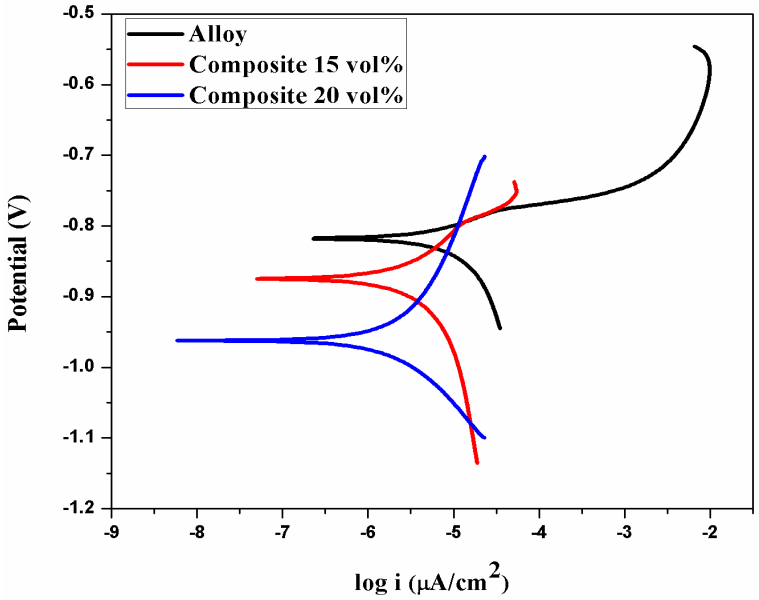

Figure 3.17. Potentiodynamic polarizations curves of unreinforced squeeze cast Al6061 alloy and the infiltrated composite reinforced with 15 and 20 vol% of aluminosilicate fiber.

The corrosion rate is directly proportional to corrosion current (flow of electrons), which in turn depends on the polarization resistance (resistance to oxidation). From the potentiodynamic polarization curves, infiltrated composite with 20 vol% aluminosilicate fiber obtains the lowest corrosion current density (i_{corr}) and high polarization resistance (R_p) value leading to better corrosion resistance compared to that of base squeeze cast alloy and 15 vol% fiber infiltrated composite. Rodriguez[208] revealed that the weakest portion of a fiber composite will be the matrix/reinforcement interface; therefore, the nature of bonding will be crucial in its corrosion determination. Strong interfacial bonding between aluminosilicate fiber and the matrix aluminum may help in improving the corrosion resistance of the composite compared to base alloy. Enhancement in the corrosion resistance of the composite is observed with the higher volume fraction of the reinforcement, which supports the above phenomenon. The minor negative shift in the corrosion potential (E_{corr}) value of the composites compared to that of alloy is mainly due to the presence of non conducting aluminosilicate fiber in the composite which obstruct the flow of electrons at the interface region and cause unequal distribution of electric charge. As a result, accumulation of negative charges at the composite surface increases that result in the shift of potential towards the

negative direction.[209-210] Formation of interfacial products like Al_2O_3 and $MgAl_2O_4$ spinel are observed at the interface which generally act as a protective film thereby preventing the attack of corrosive species. Mostly continuous alumina phase with 5-10 nm thickness are observed (Figure 3.5a).

3.4. Conclusion

In the present studies, Al6061/aluminosilicate composite reinforced with 15 and 20 vol% of fiber were successfully fabricated by direct squeeze infiltration process and their properties were evaluated. The major conclusions are

- Uniform distribution of aluminosilicate fiber throughout the matrix and complete penetration of molten aluminum through the aluminosilicate fiber preform is observed in the composite microstructure with the elimination of prefrom breakage, porosities, and shrinkage.
- HRTEM observation shows the formation of Al_2O_3 at the aluminum-aluminosilicate fiber interface, which controls the interfacial reaction and improves the bonding strength between the matrix and the reinforcement.
- Al6061/aluminosilicate composite reinforced with 15 and 20 vol% fiber exhibits better hardness and compressive strength than that of unreinforced alloy and it improves with the increase in reinforcement volume fraction. The inclusion of fiber in the matrix alloy reduces the soft matrix plastic flow behavior by preventing dislocations thereby improving the hardness and compressive properties.
- Composite reinforced with 15 and 20 vol% fibers obtained a lower density value of 2.67 g/cc and 2.66 g/cc respectively, compared to monolithic base alloy (2.7 g/cc).
- The composite shows lesser wear rate compared to base squeeze cast alloy owing to the incorporation of hard aluminosilicate fiber. Wear resistance of the composite improves with the increase in fiber content but sliding speed overcomes the volume fraction concept attributed to the formation of MML, which acts as a coating on the pin surface.
- Electrochemical corrosion studies and Tafel plot analysis reveals that Al6061/aluminosilicate composite reinforced with 15 and 20 vol% fiber

manifest better corrosion resistance properties than base alloy. This is due to the strong interfacial bonding between the matrix and the reinforcement and by the formation of protective interfacial reactions, both preventing the extensive attack of corrosion to the inner depth.

- The electrical resistivity of the composite improves with the higher volume fraction of reinforcement fiber and considerably escalated compared to base alloy. The above phenomenon also may be a reason behind the enhanced corrosion resistance of the composite reinforced with the higher volume fraction of fiber due to the resistivity offered by the fiber without conducting current thus retarding electrochemical corrosion.

Chapter 4

Structure and Properties of Modified Compocast Microsilica Reinforced Aluminum Matrix Composite

Abstract

A356 aluminum alloy reinforced with 7 wt. % microsilica composites were produced by the three different processing routes viz. liquid metal stir casting followed by gravity casting, compocasting followed by squeeze casting and modified compocasting route and their properties were examined. Microstructure of liquid metal stir cast Al MMC shows agglomeration of particles leading to high porosity level in the developed material. Adopting new route of compocasting followed by squeeze casting process prevent the agglomeration sites with uniform distribution and dispersion of the dispersoids in the matrix metal. Modified compocasting process reduces the segregation of particles in the final composites thus enhancing the mechanical, tribological and corrosion properties of the composites. Superior wear-resistance properties were exhibited by the modified compocast composite compared to the unreinforced squeeze cast alloy and an abrasive type wear mechanism was observed in the case of composite. Increasing the sliding speed resulted in the quick evolution of tribolayer and the wear rate of composite gets reduced. The Presence of phases like $MgAl_2O_4$ spinel, $NaAlSi_3O_8$ and $KAlSi_3O_8$ has a favorable effect on increased corrosion resistance of the composite. Microsilica particles significantly enhanced the compressive strength of modified compocast composites compared to the unreinforced squeeze cast Al alloy.

4.1. Introduction

In the present scenario of materials world, evolution of metal matrix composites (MMCs) from science and intellectual interest to an industrial technology is due to their unique combination of engineering properties like high strength to weight ratio, enhanced thermal, tribo-mechanical and corrosion properties compared to base alloys. This spans a significant range of applications in ground transportation, thermal management, aerospace, industrial,

infrastructure and recreation sectors.[211] Different techniques have been implemented for processing aluminum matrix composites (AMCs), which includes powder metallurgy, spray codeposition, molten metal infiltration and casting methods.[212,145,85,82,213,214] Stir casting is one of the simplest and economic techniques for the large scale production of particulate composites which involves the addition of reinforcement particles into the molten metal in a vortex created using a mechanical stirrer aiming to obtain a better bonding between matrix-reinforcement.[144-215] However, the disadvantage of the liquid metal stir casting process is the agglomeration of ceramic particles in molten metal due to the low wettability between the reinforcement and the matrix phase. Few studies have identified compocasting as one of the economic method to produce AMCs by reducing the casting temperature and adding ceramic particles into the semi solid state aluminum, which enhances wettability and better distribution of reinforcement particles compared to stir casting.[151-216] Secondary processing methods like squeeze casting are adopted to refine the grain size and to reduce the porosity in the final composites.[217] Most of the previous studies on compocasting are carried out in SiC, fly ash, Al_2O_3 and carbon nano-tubes reinforced aluminum matrix composites.[159,218,219,220,221] Microsilica is an artificially synthesized ceramic particle which is widely used as filler in polymer composites. Microsilica stands out as one of the attractive reinforcement with its distinct advantages like low density coupled with thermal stability as well as other properties that stand equal to other commercial reinforcements. Microsilica ceramic particles are fine in size, semi-transparent, white-colored and high-strength microspheres typically used to improve hardness and abrasion resistant coatings. They have utility in radiation-curable and thin-film powder coatings, and they are also UV transparent down to 250 nm due to its chemistry. The studies on the production of microsilica reinforced aluminum composite are very rare.[222] The present investigation attempts to fabricate Al A356-7% microsilica composite by liquid metal stir casting, compocasting and modified compocasting methods using fine reinforcement particles. The influence of microspheres addition on microstructure and properties of Al A356-7 % microsilica composites are evaluated.

4.2. Experimental Procedure

A356 cast aluminum alloy supplied by Sargam Metals, Chennai was chosen as the matrix material with a nominal composition of Al–7Si–0.35Mg (in wt %). The microsilica particles supplied by 3M India Ltd, Bangalore was used as the reinforcement with particle size in the range from 15 to 24 μm. The density of the microsilica particles used was 2.4 g/cm^3 having a softening point of 1020^{0}C (from materials data sheet of supplier). As received microsilica were surface treated in distilled water followed by acetone under ultrasonication to deflocculate and clean the surface of the particles and later filtered and dried in an oven. Liquid metal stir casting, compocasting and modified compocasting were used for the primary synthesis of the 356 Aluminum - 7 wt% Microsilica composites and solidified using permanent mold and squeeze casting processes. The unreinforced A356 alloy was subjected to squeeze casting process for comparison of characteristics with respect to the composites. Magnesium (1 wt. %) in pure form was added into the molten metal to improve the wettability of the particles during the processing of composites. Microsilica composites were cast in three different ways viz. (a) liquid metal stir casting followed by gravity casting, (b) compocasting following squeeze casting and (c) modified compocasting- recast the compocast ingot by remelting, stirring and squeeze casting. In the case of liquid metal stir casting route, the incorporation of microsilica particle into the melt and pouring of composite melt into the mold were carried out above liquidus temperature of the matrix alloy (730^{0}C). Compocasting process involves the incorporation of microsilica particles into the melt at a temperature between the solidus (585^{0}C) and liquidus (615^{0}C) temperatures of the matrix alloy (that was in a semisolid state) and pouring steps were carried out above liquidus temperature of the aluminum alloy (730^{0}C). Preheated (100^{0}C) microsilica particles were added to the molten melt at a feed rate of 2 g/min and the aluminum alloy melt was mechanically stirred using an impeller driven by an electric motor. Secondary processing of the compocast melt was executed using 25T hydraulic press by squeeze casting process.

The T6 heat treatment schedule was adopted for both the unreinforced alloy and composite, i.e., solution treatment (525^{0}C for 12 h) followed by quenching in warm water (80^{0}C) and then precipitation or age hardening at 165^{0}C

for 8 h. Heat treated samples of unreinforced squeeze cast alloy and composite were used for characterization in the present study. Microstructural characteristics of alloys and composites were characterized using JEOL SEM with Oxford EDAX and Leica DMRX Optical Microscope. The metallographic samples were prepared by initial polishing using 100, 220, 400, 600 and 1000 grit size emery papers followed by final selvyt cloth polishing using diamond paste of particle size 6μ, 3μ and 0.25μ. The SDAS (secondary dendrite arm spacing) values of unreinforced alloy and composite were measured in the microstructures using linear intercept method. Philips XRD was used to characterize microsilica particles and composite using Cu K_α radiation (wavelength λ =0.154 Å) to identify the phases. The hardness tests were carried out using Zwick Brinell hardness testing machine with a 2.5 mm ball indenter and 62.5 kg load. The test was conducted at room temperature, and the measurement of hardness was taken at different places on each sample to obtain an average value of hardness. The dry wear tests were conducted using DUCOM (TR20LE) pin-on-disk tribometer with various loads of 10 N, 20 N, 30 N and 40 N at a sliding velocity of 2m/s and 4 m/s for the constant sliding distance of 1500m. The counter surface disk used for pin-on-disk wear testing was EN31high carbon alloy steel with chemical composition, Fe-1C-0.5Mn-1.4Cr-0.25Si (in wt %), hardness of 63HRC and surface roughness (R_a) of 0.4μm, which was measured using Bruker profilometer. The dimension of the wear testing pin was 6 mm diameter and 30 mm length with the surface roughness of the wear surface was 0.5μm. The differential thermal analysis (DTA) analysis was performed using a Hitachi STA7300 (TG-DTA) instrument at a heating rate of 10^oC/min in argon atmosphere. The density and compression tests were evaluated using Archimedes principle and Instron machine respectively. The strain rate used for the compression tests were 0.5mm/min. The corrosion behavior of the alloy and composite were evaluated by an electrochemical workstation (CH Instruments) using a three-electrode cell, with A356 squeeze cast alloy and A356-7% microsilica reinforced modified compocast composite as working electrode, platinum as auxiliary electrode and calomel as reference electrode using a potentiodynamic system. The working electrode, in each case the material under study, was subjected to 3.5 wt % NaCl solution and the scan rate was 0.2 mV/sec.

4.3. Result and Discussion

4.3.1. Microstructural Analysis

Figure 4.1a shows the SEM micrograph of the microsilica solid particles which are observed to be spherical in shape. The different size particles are mixed together in such a way that some of the fine particles gets sticked over the surface of the larger particles. EDS analysis confirms the chemical constituents of microsilica particles made of alkali aluminosilicate ceramic (Figure 4.1b).

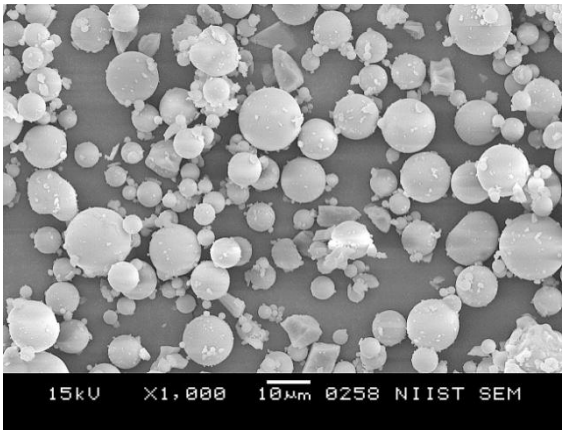

(a)

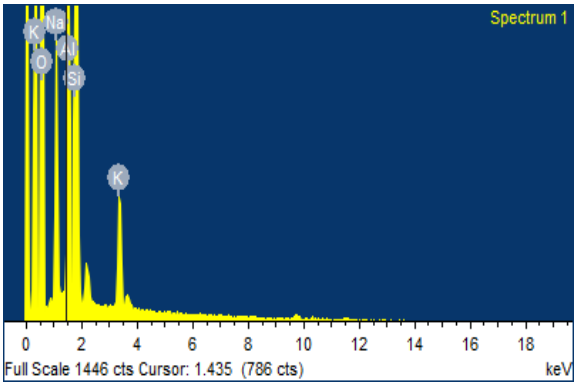

(b)

Figure 4.1. (a) SEM photomicrographs and (b) EDX spectrum of surface treated microsilica particles.

Figure 4.2a shows the microstructure of squeeze cast hypoeutectic A356 aluminum alloy in as cast conditions that begins with the formation of a primary phase α-Al solid solution (white phase) and Al-Si eutectic mixture (gray phase) between the dendrite arms during solidification. Microstructure depicts the formation of very fine grain morphology having a secondary dendrite arm spacing

of 13μm with the elimination of shrinkage and gas porosities since solidification takes place under pressure, which demonstrates the quality of squeeze casting process. A356-7% microsilica composite microstructure processed by liquid metal stir casting followed by gravity casting route at 730^0C resulted in agglomeration of particles which induces the formation of high level porosity in the developed material (Figure 4.2b) having a secondary dendrite arm spacing of 20μm. From the present exploration it is found that the sticking nature between the particles of microsilica is very high with agglomerated fine particles and it is directly proportional to the increase in processing temperature. Hence the possibility of incorporating microsilica particles without agglomeration in the matrix material at high temperature liquid metal stir casting is limited and it can be evident from the microstructure. Figure 4.2c shows the microstructure of Al-7 % microsilica composite prepared by the compocasting process (semisolid stir casting) at 590˚C followed by squeeze casting to refine the grain size having a secondary dendrite arm spacing of 9μm and to reduce the porosity in the composite. The above process prevents the agglomeration sites with uniform distribution and dispersion of the dispersoids in the metal compared to the liquid stir casting method with few segregation of particles through which the liquid metal gets infiltrated during squeeze casting process. During compocasting process higher viscosity of the semisolid molten metal slurry transmits shear force over the agglomerated particles leads to the better separation of the reinforcement.[150]

Segregation of the particles in the composite can be removed by modified compocasting process directly at a temperature of around 730˚C by stirring process followed by squeeze casting to obtain a uniform distribution of particles in the final microstructure as shown in Figure 4.2d. The SDAS value of modified compocast composite is 7 μm, which seems to be lower compared to other processing technique due to the better distribution of particles without segregation and agglomeration. Addition of Mg in the matrix material helps to promote wetting and it has to be limited to 4.7 wt.% due to the formation of relatively brittle intermetallic compound such as Al_3Mg_2 which decreases the strength of the composites.[59] However, in the present study only 1 wt.% Mg is added as wetting promoter.

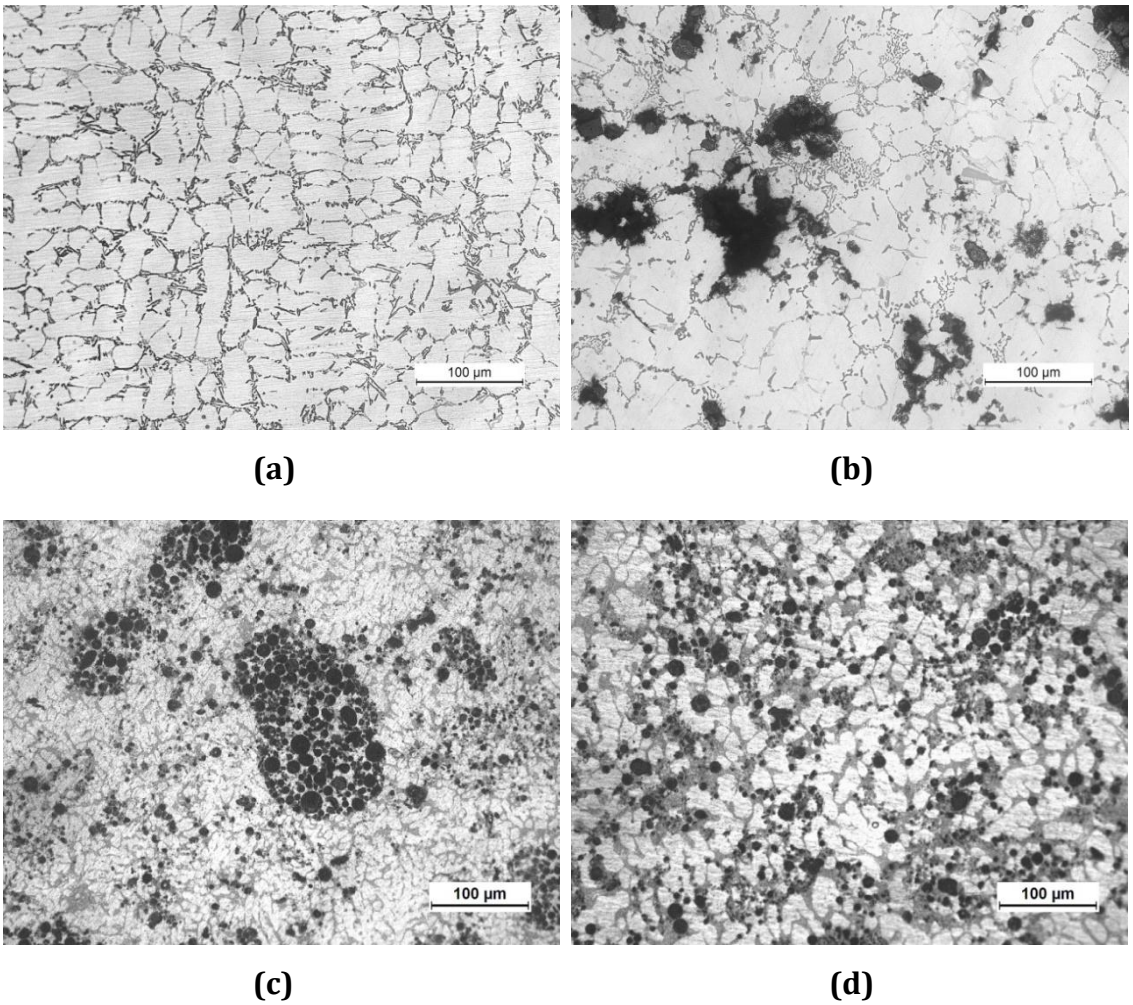

Figure 4.2. Microstructures of (a) Al A356 squeeze cast base alloy (b) A356-7% microsilica composite synthesized by liquid metal stir casting and gravity cast (c) A356-7% microsilica composite processed by compocasting followed by squeeze casting (d) Modified compocast- recast final composite by remelting, stirring and squeeze casting.

4.3.2. Thermal and Physical Characteristics

Differential thermal analysis curves of the squeeze cast alloy and the modified compocast composite in Figure 4.3 show a major peak at the temperature of 577 ^{o}C corresponding to the precipitation of L $\rightarrow$ α-Al + eutectic Si (solidus) and the adjacent peak at 613ºC corresponds to L $\rightarrow$ α-Al dendrites (liquidus). The peak at 370 ^{o}C corresponds to the Mg_2Si precipitate formation. The minor shift in liquidus temperature of composite towards the lower temperature is due to the colligative property of depression in freezing point by the addition of microsilica particles into the alloy. Similar observation of depression in liquidus

temperature by the addition of silicon carbide particles into A356 aluminum alloy was found in earlier studies.[179] The compocasting was carried out at the temperature between the liquidus and the solidus, where the semisolid alloy containing the α-Al dendrites were stirred in the temperature range of 585 - 590ºC. The α-Al which is in a semi solid state provides shear action during stirring to provide better and uniform dispersion of particles in the matrix than the pure liquid metal stirring process. The density of the modified compocast composite sample is 2.52 g/cm^3 which is lower than those of the monolithic alloy (2.68 g/cm^3).

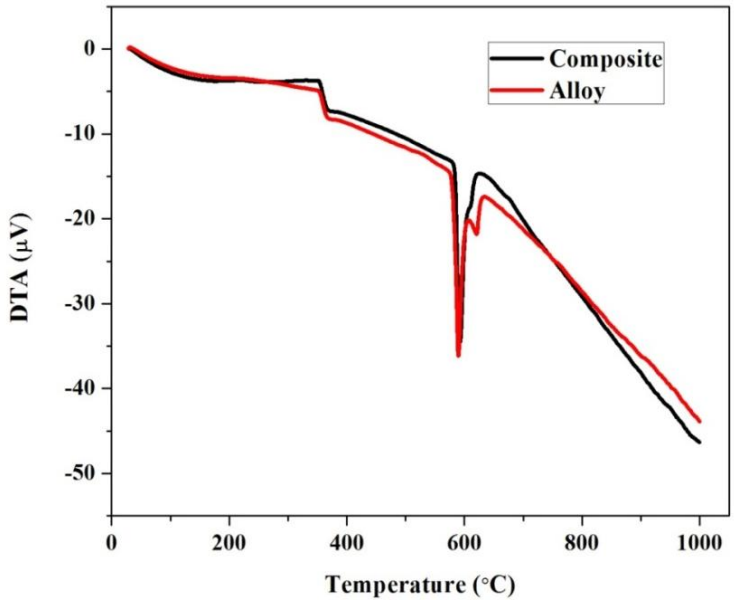

Figure 4.3. DTA analysis of unreinforced A356 alloy and modified compocast composite.

4.3.3. Mechanical Properties

The Brinell hardness of Al A356 base squeeze cast alloy and their composites containing 7% microsilica fabricated by different processing techniques in as cast and heat treated conditions are presented in Figure 4.4. From the figure, it can be observed that by incorporating microsilica particles into matrix conspicuously enhances the hardness properties compared to base alloy, however the property is also dependent on the quality of composite produced. Particles in the matrix act as heterogeneous nucleation sites for the grain refinement and also difference in the thermal expansion coefficient between

particles and the alloy induces mismatch strains in the interface which act as a barrier to the movement of dislocations.

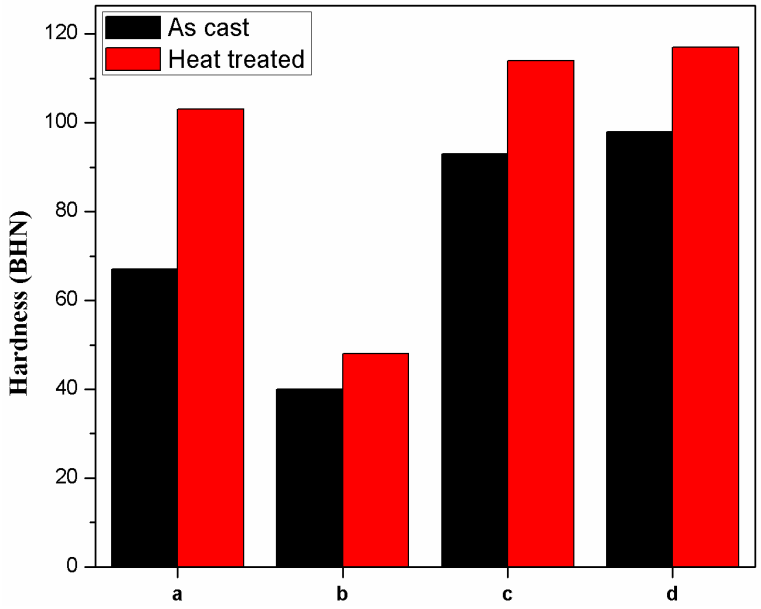

Figure 4.4. Hardness of (a) A356 alloy squeeze cast (b) A356-7% micro silica composite by stir casting (c) A356-7% micro silica composite by compocasting and squeeze casting (d) Modified compocast.

The hardness of the composite strictly depends on the processing techniques and consistency in particle distribution which acts as an impediment to the motion of dislocation. A356-7% microsilica composite processed by liquid metal stir casting followed by gravity casting in as cast and heat treated condition shows significant reduction in the hardness value compared to base alloy. Microsilica particles clustering occurred at higher temperature processing induced agglomeration and porosities, consequently remarkable changes in the hardness value are obtained. Composite fabricated by compocasting followed by squeeze casting technique in as cast and heat treated condition shows superior hardness compared to other processing techniques due to the better distribution of particles in the matrix as well as the finer grain size since solidification takes place under pressure. The dendrite arm spacing (DAS), which represents the size reduction of primary aluminum shows a DAS of squeeze cast unreinforced alloy is 13 μm, whereas the modified compocasting shows 7 μm. The modified compocast composite in as cast and heat treated conditions results in enhanced hardness properties by avoiding

the segregation of particles in the metal matrix. Among the various processing conditions used, the A356-7% microsilica composite processed by modified compocasting technique provides better distribution of particles and higher hardness. Hence further characterizations are made on modified compocast composite.

The average compressive strength obtained for Al A356–7% microsilica reinforced modified compocast composite in T6 condition is 656 MPa, which is significantly higher than the squeeze cast matrix alloy of 516 MPa. The enhanced compressive strength of composite is due to the resistance to deformation stress of the matrix by the hard microsilica particles. The plastic flow of the matrix is constrained due to the smaller inter-particle spacing of the microsilica, which prevents the dislocation motion and thereby promoted strain hardening of the composite matrix functioned as a strain hardening effect in the composite.

4.3.4. XRD Analysis

The XRD pattern of as received and extracted microsilica particles from the modified compocast composite using NaOH is shown in Figure 4.5a and b respectively. The major diffraction peaks observed in as received microsilica particles belongs to $NaAlSi_3O_8$, $KAlSi_3O_8$, SiO_2 and Al_2O_3 phases. Various techniques have been adopted for synthesizing alkali aluminosilicate in which aqueous alkali hydroxide solution of Na or K was added for the formation of $NaAlSi_3O_8$ and $KAlSi_3O_8$ phases. These phases act as a corrosion resistance agent having a melting point of approximately 1750 °C and 1690 °C respectively, which is an added advantage and strengthens the alkali aluminosilicate particle to a further extent.[223] The pattern of XRD peaks of the as-received microsilica particle shows slightly amorphous in nature by the presence of shallow diffraction peak, however the extracted particle are more crystalline in nature. Chemical interaction between the magnesium in the matrix and the constituents, i.e., Al_2O_3 and SiO_2 present in the microsilica leads to the formation of $MgAl_2O_4$ spinel and intermetallic phase $Mg_{17}Al_{12}$. The Mg in the alloy improves the wettability between the matrix and the reinforcement by the formation of $MgAl_2O_4$ spinel by scavenging the oxides.[35] The modification of intermetallic phase $Mg_{17}Al_{12}$ by heat treatment process enhances the mechanical properties of the material.[224]

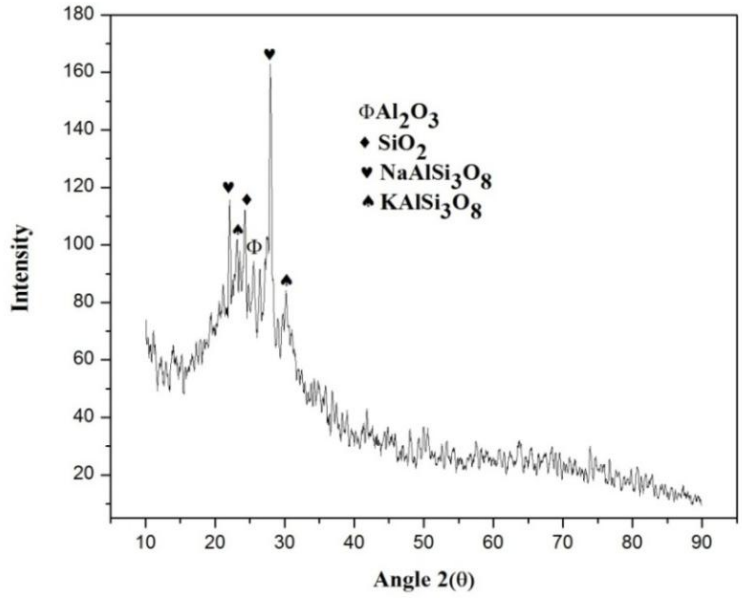

(a)

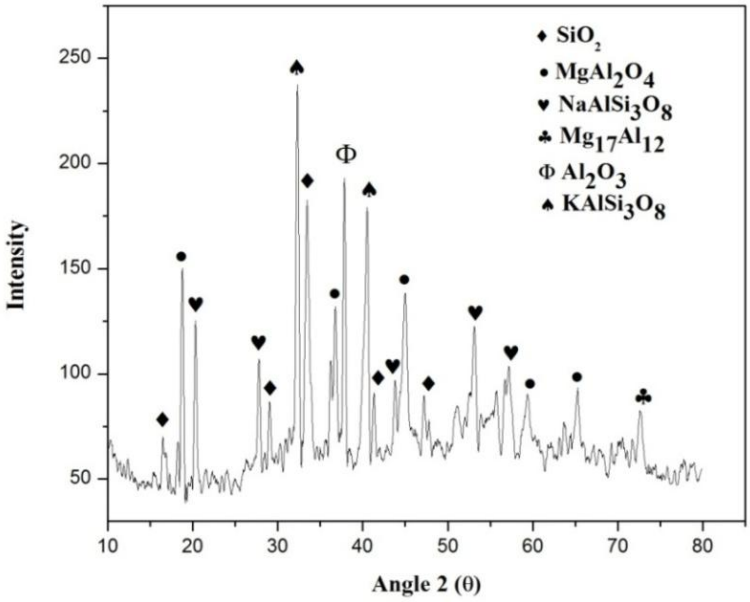

(b)

Figure 4.5. XRD pattern of (a) As received micro silica particles (b) extracted microsilica particles from modified compocast composite using NaOH solution showing interfacial reaction products.

4.3.5. Wear Characteristics

The wear behavior of A356 squeeze cast alloy and the modified compocast composite with respective to variation in load and velocity is shown in Figure 4.6. The wear rate of both alloy and composite increases with increase in load owing to

the higher temperature caused by shear stress at higher load. It is evident from the graph that the wear rate of microsilica reinforced composites is significantly lower than the base alloy which is attributed to the presence of hard microsilica particles. The unreinforced alloy is softer compared to composites and thus encountering heavy plastic deformation on the sliding surface and causing high wear rate. A drastic wear transition region, ie mild to sever wear transition is observed in the case of A356 squeeze cast alloy at a speed of 2 m/s in 30 N load. When the load was increased to 40 N heavy material damage and lot of vibration was observed during testing, hence further wear studies for unreinforced alloy was discontinued. On the other hand reinforcement in the composite act as a stress bearing component of the material thereby reducing the severe plastic deformation, further, it plays as a role in strengthening material to the composite by increasing the hardness which is inversely proportional to the wear loss.

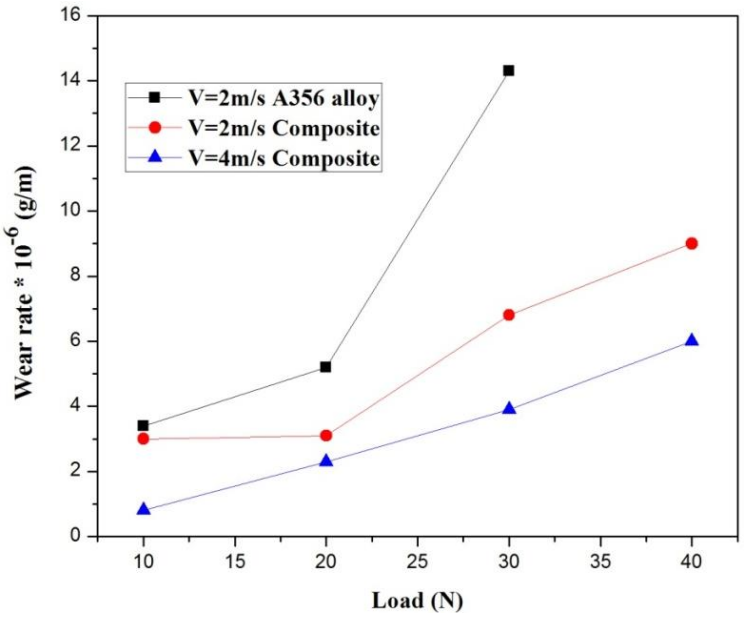

Figure 4.6. Wear rate of unreinforced A356 squeeze cast alloy and A356-7% micro silica reinforced modified compocast composite with varying loads and sliding speeds.

It is discerned from the plot that an increase in sliding velocity results in decreased wear rates in case of composites resulted in the increased formation of tribolayer. This mechanically mixed layer (MML) was found to be composed of plastically deformed wear debris and oxidized particles formed during sliding

which act as a wear resistance layer.[225] Obviously increased sliding speed may result in the quick evolution of tribolayer and the wear rate of composite gets reduced. Similar observation has been depicted in the investigation on hybrid Al-Gr and Al-SiC particulates composites.[226]

Worn surfaces of the Al A356 squeeze cast alloy sliding at room temperature are shown in the SEM micrographs (Figure 4.7). From the micrograph, it is observed that deeper and wider grooves (marked A) with flow of material (marked B) along the sliding direction with the formation of cavities were formed in case of unreinforced alloy at a speed of 2m/s at 10 N load (Figure 4.7a-b).

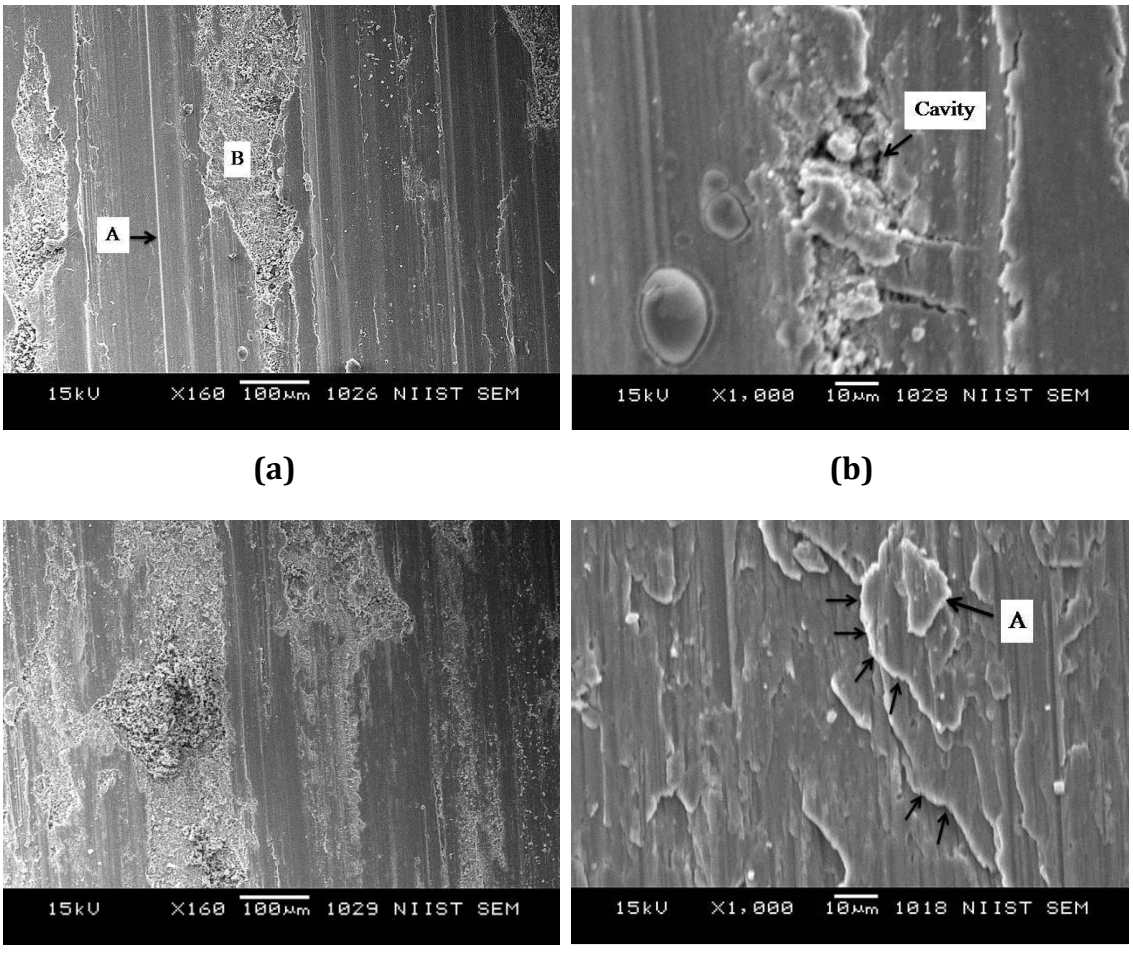

(a) **(b)**

(c) **(d)**

Figure 4.7. SEM micrographs (Lower and Higher magnification) of worn out surface of (a) and (b) Squeeze cast A356 unreinforced alloy at an applied velocity of 2m/s in 10 N load (c) and (d) Squeeze cast A356 unreinforced alloy-2m/s in 30 N load.

The degree of shear deformation in alloy increased at a higher load of 30 N (Figure 4.7c-d) with radical delamination (marked A) of the material surface resulted in localized crack propagation (arrow marked). This induced the adhesion wear mechanism of matrix alloy which displayed highest wear rate compared to composite.

Worn surfaces of 7% microsilica reinforced modified compocast composite seems to be reasonably smooth compared to alloy (Figure 4.8a-f) at 10 N and 40 N load with the formation of MML with increase in velocity, which can be observed from the patches on the wear track (Figure 4.8e and f). Effect of delamination is lessened in the case of composite (Figure 4.8b and d) with shallow grooves (Figure 4.8a and c marked A) and these phenomenon gets reduced significantly at higher sliding speed due to the formation of tribolayer which resist the plastic flow of the material. This clearly specifies that wear loss can be correlated to the presence of tribolayer, which may act as a protective layer.

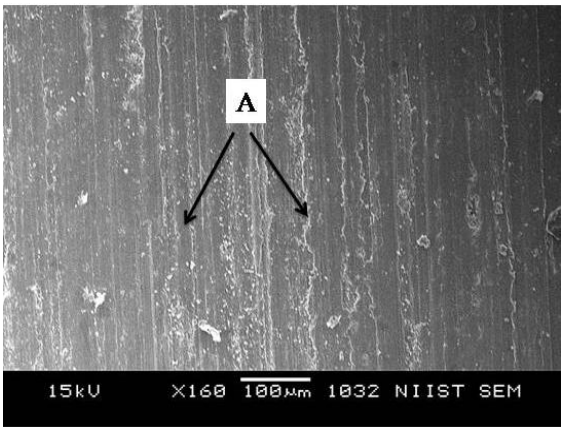

(a)

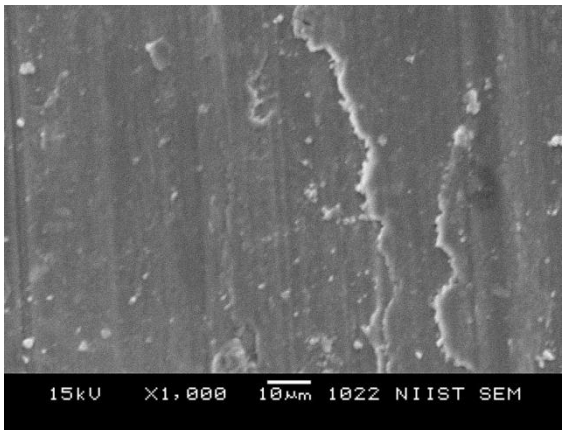

(b)

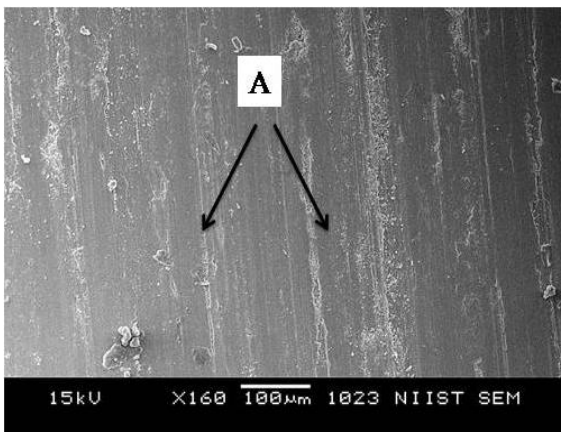

(c)

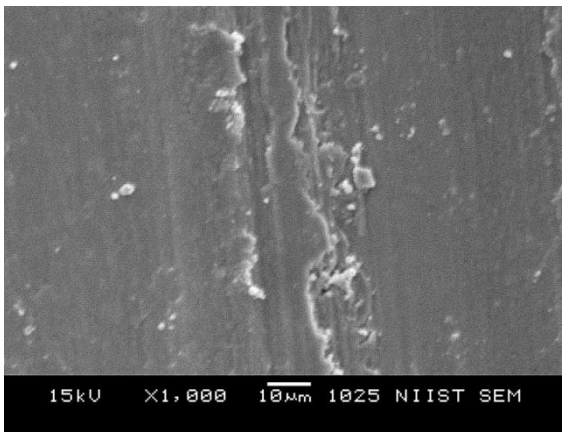

(d)

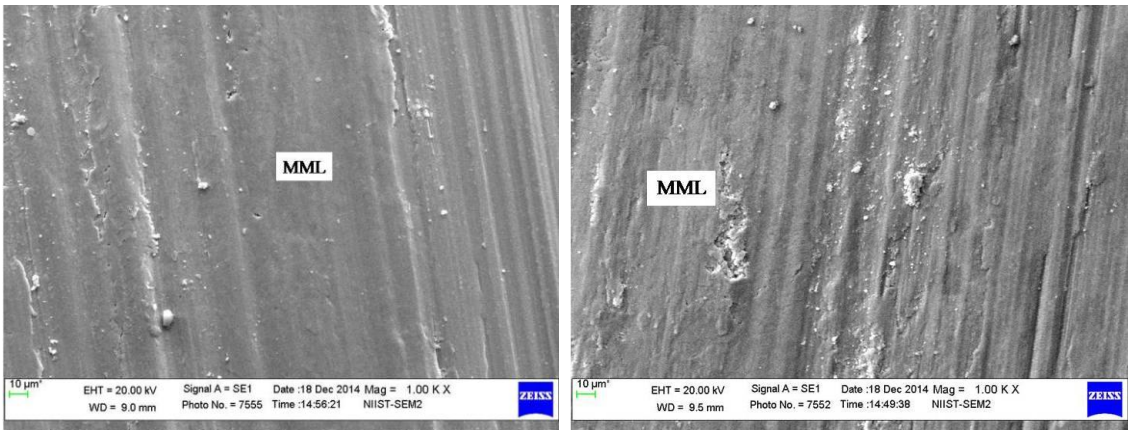

(e) **(f)**

Figure 4.8. SEM micrographs (Lower and Higher magnification) of worn out surface of (a) and (b) composite at an applied velocity of 2m/s in 10 N load (c) and (d) composite-2m/s in 40 N load (e) composite-4m/s in 10 N load (f) composite-4m/s in 40 N load.

With the increase in load, an excessive flow of material is observed in alloy pin surface compared to the composite. As the load increases the rate of material loss in all systems increased and may be ascribed to the nature of plastic flow at higher load. According to the earlier studies the stability of the MML gets reduced due to the increasing thickness of these layers at the higher load conditions. The adhesion of the MML decreases with increase in the layer thickness and it is more stable in thin layer [227-229].

EDS spectrum of the worn surface of the modified compocast composite at sliding speed of 4 m/s and load 40 N shows the presence of Si, iron and oxide layers like $MgAl_2O_4$, Al_2O_3, MgO (Figure 4.9). Thermal stability of these oxide layers withstands the heat generated during friction and thereby reduces adhesion mechanism due to the softening and deformation of material surface which directly relates with the wear rate. The presence of oxides is observed in the mechanically mixed layer by the presence of strong oxygen peak in EDS. This confirms that tribolayer formed between two sliding surfaces contain various oxides formed both from the pin and counter surface. The iron from the counter body (EN31 steel) surface gets transferred to the pin surface convincing the abrasive wear mechanism observed in the composite.

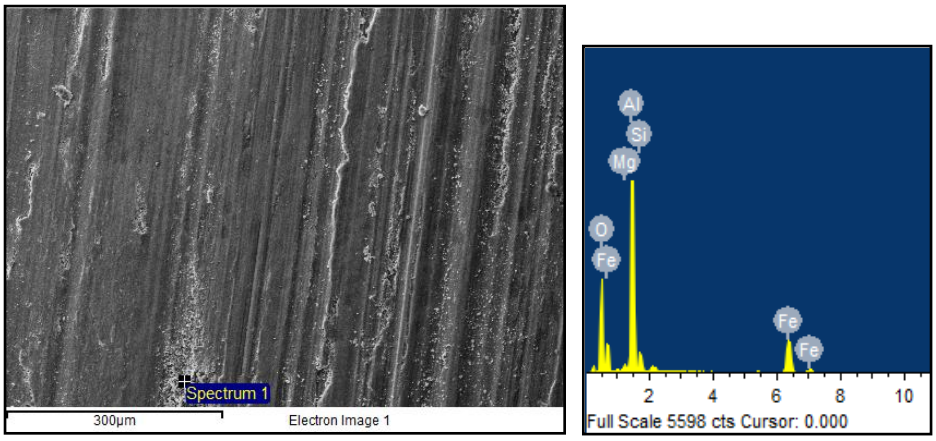

Figure 4.9. SEM micrograph and EDS spectrum of worn out track of composite wear pin (sliding speed -4 m/s, load - 40 N).

4.3.6. Corrosion Characteristics

Corrosion potential and corrosion current values of both squeeze cast alloy and the modified compocast composite were obtained from the extrapolation of anodic and cathodic Tafel lines (Figure 4.10). It is well known phenomenon that the corrosion rate is directly proportional to the corrosion current, which in turn depends on the polarization resistance. It can be seen from the polarization curve that there is a minor negative shift in the corrosion potential (E_{corr}) value of composite (-0.83 V) with reference to the alloy (-0.80 V). From the polarization measurements the corrosion current density (I_{corr}) value for the modified compocast composite is 10 µA/cm^2, whereas the unreinforced alloy shows an I_{corr} value of 11 µA/cm^2. Both the composite and alloy shows comparable corrosion resistance with respect to corrosion current density values. According to the Stern-Geary equation, polarization resistance (R_P) of the material can be calculated from

$$\Delta E/\Delta i = R_P = \frac{\beta_A \beta_C}{2.3 i_{CORR} (\beta_A + \beta_C)} \qquad (1)$$

Where, $\Delta E/\Delta i$ is the slope of the linear region, β_A is the anodic Tafel constant expressed in volts per decade of current and β_C is the cathodic Tafel constant expressed in volts per decade of current. From the above formula it can be discerned that the polarization resistance of the composite (2552.86 Ω) is higher compared to alloy (1105 Ω). Based on polarization resistance (R_P) determination,

the Al A356-7% microsilica reinforced modified compocast composite shows enhanced corrosion resistance compared to the unreinforced base alloy.

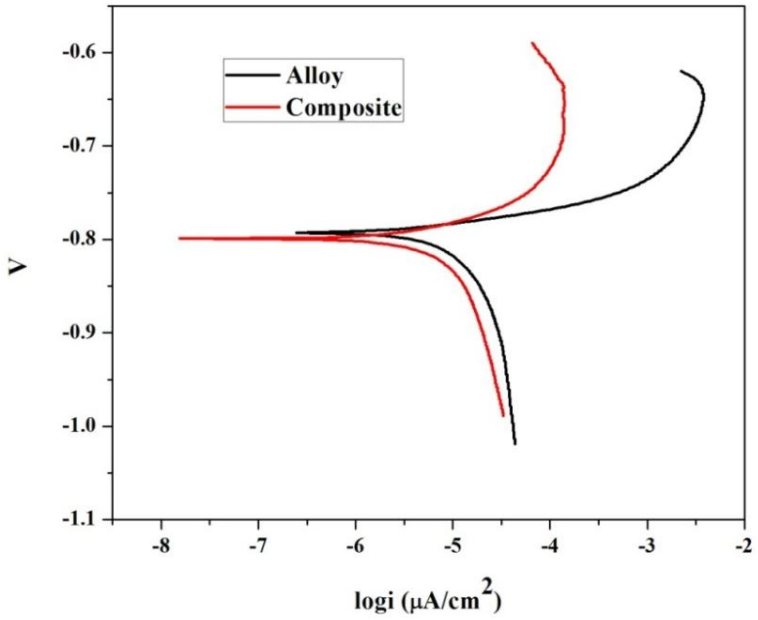

Figure 4.10. Potentiodynamic polarizations curves of A356 squeeze cast alloy and modified compocast composite exposed to 3.5 wt % NaCl aerate solution with calomel as reference electrode.

Formation of interfacial products obtained from the reaction between Al, Mg and microsilica particles has a favorable effect on corrosion resistance of the composite. The corrosive species have less tendency to attack the oxides and spinel compared to the alloy. Predominant phases include $MgAl_2O_4$, Al_2O_3, and SiO_2 act as a protective passive film (oxide layer) on the material surface. The intermetallic Mg_2Si acts as anodic region to the matrix, thus leading to catastrophic localized corrosion[127] and formation of such reactions are limited as the oxygen content was high enough to react with Mg emerging spinel and magnesium oxide phases. Bonding between the matrix and reinforcement should be strong, since weak interfaces act as favorable site for oxide layer break down and pit nucleation.

4.4. Conclusion

- Better separation, dispersion and distribution of the microsilica particles in the solidified matrix is obtained by compocasting cum squeeze casting process than in liquid metal stir casting. However, segregation of particles in the resultant composite can be avoided by recasting process.
- Hardness of the composites predominantly depends upon the processing method, related to the reinforcement distribution. Composite samples obtained by recasting process attain higher hardness compared to other systems.
- Sliding wear behavior of Al A356 squeeze cast alloy and 7% microsilica reinforced modified compocast composite was studied as a function of varying load and speed. Adhesive wear mechanism is observed in the case of alloy with severe material flow and delamination due to localized crack propagation.
- Composites exhibit a remarkable wear resistance with decreased wear rates at an increased sliding velocity due to the formation of tribolayer containing oxygen and iron on the pin surface and abrasive wear mechanism is observed in the system.
- Tafel curve and polarization resistance measurements reveal that Al A356-7% microsilica reinforced modified compocast composite shows similar corrosion resistance compared to squeeze cast alloy by the presence of mixed oxide layers like $MgAl_2O_4$, $NaAlSi_3O_8$ and $KAlSi_3O_8$. These oxide layers act as a protective film on the material surface thereby preventing the pitting corrosion to further depth.
- The compression strength of modified compocast composite is enhanced compared to the squeeze cast matrix alloy and the density of the modified compocast composite sample is less than those of the monolithic alloy.
- These composites are more predominantly applied for fabrication of wear resistant engineering components where higher hardness and compressive strength are preferentially required.

Chapter 5

Effect of Alumina Nanoparticle on Strengthening of Al-Si-Mg Alloy Processed by Modified Compocasting

Abstract

The present investigation evaluates the effect of varying percentage of alumina nanodispersions in strengthening and interfacial bonding with cast A356 aluminum alloy by modified compocasting followed by solidification using squeeze casting. Addition of 0.5 wt% Al_2O_3 nanoparticles to cast alloy shows remarkable enhancement in the yield strength from 204 to 323 MPa. They also exhibit higher hardness, UTS, compressive strength, thermal, tribological and corrosion properties. HRTEM image showed the insertion of Al lattice into the Al_2O_3 crystalline lattice contributing to strengthening of the alloy. The Al_2O_3 nanoparticles and the β'' are involved in the Orowan strengthening of Al nanocomposite. The presence of hard Al_2O_3 nanoparticles and the stronger bonding between particle and alloy constrain the dislocation motion leading to dislocation bowing. The theoretical estimation of Al -0.5 wt% Al_2O_3 nanocomposite yield strength shows that the contribution of Hall-Petch is predominant followed by Orowan and solid solution strengthening.

5.1. Introduction

Aluminum alloys with nanodispersions are gaining considerable attention as lightweight metallic materials in high-performance application areas of aerospace and defense sectors. Aluminum Nanocomposites (ANC) exhibits excellent mechanical properties, resistance to creep at the higher temperature and good fatigue strength compared to base aluminum alloys.[230-231] The nanoscale reinforcement has more reinforcing effect than micron size in metallic systems due to the strong bonding at atomic level between the matrix and nano reinforcement.[232] Furthermore, since the distribution of nano-reinforcement in metal matrix is inter and intra-granular types, the concepts of Hall-Petch and Orowan mechanism contribute for material strengthening.[233] However, the major challenge while developing metallic nanocomposite is on uniform distribution of

dispersoids in the matrix and the properties of the final composite depend on the same.[234,144] A variety of techniques have been developed to integrate nanoscale reinforcements with metal matrix like powder metallurgy,[235] stir casting,[236] compocasting,[237] infiltration,[238] ultrasonic technique[239] etc. Among them, stir casting is attractive due to its simplicity and low cost in processing. However, the disadvantages are the agglomeration of reinforcement due to low wettability with the matrix and the formation of interfacial reactions. In recent years, researchers have identified compocasting as one of the effective methods for fabricating ANC over other conventional methods due to its advantages like uniform distribution of reinforcement without agglomeration, good wettability and better matrix-reinforcement bonding.[142] Compocasting is a solid-liquid state method in which a vortex is created in the semisolid molten metal and the reinforcements are added into the vortex under stirring.[150]

Sajjadi et al. reported the studies on Al A356 nanocomposites processed by the compocasting process, however the mechanical properties reported are 162 MPa for 3wt% of alumina nanoparticle addition.[151] Mazahery et al. identified that the porosity level of nanocomposites increases with increasing nanoparticles content, fabricated by stir casting process.[160] Squeeze casting technique has great potential in reducing the porosity level in final composite.[207] The literature survey shows that most of the works on Al-nanocomposites have been focused on improving the mechanical properties with the high weight percentage of nanoparticles without tailoring the process parameters. Hence, the basic study on the effects of tailoring the process parameters in strengthening the Al-nanocomposites at the atomic level is almost non-existent. One of the major requirements of composite materials is a strong interface bonding for effective load transfer from the matrix to the reinforcement.[240] Accordingly, in the present investigation Al-Al_2O_3 nanocomposites are processed by modified compocasting technique and solidified under squeeze casting process. The paper deals with the evaluation of interfacial characteristics between the nanoparticles and aluminum matrix, and the influence of interfacial bonding on the strengthening of cast aluminum alloys. The nanocomposites are characterized with respect to structural, interfacial, physical, mechanical, tribological, and corrosion characteristics.

5.2. Experimental Procedure

5.2.1. Processing of Al-Al_2O_3 Nanocomposite

Al A356 cast alloy supplied by Sargam Metals, India was used as the matrix material with a chemical composition of Al–7Si–0.35Mg (in wt%). The Al_2O_3 nanoparticles with the weight percentage of 0.25 wt%, 0.5wt%, and 1 wt% were used as the reinforcement with average particle size of 40 nm obtained from Alfa Aesar. The density of Al_2O_3 nanoparticles used was 3.6 g/cc with a melting point of 2045 ^oC. The stir casting and modified compocasting routes were used for fabricating Al-Al_2O_3 nanocomposites and solidified using squeeze casting by 25T hydraulic press. The Al_2O_3 nanoparticles were preheated at 200 ^oC for 1 hr. Stir casting process involves the incorporation of Al_2O_3 nanoparticles into the vortex of mechanically stirred molten metal and solidified by squeeze casting above the liquidus temperature of the matrix material (730 °C). In modified compocasting process, the Al_2O_3 nanoparticles were incorporated into the vortex of semisolid metal at a temperature between the solidus and liquidus (585-595°C) range of the matrix material and solidified the composite melt using squeeze casting above the liquidus temperature of the matrix material (730 °C). To ascertain better dispersion of nanoparticles, the compocast ingot was reprocessed by remelting, stirring and squeeze casting. The effects of modified compocasting over compocasting were described in our previous study.[207] The squeeze casting of Al A356 alloy was carried out for comparison of properties. During the fabrication of composites, 1 wt% Mg in pure form was added into the molten aluminum metal to improve the wettability between the nanoparticles and the matrix.

5.2.2. Characterization

Structure and properties of Al-Al_2O_3 nanocomposites were characterized by different techniques and compared with base alloy. The T6 heat treatment condition was used for base alloy and Al-Al_2O_3 nanocomposites, i.e., solution treatment (525 °C for 12 h) followed by quenching in warm water (80 °C) and then precipitation or age hardening at 165 °C for 8 h. The microstructures were investigated by Leica DMRX optical microscope, JEOL Scanning electron microscope and JEOL-JEM-2100 transmission electron microscope with Oxford energy dispersive X-ray spectroscopy (EDS). The secondary dendrite arm spacing (SDAS) values were measured using linear intercept method. The coefficient of

thermal expansion (CTE) was measured using EXSTAR-TMA/SS6100 thermo mechanical analyser at a heating rate of 10 ^{o}C/min. The differential thermal analysis (DTA) was carried out using Hitachi STA7300 (TG–DTA) instrument at a heating rate of 10 °C/min in the argon atmosphere. The density was measured using Archimedes principle method. Heat-treated samples were used for mechanical properties and wear characterization. The tensile and compression tests were carried out using universal testing machine (INSTRON 1195-5500R). The hardness was measured using ZwickBrinell hardness testing machine with a 2.5 mm ball indenter and 62.5 kg load. The dry wear tests were carried out in DUCOM (TR20LE) pin-on-disk tribometer with applied loads of 10 N, 20 N, 30 N, 40 N and 50 N at a sliding velocity of 2 m/s for the constant sliding distance of 1500 m. The corrosion tests were carried out using electrochemical workstation (CH Instruments, 680) with three-electrode cell system. The Al A356 alloy and Al-Al_2O_3 nanocomposites were used as the working electrode, platinum was used as the auxiliary electrode and calomel as the reference electrode. In all the tests the working electrode under study was subjected to 3.5 wt% NaCl solution and the scan rate was 1mV/sec.

5.3. Result and Discussion

5.3.1. Microstructural Characteristics

Figure 5.1a showed the optical microstructure of squeeze cast Al A356 base alloy, in which the formation of primary phase α-Al dendrites (white region) and Al–Si eutectic mixture (gray region) between the dendrite arms during solidification is observed. The elimination of porosities and the formation of fine grains are perceived in the microstructure (secondary dendrite arm spacing of 17μm) since solidification takes place under pressure with the higher degree of heat dissipation during squeeze casting process. Figure 5.1(b, c, and d) shows the microstructures of Al A356-0.25 wt%, 0.5 wt%, and 1 wt% Al_2O_3 nanoparticles reinforced composites respectively, prepared by modified compocasting process. It is clear from the microstructures that the incorporation of Al_2O_3 nanoparticles into the aluminum matrix refines the phases of the composites compared to squeeze cast A356 base alloy. As the sizes of Al_2O_3 particles are in nanometer scale, the surface area of particles in the matrix increases thereby enhancing the

grain nucleation sites and breaking of dendrites resulting in refined grain size of the composite microstructure during solidification. The addition of 0.25 wt% Al_2O_3 nanoparticles into the aluminum matrix alters the grains size (Figure 5.1b) with a secondary dendrite arm spacing of 13.5 μm. When 0.5 wt% Al_2O_3 nanoparticles are added into the matrix aluminum, the size of aluminum dendrites and eutectic Al-Si morphology gets refined significantly (Figure 5.1c) compared to the former one. The SDAS value of Al-0.5 wt % Al_2O_3 nanocomposite is 9μm, which is lower compared to all other variants due to the incorporation of optimum weight percentage of nanoparticles into the matrix with better dispersion and distribution of particles. Further addition of Al_2O_3 nanoparticles (1 wt %) into the matrix increased the secondary dendrite arm spacing to 11 μm (Figure 5.1d) compared to 0.5 wt% Al_2O_3 nanoparticles added composite due to the agglomeration of nanoparticles in the matrix aluminum. Al A356-0.5wt% Al_2O_3 nanoparticles reinforced composite processed by stir casting technique also results in the agglomeration of particles in the matrix, which extensively increase the grain size of the composite with a secondary dendrite arm spacing of 15 μm (Figure 5.1e). During compocasting process, the higher viscosity of semisolid aluminum molten metal slurry transmits shear force over the agglomerated nanoparticles which lead to better dispersion and distribution of reinforcement in the matrix.[150] Also, good wettability between the nanoparticles and the melt is maintained in the semisolid state.

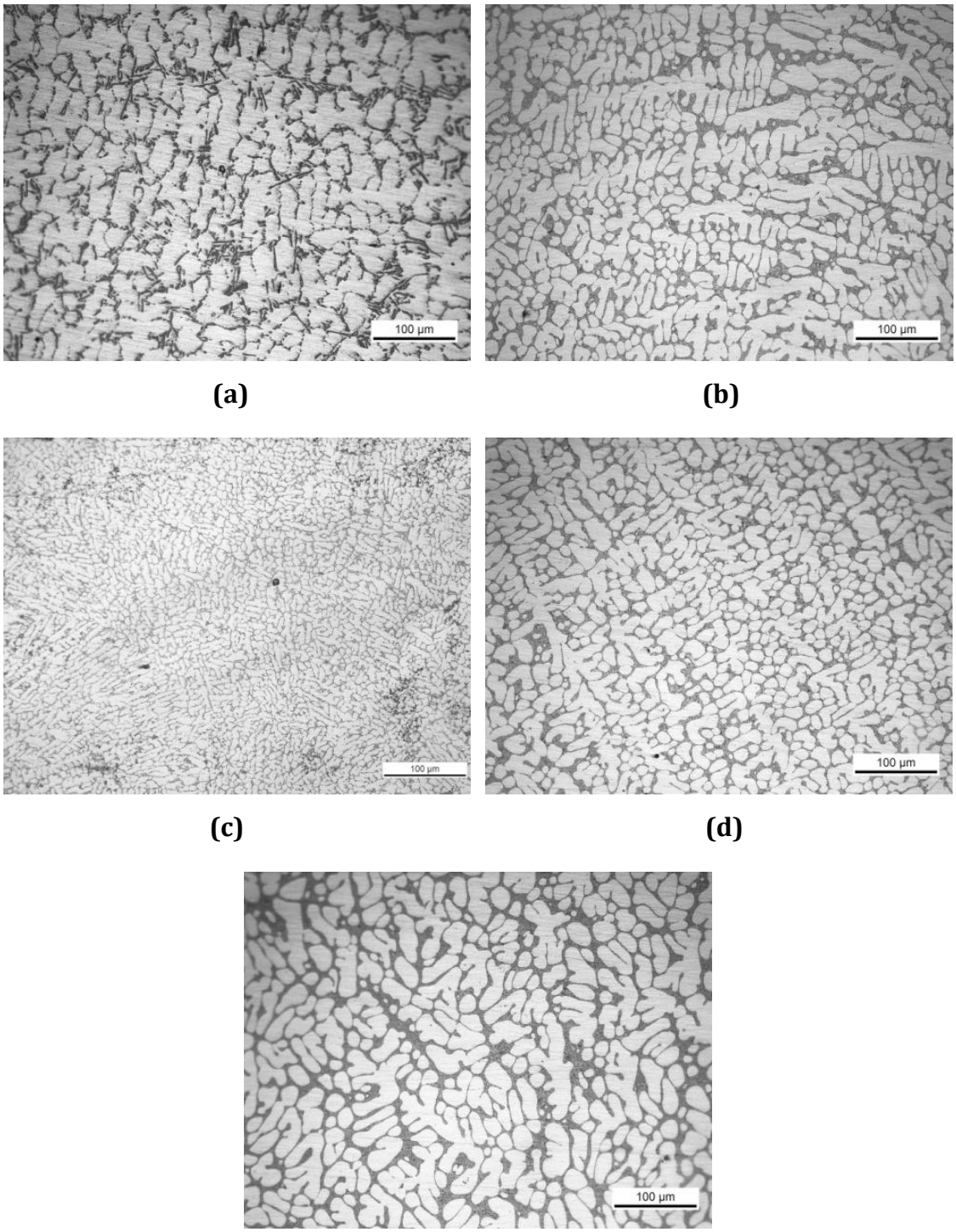

Figure 5.1. Optical Microstructures of (a) Al A356 squeeze cast base alloy; (b) A356-0.25 wt%, (c) A356-0.5 wt%, and (d) A356-1 wt% Al_2O_3 nanoparticles reinforced composites by modified compocasting technique; (e) A356- 0.5 wt% Al_2O_3 nanoparticles reinforced composite by stir casting technique.

5.3.2. Strengthening by Nanodispersion

HRTEM images of Al-0.5 wt% Al_2O_3 nanoparticles reinforced composite by modified compocast method is shown in Figure 5.2, in which the distribution of Al_2O_3 nanoparticles in the aluminum matrix is perceived (Figure 5.2a). Figure 5.2b shows the crystalline lattice inside an Al_2O_3 nanoparticle having an interplanar distance $d_{(440)}$ of 0.13 nm. The strong adhesion at atomic level between the aluminum and Al_2O_3 nanoparticle is observed at the interface (marked as I) (Figure 5.2c), in which the lattice planes of aluminum get inserted into the Al_2O_3 crystalline lattice, thereby providing a 'Key Lock' effect. The 'Key Lock' effect in Al-Al_2O_3 nanocomposite may be due to two factors: (a) atomic diffusion of aluminum into Al_2O_3 nanoparticle, and (b) solidification of the composite under high pressure. The presence of nanoparticles hinders the motion of dislocations in the matrix by trapping the dislocations between the particles (Orowan mechanism), thereby improving the yield strength of the material. Orowan looping and bowing are observed in the matrix (Figure 5.2d), later the dislocations bypass the nanoparticles. The dislocation bowing is directly proportional to the resistance force offered by the nanoparticle which in turn depends on the matrix-reinforcement bonding, and the hardness of reinforcement. Figure 5.2e shows the dislocation mechanisms in three different types of AMNC (a) composite with hard nanoparticles and low bonding strength (matrix/nanoparticles) - wherein, the high dislocation force / plastic flow of the matrix moves the nanoparticles from its original position and encounters heavy material deformation, (b) composite with soft nanoparticles and high bonding strength- wherein, the high bonding strength of nanoparticles shows some resistant force against the dislocation force, but due to its softness nanoparticles breaks and encounters material deformation, and (c) composite with hard nanoparticles and high bonding strength- wherein, the nanoparticles shows high resistance force against the dislocation force, resulting in dislocation looping and bowing with less material deformation. In the present case of nano alumina dispersed composite the last mechanism is prevalent.

5.3.2.1. Strengthening by Squeeze Pressure and Phase Refinement

During squeeze casting, a large number of dislocations will be generated in the matrix and they entangle with each other causing dislocation density sites (Figure 5.3a). As a result, more stress is needed to plastically deform the material

resulting in the higher yield strength of the material. At the same time, faster cooling rate during solidification in squeeze casting process causes the formation of metastable phases[241] like AlFeSi (Figure 5.3b) and Mg_2Si, which act as hurdles and arrest the dislocation density sites. Two types of Mg_2Si morphologies are observed in the aluminum matrix: (a) rod shape-β' (Figure 5.4a), and (b) needle shape-β" (Figure 5.4b).[242] In which, β" precipitate has more efficiency in locking the dislocations mobility over β' due to its nanoscale-size (50-100 nm length), thereby playing the similar role like Orowan mechanism. The uniform arrangement of β" precipitates perpendicular to the dislocations are observed with a texture like 'Zebra Crossing'. Since, the morphology of β" precipitates are 'needle' shape the dislocations bypassing the β" precipitates encounter high tension, which leads to breakup and scattering of dislocation (marked as D) (Figure 5.4b). As a result, the overall stress caused by the dislocation in the material is reduced. The two reasons behind the breakup and scattering of dislocation are (a) the edge of β" precipitates- which creates distortion in the contact point of dislocation lines, and (b) the length of β" precipitates-which exceeds the limit of dislocation bowing (Figure 5.4c). Figure 5.4d showed the force in dislocation line when it contact with the β" precipitate. It can be expressed as[243]

$$F = 2T\sin\theta \qquad (1)$$

Where, F is the resistance force of precipitate and T is the tension of dislocation line. In which, if the resistance force F increases then the dislocation line tension T decreases due to increase in θ value. Also, the alloying elements like Si in the matrix play the similar role in locking dislocations (Figure 5.5).

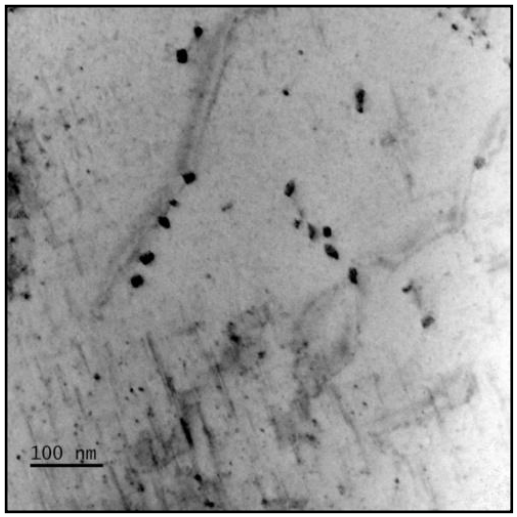

(a)

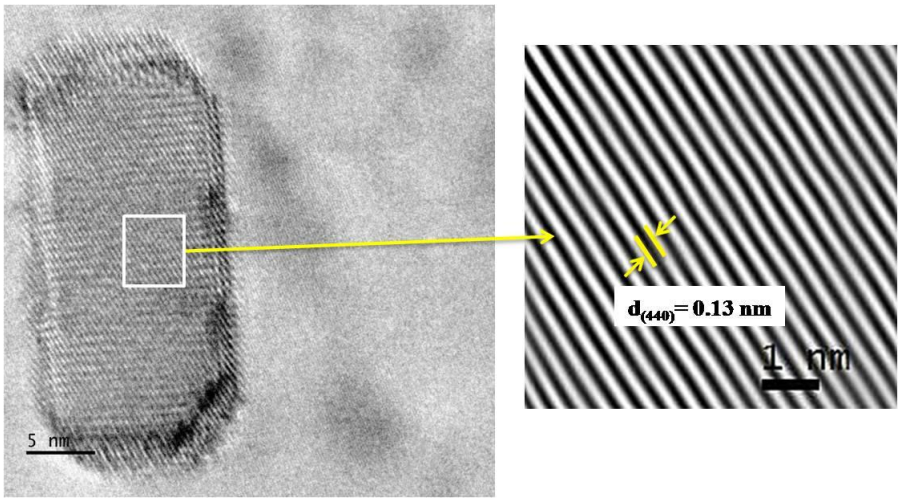

(b)

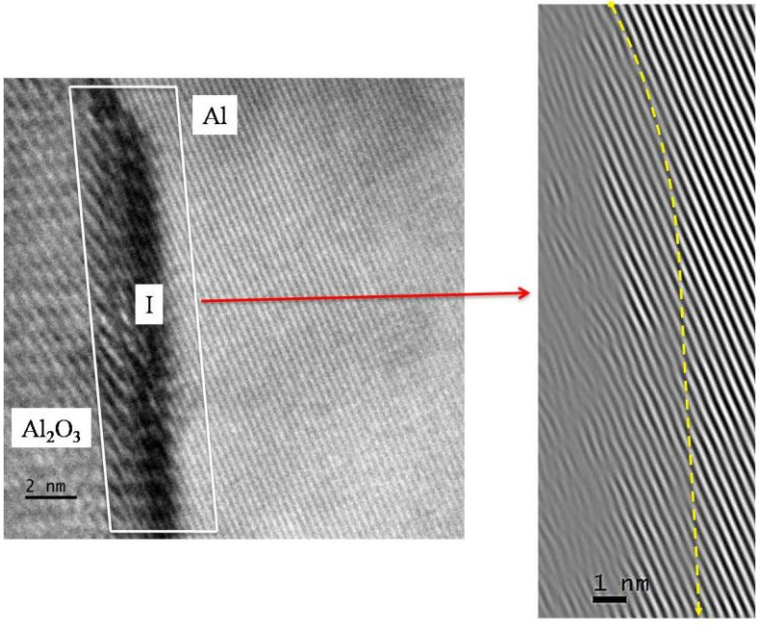

(c)

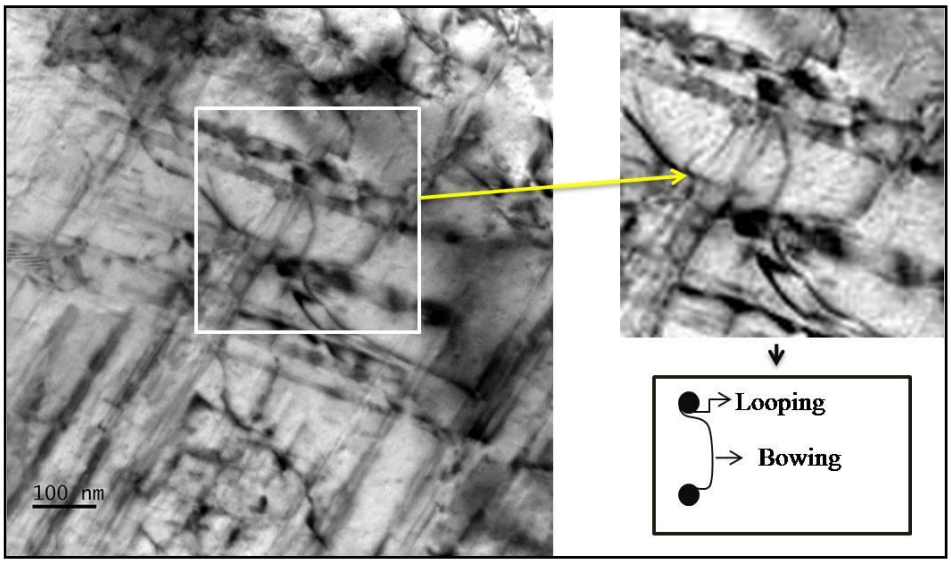

(d)

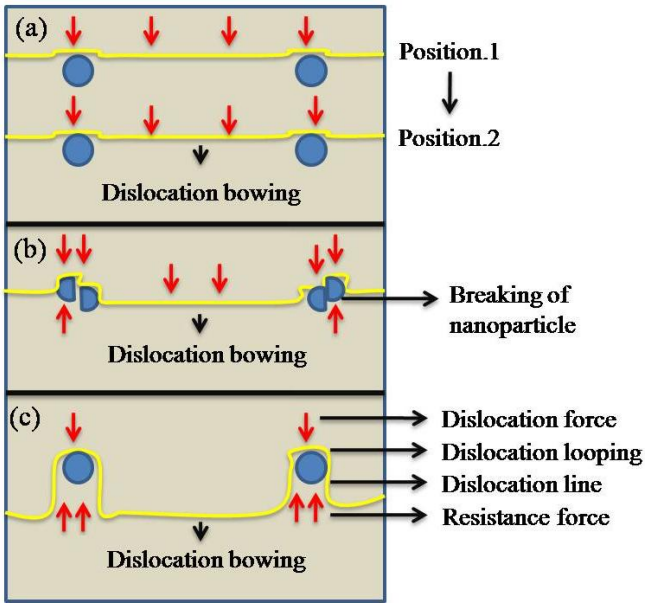

(e)

Figure 5.2. HRTEM images of Al-0.5 wt% Al_2O_3 nanocomposite by modified compocasting process showing (a) Al_2O_3 nanoparticles in aluminum matrix; (b) Crystalline lattice of Al_2O_3 nanoparticle; (c) Al-Al_2O_3 interface bonding; (d) Dislocation looping and bowing in the Al-Al_2O_3 nanocomposite. Schematic diagram of (e) Dislocation mechanisms in three different types of AMNC.

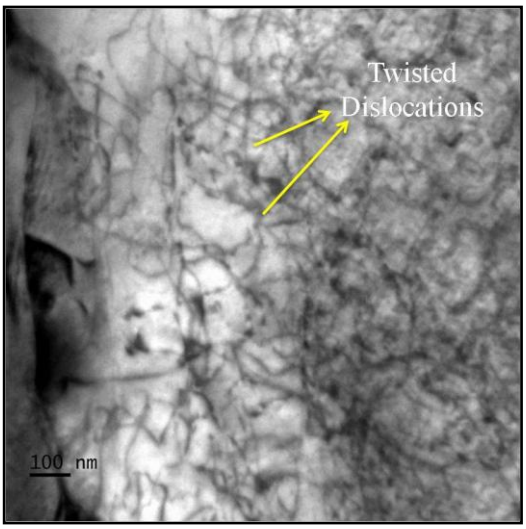

(a)

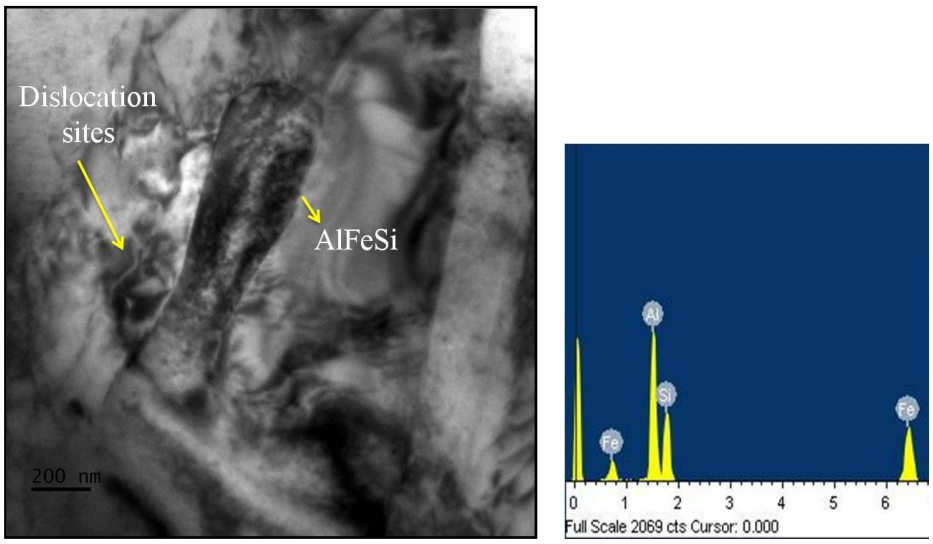

(b)

Figure 5.3. HRTEM images of Al-0.5 wt% Al_2O_3 nanocomposite by modified compocasting process showing (a) Dislocation density sites; (b) Intermetallic phase AlFeSi arresting dislocation density sites and its corresponding TEM-EDS (Atomic%: Al-55.56, Si-24.84, Fe-19.60).

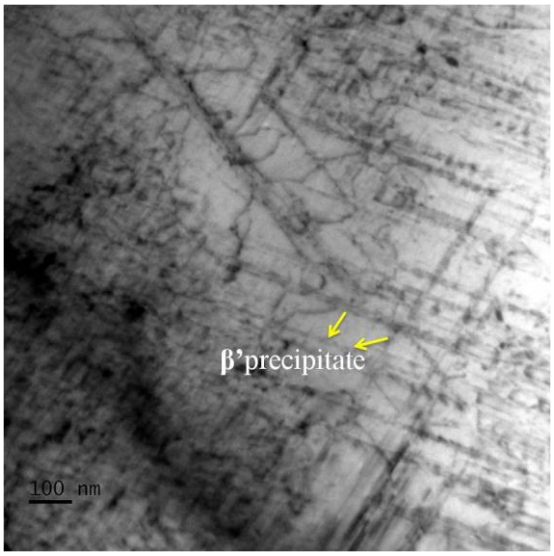
β'precipitate
100 nm

(a)

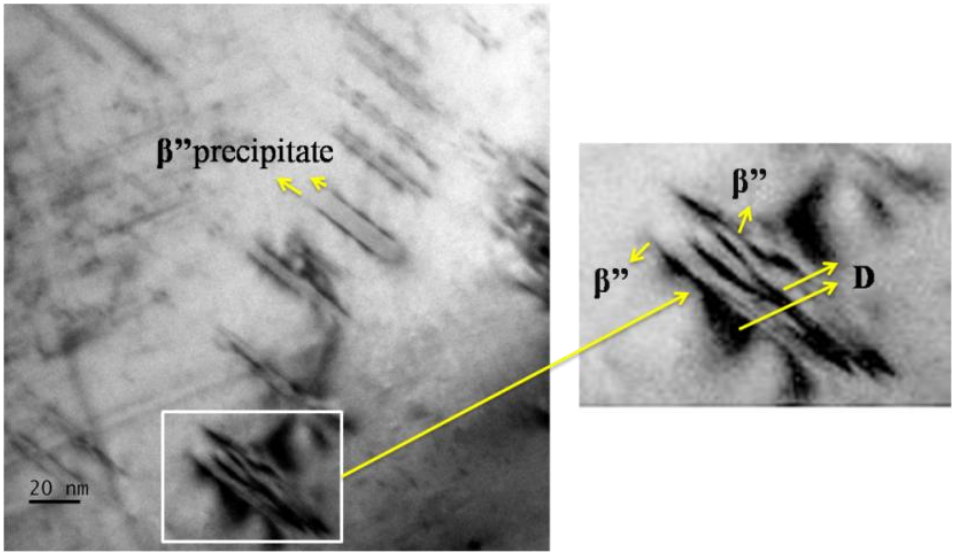
β"precipitate
20 nm
β"
β"
D

(b)

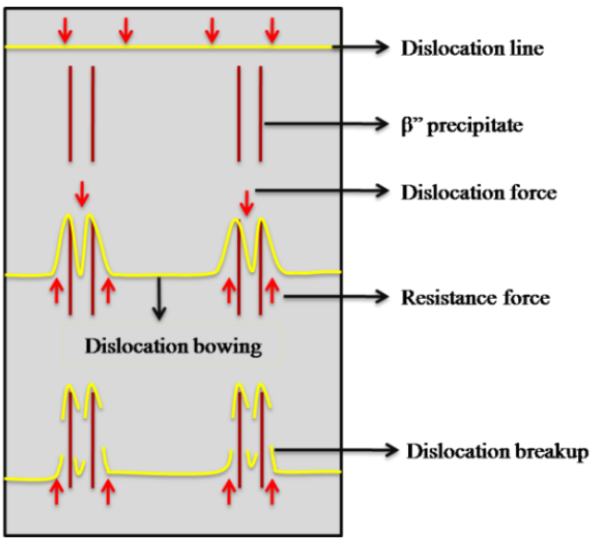
Dislocation line
β" precipitate
Dislocation force
Resistance force
Dislocation bowing
Dislocation breakup

(c)

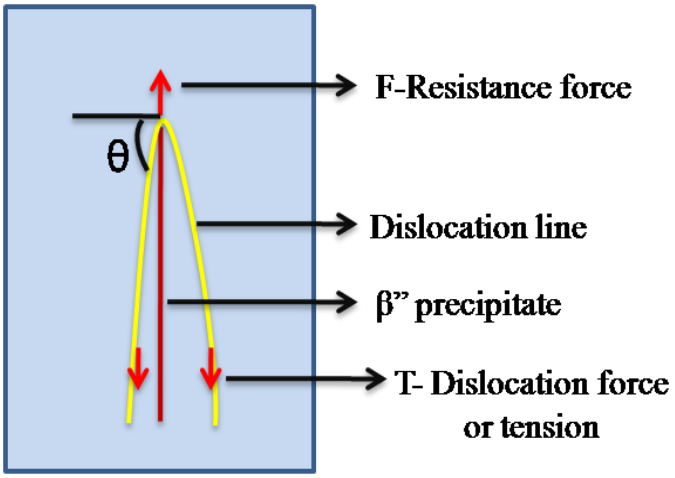

(d)

Figure 5.4. HRTEM images of Al-0.5 wt% Al_2O_3 nanocomposite by modified compocasting process showing (a) β' precipitates in the aluminum matrix-rod shape; (b) Breakup and scattering of dislocation when it bypass the β'' precipitate (needle shape). Schematic diagrams of (c) Dislocation mechanism in the matrix containing β'' precipitates; (d) Force in dislocation line when it contact with the β'' precipitate.

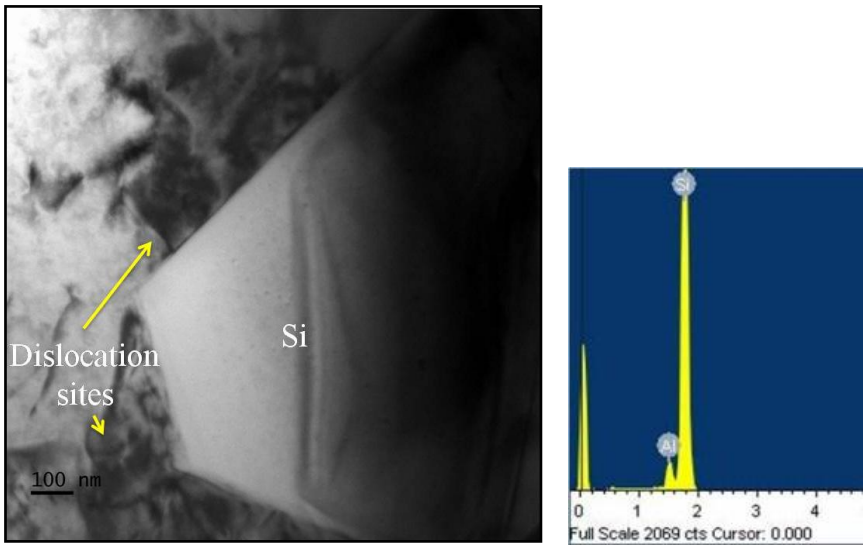

Figure 5.5. HRTEM image of Al-0.5 wt% Al_2O_3 nanocomposite by modified compocasting process showing the locking of dislocations by the alloying element Si in the matrix and its corresponding TEM-EDS (Atomic%: Si-93.15, Al-6.85).

5.3.3. Thermal and Physical Characteristics

Differential thermal analysis curves of squeeze cast Al A356 base alloy and Al-nanocomposites reinforced with varying weight percentage of Al_2O_3 nanoparticles by modified compocast method are shown in Figure 5.6. The squeeze cast Al A356 alloy showed a major endothermic peak at 577 °C corresponding to the precipitation of L→α-Al+eutectic Si (solidus) at which the compocasting process was carried out. The Al-nanocomposites shows a minor shift in the liquidus temperature towards the lower temperature at 570 °C, due to the colligative property of depression in freezing point by the addition of Al_2O_3 nanoparticles into the matrix aluminum. Both the alloy and Al-nanocomposites obtains an adjacent peak at 613 °C corresponding to L→α-Al dendrites (liquidus).

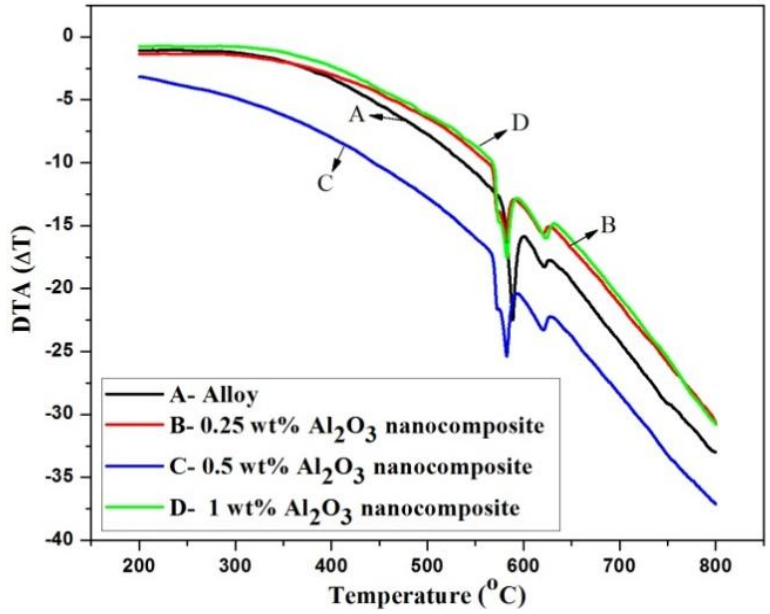

Figure 5.6. DTA curves of squeeze cast Al A356 base alloy and Al-nanocomposites reinforced with varying weight percentage of Al_2O_3 nanoparticles by modified compocast method.

Figure 5.7 showed the measured CTE values of unreinforced squeeze cast Al A356 base alloy and Al-nanocomposites reinforced with varying weight percentage of Al_2O_3 nanoparticles by modified compocasting method. The low CTE value of reinforced Al_2O_3 nanoparticles helps in reducing the CTE of composites. Also, being nanoparticles it provides more interface area with the matrix, which in turn act as additional barrier sites for matrix thermal expansion by holding the

matrix grains without expansion. The increase in weight percentage of Al_2O_3 nanoparticles in the matrix decrease the CTE value of composite, apart from 1 wt% Al_2O_3 nanoparticles reinforced composite which increases the CTE value of composite. This can be attributed to non uniform distribution of Al_2O_3 nanoparticles in the matrix. The density of squeeze cast Al A356 base alloy, 0.25 wt%, 0.5 wt% and 1 wt% Al_2O_3 nanoparticles reinforced composites are in the range of 2.7 - 2.75 g/cc.

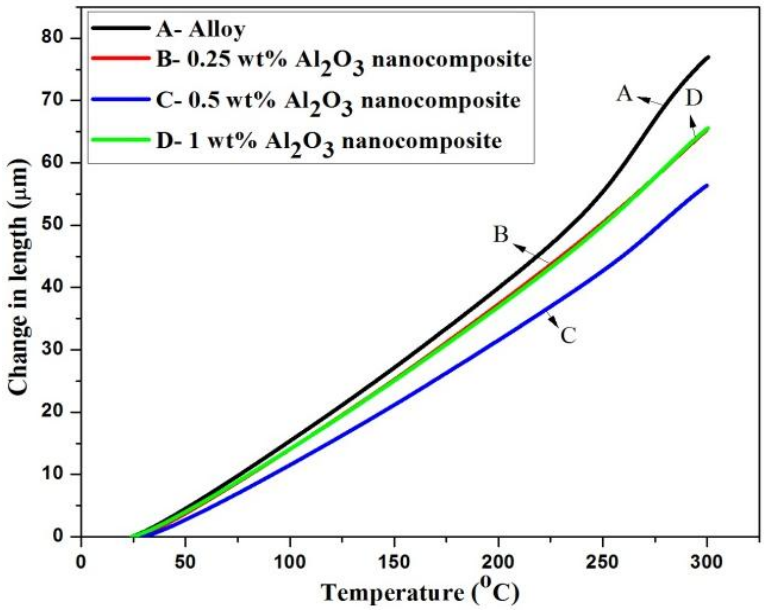

Figure 5.7. CTE analysis of squeeze cast Al A356 base alloy and Al-nanocomposites reinforced with varying weight percentage of Al_2O_3 nanoparticles by modified compocast method.

5.3.4. Mechanical Characteristics

5.3.4.1. Hardness

Figure 5.8 shows the histogram of the Brinell hardness values (as-cast and heat treated conditions) of squeeze cast Al A356 base alloy and their composites containing 0.25 wt%, 0.5 wt% and 1 wt% Al_2O_3 nanoparticles developed by different processing technique. The heat-treated sample shows higher hardness values than that of as-cast mode due to the precipitation hardening effect. Al_2O_3 nanoparticles dispersed in aluminum alloy significantly improve the hardness properties compared to base alloy. The hard Al_2O_3 nanoparticles in the aluminum matrix act as barriers to the motion of dislocations generated in the matrix and the

higher particle density causes Orowan mechanism. Composite reinforced with 0.5 wt% Al_2O_3 nanoparticles processed by modified compocasting process shows higher hardness of 147 BHN in heat treated condition compared to other systems. With further increase in the weight percentage (1 wt%) of Al_2O_3 nanoparticles in the matrix by modified compocasting process showed a decrease in the hardness value compared to the former ones owing to the agglomeration of nanoparticles. As the nanoparticles possess high surface energy due to high surface area to volume ratio, the propensity of nanoparticles to stick with each other and forming agglomerated zones in the matrix increases with increase in the addition of nanoparticles exceeding the limit. The hardness of the composite also depends on processing technique and consistency in uniform reinforcement distribution. Al-0.5 wt% Al_2O_3 nanocomposite developed by stir casting process shows a significant reduction in the hardness value in as-cast and heat treated conditions compared to Al-0.5 wt% Al_2O_3 nanocomposite fabricated by modified compocasting process. The non-uniform distribution of reinforcement during stir casting process cause clustering of Al_2O_3 nanoparticles in the matrix, consequently a remarkable change in the hardness value is obtained.

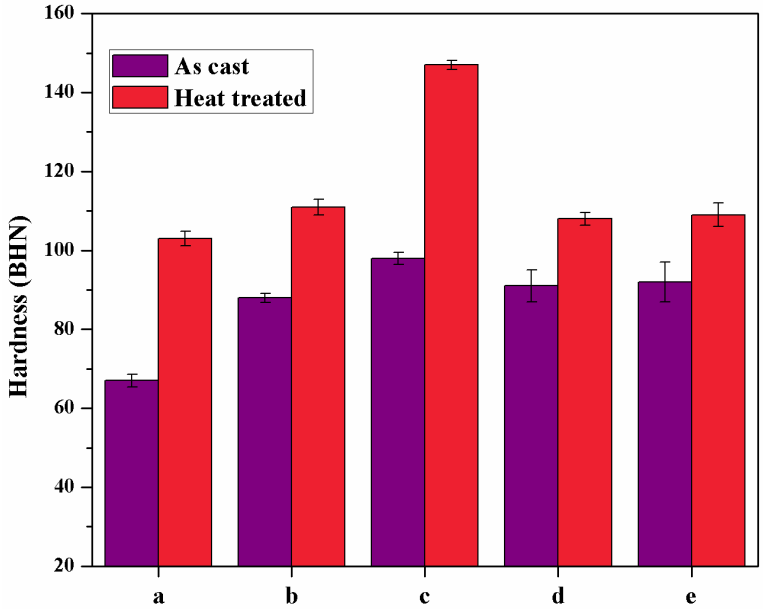

Figure 5.8. Hardness values of (a) squeeze cast Al A356 alloy; (b) Al-0.25 wt% Al_2O_3, (c) Al-0.5 wt% Al_2O_3, and (d) Al-1wt% Al_2O_3, nanocomposites by modified compocasting process; (e) Al-0.5 wt% Al_2O_3 nanocomposite by stir casting process.

5.3.4.2. Tensile Strength

The ultimate tensile strength (UTS) and yield strength (YS) of squeeze cast Al A356 base alloy and Al-nanocomposites reinforced with varying weight percentage of Al_2O_3 nanoparticles processed by modified compocasting are shown in Figure 5.9. The composite reinforced with 0.5 wt% Al_2O_3 nanoparticles showed higher UTS (345 MPa) and YS (323 MPa) compared to base alloy (UTS -292 MPa and YS-204MPa) and other varying weight percentages of Al_2O_3 nanoparticle reinforced composites. This can be ascribed to the factors like (i) uniform distribution of Al_2O_3 nanoparticles in the aluminum matrix, so that tensile load is transferred uniformly from the matrix to nanoparticles, (ii) grain refinement by squeeze casting and nanoparticle strengthening mechanism thereby satisfying Hall-Petch relation, (iii) dislocations arrest by strain fields developed from CTE mismatch between the aluminum matrix and Al_2O_3 nanoparticles during solidification, and (iv) effective grain boundary pinning[244] by nanoparticles due to strong bonding with the matrix in atomic level. Table 5.1 shows the UTS and YS values of Al-Al_2O_3 nanocomposites reported from previous studies in comparison with the present work.

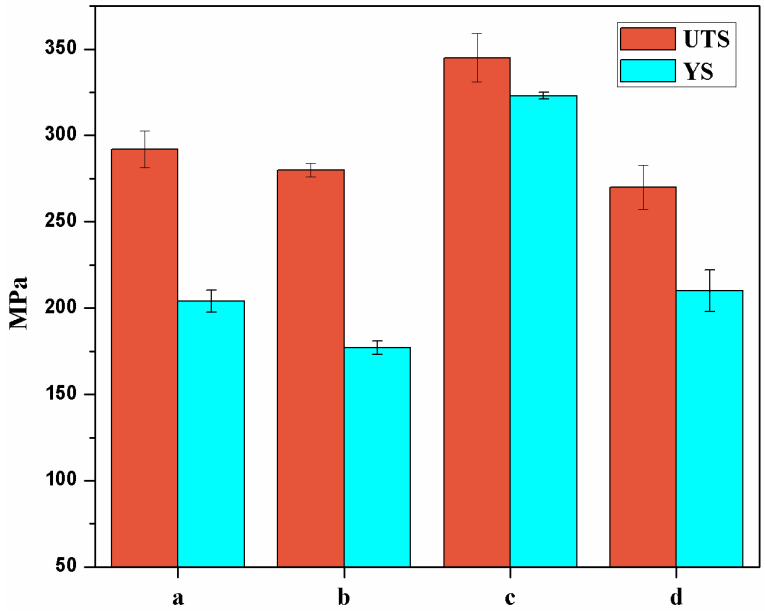

Figure 5.9. UTS and YS of (a) squeeze cast Al A356 alloy; (b) Al-0.25 wt% Al_2O_3, (c) Al-0.5 wt% Al_2O_3, and (d) Al-1wt% Al_2O_3, nanocomposites by modified compocasting process.

Table 5.1: Comparison of UTS and YS of Al-Al_2O_3 nanocomposites of present work with reported in previous studies.

System	wt%	Process	Heat Treatment	UTS MPa	YS MPa
A356-Al_2O_3 particles (50 nm)[237]	2	Compocasting	T6	259	-
A356-Al_2O_3 particles (50 nm)[160]	2	Stir casting	As cast	183	113
A356-Al_2O_3 particles (50 nm)[151]	3	Compocasting	As cast	161	111
A356-Al_2O_3 particles (40 nm)[245]	2	Compocasting	As cast	195	-
A356-Al_2O_3 particles (40 nm) Present work	**0.5**	**Compocasting followed by squeeze casting**	**T6**	**345**	**323**

Figure 5.10 shows the tensile fracture surface of Al A356 base alloy and Al-nanocomposites reinforced with varying weight percentage of Al_2O_3 nanoparticles. The fracture surface of Al A356 alloy showed (Figure 5.10a) large dimples (marked as LD) with recurrent material cracks (marked as MC). As shown in Figure 5.10c, Al- 0.5 wt% Al_2O_3 nanocomposite obtain deep dimples (marked as DD) with less material cracking compared to base alloy and other varying weight percentages of Al_2O_3 nanoparticles reinforced composites. Small dimples (marked as SD) are observed in Al-0.25 wt% Al_2O_3 nanocomposite (Figure 5.10b) and incase of Al-1 wt% Al_2O_3 nanocomposite (Figure 5.10d) mixed mode of dimples (SD and LD) are noticed.

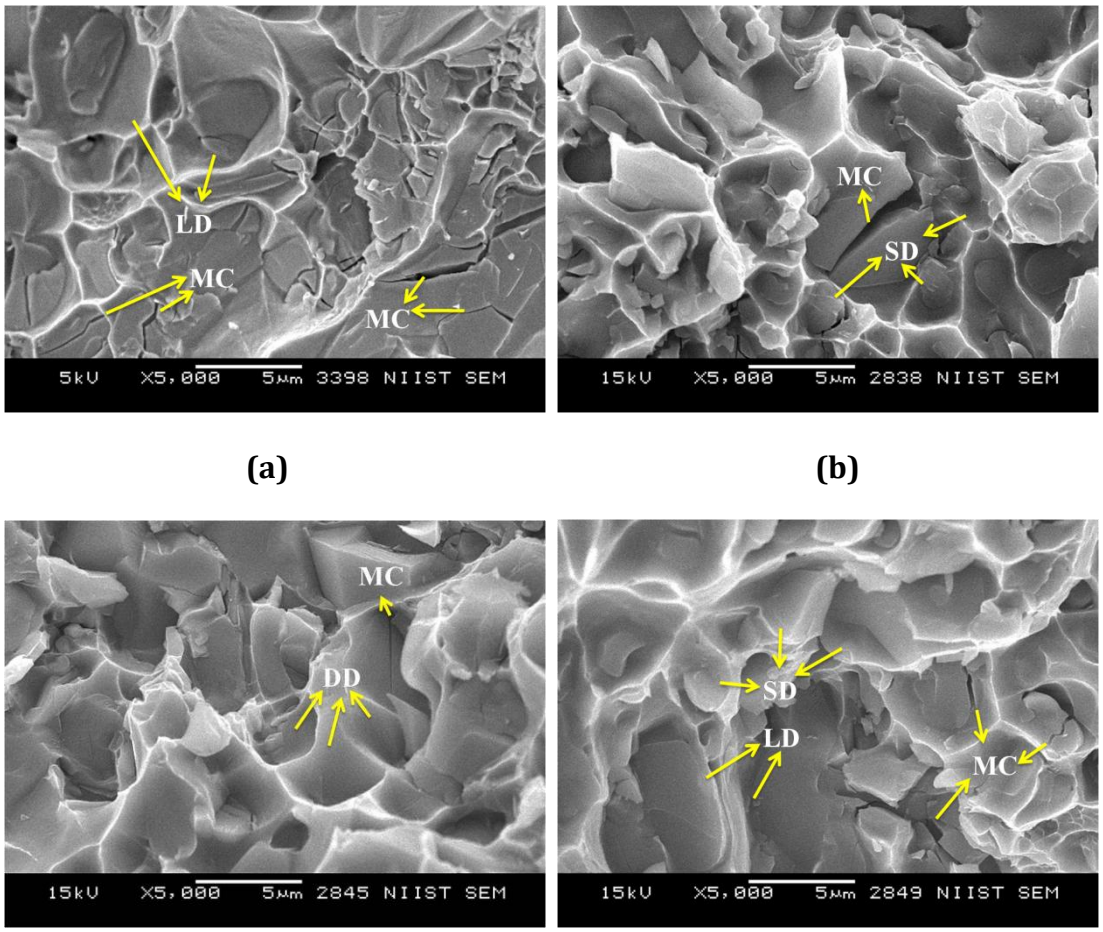

Figure 5.10. SEM images of the tensile fracture surfaces of (a) squeeze cast Al A356 alloy; (b) Al-0.25 wt% Al_2O_3, (c) Al-0.5 wt% Al_2O_3, and (d) Al-1wt% Al_2O_3, nanocomposites by modified compocasting process (LD- large dimples, MC- material cracks, DD- deep dimples, SD- small dimples). .

5.3.4.3. Impact of Pinning Dislocation Mobility on Mechanical Properties.

The significant rise in the yield strength (tensile) of Al-0.5 wt% Al_2O_3 nanocomposite by modified compocasting process is due to the effective holding of dislocation motion in the material. The obstacles in the material to delay the movement of dislocation can be grain boundaries, nanoparticles, precipitates and solute atoms. The contributions of aforesaid barriers in hindering dislocation motion (thereby strengthening nanocomposite) can be estimated by the equation (2)[246]

$$YS = \sigma_{HP} + \sigma_{Or} + \sigma_{SS} \qquad (2)$$

Where YS is the yield strength (tensile), σ_{HP} is the Hall-Petch strengthening (grain size), σ_{Or} is the Orowan strengthening which consists of strengthening by particles and precipitates, and σ_{SS} is the solid solution strengthening (solute atoms). The Hall-Petch relation can be expressed as[247]

$$\sigma_{HP} = \sigma_0 + \mathrm{K(d)}^{-0.5} \quad (3)$$

In which, σ_0 is the overall crystal lattice resistance to the mobility of dislocation (122 MPa) and K is the Hall-Petch coefficient (1.1 MPa $m^{-1/2}$). The d is the average grain size and here d is related to average secondary dendrite arm spacing.[247] The Orowan strengthening can be estimated by[248]

$$\sigma_{Orowan} = \frac{0.13Gb}{\lambda} \ln \frac{r}{b} \quad (4)$$

Where G is the shear modulus of Al (27 GPa), b is the burgers vector of Al (0.286 nm), r is the radius of nanoparticle/precipitate, and λ is the inter-particle/precipitate spacing, expressed as[248]

$$\lambda = d_{\mathrm{p}}[(\frac{1}{2V_{\mathrm{p}}})^{\frac{1}{3}} - 1] \quad (5)$$

Where d_{p} is the diameter of the nanoparticle and V_{p} is the volume fraction of the particle. Since the nanoparticles and the β'' precipitates are involved in the Orowan strengthening mechanism both their contributions are considered and estimated by

$$\sigma_{Orowan} = \sigma_{Or_{particle}} + \sigma_{Or_{precipitate}} \quad (6)$$

Finally, the contribution of solid solution strengthening is estimated by subtracting the Hall-Petch and Orowan strengthening from the experimental yield strength. Figure 5.11 showed the theoretical analysis of the contributions of Hall-Petch, Orowan and solid solution strengthening in the yield strength of Al-0.5 wt% Al_2O_3 nanocomposite by modified compocasting process. It is clear from the stack column that the Hall-Petch strengthening is contributed more in the yield strength of nanocomposite. In the case of Orowan mechanism, strengthening by nanoparticles are contributed more than β'' precipitates. Regarding solid solution

strengthening, their contribution in pinning dislocation motion is minimal due to the conversion of solute atoms to intermetallic precipitates.

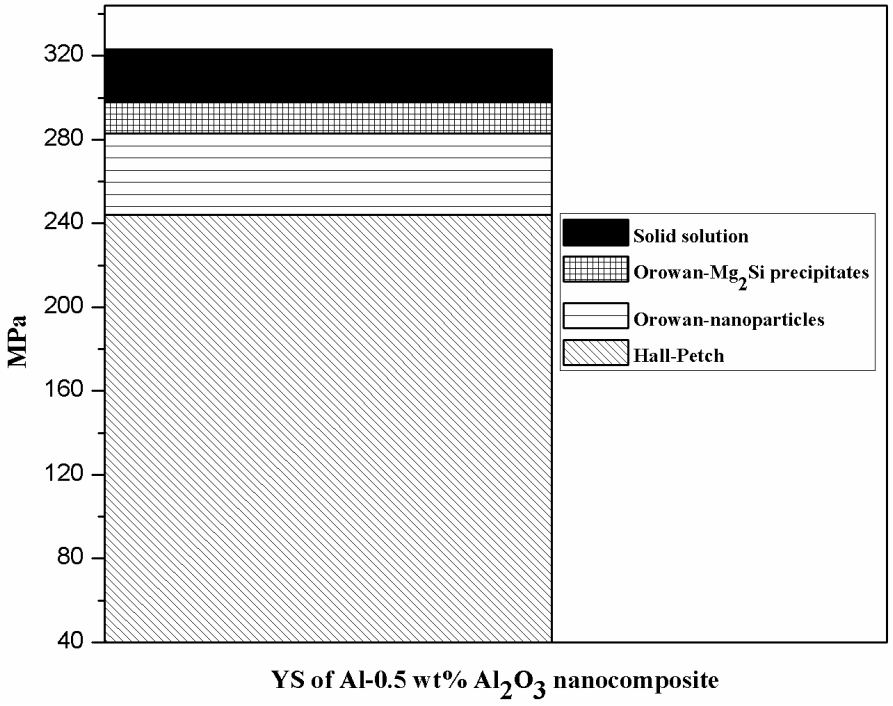

Figure 5.11. Theoretical estimation of the contributions of Hall-Petch, Orowan and solid solution strengthening in the yield strength of Al-0.5wt% Al_2O_3 nanocomposite by modified compocasting process.

5.3.4.4. Compression

The average compressive strength obtained for Al nanocomposites reinforced with 0.25 wt%, 0.5 wt%, and 1 wt% Al_2O_3 nanoparticles by modified compocasting are 861 MPa, 995 MPa, and 735 MPa respectively, which are significantly higher than squeeze cast Al A356 alloy (516 MPa). The significant raise in the compressive strength of Al-nanocomposites compared to unreinforced alloy is due to the presence of hard nanoparticles into the matrix, which resists the soft matrix distortion caused by compressive stress. The Al-nanocomposite reinforced with the higher weight percentage of Al_2O_3 nanoparticles showed a decrease in compressive strength, may be due to the formation of larger particle agglomeration sites in the matrix.

5.3.5. Wear Behavior

The tribological behavior of squeeze cast Al A356 base alloy and Al A356-nanocomposites reinforced with 0.25 wt%, 0.5 wt% and 1 wt% Al_2O_3 nanoparticles with respective to variation in load are shown in Figure 5.12. The wear rate of both Al alloy and Al-Al_2O_3 nanocomposites increases with increase in load because of higher temperature caused by shear stress at higher load.

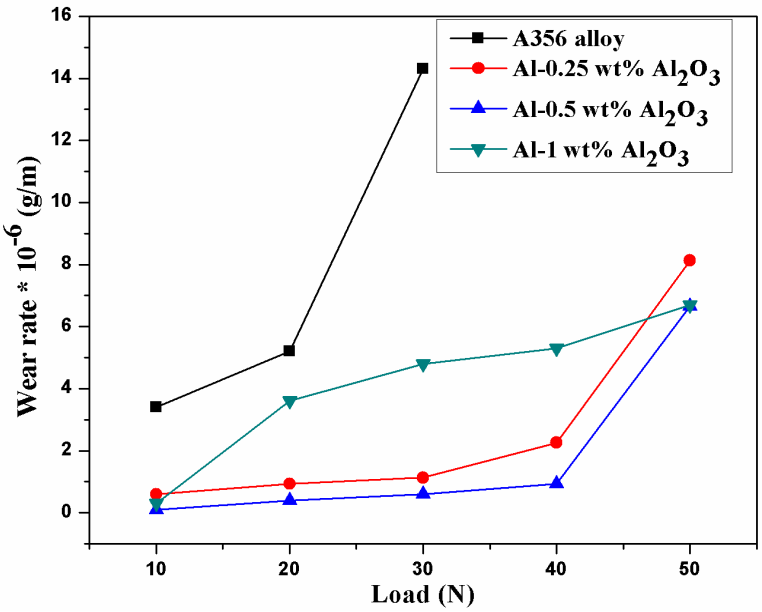

Figure 5.12. Wear rate of squeeze cast Al A356 alloy and Al-nanocomposites reinforced with varying weight percentage of Al_2O_3 nanoparticles by modified compocasting process.

It is intelligible from the graph that the wear resistances of Al-Al_2O_3 nanocomposites are exceptionally high compared to that of base alloy and this can be ascribed to the presence of hard nanoparticles in the aluminum matrix. As the surface of the unreinforced alloy is softer compared to developed composites, the alloy loses its hardness property due to thermal softening during wear and encounters heavy plastic deformation, resulted in severe wear. At the same time, the addition of Al_2O_3 nanoparticles into the matrix improves the high-temperature properties of the composites thereby resisting the localized deformation caused by thermal softening during wear and retains the hardness. At a speed of 2m/s in 30 N load an extreme wear transition region is noticed in the case of unreinforced alloy and a further increase in load causes heavy vibration and damage to the pin

material; therefore, the test for alloy was stopped. The wear curves of composites confirm the assertion that the wear rate of the material is inversely proportional to the hardness. The wear rate of composite decreases with increase in the weight percentage of Al_2O_3 nanoparticles apart from 1 wt% Al_2O_3 nanoparticles reinforced composite. The higher weight percentage (1 wt%) of Al_2O_3 nanoparticles in the composite may cause agglomeration of particles in the matrix and during wear testing the particle free matrix get exposed to the counter disc, resulting in higher wear rate.

5.3.5.1. Worn Surface Morphology

The SEM images of the worn surfaces of unreinforced Al A356 alloy and Al-Al_2O_3nanocomposites are shown in Figure 5.13. Heavy material flow (marked as MF) due to wear and localized material exfoliations (marked as ME) due to severe plastic deformations are observed in the case of alloy rotated at a speed of 2 m/s in 30 N load, manifesting adhesive wear mechanism (Figure 5.13a). The worn surface of Al-0.25 wt% Al_2O_3 nanocomposite rotated at a speed of 2 m/s in 50 N load (Figure 5.13b) showed shallow grooves (marked as SG) along the sliding direction. In the case of Al-0.5 wt% Al_2O_3 nanocomposite rotated at a speed of 2 m/s in 50N load, the worn surface looks smooth with fine grooves (marked as FG) (Figure 5.13c) compared to the foregoing one due to the incorporation of an optimum percentage of Al_2O_3 nanoparticles into the matrix, which resist the material flow. On the other hand, in the case of Al-1wt % Al_2O_3 nanocomposite rotated at a speed of 2 m/s in 50 N load, the worn surface showed deeper and wider grooves (marked as DW) with materials accumulated (marked as MA) on the edges of the grooves (Figure 5.13d). This can be due to the wear out of particle free or low particle concentrated matrix region wherein the material is relatively soft. During wear, some of the hard Al_2O_3 nanoparticles from the composites pin surface get detached and entrapped between the pin and the counter surface causing deep scratches on the worn area and later it converted into fine, shallow and deep parallel grooves along the sliding direction, revealing abrasive wear mechanism.

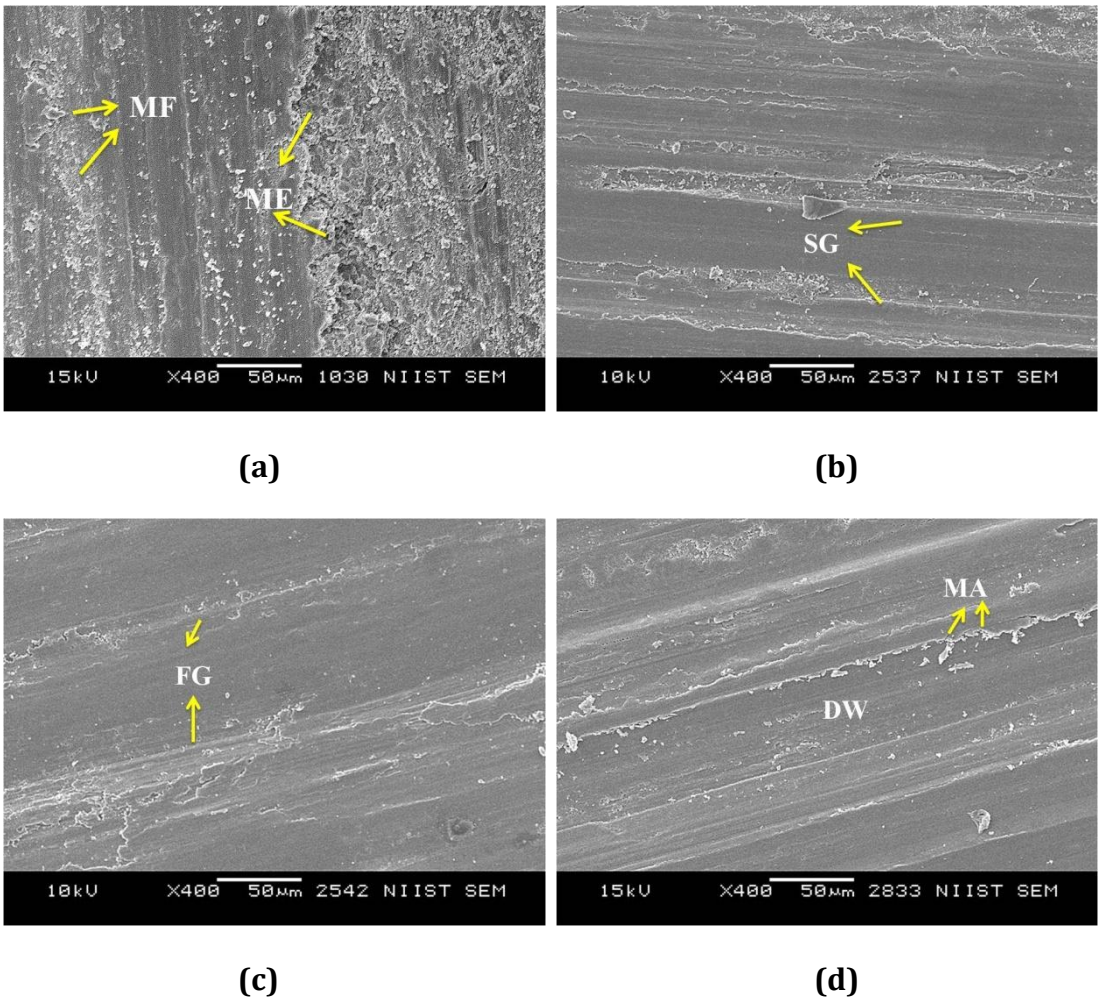

Figure 5.13. SEM images of the worn out surfaces of (a) squeeze cast Al A356 alloy; (b) Al-0.25 wt% Al_2O_3, (c) Al-0.5 wt% Al_2O_3, and (d) Al-1wt% Al_2O_3, nanocomposites by modified compocasting process (MF- material flow, ME- material exfoliations, SG- shallow grooves, DW- deeper and wider grooves, MA- materials accumulated) .

5.3.6. Corrosion Characteristics

The potentiodynamic polarization curves and the corrosion parameters of squeeze cast Al A356 base alloy and Al –nanocomposites reinforced with varying weight percentages of Al_2O_3 nanoparticles are shown in Figure 5.14 and Table 5.2. The potentiodynamic polarization curves indicate that the Al-nanocomposites shows comparable corrosion resistance to that of Al A356 alloy with respect to corrosion current density values. This is due to strong bonding between the matrix aluminum and the Al_2O_3 nanoparticles. However, Al-0.5 wt% Al_2O_3 nanocomposite

obtain the highest polarization resistance (R_p) value compared to that of base alloy and other varying weight percentage Al_2O_3 nanoparticles reinforced composites.

Table 5.2: Corrosion parameters of unreinforced squeeze cast Al A356 alloy and Al (A356) nanocomposites reinforced with varying weight percentage of Al_2O_3 nanoparticles.

Sample type	**E_{corr} Corrosion potential (V)**	**i_{corr} Corrosion current (A/cm^2)**	**Resistance (Ω)**
A356 Al Alloy	-0.89	9.82×10^{-7}	40183
Al-0.25 wt% Al_2O_3 nanocomposite	-0.84	2.28×10^{-7}	50293
Al-0.5 wt% Al_2O_3 nanocomposite	-1.02	7.6×10^{-7}	55897
Al-1 wt% Al_2O_3 nanocomposite	-0.88	5.7×10^{-7}	55487

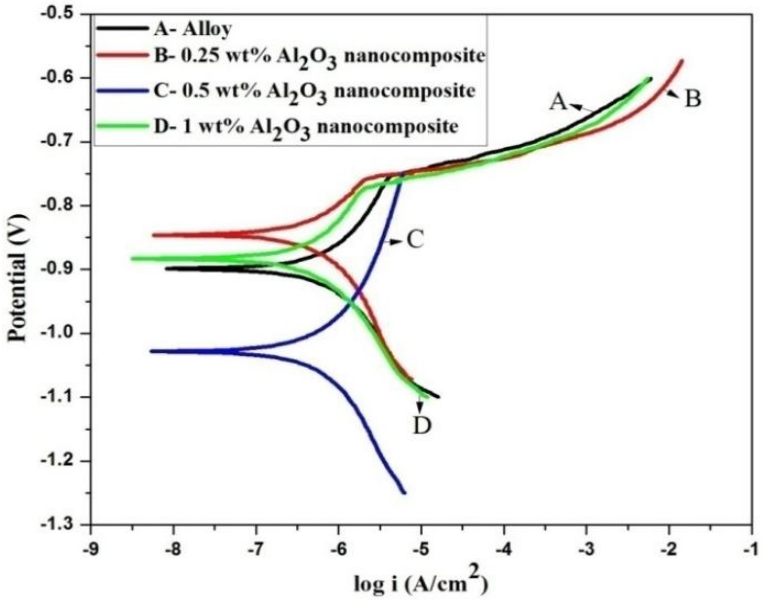

Figure 5.14. Potentiodynamic polarization curves of squeeze cast Al A356 alloy and Al-nanocomposites reinforced with varying weight percentage of Al_2O_3 nanoparticles by modified compocasting process.

The Al_2O_3 nanoparticles in the composite act as an inert material to the corrosive liquid and protect the matrix from the chemical reaction, resulting in better polarization resistance. The corrosion resistance in Al alloy and nanocomposites are attributed to the fine grains leading to high grain boundary density which can produce more passivation sites.[249] The uniform distribution of non-conductive Al_2O_3 nanoparticles in the matrix obstruct the mobility of electrons to electrolyte during reduction process and cause accumulation of negative charges at the particle-matrix interface of composite, which shift the potential of Al-0.5 wt% Al_2O_3 nanocomposite towards the negative direction.[250]

5.4. Conclusions

The present study concentrated on strengthening of cast A356 aluminum alloy through Al_2O_3 nanodispersoid addition by modified compocasting process followed by solidification under squeeze casting technique.The major conclusions are

- The optimum weight percentage of Al_2O_3 nanoparticles in the Al A356 matrix for properties enhancement are 0.5 weight percentage. Al A356-0.5 wt% Al_2O_3 nanocomposite by modified compocasting process shows a refined dendritic structure with better thermal, mechanical and tribological characteristics compared to base alloy and other varying weight percentages of Al_2O_3 nanoparticles reinforced composites studied.
- HRTEM image of Al-0.5 wt% Al_2O_3 nanocomposite by modified compocasting process showed the intimate bonding of Al lattice into the Al_2O_3 nanoparticles, thereby providing a 'Key Lock' effect. The AlFeSi, β', and β'' precipitates are observed in the composites. The Al_2O_3 nanodispersions and the β'' precipitates are involved in the Orowan strengthening mechanism thereby enhancing the mechanical properties of the composite.
- Hall-Petch, Orowan, and solid solution strengthening are involved in the yield strength of Al-0.5 wt% Al_2O_3 nanocomposite by modified compocasting process. The theoretical estimation shows that the Hall-Petch strengthening is contributed more followed by Orowan and solid solution

strengthening. In the case of Orowan mechanism particle strengthening is contributed more than precipitate.

- Remarkable enhancement in tensile strength is observed in Al-0.5 wt% Al_2O_3 nanocomposite (UTS - 345 MPa and YS - 323 MPa) compared to squeeze cast A356 base alloy (UTS -292 MPa and YS-204 MPa) and other varying weight percentages of Al_2O_3 nanoparticles reinforced composites. Al-0.5 wt% Al_2O_3 nanocomposite shows a compressive strength of 995 MPa, which is significantly higher than squeeze cast Al A356 alloy (516 MPa) and other composites.
- Higher hardness of 147 BHN in heat treated condition is observed for Al-0.5 wt% Al_2O_3 nanocomposite compared to other systems. Al nanocomposites exhibit superior wear properties than squeeze cast Al A356 base alloy due to the addition of Al_2O_3 nanoparticles which resist the matrix flow.
- Potentiodynamic polarization curves show that the Al-Al_2O_3 nanocomposites exhibit comparable corrosion resistance value to that of Al A356 alloy. However, Al-0.5 wt% Al_2O_3 nanocomposite by modified compocasting process manifest better polarization resistance (Rp) value owing to higher grain boundary density which can produce more passivation sites.

Chapter 6

Summary

Significant Observations

The present investigation deals with the fabrication and evaluation of aluminum composites using squeeze infiltration and compocasting techniques. Squeeze infiltration and modified compocasting techniques were found to be effective methods for fabricating Al composites with high volume fraction and fine and nano size reinforcements respectively in the matrix with uniform distribution. Bidirectional (BD) satin weave polyacrylonitrile (PAN) based carbon fiber (C_f) fabric preform and discontinuous zirconia grade aluminosilicate fiber preform was used for infiltration process. Finer size microsilica and nano Al_2O_3 particles were used as reinforcements for modified compocasting process. Solidification of composites was carried out under squeeze pressure to refine the grain size and to reduce the porosity in the final composites. The structural, physical, mechanical, tribological, interfacial and corrosion characteristics were evaluated.

In the first part of the thesis bidirectional (BD) satin weave polyacrylonitrile (PAN) based carbon fiber (C_f) fabric preform was successfully infiltrated with Al6061 alloy by squeeze infiltration process. The infiltrated composite shows a uniform distribution of carbon fibers in the matrix with the elimination of porosities, fiber damage and close control in deleterious aluminum carbide (Al_4C_3) phase formation, by using optimized process parameters. The complete penetration of molten aluminum metal between each and every carbon fiber in the preform with perfect adhesion between the carbon fiber and aluminum was observed. The surface of the extracted carbon fiber from the infiltrated composite was found to be relatively smooth without any damage showing no remarkable interfacial reaction product of Al_4C_3. HRTEM observation shows the presence of Al_2O_3 and $MgAl_2O_4$ spinel, confirmed by EDS and SAD pattern, at the interface between the carbon fiber and matrix thereby controlling the growth of Al_4C_3 crystals. C_f/Al6061 composite exhibits superior wear

resistance compared to unreinforced alloy due to the formation of self-lubricant tribo-film on the pin surface, which intercepts the matrix metal to counter surface contact. The introduction of BD carbon fiber in the matrix enhanced the hardness and compressive strength of the composite remarkably by restraining the matrix plastic flow behavior. The tensile strength of composite decreased due to interfacial delamination of transverse oriented fibers at lower load. The tensile fractrograph of the composite shows a multimode fracture of ductile matrix failure and brittle fiber breakage. Honeycomb cell morphology was observed around the longitudinal fiber due to the necking of ductile aluminum matrix. The C_f/Al6061 shows the lower density of 2.16 g/cm^3 which is a major advantage for weight reduction compared to the monolithic alloy (2.7 g/cm^3). Electrochemical and Immersion test of composite show no significance reduction in corrosion characteristics.

In the second part squeeze infiltration process was successfully adopted to develop Al6061 metal matrix composite reinforced with zirconia grade aluminosilicate short fiber using 15 and 20 vol% preforms. Uniform distribution of aluminosilicate fiber throughout the matrix and complete penetration of molten aluminum through the aluminosilicate fiber preform was observed in the composite microstructure with the elimination of prefrom breakage, porosities, and shrinkage. HRTEM observation shows the formation of Al_2O_3 at the aluminum-aluminosilicate fiber interface, which controls the chemical interaction and improves the bonding strength between the matrix and the fiber. Al6061/aluminosilicate composite reinforced with 15 and 20 vol% fiber exhibits better hardness and compressive strength than that of unreinforced alloy and it improves with the increase in reinforcement volume fraction. The inclusion of fiber in the matrix alloy reduces the soft matrix plastic flow behavior by preventing dislocations thereby improving the hardness and compressive properties. The tensile and impact strength of the base squeeze cast alloy was slightly higher than that of the composite due to its tough and ductile nature. Infiltrated composite shows enhanced wear resistance behavior compared to base squeeze cast alloy owing to the incorporation of hard aluminosilicate fiber. Wear resistance of the composite improves with the increase in volume fraction of the reinforcement. However, sliding speed overcomes the volume fraction concept in

improving the wear resistance of the composite by the quick formation of mechanically mixed layer (MML) at increased sliding speed. Composite reinforced with 15 and 20 vol% fibers obtained a lower density value of 2.67 g/cc and 2.66 g/cc respectively, compared to monolithic base alloy (2.7 g/cc). Electrochemical corrosion studies and Tafel plot analysis reveals that Al6061/aluminosilicate composite reinforced with 15 and 20 vol% fiber manifest better corrosion resistance properties than base alloy. This was due to the strong interfacial bonding between the Al matrix and aluminosilicate fiber and by the formation of protective interfacial reactions, both preventing the extensive attack of corrosion to the inner depth.

In the third part of the thesis A356 aluminum alloy reinforced with 7 wt. % microsilica composites were produced by the three different processing routes viz. liquid metal stir casting, compocasting and modified compocasting followed by squeeze casting. The microstructure of liquid metal stir cast Al MMC shows agglomeration of particles leading to high porosity level in the developed material. Better separation, dispersion and distribution of the microsilica particles in the solidified matrix was obtained by compocasting cum squeeze casting process than in liquid metal stir casting. Modified compocasting process (recasting the compocast ingot) reduces the segregation of particles in the final composites. The hardness of the composites predominantly depends upon the processing method, related to the reinforcement distribution. Composite samples obtained by recasting process attain higher hardness compared to other systems. Modified compocast composite exhibit a superior wear resistance properties with decreased wear rates at an increased sliding velocity due to the formation of tribolayer containing oxygen and iron on the pin surface and abrasive wear mechanism is observed in the system. Tafel curve and polarization resistance measurements reveal that Al A356-7% microsilica reinforced modified compocast composite shows similar corrosion resistance compared to squeeze cast alloy by the presence of mixed oxide layers like $MgAl_2O_4$, $NaAlSi_3O_8$ and $KAlSi_3O_8$. Microsilica particles significantly enhanced the compressive strength of modified compocast composites compared to the unreinforced squeeze cast Al alloy and the density of the modified compocast composite sample was less (2.52 g/cm^3) than those of the monolithic alloy (2.68 g/cm^3).

The final part of the investigation evaluates the effect of alumina nanoparticles in strengthening of cast A356 aluminum alloy by modified compocasting followed by solidification using squeeze casting. The optimum weight percentage of Al_2O_3 nanoparticles in the Al A356 matrix for properties enhancement was 0.5 weight percentage. Al A356-0.5 wt% Al_2O_3 nanocomposite by modified compocasting process shows a refined dendritic structure with a lower SDAS value of 9 μm. HRTEM image of Al-0.5 wt% Al_2O_3 nanocomposite by modified compocasting process showed the intimate bonding of Al lattice into the Al_2O_3 nanoparticles, thereby providing a 'Key Lock' effect. The Al_2O_3 nanodispersions and the β'' precipitates were involved in the Orowan strengthening of Al nanocomposite. The presence of hard Al_2O_3 nanoparticles and the stronger bonding between particle and alloy constrain the dislocation motion leading to dislocation bowing. The composite reinforced with 0.5 wt% Al_2O_3 nanoparticles by modified compocasting process showed higher UTS (345 MPa) and YS (323 MPa) compared to base alloy (UTS -292 MPa and YS-204MPa) and other varying weight percentages of Al_2O_3 nanoparticle reinforced composites. Hall-Petch, Orowan, and solid solution strengthening contributes in the yield strength of Al-0.5 wt% Al_2O_3 nanocomposite processed by modified compocasting. The theoretical estimation of Al -0.5 wt% Al_2O_3 nanocomposite yield strength shows that the contribution of Hall-Petch was predominant followed by Orowan and solid solution strengthening. In the case of Orowan mechanism particle strengthening was contributed more than precipitate. Al-0.5 wt% Al_2O_3 nanocomposite by modified compocasting process shows a compressive strength of 995 MPa, which was significantly higher than squeeze cast Al A356 alloy (516 MPa) and other composites. Higher hardness of 147 BHN in heat treated condition was observed for Al-0.5 wt% Al_2O_3 nanocomposite by modified compocasting process compared to other systems. Al nanocomposites exhibit superior wear properties than squeeze cast Al A356 base alloy due to the addition of Al_2O_3 nanoparticles which resist the matrix flow. The electrochemical corrosion studies reveal that the Al-Al_2O_3 nanocomposites exhibit comparable corrosion resistance value to that of Al A356 alloy.

Scope of Future Studies

- Synthesizing and characterisation of mechanically self-sustaining graded porous ceramic preforms for squeeze infiltration process of developing functionally graded materials (FGM).
- Development of selectively reinforced composites for location specific applications by the infiltration process.
- Development of unidirectional carbon fiber/Al composite by squeeze infiltration process.
- Processing and evaluation of Al/CNT composites and other Al composites using various new nanoparticles as reinforcement by modified compocasting.

References

[1] Nassim Samer, Jérôme Andrieux, Bruno Gardiola, Nikhil Karnatak, Olivier Martin, Hiroki Kurita, Laurent Chaffron, Sophie Gourdet, Sabine Lay and Olivier Dezellus: Compos. Part. A. Appl. S, 2015, vol. 72, pp. 50-57.

[2] M. Rosso: Ceramic and metal matrix composites: route and properties, 12th international scientific conference on Achievements in Mechanics and Materials Engineering, 2003.

[3] Biao Chen, Shufeng Li, Hisashi Imai, Lei Jia, Junko Umeda, Makoto Takahashi and Katsuyoshi Kondoh: Comp. Sci. and Tech, 2015, vol. 113, pp. 1-8.

[4] Hajo Dieringa: J. Mater. Sci, 2011, vol. 46, pp. 289–306

[5] D. T. Kountouras, C. A. Vogiatzis, F. Stergioudi, A. Tsouknidas and S. M. Skolianos: J. Mater. Eng. Perform, 2014, vol. 23, pp. 2015-19.

[6] K. Naplocha, A. Janus, J.W. Kaczmar and Z. Samsonowicz: J. Mater. Process. Tech, 2000, vol. 106, pp. 119-22.

[7] M. Scheffler and P. Colombo: Cellular Ceramics: Structure, Manufacturing, Properties and Applications, Wiley-VCH, Weinheim, Germany, 2005, p.645.

[8] Paolo Colombo: Phil. Trans. R. Soc. A, 2006, vol. 364, pp. 109-24.

[9] P. Colombo and J. R. Hellmann: Mater. Res. Innovat, 2002, vol. 6, pp.260-72.

[10] P. Sepulveda: Am. Ceram. Soc. Bull, 1997, vol. 76, pp. 61-65.

[11] L. Montanaro, Y. Jorand, G. Fantozzi and A. Negro: J. Eur. Ceram. Soc, 1998, vol. 18, pp. 1339-50.

[12] J. Luyten, I. Thijs, W. Vandermeulen, S. Mullens, B. Wallaeys and R. Mortelmans: Adv. Appl. Ceram, 2005, vol. 104, pp. 4-8.

[13] Y.W. Kim, S.H. Kim, C. Wang, C.B. Park: J. Am. Ceram. Soc, 2003, vol. 86, pp. 2231-33.

[14] T. J. Fitzgerald, V. J. Michaud, and A. Mortensen: J. Mater. Sci, 1995, vol. 30, pp. 1037-45.

[15] Andre R. Studart, Urs T. Gonzenbach, Elena Tervoort and Ludwig J. Gauckler: J. Am. Ceram. Soc, 2006, vol. 89, pp. 1771-89.

[16] T. Yamanaka, Y.B. Choi, K. Matsugi, O. Yanagisawa and G. Sasaki: J. Mater. Process. Tech, 2007, vol. 187-188, pp. 530-32.

[17] A. Rodriguez-Guerrero, S.A. Sanchez, J. Narciso, E. Louis and F. Rodriguez-Reinoso: Acta. Mater, 2006, vol. 54, pp. 1821-31.

[18] L.A. Dobrzański, M. Kremzer, A. Nagel and B. Huchler: JAMME, 2006, vol. 18, pp. 71-74.

[19] E.C. Hammel, O.L.-R. Ighodaro and O.I. Okoli: Ceram. Int, 2014, vol. 40, pp. 15351-370.

[20] P. Putyra, P. Kurtyka, L. Jaworska, M. Podsiadlo and B. Smuk: AMSE, 2008, vol. 33, pp. 97-100.

[21] O. Raddatz, G.A. Schneider and N. Claussen: Acta.Mater, 1998, vol. 46, pp. 6381-95.

[22] A. Mortensen: Comprehensive Composite materials, 2000, vol. 3.20, pp. 521-554.

[23] A.M. Zahedi, H.R. Rezaie, J. Javadpour, Mehdi Mazaheri and M.G. Haghighi: Ceram. Int, 2009, vol. 35, pp. 1919-26.

[24] B. Srinivasa Rao and V. Jayaram: Acta. Mater, 2001, vol. 49, pp. 2373-85.

[25] M.I. Pech-Canul, R.N. Katz and M.M. Makhlouf: J. Mater. Process. Tech, 2000, vol. 108, pp. 68-77.

[26] Kon Bae Lee and Hoon Kwon: Scripta. Mater, 1997, vol. 36, pp. 847-52.

[27] M. Rodríguez-Reyes, M.I. Pech-Canul, J.C. Rendón-Angeles and J. López-Cuevas: Comp. Sci. and Tech, 2006, vol. 66, pp. 1056-62.

[28] K.B. Lee, J.H. Choi and H. Kwon: Met. Mater. Int, 2009, vol. 15, pp. 33-36.

[29] M. Guedes, J.M.F. Ferreira, L.A. Rocha and A.C. Ferro: Ceram. Int, 2011, vol. 37, pp. 3631-35.

[30] F. Ortega-Celaya, M.I. Pech-Canul and M.A. Pech-Canul: J. Mater. Process. Technol, 2007, vol. 183, pp. 368-73.

[31] A.M. Bahraini, T. Minghetti, M. Zoellig, J. Schubert, K. Berroth, C. Schelle, T. Graule and J. Kuebler: Compos. Part A. Appl. S, 2009, vol. 40, pp. 1566-72.

[32] K. Lemster, T. Graule and J. Kuebler: Mat. Sci. Eng. A. Struct. 2005, vol. 393, pp. 229-38.

[33] D. Wittig, A. Glauche , C.G. Aneziris, T. Minghetti, C. Schelle, T. Graule and J. Kuebler: Mat. Sci. Eng. A. Struct, 2008, vol. 488, pp. 580-85.

[34] A. Contreras, V.H. Lopez and E. Bedolla: Scripta. Mater, 2004, vol. 51, pp. 249-53.

[35] B.C. Pai, G. Ramani, R.M. Pillai and K.G. Satyanarayna: J. Mater. Sci, 1995, vol. 30, pp. 1903-11.

[36] G.H. Schiroky, D.V. Miller, M.K. Aghajanian and A.S. Fareed: Key. Eng. Mater, 1997, vol. 127-131, pp. 141-52.

[37] H. Nakae and Y. Hiramoto: Int. J. Metalcast, 2011, vol. 5, pp. 23-28.

[38] T.P.D. Rajan, R.M. Pillai and B.C. Pai: J. Mater. Sci, 1998, vol. 33, pp. 3491-503.

[39] Xiao Mei Xi, Xiao Feng Yang: J. Am. Ceram. Soc, 1996, vol. 79, pp. 102-08.

[40] R.Y. Lin, R. J. Arsenault, G. P. Martins and S. G. Fishman: Interfaces in Metal–Ceramic Composites, Minerals, Metals and Materials Society, Warrendale, PA 1990, pp.291.

[41] G. Mingyuan, J. Yanping, M. Zhi, W. Zengan and W. Renjie, Mater. Sci. Eng. A. Struct, 1998, vol. 252, pp. 188-98.

[42] Idem. Jpn. Kokai. Tokkyo. Koho. JP 01279721 A2, 10 Nov, 1989, Heisei, pp.13.

[43] R.K. Dwivedi, V. Irick Jr, US patent 4871008, 1989.

[44] P.K. Rohatgi, J.K. Kim, N. Gupta, Simon Alaraj and A. Daoud: Compos. Part A. Appl. S, 2006, vol. 37, pp. 430-37.

[45] E. Carreno-Morelli, T. Cutard, R. Schaller and C. Bonjour: Mater. Sci. Eng. A, 1998, vol. 251, pp. 48-57.

[46] L.H. Qi, L.Z. Su, J.M. Zhou, J.T. Guan, X.H. Hou and H.J. Li: J. Alloy. Compd, 2012, vol. 527, pp. 10-15.

[47] Adem Demir and Necat Altinkok: Comp. Sci. and Tech, 2004, vol. 64, pp. 2067-74.

[48] T. Joseph Blucher: J. Mater. Process. Tech, 1992, vol. 30, pp. 381-90.

[49] Zhenjun Wang, Zhifeng Xu, Huan Yu, Qingsong Yan and Bo Wen Xiong: Adv. Mat. Res, 2013, vol. 634-638, pp. 1914-17.

[50] W. Hufenbach, M. Gude, A. Czulak, J. Sleziona, A. Dolata-Grosz, M. Dyzia: JAMME, 2009, vol. 35, pp. 177-83.

[51] A. Daoud: Mater. Sci. Eng. A, 2005, vol. 391, pp. 114-20.

[52] N. W. Rasmussen, P. N. Hansen and S. F. Hansen: Mater. Sci. Eng. A, 1991, vol. 135, pp. 41-43.

[53] J. Wannasin and M.C. Flemings: J. Mater. Process. Tech, 2005, vol. 169, pp. 143-49.

[54] M. Sanchez, J. Rams and A. Urena, Compos. Part A. Appl. S, 2010, vol. 41, pp. 1605-611.

[55] Y. Nishida, I. Shirayanagi and Y. Sakai: Metall. Mater. Trans A, 1996, vol. 27, pp. 4163-69.

[56] R. M. Andrews and A. Mortensen: Mater. Sci. Eng. A. Struct, 1991, vol. 144, pp. 165-68.

[57] J. Pan, D.M. Yang, H. Wan and X.F. Yin: Key. Eng. Mater, 1995, vol. 104-107, pp. 275-82.

[58] Yang Deming, Yin Xinfang and Pan Jin: J. Mater. Sci. Lett, 1993, vol. 12, pp. 252-53.

[59] Tadashi Matsunaga, Kenji Matsuda, Tomei Hatayama, Kenji Shinozaki and Makoto Yoshida: Compos. Part A. Appl. S, 2007, vol. 38, pp. 1902-11.

[60] Tadashi Matsunaga, Kenji Ogata, Tomei Hatayama, Kenji Shinozaki and Makoto Yoshida: Compos. Part A. Appl. S, 2007, vol. 38, pp. 771-78.

[61] Gen Sasaki, Junichi Adachi, Yong-Bum Choi, Jin Pan, Toshio Fujii, Kazuhiro Matsugi and Osamu Yanagisawa: Mater. Sci. Forum, 2005, vol. 475 – 479, pp. 921-24.

[62] Ferhat Gul and Mehmet Acilar: Comp. Sci. and Tech, 2004, vol. 64, pp. 1959-70.

[63] Wen-Sheng Chung and SuJien Lin: Mater. Res. Bull, 1996, vol. 31, pp. 1437-47.

[64] Jingyu Yang and D. D. L. Chung: J. Mater. Sci, 1989, vol. 24, pp. 3605-12.

[65] Bowen Xiong, Huan Yu, Zhifeng Xu, Qingsong Yan and Changchun Cai: J. Alloys and Comp, 2011, vol. 509, pp. L279-83.

[66] Olivier Beffort, Siyuan Long , Cyril Cayron, Jakob Kuebler and Philippe-Andre Buffat: Comp. Sci. and Tech, 2007, vol. 67, pp. 737-45.

[67] K. Pradeep Rohatgi, Vindhya Tiwari and Nikhil Gupta: J. Mater. Sci, 2006, vol. 41, pp. 7232-39.

[68] Wang Deqing, Shi Ziyan, Gao Hong and H. F. Lopez: J. Mater. Synth. Proces, 2001, vol. 9, pp. 247-51.

[69] D. Coupard, J. Goni and J. F. Sylvain: J. Mater. Sci, 1999, vol. 34, pp. 5307-13.

[70] R. Saha, E. Morris and N. Chawla: J. Mater. Sci. Lett, 2002, vol. 21, pp. 337-39.

[71] L.M. Peng and K.S. Han: J. Mater. Sci. Lett, 2003, vol. 22, pp. 279-82.

[72] C.P. Ju, K. I. Chen and J. H. Chern Lin: J. Mater. Sci, 1994, vol. 29, pp. 5127-34.

[73] Jun-tao GUAN, Le-hua QI, Jian LIU, Ji-ming ZHOU and Xin-liang WEI: Trans. Nonferrous Met. Soc. China, 2013, vol. 23, pp. 3173-79.

[74] J. Bear: Dynamics of fluids in porous media, Dover Publications, New York, NY, 1988.

[75] C. Garcia-cordovillaa, E. Louisb and J. Narciso: Acta. Mater, 1999, vol. 47, pp. 4461-79.

[76] V.Michaud and A.Mortensen: Compos. Part A. Appl. S, 2001, vol. 32, pp. 981-96.

[77] M. Bahraini, J.M. Molina, M. Kida, L. Weber, J. Narciso and A. Mortensen: Curr. Opin. Solid. St. M, 2005, vol. 9, pp. 196-201.

[78] V. Sampath, N. Ramanan and R. Palaninathan: Mater. Manuf. Process, 2006, vol. 21, pp. 495-05.

[79] Adam Papworth and Peter Fox: Mater. Lett, 1996, vol. 29, pp. 209-13.

[80] T.R. Vijayaram, S. Sulaiman, A.M.S. Hamouda and M.H.M. Ahmad: J. Mater. Process. Tech, 2006, vol. 178, pp. 34-38.

[81] Hasan Ali Alhashmy and Michel Nganbe: Mater. Design, 2015, vol. 67, pp. 154-58.

[82] K.M. Sree Manu, V.G. Resmi, M. Brahmakumar, N. Anand, T.P.D. Rajan, C. Pavithran, B.C. Pai and K. Manisekar: Mater. Sci. Forum, 2012, vol. 710, pp. 371-76.

[83] S.S. Wang: J. Compos. Mater, 1983, vol. 17, pp. 210-23.

[84] B. Kieback, A. Neubrand and H. Riedel: Mat. Sci. Eng. A-Struct, 2003, vol. 362, pp. 81-106.

[85] K.M. Sree Manu, V. G. Resmi, M. Brahmakumar, P. Narayanasamy, T. P. D. Rajan, C. Pavithran and B. C. Pai: Trans. Indian. Inst. Met, 2012, vol. 65, pp. 747-51.

[86] T.Y. Kosolapova: Carbides Properties, Production and Applications (New York: Plenum), 1971.

[87] F. Delannay, L. Froyen and A. Deruyttere: J. Mater. Sci, 1987, vol. 22, pp. 1-16.

[88] H. Ribes, M. Suery, G. Esperance and J.G. Legoux: Metall. Trans. A, 1990, vol. 21, pp. 2489-96.

[89] M.Y. Gu, Z. Mei, Y.P. Jin and Z.G. Wu: Scripta. Mater, 1999, vol. 40, pp. 985-91.

[90] Chun-xue Ma, Jia-Kang Yu, Chen Xue And Zhi-Qing Zhang: Trans. Nonferrous Met. Soc. China, 2013, vol. 23, pp. 2229-35.

[91] Shaofeng Zhang , Guoqin Chen, Risheng Pei , Murid Hussain , Yaping Wang, Daguang Li, Pingping Wang and Gaohui Wu: Mater. Design, 2015, vol. 65, pp. 567-74.

[92] Diego Manfredi, Matteo Pavese, Sara Biamino, Andrea Antonini, Paolo Fino and Claudio Badini: Compos. Part A. Appl. S, 2010, vol. 41, pp. 639-45.

[93] N. Nagendra, B.S. Rao and V. Jayaram: Mater. Sci. Eng. A. Struct, 1999, vol. 269, pp. 26-37.

[94] Lin Zhang , Xuanhui Qu, BohuaDuan, Xinbo He, Shubin Ren and Mingli Qin: Comp. Sci. and Tech, 2008, vol. 68, pp. 2731-38.

[95] S.G. Warrier, C.A. Blue and R.Y. Lin: J. Mater. Sci. Lett, 1993, vol.12, pp. 865-868

[96] E. Hajjari , M. Divandari and A.R. Mirhabibi: Mater. Des, 2010, vol. 31, pp. 2381-86.

[97] Yu-qin MA, Le-hua QI, Wu-qiang Zheng, Ji-ming Zhou and Lu-yan Ju: Trans. Nonferrous Met. Soc. China, 2013, vol. 23, pp. 1915-21.

[98] Qiurong Yang, Jinxu Liu , Shukui Li, Fuchi Wang and Tengteng Wu: Mater. Des, 2014, vol. 57, pp. 442-48.

[99] M. Lancin and C. Marhic: J. Eur. Ceram. Soc, 2000, vol. 20, pp. 1493-503.

[100] M. H. Vidal- Sétif, M. Lancin, C. Marhic, R. Valle, J.-L. Raviart, J.-C. Daux and M. Rabinovitch: Mater. Sci. Eng. A. Struct, 1999, vol. 272, pp. 321-33.

[101] Lehua Qi, Luyan Ju and Jiming Zhou: Procedia Eng, 2014, vol. 81, pp. 1577-82.

[102] L.A. Dobrzanski, M. Kremzer and A. Nagel: JAMME, 2007, vol. 24, pp. 183-186.

[103] T. Etter, M. Papakyriacou, P. Schulz and P.J. Uggowitzer: Carbon, 2003, vol. 41, pp. 1017-24.

[104] Shubin Ren, Xinbo He, Xuanhui Qu, Islam S. Humail and Yan Li: Comp. Sci. and Tech, 2007, vol. 67, pp. 2103-13.

[105] H.S. Lee and S.H. Hong: Mater. Sci. Tech, 2003, vol. 19, pp. 1057-64.

[106] M.I. Pech-Canul, R.N. Katz and M.M. Makhlouf: J. Mater. Process. Tech, 2000, vol. 108, pp. 68-77.

[107] Moonhee Lee, Yongbum Choi , Kenjiro Sugio, Kazuhiro Matsugi and Gen Sasaki: Comp. Sci. and Tech, 2014, vol. 97, pp. 1-5.

[108] Ayse KALEMTAS, Gulsum TOPATES, Ozlem BAHADIR, Pinar KAYA ISCI and Hasan MANDAL: Trans. Nonferrous Met. Soc. China, 2013, vol. 23, pp. 1304-13.

[109] X.Y. Qin, B.M. Wu, Y.L. Du, L.D. Zhang and H.X. Tang: Nanostruct. Mater, 1996, vol. 7, pp. 383-91.

[110] S. M. Seyed Reihani: Mater. Des, 2006, vol. 27, pp. 216-22.

[111] G.M. Song, Y.J. Wang and Y. Zhou: J. Mater. Sci, 2001, vol. 36, pp. 4625-31.

[112] Yan-Wei Zhao, Yu-Jin Wang, Lei Chen, Yu Zhou, Gui-Ming Song and Jun-Ping Li: Int. J. Refract. Met. H, 2013, vol. 37, pp. 40-44.

[113] Yonggang Tong, Shuxin Bai, Qing H Qin, Hong Zhang and Yicong Ye: Ceram. Int, 2015, vol. 41, pp. 4014-20.

[114] Yulin Zhu, Song Wang, Hongmei Chen, Wei Li, Jinming Jiang and Zhaohui Chen: Ceram. Int, 2013, vol. 39, pp. 9085-89.

[115] Shubin Ren , Xinbo He, Xuanhui Qu, Islam S. Humail and Yan Li: Comp. Sci. and Tech, 2007, vol. 67, pp. 2103-13.

[116] Xiao-fen TAN, Fan-hao ZENG, Shu-qiu WANG, Fei ZHOU and Xiang XIONG: Trans. Nonferrous Met. Soc. China, 2014, vol. 24, pp. 2359-65.

[117] Yulin Zhu, Song Wang, Hongmei Chen, Wei Li and Zhaohui Chen: Ceram. Int, 2014, vol. 40, pp. 2793-98.

[118] S. Can Kurnaz: Mater. Sci. Eng. A. Struct, 2003, vol. 346, pp. 108-15.

[119] E. Schlenther, C.G. Aneziris, T. Graule and J. Kuebler: Mater. Sci. Eng. A. Struct, 2012, vol. 556, pp. 751-57.

[120] C.A. Lewis and P.J.Withers: Acta. Metall. Mater, 1995, vol. 43, pp. 3685-99.

[121] J.F. Zhang, L.C. Zhang and Y.W. Mai: J Mater Sci, 1995, vol. 30, pp. 1961-66.

[122] ZHANG Lin, QU Xuan-hui, DUAN Bo-hua, HE Xin-bo and QIN Ming-li: Trans. Nonferrous Met. Soc. China, 2008, vol. 18, pp. 1076-82.

[123] A. Daoud: Mater. Lett, 2004, vol. 58, pp. 3206-13.

[124] Sheng-ming Zhou, Xiao-bin Zhang, Zhi-peng Ding, Chun-yan Min, Guo-liang Xu and Wen-ming Zhu: Compos. Part A. Appl. S, 2007, vol. 38, pp. 301-306.

[125] Hong Chang, Jon Binner and Rebecca Higginson: Wear, 2010, vol. 268, pp. 166-71.

[126] L.A. Dobrzanski, M. Kremzer and M. Drak: JAMME, 2008, vol. 30, pp. 121-28.

[127] R. Escalera-Lozano, C.A. Gutiérrez, M.A. Pech-Canul and M.I. Pech-Canul: Mater. Charact, 2007, vol. 58, pp. 953-60.

[128] Sennur Candan: Corros. Sci, 2009, vol. 51, pp. 1392-98.

[129] Sennur Candan: Mater. Lett, 2004, vol. 58, pp. 3601-05.

[130] Z. Ahmad, P.T. Paulette and B.J.A. Aleem: J. Mater. Sci, 2000, vol. 35, pp. 2573-79.

[131] M.K. Surappa: Aluminium matrix composites: Challenges and opportunities, Sadhana, Vol. 28, Parts 1 & 2, February/April 2003, pp. 319.

[132] Cetin Toy and William D. Scott: J. Am. Ceram. Soc, 1990, vol. 73, pp. 97-101.

[133] H. S. Lee and S. H. Hong: Mater. Sci. and Tech, 2003, vol. 19, pp. 1057-64.

[134] R. Mahadevan and R. Gopal: 68th WFC - World Foundry Congress, 2008, 379.

[135] J. Goni, I. Sarries. J. Barcena, M. Garcia de Cortazar, P.Egizabal and J. Coleto: Developments in novel production processes for metal matrix composites, Proc. 16thInternational Conference on Composite materials, Kyoto, Japan, 8 - 13 July 2007.

[136] F.C. Campbell: Lightweight Materials: Understanding the Basics, ASM International, Materials Park, Ohio 2012, pp. 459.

[137] M. Ebisawa, T. Hara, T. Hayashi and H. Ushio: Production Process for Metal Matrix Composite (MMC) Engine Block, SAE Special Paper Series, 910835.

[138] Grigorios Itskos, Pradeep K. Rohtagi, Angeliki Moutsatsou Charalampos Vasilatos, John D. Defow and Nikolaos Koukouzas: Pressure infiltration technique for the synthesis of A356 Al/fly ash composites: microstructure

and tribological performance, World of Coal Ash Conference (WOCA), Denver, CO, USA, 2011.

[139] Włodzimierz Wilk and Barbara Staniewicz-Brudnik: Abrasive Machining of Metal Matrix Composites, 8th International conference Advanced Manufacturing Operations, 2008, pp.373.

[140] B.S. Lee and S. Kang: Mater. Chem. Phys, 2001, vol. 67, pp. 249-55.

[141] Alexander Evans, Christopher San Marchi and Andreas Mortensen: Metal Matrix Composites in Industry: An Introduction and a Survey, Springer, New York, 2003.

[142] M. Rosso: J. Mater. Process. Technol, 2006, vol. 175, pp. 364–375.

[143] Satish Kumar Thandalam, Subramanian Ramanathan and Shalini Sundarrajan: J. Mater. Res. Technol, 2015, vol. 4, pp. 333–347.

[144] M. Kok: J. Mater. Process. Technol, 2005, vol. 161, pp. 381–387.

[145] A. Mortensen and I. Jin: Int. Mater. Rev, 1992, vol. 37, pp. 101–128.

[146] Ali Mazahery and Mohsen Ostad Shabani: Trans. Nonferrous Met. Soc. China, 2013, vol. 23, pp. 1905−14.

[147] Ali Mazahery and Mohsen Ostad Shabani: Ceram. Int, 2012, vol. 38, pp. 1887–95.

[148] Hamed Khosravi, Hamed Bakhshi and Erfan Salahinejad: Trans. Nonferrous Met. Soc. China, 2014, vol. 24, pp. 2482−88.

[149] F. Akhlaghi, A. Lajevardi and H.M. Maghanaki: J. Mater. Process. Technol, 2004, vol. 155–156, pp. 1874–80.

[150] T.P.D. Rajan, R.M. Pillai, B.C. Pai, K.G. Satyanarayana and P.K. Rohatgi: Compos. Sci. Technol, 2007, vol. 67, pp. 3369–77.

[151] S.A. Sajjadi, H.R. Ezatpour and M. Torabi Parizi: Mater. Des, 2012, vol. 34, pp. 106–111.

[152] B. Ashok Kumar and N. Murugan: Mater. Des, 2012, vol. 40, pp. 52−58.

[153] K. Kalaiselvan, N. Murugan and S. Parameswaran: Mater. Des, 2011, vol. 32, pp. 4004−4009.

[154] C.S. Ramesha, R. Keshavamurthy, B.H. Channabasappa and A. Ahmed: Mater. Sci. Eng. A, 2009, vol. 502, pp. 99−106.

[155] J. Allwyn Kingsly Gladston, N. Mohamed Sheriff, I. Dinaharan, J. David Raja Selvam: Trans. Nonferrous Met. Soc. China, 2015, vol. 25, pp. 683−691.

[156] Lorella Ceschini, Arne Dahle, Manoj Gupta, Anders Eric Wollmar Jarfors, S. Jayalakshmi, Alessandro Morri, Fabio Rotundo, Stefania Toschi and R. Arvind Singh: Metal matrix nanocomposites: An overview, Aluminum and magnesium metal matrix nanocomposites, Springer, 2017, pp. 1-17, DOI 10.1007/978-981-10-2681-2_1.

[157] Gennadiy Kosnikov, Oleg Figovsky and Adnan Eldarkhanov: Ch&ChT, 2015, vol. 9, pp. 165-170.

[158] V. Aniruddha Muley, S. Aravindan and I.P. Singh: Manufacturing. Rev, 2015, vol. 2, Article number 15, pp. 1-13.

[159] S.A. Sajjadi, M. Torabi Parizi, H.R. Ezatpour and A. Sedghi: J. Alloys. Compd, 2012, vol. 511, pp. 226– 231.

[160] A. Mazahery, H. Abdizadeh and H.R. Baharvandi: Mater. Sci. Eng. A, 2009, vol. 518, pp. 61–64.

[161] Ali Mazahery and Mohsen Ostadshabani: J. Compos. Mater, 2011, vol. 45, pp. 2579-2586.

[162] S.E. Ede, J.U. Odo, I.D. Adiele, J.N. Ani, C.W. Onyia and B.A. Okorie: IJSRP, 2015, vol. 5, pp. 1-6, ISSN 2250-3153.

[163] S. Iman El-Mahallawi, Ahmed Yehia Shash and Amer Eid Amer: Metals, 2015, vol. 5, pp. 802-821.

[164] S. Chand: J. Mater. Sci, 2000, vol. 35, pp. 1303–13.

[165] Amanda Jacob: Reinforced Plastics, 2014, vol. 58, pp. 18-19.

[166] Ming Yang and V.D. Scott: Carbon, 1991, vol. 29, pp. 877-879.

[167] M. De Sanctis, S. Pelletier and Y. Bienvenu: Carbon, 1994, vol. 32, pp. 925-30.

[168] Z. Qingbing: J. Appl. Polym. Sci, 1998, vol. 70, pp. 177–83.

[169] C.W. Lee, Kim Il-Ho, W. Lee, S.H. Ko, J.M. Jang and T.W. Lee: Surf. Interface. Anal, 2010, vol. 42, pp. 1231–4.

[170] Y. Tang, L. Liu, W. Li, B. Shen and W. Hu: Appl. Surf. Sci, 2009, vol. 255, pp. 4393–400.

[171] H. Naji, S.M. Zebarjad and S.A. Sajjadi: Mat. Sci. Eng. A-Struct, 2008, vol. 486, pp. 413–20.

[172] J.C. Xu, H. Yu, L. Xia, X.L. Li and H. Yang: Mater. Des, 2004, vol. 25, pp. 489–93.

[173] Alain Léger, Ludger Weber and Andreas Mortensen: Acta. Mater, 2015, vol. 91, pp. 57-69.

[174] Julien Stein, Blanka Lenczowski, Eric Anglaret and Nicole Frety: Carbon, 2014, vol. 77, pp. 44-52.

[175] Lehua Qi, Juntao Guan, Jian Liu, Jiming Zhou and Xinliang Wei: Wear, 2013, vol. 307, pp. 127–133.

[176] W.G. Wang, B.L. Xiao and Z.Y. Ma: Compos. Sci. Technol, 2013, vol. 87, pp. 69–76.

[177] S.R. Bakshi, D. Lahiri and A. Agarwal: Int. Mater. Rev, 2010, vol. 55, pp. 41-64.

[178] Jong Gil Park, Dong Hoon Keum and Young Hee Lee: Carbon, 2015, vol. 95, pp. 690-98.

[179] T.P.D. Rajan, K. Narayan Prabhu, R.M. Pillai and B.C. Pai: Compos. Sci. Technol, 2007, vol. 67, pp. 70–78.

[180] F. Stephen Bartoluccia, Joseph Paras, A. Mohammad Rafiee, Javad Rafiee, Sabrina Lee, Deepak Kapoor and Nikhil Koratkar: Mat. Sci. Eng. A-Struct, 2011, vol. 528, pp. 7933–37.

[181] Jingyue Wang, Zhiqiang Li, Genlian Fan, Huanhuan Pan, Zhixin Chen and Di Zhang: Scripta. Mater, 2012, vol. 66, pp. 594–97.

[182] D.J. Woo, F.C. Heer, L.N. Brewe, J.P. Hooper and S. Osswald: Carbon, 2015, vol. 86, pp. 15-25.

[183] T. Suzuki and H. Umehara: Carbon, 1999, vol. 37, pp. 47–59.

[184] M. Yang and V.D. Scott: J. Mater. Sci, 1991, vol. 26, pp. 1609-17.

[185] H.D. Steffens, B. Reznik and V. Kruzhanov: J. Mater. Sci, 1997, vol. 32, pp. 5413-17.

[186] S. Santhosh Kumar, V. Seshu Bai and T. Rajasekharan: J. Phys. D. Appl. Phys, 2008, vol. 41, Article number. 105403, pp. 1-6.

[187] Y.Q. Wang and J.I. Song: Wear, 2011, vol. 270, pp. 499–505.

[188] Peter Morgan: Carbon fibers and their composites. Taylors and Francis publication. Carbon fiber production using a PAN precursor; 2005, p. 203-214.

[189] J.D. Richard Tilley: Understanding solids: The science of materials. John Wiley and Sons publication. Mechanical properties of solids; 2013, p. 312.

[190] S.V. Prasad and K.R. Mecklenburg: Wear, 1993, vol. 162, pp. 47-56.

[191] S. Canumalla, S.A. Dynan, D.J. Green, R.B. Bhagat and R.N. Panborn: J. Compos. Mater, 1995, vol. 29, pp. 653-70.

[192] M.H. Stacey: Mater. Sci. Technol, 1988, vol. 4, pp. 227-239.

[193] Junjia Zhang, Shichao Liu, Yingxin Zhang, Yong Dong, Yiping Lu and Tingju Li: J. Mater. Process. Tech, 2015, vol. 226, pp. 78–84.

[194] Shaolin Li, Lehua Qi, Ting Zhang, Jiming Zhou and Hejun Li: J. Alloy. Compd, 2016, vol. 663, pp. 686-692.

[195] Caiyu Guo, Xinbo He, Shubin Ren and Xuanhui Qu: J. Alloy. Compd, 2016, vol. 664, pp. 777-783.

[196] V. Michaud and A. Mortensen: Compos. Part A-Appl. S, 2001, vol. 32, pp. 981–996.

[197] Adam Papworth and Peter Fox: Mater. Lett, 1996, vol. 29, pp. 209-213.

[198] Meihui Song, Gaohui Wu, Wenshu Yang, Wei Jia, Ziyang Xiu and Guoqin Chen: J. Mater. Sci. Technol, 2010, vol. 26, pp. 931-935.

[199] W.J. Clegg, I. Horsfall, J.F. Mason and L. Edwards: Acta. Metall, 1988, vol. 36, pp. 2151-2159.

[200] C.M. Friend and S.D. Luxton: J. Mater. Sci, 1988, vol. 23, pp. 3173-3180.

[201] S.Q. Wu, H.Z. Wang and S.C. Tjong: Compos. Sci. Technol, 1996, vol. 56, pp. 1261-1270.

[202] MMTCL Ceramic Fibre–Thermal Ceramics Products Leaflet– Murugappa, Morgan Thermal Ceramics Ltd., Chennai, 2011.

[203] L.M. Tham, M. Gupta and L. Cheng: Acta. Mater, 2001, vol. 49, pp. 3243-3253.

[204] Małgorzata Warmuzek: Aluminum-Silicon Casting Alloys: Atlas of Microfractographs, ASM International, Ohio, 2004.

[205] T.P.D. Rajan, R.M. Pillai and B.C. Pai: Metall. Mater. Trans. A, 2002, vol. 33A, pp. 2755-2761.

[206] W.M. Zhong, G.L. Esperance and M. Suery: Metall. Mater. Trans. A, 1995, vol. 26, pp. 2625-2635.

[207] K.M. Sree Manu, K. Sreeraj, TPD. Rajan, R.M. Shereema, B.C. Pai and B. Arun: Mater. Design, 2015, vol. 88, pp. 294-301.

[208] E.L. Rodriguez: J. Mater. Sci. Lett, 1987, vol. 6, pp. 718–720.

[209] I.B. Singh, D.P. Mondal, M. Singh, Anshul Bhadkul and Nidhi Jha: Indian. J. Chem. Technol, 2014, vol. 21, pp. 168-175.

[210] L.L. Shreir: Corrosion: Volume 1: Metal /Environment reactions. 2nd edition, Newnes-Butterworth, London, 1976.

[211] D.B. Miracle: Compos. Sci. Technol, 2005, vol. 65, pp. 2526–2540.

[212] V.V. Bhanu Prasad, K.S. Prasad, A.K. Kuruvilla, A.B. Pandey, B.V.R. Bhat and Y.R. Mahajan: J. Mater. Sci, 1991, vol. 26, pp. 460–6.

[213] Hai Su, Wenli Gao, Zhaohui Feng and Zheng Lu: Mater. Des, 2012, vol. 36, pp. 590-596.

[214] Hamid Reza, Ezatpour, Seyed Abolkarim Sajjadi, Mohsen Haddad Sabzevar and Yizhong Huang: Mater. Des, 2014, vol. 55, pp. 921-928.

[215] M.A. Taha and N.A. El-Mahallawy: J. Mater. Process. Technol, 1998, vol. 73, pp. 139–146.

[216] L. Ceschini, G. Minak and A. Morri: Compos. Sci. Technol, 2006, vol. 66, pp. 333–42.

[217] G.R. Li, Y.T. Zhao, H.M. Wang, G. Chen, Q.X. Dai and X.N. Cheng: J. Alloys. Compd, 2009, vol. 471, pp. 530–535.

[218] B. Abbasipour, B. Niroumand and S.M. Monir vaghefi: Trans. Nonferrous. Met. Soc. China, 2010, vol. 20, pp. 1561-1566. 15.

[219] S. Amirkhanlou and B. Niroumand: Trans. Nonferrous. Met. Soc. China, 2010, vol. 20, pp. s788-s793.

[220] J. David Raja Selvam, D.S. Robinson Smart and I. Dinaharan: Mater. Des, 2013, vol. 49, pp. 28–34.

[221] Umit Cocen and Kazim Onel: Mater. Sci. Eng. A, 1996, vol. 221, pp. 187-191.

[222] K.M. Sree Manu, P.S. Rahul, L. Ajay Raag, T.P.D. Rajan, M. Brahmakumar and B.C. Pai: Mater. Sci. Forum, 2015, vol. 830-831, pp. 489-492.

[223] Nora Brachhold and G. Christos Aneziris: Int. J. Appl. Ceram. Technol, 2012, pp. 1–9.

[224] M. Thirumurugan and S. Kumaran: T. Nonferr. Metal. Soc, 2013, vol. 23, pp. 1595-1601.

[225] R.L. Deuis, C. Subramanian and J.M. Yellup: Compos. Sci. Technol, 1997, vol. 57, pp. 415-435.

[226] S. Suresha and B.K. Sridhara: Compos. Sci. Technol, 2010, vol. 70, pp. 1652–1659.

[227] S.R.J. Saunders and J.R. Nicolls: Mater. Sci. Tech. Ser, 1989, vol. 5, pp. 780–798.

[228] G. Sundararajan: Wear, 1991, vol. 145, pp. 251.

[229] B. Venkataraman and G. Sundararajan: Wear, 2000, vol. 245, pp. 22-38.

[230] Lin Jiang, Hanry Yang, K. Joshua Yee, Xuan Mo, Troy Topping, J. Enrique Lavernia and M. Julie Schoenung: Acta. Mater, 2016, vol. 103, pp. 128-140.

[231] C.J. Hsu, C.Y. Chang, P.W. Kao, N.J. Ho and C.P. Chang: Acta. Mater, 2006, vol. 54, pp. 5241-5249.

[232] Haoyue Zhang, Nikica Maljkovic and S. Brian Mitchell: Mater. Sci. Eng. A, 2002, vol. 326, pp. 317-323.

[233] P.M. Hazzledine: Scripta. Metall. Mater, 1992, vol. 26, pp. 57-58.

[234] D.K. Koli, G. Agnihotri and R. Purohit: Proc. Mater. Sci, 2014, vol. 6, pp. 567–589.

[235] Fuzeng Ren, Weiwei Zhu, Kangjie Chu and Cancan Zhao: J. Alloy. Compd, 2016, vol. 676, pp. 164-172.

[236] Se-Il Oh, Jun-Young Lim, Yu-Chan Kim, Juil Yoon, Gyeung-Ho Kim, Joonho Lee, Yun-Mo Sung and Jun-Hyun Han: J. Alloy. Compd, 2012, vol. 542, pp. 111-117.

[237] I. El-Mahallawi, H. Abdelkader, L. Yousef, A. Amer, J. Mayer and A. Schwedt: Mater. Sci. Eng. A, 2012, vol. 556, pp. 76–87.

[238] Bowen Xiong, Zhifeng Xu, Qingsong Yan, Changchun Cai, Yuhui Zheng and Baiping Lu: J. Alloy. Compd, 2010, vol. 497, pp. L1-L4.

[239] Marc Estruga, Lianyi Chen, Hongseok Choi, Xiaochun Li and Song Jin: ACS. Appl. Mater. Interfaces, 2013, vol. 5, pp. 8813–8819.

[240] Yongfeng Zhao, Zhao Qian, Xia Ma, Houwen Chen, Tong Gao, Yuying Wu and Xiangfa Liu: ACS. Appl. Mater. Interfaces, 2016, DOI: 10.1021/acsami.6b08913.

[241] K.Y. Wen, W. Hu and G. Gottstein: Mater. Sci. Technol, 2003, vol. 19, pp. 762-768.

[242] M. Cabibbo, S. Spigarelli and E. Evangelista: Mater. Charact, 2003, vol. 49, pp. 193-202.

[243] R.R. Ambriz and D. Jaramillo: Mechanical behavior of precipitation hardened aluminum alloys welds. Waldemar Monteiro A, editor. Light metal alloys applications. InTech, 2014. DOI: 10.5772/58418.

[244] X.L. Zhong, Wong WLE and M. Gupta: Acta. Mater, 2007, vol. 55, pp. 6338–6344.

[245] A.Y. Shash, A.E. Amer and M. El-Saeed: Mechanical and Materials Engineering of Modern Structure and Component Design, A. Öchsner and H. Altenbach (eds.), Advanced Structured Materials, pp. 13-24, DOI 10.1007/978-3-319-19443-1_2.

[246] M. Mondet, E. Barraud, S. Lemonnier, J. Guyon, N. Allain and T. Grosdidier: Acta. Mater, 2016, vol. 119, pp. 55-67.

[247] J.Z. Yi, Y.X. Gao, P.D. Lee and T.C. Lindley: Metall. Mater. Trans. B, 2006, vol. 37B, pp. 301-311.

[248] Z. Zhang and D.L. Chen: Scr. Mater. 2006, vol. 54, pp. 1321–1326.

[249] K.D. Ralston and N. Birbilis: Corrosion 2010; 66: 075005-075005-13.

[250] K.M. Sree Manu, T.P.D. Rajan and B.C. Pai: J. Alloy. Compd, 2016, vol. 688, pp. 489-499.

Publications

1. **K.M. Sree Manu**, S. Arun Kumar, T.P.D. Rajan, M. Riyas Mohammed, B.C. Pai 'Effect of Alumina Nanoparticle on Strengthening of Al-Si alloy through Dendrite Refinement, Interfacial Bonding and Dislocation Bowing' *Journal of Alloys and Compounds 712 (2017) 394-405.*

2. **K.M. Sree Manu**, L. Ajay Raag, T.P.D. Rajan, Manoj Gupta, B.C. Pai 'Liquid metal infiltration processing of metallic composites - A critical review' *Metallurgical and Materials Transaction B* 47 (2016) 2799-2819.

3. **K.M. Sree Manu**, T.P.D. Rajan, B.C. Pai 'Structure and properties of squeeze infiltrated zirconia grade-aluminosilicate short fiber reinforced aluminum composites' *Journal of Alloys and Compounds* 688 (2016) 489-499.

4. **K.M. Sree Manu**, K. Sreeraj, T.P.D. Rajan, R.M. Shereema, B.C. Pai, B. Arun 'Structure and properties of modified compo cast microsilica reinforced aluminum matrix composite' *Materials and Design* 88 (2015) 294–301.

5. V.G. Resmi, **K.M. Sree Manu**, V. Lakshmi, M. Brahmakumar, T.P.D. Rajan, C. Pavithran, B.C. Pai 'Processing of silica bonded porous SiC preform for metallic composites' *Journal of Porous Materials* 22(2015) 1445-1454.

6. **K.M. Sree Manu**, P.S. Rahul, L. Ajay Raag, T.P.D. Rajan, M. Brahmakumar, B.C. Pai 'Development of Al 319-micro silica metallic composite by squeeze infiltration technique' *Materials Science Forum* 830-831 (2015) 489-492.

7. V.G. Resmi, **K.M. Sree Manu**, J.P. Deepa, V. Lakshmi, T.P.D. Rajan, C. Pavithran, B.C. Pai 'Processing of porous ceramics using aluminium derived binders and sacrificial porogen leaching method' *Materials Science Forum* 830-831 (2015) 448-451.

8. **K.M. Sree Manu**, V.G. Resmi, M. Brahmakumar, P. Narayanasamy, T.P.D. Rajan, C. Pavithran, B.C. Pai 'Squeeze infiltration processing of functionally

graded aluminum–SiC metal ceramic composites' *Transactions of the Indian Institute of Metals* 65 (2012) 747–751.

9. **K.M. Sree Manu**, V.G. Resmi, M. Brahmakumar, T.P.D. Rajan, B.C. Pai 'Synthesis of porous SiC preform and squeeze infiltration processing of aluminium-SiC metal ceramic composites' *Materials Science Forum* 710 (2012) 371-376.

10. T.P.D. Rajan, E. Jayakumar, **K.M. Sree Manu**, Akhil S. Karun, B.C.Pai 'Processing of functionally graded aluminium alloy and composite engineering components by centrifugal and squeeze casting techniques' *Indian Foundry Journal* 62(2016) 21-25.

Conference proceedings / presentation

1. **K.M. Sree Manu**, V.G. Resmi, T.P.D. Rajan, Prince Joseph, B.C. Pai, T.S. Srivatsan 'Use of squeeze infiltration processing for fabricating micro silica reinforced aluminium alloy-based metal matrix composite' Advanced Composites for Aerospace, Marine and Land applications, The Minerals Metals and Materials Society (TMS), TMS 2014, San Diego, California, USA.

2. **K.M. Sree Manu**, V.G. Resmi, T.P.D. Rajan, Prince Joseph, B.C. Pai, T.S. Srivatsan 'Fabrication and characterisation of a hybrid functionally graded metal-matrix composite using the technique of squeeze infiltration' Advanced Composites for Aerospace, Marine and Land applications, The Minerals Metals and Materials Society (TMS), TMS 2014, San Diego, California, USA.

3. **K.M. Sree Manu**, V.G. Resmi, Prince Joseph, T.P.D. Rajan, C. Pavithran, B.C. Pai 'Synthesisof porous aluminosilicate-silicon carbide fibre-particulate hybrid preform for infiltration processing of A319 metal-ceramic composites' Oral presentation in International Symposium for Research Scholars on Metallurgy, Materials Science and Engineering (ISRS-2012), December 13-15, IIT Madras, Chennai, India.

4. **K.M. Sree Manu**, V G. Resmi, V. Lakshmi, T.P.D.Rajan, B.C. Pai, P. Narayanasamy, M. Brahmakumar, K. Manisekhar 'Structural and mechanical characteristics of infiltration processed metal matrix composites' Oral presentation in National Aerospace Manufacturing seminar (NAMS) organized by Society of Aerospace Manufacturing Engineers, November 2011, Trivandrum, India.

Patent

1. **K.M. Sree Manu**, T.P.D. Rajan, Vijay Petley, Shweta Namdeo Verma, G. Rajendran, 'A new process for fabricating metallic composites by novel liquid metal infiltration technique' (Indian Patent-Filing under process).

Awards

1. **Best Poster Award**- International Conference on Advanced Materials and Manufacturing Process for Strategic Sectors (ICAMPS 2015) organized by Indian Institute of Metals (IIM), Trivandrum Chapter, May 13-15, Trivandrum, India.

2. **Best Poster Award**- 53rd National Metallurgists Day (NMD ATM 2015) on New Horizons in Materials Processing and Applications organized by Indian Institute of Metals (IIM), November 13-16, Coimbatore, India.

3. **Best Paper Award**- National Conference on Recent Engineering Advances and Trends 2015 (NCREAT-15) held at Pankajakasthuri College of Engineering and Technology, March 20, Trivandrum, India.